

**Exploiting natural variation to uncover genes modulating
root foraging responses to low nitrogen
in *Arabidopsis thaliana***

Dissertation

zur Erlangung des
Doktorgrades der Naturwissenschaften (Dr. rer. nat.)

der

Naturwissenschaftlichen Fakultät I
-Biowissenschaften-

der Martin-Luther-Universität
Halle-Wittenberg

vorgelegt

von Herrn M.Sc. Zhongtao Jia
geb. am 21.03.1990 in Xinyang City, China

verteidigt am 12.11.2019

Gutachter:

1. Prof. Dr. Nicolaus von Wirén
2. Prof. Dr. Klaus Humbeck
3. Prof. Dr. Malcolm Bennett

Table of Contents

1 Summary	1
2 Introduction.....	3
2.1 Root system architecture.....	3
2.1.1 Primary root elongation	3
2.1.2 Lateral root branching	9
2.2 Root system plasticity under varying nutrient availability.....	14
2.2.1 Nitrogen-dependent reprogramming of root system architecture	14
2.2.2 Root system architectural responses to other nutrients	19
2.3.3 Interdependence of nutrient signals in shaping root system architecture..	25
2.3 Aim of the thesis.....	26
3. Materials and methods	28
3.1 Plant materials and growth conditions.....	28
3.2 Root phenotyping, determination of dry mass, shoot N concentration and content	29
3.3 Chemical treatments	29
3.4 GWA mapping and sequence mining.....	30
3.5 Cloning and plant transformation.....	30
3.6 Histological and microscopic analysis	31
3.7 Quantitative real-time PCR.....	31
3.8 Climate data	31
3.9 Statistical analysis	32
4 Results.....	33
4.1 Natural variation of Arabidopsis root system architectural traits and biomass under two nitrogen conditions	33
4.2 Nitrogen independently modulates root system architectural traits	35
4.3 Low nitrogen-dependent root responses overcome inherent developmental differences.....	37
4.4 Root response to low nitrogen positively correlates with shoot nitrogen content	38
4.5 Low nitrogen promotes root elongation by stimulating cell elongation and cell division	39
4.6 Identification and characterization of BSK3 and its role in the primary root response to low nitrogen	42

4.6.1 GWAS maps primary root length variation under low N to <i>BSK3</i>	42
4.6.2 <i>BSK3</i> and <i>BSK</i> homologs modulate root growth under low N.....	45
4.6.3 Allelic variation of <i>BSK3</i> determines root growth and BR sensitivity	49
4.6.4 <i>BSK3</i> -dependent brassinosteroid signaling fine-tunes root responsiveness to low nitrogen.....	57
4.6.5 <i>BSK3</i> is strongly expressed in outer root cell layers but not regulated by nitrogen	59
4.6.6 Low nitrogen interferes with brassinosteroid signaling by upregulating <i>BAK1</i>	60
4.6.7 <i>BSK3</i> variants are likely adaptive to selection pressure of precipitation	65
4.7 Identification and characterization of <i>YUC8</i> in the lateral root response to low nitrogen	66
4.7.1 GWAS maps natural variation of lateral root response to <i>YUC8</i>	66
4.7.2 <i>YUC8</i> and its homologs modulate root growth at low nitrogen.....	69
4.7.3 The <i>yucQ</i> mutant reduces cell elongation under low nitrogen.....	74
4.7.4 Low nitrogen increases auxin biosynthesis by upregulating gene expression of <i>YUC8</i> and some of its homologs	75
4.7.5 Allelic variation of <i>YUC8</i> determines lateral root elongation under low nitrogen.....	78
4.7.6 Growth responses of allelic variants of <i>YUC8</i> associate with temperature variability	84
4.8 Identification of <i>DWF1</i> and characterization of its role in root responses to low nitrogen supply	87
4.8.1 Natural variation of total lateral root length and total root length under two N supply levels	87
4.8.2 GWAS maps natural variation of total lateral root length and total root length under low nitrogen to <i>DWF1</i>	88
4.8.3 Low nitrogen upregulates gene expression of <i>DWF1</i>	92
4.8.4 Low nitrogen enhances brassinosteroid biosynthesis to modulate root growth	94
4.8.5 Decreasing the endogenous brassinosteroid level attenuates the root response to low nitrogen in natural accessions.....	97
4.8.6 Variation in transcript levels of <i>DWF1</i> associates with natural variation of root length	99
4.8.7 Overexpression of <i>DWF1</i> improves shoot growth and N uptake.....	102
5 Discussion	104

5.1 Root size relates to plant performance and N accumulation	105
5.2 Employing natural variation enables identification of key regulators in hormonal pathways modulating the root foraging response	106
5.3 Brassinosteroid synthesis and signaling regulate root foraging responses to low nitrogen	108
5.4 Role of auxin in regulating root responses to low nitrogen	114
5.5 Allelic variation in genes shaping phytohormone signaling pathways associates with local environmental adaptation	116
6 References	119
7 Appendix.....	143
8 Acknowledgements	163
9 Curriculum Vitae	165
10 Eidesstattliche Erklärung/Declaration under Oath	167
11 Erklärung über bestehende Vorstrafen und anhängige Ermittlungsverfahren/Declaration concerning Criminal Record and Pending Investigations.....	168

1 Summary

Being sessile, plants have evolved sophisticated sensing mechanisms to respond to environmental factors by adjusting an array of morphological and physiological processes. To adapt to limited nitrogen (N) availability in soils, most plant species develop longer roots by stimulating the elongation of primary and lateral roots. An expanded root system allows plants to forage larger soil volumes and thus to improve water and nutrient uptake from deeper soil layers. Even though this foraging response to N limitation has been known for long, the mechanism underlying this plasticity in root development has remained unknown.

The present thesis set out with an assessment of the natural variation of root architectural traits as well as their responsiveness to N deficiency in 200 genotyped *Arabidopsis* ecotypes. These comprehensive phenotypic analyses not only revealed a high degree of independence of individual root traits and their responses to N deficiency, but also suggested an adaptive role of an expanded root system to low N availability in the growth system. At the cellular level, microscopic analyses indicated that the stimulatory effect of N deficiency on primary and lateral root elongation is attributed to enhanced cell elongation and to some extent also to enlarged meristem size in a genotype-specific manner.

Genome-wide association studies (GWAS) allowed the identification of three genes, *BSK3*, *YUC8* as well as *DWF1*, which regulate the natural variation of primary root length, average and total lateral root length as well as total root length under low N growth conditions. *BSK3*, encoding a BRASSINOSTEROID (BR) SIGNALING KINASE, was identified to modulate primary root elongation and partially also lateral root elongation under mild N deficiency. Irrespective of its variation in gene expression, allelic complementation tests demonstrated that a proline to leucine substitution in the predicted kinase domain of *BSK3* enhances BR sensitivity and signaling and increases the extent of root elongation. While prolonged growth under low N supply had no significant impact on *BSK3* transcript levels, transcript levels of the BR co-receptor *BAK1* increased. It was concluded that this response contributes to activate BR signaling and stimulate root elongation.

In the same phenotypic analysis, another prominent QTL was identified on chromosome 4 and found to associate primarily with the lateral root response to low

N. This marker-trait association was traced down to *YUCCA8* (*YUC8*), encoding a key protein in auxin biosynthesis. Expression analyses using *qRT-PCR* and *proYUC8-GUS* revealed that low N upregulated the expression of *YUC8* in the root tip. In addition to *YUC8*, low N also enhanced transcript levels of *YUC3*, *YUC5*, *YUC7* and *YUC9* that show closest homology to *YUC8*. Reverse-genetics approaches employing T-DNA insertion lines and pharmacological assays indicated an essential role of YUCCA-dependent auxin biosynthesis in the root foraging response to low N. Similar as for *BSK3*, allelic variation in *YUC8* caused an amino acid substitution in the coding region. Subsequent protein haplotype analysis and transgenic complementation tests demonstrated that a leucine to serine substitution in *YUC8* can alter the lateral root response to low N in the growth medium.

Apart from *BSK3* and *YUC8*, *DWARF1* (*DWF1*) associated with total lateral root length and total root length under low N. *DWF1* catalyzes an early step in the biosynthetic pathway of BRs. At the transcriptional level, *DWF1* transcript levels were significantly enhanced under low N supply. In addition to *DWF1*, expression levels of *CONSTITUTIVE PHOTOMORPHOGENIC DWARF* (*CPD*), *DWARF4* (*DWF4*) and *BRASSINOSTEROID-6-OXIDASE 2* (*BR6OX2*) that are central in BR biosynthesis were also upregulated by N deficiency. Characterization of corresponding T-DNA insertion lines and pharmacological experiments indicated that a low N nutritional status enhanced the transcript levels of these genes and their contribution to root elongation under low N. Unlike *BSK3* and *YUC8*, *DWF1* showed no consistent variation in the coding region that associated with root elongation. Instead, expression analysis of *DWF1* in different accessions suggested natural variation at the transcript level. Further supporting this conclusion, suppressed or enhanced expression of *DWF1* decreased or increased root growth, respectively.

Taken together, the present study shows how allelic variation in the coding region of BR signalling and auxin biosynthesis genes as well as in the transcript level of BR biosynthesis genes can contribute to enhanced root elongation under low N availability. Together with their allelic variants, the genes identified here provide promising targets for genetically improving N uptake efficiency in crops by developing cultivars with larger root systems.

2 Introduction

2.1 Root system architecture

Plant growth and survival strongly relies on a well developed root system, as the root not only provides shoot anchorage, but also determines how efficiently plants explore the soil to acquire nutrients and water. In dicotyledonous plants, such as *Arabidopsis thaliana*, the root system is composed of two basic components, i.e. an embryonically formed primary root and individual post-embryonic lateral roots (Kemmerling et al., 2007). The graminaceous plants like maize or rice have a fibrous root system composed of not only embryonic primary root and seminal roots but also post-embryonic shoot-borne nodal or crown roots, from which the lateral roots emerge (Kemmerling et al., 2007). The spatial three-dimensional arrangement of the primary and seminal roots together with their lateral roots of different orders including associated root hairs shape the root system architecture (RSA), which is of prime importance for exploitation of the soil and plant productivity (Lynch, 1995). For instance, by genetically altering root growth angle and root length, it has been shown that rice plants increase tolerance to drought or phosphate deficiency (Uga et al., 2013; Gamuyao et al., 2012). Hence, understanding the mechanisms of how plant roots develop bears great potential for increasing crop yield and optimizing resource efficiency in agricultural plant production. Root development is under control of various intrinsic and external factors (Malamy, 2005). Amongst the endogenous factors, plant hormones play a pivotal role in shaping root system architecture (RSA). Therefore, the following section describes how plant hormones modulate root elongation and lateral root branching, with knowledge and references mainly derived from *Arabidopsis thaliana*.

2.1.1 Primary root elongation

Post-embryonic root development is achieved by a balance between cell division, differentiation and elongation (Beemster & Baskin, 1998). Hence factors affecting the rate of cell proliferation in the meristematic zone and cell expansion in the elongation zone are of crucial importance in determining root growth rate. Cell proliferation takes place in the root apical meristem (RAM), which is formed by a pool of stem cells around the quiescent center (QC) (Petricka et al., 2012). It has been shown that

establishment and maintenance of the RAM is orchestrated by a tightly coordinated action of transcription factors and plant hormones. The *SHR/SCR* module consisting of two GRAS-family transcription factors is essential for ground tissue patterning and root meristem maintenance (DiLaurenzio et al., 1996; Cui et al., 2007). SHR is transcribed and translated in the stele but moves to adjacent ground tissue where SHR is sequestered by SCR in the nucleus to upregulate *SCR* expression in the endodermal cells and QC. In turn, activation of SCR in the QC transcriptionally activates *WOX5* to maintain the QC and stem cell identity in a cell-autonomous manner (Sabatini et al., 2003). Parallel to the *SHR/SCR* pathway, auxin maxima formed at the root apex also maintain the identity of stem cell niche (Sabatini et al., 1999). Establishment of auxin maxima in the root apex requires a concerted action of local auxin biosynthesis and polar auxin transport from the shoot, mediated by PIN-family auxin efflux carriers (Sabatini et al., 1999; Blilou et al., 2005; Liu et al., 2017; Brumos et al., 2018). Downstream of auxin, two auxin-inducible AP2-type transcription factors, *PLT1* and *2*, regulate several *PIN* genes. The expression level of *PLTs* regulates auxin maxima that maintain the identity of the stem cell niche and determine where cells start to differentiate (Aida et al., 2004; Blilou et al., 2005; Galinha et al., 2007). Further studies showed that PLTs may act through HYP2, a SUMO E3 ligase, to promote mitotic activity, because proper expression of *HYP2* in proliferating cells of root meristem requires *PLT2*, and activation of *PLT2* in *hyp2* mutants fails to enlarge the root meristem (Ishida et al., 2009). Apart from a role in specifying the stem cell niche, auxin also promotes root growth by regulating cell proliferation and expansion. Auxin is able to modulate cell cycle progression by inducing expression of cell cycle regulators (*CDKA;1* and *CYCD3;1*) and also by stimulating ubiquitin-dependent degradation of *SKP2A*, an F-box proteolysis regulator, to promote degradation of the cell cycle inhibitor E2FD/Del2 (Hemerly et al., 1993; Dewitte & Murray, 2003; Sozzani et al., 2010). Regarding cell expansion, it is thought that auxin stimulates the activity of plasma membrane bound H^+ -ATPase, leading to apoplastic acidification and subsequent cell wall loosening (Barbez et al., 2017).

Although auxin plays a critical role in determining root growth rate, other plant hormones are also required for proper root development. Cytokinins (CKs) promote

cell differentiation and antagonize the stimulatory effect of auxin on cell division in roots (Dello Ioio et al., 2007). Exogenous application of CKs to roots greatly reduces meristem size, while impaired cytokinin biosynthesis or genetically enhanced degradation of CKs increases root meristem size (Dello Ioio et al., 2007; Ruzicka et al., 2009). The antagonistic interplay between auxin and CKs is of particular importance in the root transition zone, where it is integrated via the AUX/IAA-type protein SHY2/IAA3 (Dello Ioio et al., 2008). In this case, CKs transcriptionally activate expression of *SHY2* through an AHK3/ARR1-dependent two-component CK signaling pathway, which in turn negatively regulates expression of *PIN* genes (esp. *PIN1*, *PIN3* and *PIN7*) and causes redistribution of auxin, thereby decreasing the meristem size. To prevent SHY2 from completely arresting cell division, auxin conversely promotes protein degradation of SHY2 via the SCF^{TIR1} pathway to sustain activity of PINs and thus increase cell division and meristem size (Dello Ioio et al., 2008). As a result, the concerted action of auxin and CKs mediated by SHY2 maintains a balance between cell proliferation and differentiation.

Gibberellin (GA) has long been known to promote plant development by stimulating degradation of growth-repressing DELLA proteins (DELLAs) (Richards et al., 2001). Tissue-specific expression of a non-degradable form of the DELLA growth repressor GAI revealed that the root endodermis is the primary responsive tissue for GA-dependent cell elongation and coordinated root growth (Ubeda-Tomas et al., 2008). Apart from DELLA-dependent regulation of cell elongation, GA also mediates DELLA protein degradation in dividing endodermal cells to restrain transcription of the cell cycle inhibitors *KRP2* and *SIM*-family genes, which in turn controls cell division activity and subsequent meristem growth (Ubeda-Tomas et al., 2009; Achard et al., 2009). Auxin induces destabilization of growth-repressing DELLA proteins and enhances GA biosynthesis (Fu & Harberd, 2003; Frigerio et al., 2006; Kim et al., 2007), which ultimately represses the inhibitory effect of CKs on root growth via repression of *ARR1* at early stages of meristem development (Moubayidin et al., 2010). As such, GA appears as an integrator for the auxin-CK antagonism in the regulation meristem growth.

Brassinosteroids (BRs) also regulate root growth and their effect on root elongation strongly depends on their concentrations. At low concentrations, BRs increase root elongation, while they inhibit root growth at high concentrations (Mussig et al., 2003; Kim et al., 2007). BRs modulate root growth by interfering with cell cycle progression and cell differentiation in the root meristem and cell expansion in the elongation zone (Takahashi et al., 1995; Gonzalez-Garcia et al., 2011). In particular, the epidermis appears to be the primary site in roots for BR signal perception (Hacham et al., 2011). In the stem cell niche, BRs promote QC division and differentiation of distal meristem cells, which requires the transcription factors *ERF115* and *BRAVO* (Gonzalez-Garcia et al., 2011; Hacham et al., 2011; Heyman et al., 2013; Vilarrasa-Blasi et al., 2014). BR signaling is intimately linked to auxin signaling partially via *BRX*, a transcription factor that was first identified as a regulator of cell proliferation and elongation (Mouchel et al., 2004; Mouchel et al., 2006). A non-functional allele of *BRX* results in a short primary root, because of BR deficiency. While *BRX* activity regulates expression of auxin-responsive genes, such as *PIN3*, auxin can conversely regulate expression and nuclear shuttling of *BRX* from the plasma membrane (Scacchi et al., 2009), suggesting that *BRX* acts as an integrator in a feedback loop that adjusts BR levels for optimal transcription of auxin-responsive genes. More recently, it has been shown that, opposing to auxin accumulation, distribution of the BR-responsive transcription factor *BZR1* follows a longitudinal gradient along the root apex, with high levels of nuclear-localized *BZR1* in epidermal cells of the transition-elongation zone but low levels in QC cells (Chaiwanon & Wang, 2015). Together with an opposite expression pattern of BR- and auxin-regulated genes, these results suggest a novel spatiotemporal and antagonistic action of BRs and auxin in modulating stem cell dynamics (Chaiwanon & Wang, 2015).

The gaseous phytohormone ethylene acts synergistically with auxin to inhibit cell elongation and subsequent root elongation (Ruzicka et al., 2007; Swarup et al., 2007). Ethylene restricts root growth through enhancing local auxin biosynthesis and PIN-mediated shootward auxin transport at the root apex (Stepanova et al., 2005; Ruzicka et al., 2007; Swarup et al., 2007; Stepanova et al., 2008). Most recently, it has been found that ethylene triggers auxin synthesis in epidermal cells of the root elongation zone and that the root epidermis is the major site of ethylene-triggered

inhibition of cell growth (Brumos et al., 2018; Vaseva et al., 2018). Independent of auxin, ethylene can also promote cell divisions in the QC (Ortega-Martinez et al., 2007).

Despite an inhibitory effect of elevated concentrations of ABA on root growth, lower concentrations of ABA stimulate root elongation (Hong et al., 2013). ABA stimulates root elongation by promoting QC maintenance and suppressing stem cell differentiation (Zhang et al., 2010). In addition, acting on the transcription factors MP and WOX5, ABA also inhibits the rate of cell division in the meristem and the speed of cell differentiation, resulting in an increased cell number in the division and the transition zones (Zhang et al., 2010). Genetic evidences has been provided that the regulation of root growth by ABA depends on a crosstalk between auxin and BRs. ABA can induce expression of *ARF2* and activation of the corresponding protein inhibits expression of the homeodomain gene *HB33* leading to enhanced root elongation (Wang et al., 2011). Although the mechanism underlying the crosstalk between ABA and BRs is still unclear, it has been shown that root elongation of BR mutants, such as *det2*, *bri1-9* and *bri1-5*, is hypersensitive to ABA due to an inhibitory effect of ABA on cell elongation (Xue et al., 2009). Most recently, it has been shown that ABA signaling inhibits BR signaling through dampening of dephosphorylation of BIN2, which requires the activity of ABI1 and ABI2 (Wang et al., 2018).

In addition to classical phytohormones, evidence has emerged that plants also utilize small secreted signaling peptides for cell-to-cell communication during root development. There are in general two broad groups of peptides, small post-translationally modified peptides (CLV3/CLEs, TDIFs, PSK, PSY1, CEPs and RGFs) and cysteine-rich peptides (RALF/RALFLs, EPFs/EPFLs), discovered in plants (Matsubayashi, 2012). Among them, the peptides of CLE, PSK, PSY1, RGF and some of the RALF/RALFL-family have been shown to play prominent roles in root development (Murphy et al., 2012). For instance, *in vitro* application of certain CLE peptides modulate root growth through alteration of the stem cell niche in the RAM (Fiers et al., 2005; Ito et al., 2006). A detailed mechanism has been reported for *CLE40*, whose loss-of-function mutant (*cle40*) shows irregular meristem organization and a short-root phenotype (Hobe et al., 2003). In this case, CLE40 modulates root

meristem maintenance through two separate pathways depending on the type of receptor. When perceived by the receptor kinases ACR4 or CLV1, CLE40 regulates distal cell differentiation by restricting expression of *WOX5* (Stahl et al., 2013). However, when CLE40 is perceived by CLV2 or CRN, this ligand/receptor complex can regulate cell differentiation in the proximal meristem likely impinging on phytohormone pathways (Pallakies & Simon, 2014).

The roles of three types of sulfated peptides, PSK, PSY1 and RGFs, have also been implicated in root growth regulation (Amano et al., 2007; Matsuzaki et al., 2010). Unlike PSK and PSY1 modulating root growth through regulation of cell elongation, RGFs coordinate root growth by maintaining the stem cell niche and cell proliferation (Matsuzaki et al., 2010). RGFs are expressed mainly in the QC and innermost columella cell layers and when secreted the corresponding peptides maintain the stem cell niche and cell division in roots (Matsuzaki et al., 2010). More recently, three independent research groups discovered that RGFs bind to RGFR-type receptors, representing a group of leucine-rich repeat receptor-like kinase(LRR-RLKs), to regulate both the transcription and protein abundance of the *PLT* genes, by which they control stem cell niche identity (Tang et al., 2015; Ou et al., 2016; Shinohara et al., 2016). Although the auxin gradient is known to shape the gradient of *PLT* expression along the root axis, it is still controversial whether RGFs function in the same pathway.

RAPID ALKALINIZATION FACTORS (RALFs) belonging to cysteine-rich peptides have also been shown to play a role in root elongation (Pearce et al., 2001; Haruta et al., 2014). Overexpression of *RALF1* reduces root elongation, whereas *RALF1* knockdown lines exhibit an increased root elongation (Haruta et al., 2014; Bergonci et al., 2014). The *RALF1* peptide binds to its receptor FERONIA4 causing phosphorylation of the plasma membrane H⁺-ATPase AHA2 and apoplastic alkalization, which in turn restrains cell elongation (Haruta et al., 2014). Interestingly, an antagonistic relationship has been shown for *RALF1* and BR signaling as exogenous application of brassinolide has a weaker effect in *RALF1*-overexpressing lines (Bergonci et al., 2014). Consistent with this notion, *RALF1* induces expression of *CPD* and *DWF4*, two genes in BR biosynthesis, that are negatively regulated by

BRs. In turn, BRs counteract RALF1-dependent induction of cell wall-remodelling enzymes, such as *PRP1*, *PRP2*, *HRPG2* and *TCH4* (Bergonci et al., 2014), suggesting that RALF1 and brassinolide act through shared signaling components. More recently, it has been found that RALF1 physically interacts with BAK1 and increases its phosphorylation, which plays an essential role in restricting cell elongation (Dressano et al., 2017).

2.1.2 Lateral root branching

Dinstinct from the primary root that is formed during embryogenesis, lateral roots are post-embryonically formed and contribute significantly to the overall root system architecture. In Arabidopsis, lateral roots are formed from xylem-pole pericycle cells (XPP) and are usually spaced along the primary root axis with a left-right alternation (Casimiro et al., 2003; De Smet et al., 2007). Lateral root formation starts with specification of a group of pericycle cells called lateral root founder cells (LRFCs) (De Smet et al., 2007). During lateral root initiation, founder cells undergo a series of tightly coordinated anticlinal and subsequent periclinal divisions, yielding a dome-shaped lateral root primodium (LRP) that eventually emerges from the parental root (Malamy & Benfey, 1997). In general, lateral root formation can be divided into three key events: Lateral root initiation, LRP establishment and lateral root emergence/elongation (Peret et al., 2009) .

Auxin plays a potent role and underpins each stage of lateral root formation. Prior to initiation, plants initiate a so-called lateral root priming process by specification of pericycle founder cells in the basal meristem of the parental root. Lateral root priming involves a complex interplay of oscillating gene expression and auxin transport as well as auxin signaling (Rogg et al., 2001; De Smet et al., 2007; Carlsbecker et al., 2010; De Rybel et al., 2010). It has been shown that the priming of lateral root founder cells (LRFCs) involves the auxin signaling module IAA28–ARF5/6/7/8/19 (De Rybel et al., 2010). The gain-of-function mutant *iaa28-1* expressing a stabilized IAA28 protein exhibits a severe defect in lateral root formation (Rogg et al., 2001). Downstream of IAA28, the transcription factor *GATA23*, whose expression is dependent on the IAA28-ARF7/19 signaling module, is found specifically expressed in lateral root founder cells before the first asymmetric division marking lateral root

induction (De Rybel et al., 2010). More importantly, tissue-specific transactivation of *GATA23* in xylem pole pericycle cells of *iaa28-1* roots is able to rescue lateral root initiation, while RNAi lines of *GATA23* showed reduced lateral root density, thus placing *GATA23* downstream of IAA28-ARF7/19 (De Rybel et al., 2010).

After priming, founder cells undergo several rounds of anticlinal asymmetric cell divisions to produce a single layer primordium consisting of a file of small cells flanked by bigger cells, marking lateral root initiation (Laskowski et al., 1995; Malamy & Benfey, 1997; Lucas et al., 2013). Auxin also is required for coordinating cell cycle progression and cell division of pre-branch sites during lateral root initiation (Himanen et al., 2002; Lavenus et al., 2013). Lateral root founder cells start to accumulate auxin and increase their responsiveness to auxin, which triggers their polarization and subsequent lateral root initiation (De Rybel et al., 2010). Perception of auxin then activates a set of genes to regulate lateral root initiation. It has been shown that auxin perception triggers degradation of IAA14 and leads subsequently to the release of ARF7/19, which in turn transcriptionally activate *LBD16* and *LBD29* required for reactivation of the cell cycle in founder cells to commence LR initiation (Fukaki et al., 2002; Fukaki et al., 2005; Okushima et al., 2007; Lee et al., 2009). Although genetic stimulation of the basic cell cycle machinery is able to bypass the IAA14-mediated control of cell division, it is not sufficient to trigger *de novo* lateral root organogenesis (Vanneste et al., 2005), suggesting additional signaling modules being involved. Consistent with this, a second auxin signaling module involving IAA12-ARF5 has been found to be active after, but not downstream of, the IAA14-ARF7/19 signaling module to regulate lateral initiation (De Smet et al., 2010).

After initiation, cells in lateral root primodium undergo a series of precise sequential anticlinal, periclinal and tangential divisions to produce a dome that breaks through the overlying tissues of the primary root (Malamy & Benfey, 1997). Here, auxin also plays an instructive role for structural organization and patterning of lateral root primodium. The formation of an auxin concentration gradient established by the coordinated action of auxin influx and efflux carriers (AUX1 and PINs) in lateral root primodium and surrounding tissues is necessarily required for proper organization of lateral root primodium (Marchant et al., 2002; Benkova et al., 2003). The proper establishment of lateral root primodium depends on the AP2-like transcription factor

PUCHI expressed in the pericycle cells and induced by auxin to regulate cell division in the proximal region of lateral root primodium (Hirota et al., 2007). Another key regulator in this process is the receptor-like kinase *ACR4* and its paralogs, whose activities have been shown to promote central pericycle cells to divide but to prevent flanking cells from dividing (De Smet et al., 2008).

On the way to the surface of the parental root, the lateral root primodium must transverse three overlying tissues, the endodermis, cortex and epidermis. Although shootward auxin transport is pivotal for lateral root initiation, lateral root emergence is finely tuned by phloem-mediated transport of auxin synthesized in the shoot (Casimiro et al., 2001; Bhalerao et al., 2002). Upon lateral root primodium growth, endodermal cells undergo a dramatic change in the cell shape, they loose volume and locally break down the Casparian strip to make way for the emerging lateral root primodium (Kumpf et al., 2013; Vermeer et al., 2014). Once the endodermis is crossed, the lateral root primodium must pass the cortex and epidermis to emerge at the root surface. Other than the endodermis undergoing a dramatic change in cell shape, the cortex and epidermis barely change their cellular organization but are rather pushed away due to loss of adherence (Kumpf et al., 2013; Vermeer et al., 2014). Regulation of this cell separation event involves the auxin signaling cascade IAA14-ARF7/19 (Swarup et al., 2008). Downstream of this module, LAX3 mediates auxin accumulation in the exactly those cortical and epidermal cells overlaying lateral root primodium (Swarup et al., 2008). However, a robust spatial expression of LAX3 in two abutting cell files requires sequential activation of another auxin efflux carrier, PIN3, which expresses at lateral, distal, shootward and rootward faces of cortical cells (Peret et al., 2013). In this model, basic auxin flow from central xylem-pole pericycle cells moves towards the outer tissue and activates expression of PIN3 to allow for auxin movement towards outer tissue layers, which subsequently turns on LAX3 expression in exactly two cell files (Peret et al., 2013). On the one hand, induction of LAX3 triggers a positive feedback signal to reinforce auxin influx in the adjacent cells, on the other hand it coordinates the spatial expression of several classes of cell wall-related enzymes to promote local cell dissociation and facilitate lateral root primodium emergence (Swarup et al., 2008; Peret et al., 2013). In addition, there is genetic evidence that auxin facilitates lateral root emergence by a

precise spatiotemporal control of water movement through the regulation of water-conducting aquaporins (Peret et al., 2012). During emergence, whilst it represses expression of *PIP2;1* in the cortex to repress water uptake in the overlying tissue, auxin activates expression of *PIP2;8* in the base of lateral root primodium and the underlying stele to promote water transport from the overlying tissue to lateral root primodium (Peret et al., 2012). As such, decreasing cell turgor in the outer tissue and increasing water pressure in the emerging lateral root primodium allow it to penetrate the parental root.

After emergence, meristem activation is marked by an increase of the number of cells in the lateral root apex (Malamy & Benfey, 1997). Lateral root elongation is realized by cell division and elongation and is further under control of auxin. It has been found that post-emergence growth of lateral root of the *alf3* mutant, defective in lateral root maturation, can be rescued by exogenous application of IAA, suggesting that meristem activation is likely related to the ability of lateral roots to synthesize auxin (Celenza et al., 1995). Despite its ability in auxin production, the lateral root still requires auxin originating from the shoot or primary root. This is suggested by impaired acropetal auxin transport in *mdr1* mutants, which show retarded lateral root elongation (Wu et al., 2007). At later developmental stages, lateral roots resemble the primary root and are thought to share the same developmental regulation as primary roots.

Although auxin plays a central role during lateral root organogenesis, other plant hormones such as CKs, ethylene, ABA and BRs also regulate lateral root formation at distinct developmental stages (Fukaki & Tasaka, 2009). CKs are considered to be antagonistic to auxin and to negatively regulate lateral root branching. For example, *Arabidopsis* plants with mutations in CK signaling components or with lower endogenous CK levels increase lateral root number, while plants with mutations in negative regulators of the cytokinin signaling pathway or with elevated cytokinin biosynthesis through ectopic expression of *IPT* exhibit defective lateral root formation (Werner et al., 2001; Werner et al., 2003; Lohar et al., 2004; To et al., 2004; Mason et al., 2005; Riefler et al., 2006). Elevating CK levels disrupt lateral root priming and initiation in pericycle founder cells by blocking cell cycle progression (Li et al., 2006;

Laplaze et al., 2007). It has been shown that the action of CK on lateral root formation is age-dependent because younger lateral root primordia are more sensitive to CK perturbation than those at later developmental stages (Bielach et al., 2012). At the molecular level, CK inhibits lateral root formation by modulating auxin transport and by preventing auxin gradient formation in developing lateral root primodium due to spatial misexpression and localization of several PINs (Laplaze et al., 2007; Marhavy et al., 2011; Marhavy et al., 2014; Bishopp & Bennett, 2014). More recently, it has been found that CRFs (CYTOKININ RESPONSE FACTORS) acting downstream of cytokinin perception transcriptionally regulate PINs expression (Simaskova et al., 2015), adding another tier in the antagonistic interaction of CK and auxin in regulating lateral root formation.

Contrary to cytokinin, BR signaling acts synergistically with auxin to promote lateral root initiation through modulating acropetal auxin transport (Bao et al., 2004). More recently, crosstalk of auxin and brassinosteroids has been also demonstrated at the signaling level. Actually, the brassinosteroid signaling kinase BIN2 phosphorylates ARF7 and ARF19 to suppress their interaction with IAAs, which in turn enhances transcriptional activity of the target genes *LBD16* and *LBD29* to promote lateral root development (Cho et al., 2014).

Ethylene has a dual role in regulating lateral root branching. Low concentrations of ethylene promote lateral root initiation, whereas high levels of ethylene inhibit the initiation of new lateral root primordium, but promote existing lateral root primodium to emerge (Negi et al., 2008; Ivanchenko et al., 2008). The inhibitory effect of high level of ethylene on lateral root initiation is dependent on elevated auxin transport involving AUX1, PIN3 and PIN7 (Negi et al., 2008; Lewis et al., 2011). Instead of modulating the auxin flow, low concentrations of ethylene increase WEI2- and WEI7-mediated auxin synthesis and also auxin signaling, thereby promoting lateral root initiation (Ivanchenko et al., 2008).

ABA can reversibly arrest lateral root growth at a specific checkpoint, i.e. immediately after lateral root primordia emergence but prior to meristem activation (De Smet et al., 2003). The inhibitory effect of ABA on lateral root development is believed to be

independent of auxin signaling as exogenous application of auxin cannot reverse post-emergence lateral root growth (De Smet et al., 2003). However, there is also genetic evidence showing the necessity of ABA and auxin interaction in lateral root formation. The B₃-type transcription factor *ABI3* involved in ABA signaling is induced by auxin in lateral root primordium and the corresponding loss-of-function mutant *abi3* shows a weaker response of lateral root formation to exogenous auxin and to auxin transport inhibitors (Brady et al., 2003). Moreover, another transcription factor, *ABI4*, mediates ABA inhibition of lateral root development via reducing root auxin levels by perturbing auxin transport (Shkolnik-Inbar & Bar-Zvi, 2010). As such, although exogenous ABA negatively impacts lateral root growth, ABA signaling is necessary for auxin-induced lateral root initiation.

2.2 Root system plasticity under varying nutrient availability

One outstanding feature of plant root systems is their inherent high degree of developmental plasticity, which enables spatial and temporal architectural changes to optimize nutrient access and uptake from most favorable sites. Experiments with *Arabidopsis thaliana* have shown that, to a large extent, nutrients can evoke specific root architectural modifications by differentially modulating root branching, elongation, angle, and spacing of roots (López-Bucio et al., 2003; Zhang et al., 2007; Forde, 2014; Giehl et al., 2014; Giehl & von Wirén, 2014; Shahzad & Amtmann, 2017; Liu & von Wirén, 2017). This section reviews how root systems respond to external or internal nutrient signals and currently known mechanisms underlying these plastic responses.

2.2.1 Nitrogen-dependent reprogramming of root system architecture

Nitrogen (N) is the mineral nutrient required in largest amounts by plants and, hence, one of the most limiting factors for plant growth and development, both in natural and agricultural ecosystems. Although nitrate (NO₃⁻) and ammonium (NH₄⁺) are two major inorganic N forms readily available for uptake from the soil, organic nitrogen in the form of amino acids or small peptides also account for a significant proportion of the soluble nitrogen pool available to plants, particularly in temperate soils of low fertility (Forde, 2014). In the soil, the distribution and availability of nitrogen drastically varies over time and space (Lark et al., 2004). To cope with this spatiotemporal fluctuations

in soil nitrogen availability, root systems must continuously sense and respond to local or temporal fluctuations in nitrogen availability. Previous experiments with *Arabidopsis thaliana* have shown that nitrogen forms and external nitrogen availability as well as the spatial distribution of these N forms can modify specific root architectural traits by signals that act locally (Remans et al., 2006; Walch-Liu et al., 2006; Lima et al., 2010; Guan et al., 2014) or systemically (Gruber et al., 2013; Kellermeier et al., 2014).

Nitrate is the predominant inorganic nitrogen form taken up by most plants grown in soil. Its availability as well as spatial distribution can evoke profound architectural changes in the root system (Zhang et al., 2007). In growth substrates with heterogeneous nitrate distribution, plant roots preferentially colonize nitrate-enriched patches by stimulating lateral root elongation (Drew, 1975; Zhang & Forde, 1998; Remans et al., 2006; Guan et al., 2014). The stimulatory effect of localized nitrate is dependent on the MADS-box transcription factor *ANR1* (Zhang & Forde, 1998) and the nitrate transceptor *NRT1.1/NPF6.3* (Remans et al., 2006; Bouguyon et al., 2016). More recently, it has been shown that the mutant *abi2-2*, which is defective in the ABA signaling phosphatase *ABI2* phenocopies the attenuated lateral root response of the *NRT1.1* mutant allele *chl1-5*. *ABI2* can interact and dephosphorylate the CIPK23/CBL1 complex, which stimulates *NRT1.1/NPF6.3*-dependent nitrate transport and signaling (Leran et al., 2015). These results place *ABI2* upstream of *NRT1.1/NPF6.3* to regulate lateral root elongation. The CIPKs/CBLs complex is of crucial importance for intracellular Ca^{2+} signal transduction (Dodd et al., 2010). Recently, a role for calcium (Ca^{2+}) as a secondary messenger has been implicated in the primary nitrate response in *Arabidopsis* roots (Riveras et al., 2015). However, whether Ca^{2+} signaling exerts a role in localized nitrate-induced lateral root elongation remains to be demonstrated.

Several studies further indicate that nitrate modulates root system architecture through auxin (Vidal et al., 2010; Krouk et al., 2010; Giehl & von Wirén, 2015). When roots are exposed to low nitrate concentrations, the nitrate transceptor *NRT1.1* inhibits lateral root emergence and elongation by facilitating shootward auxin transport (Krouk et al., 2010; Bouguyon et al., 2015; Bouguyon et al., 2016). In

addition, nitrate availability can also modulate auxin-dependent primary root and lateral root growth via a regulatory module consisting of *miR393* and the auxin receptor *AFB3* (Vidal et al., 2010). In this case, nitrate *per se* strongly induces expression of the auxin receptor gene *AFB3*. As a consequence, mutation of *AFB3* markedly abrogates the stimulatory effect of nitrate on lateral root initiation (Vidal et al., 2010). Although *AFB3* is induced by nitrate itself, its expression is under feedback regulation by downstream nitrogen assimilates via *miR393* that targets the *AFB3* transcript for degradation (Vidal et al., 2010). Downstream of *AFB3*, the transcription factor *NAC4* and its target *OBP4* specifically regulate lateral root initiation and emergence while having no effect on primary root growth (Vidal et al., 2013). This observation agrees with the finding that individual root traits display a high degree of independence across different nitrogen environments (Gifford et al., 2013).

Apart from the involvement of auxin in the modification of the root response to nitrate availability, it has also shown that excess supply of nitrate induces a systemic signal to repress the elongation of lateral roots (Zhang et al., 1999). A study with ABA biosynthesis and signaling mutants suggested involvement of the *ABI4* and *ABI5* - dependent ABA signaling pathway as well as of an ABA-independent pathway mediating this systemic repression (Signora et al., 2001). A regulatory role for ethylene has also been shown in systemic repression of lateral root growth by high nitrate (Tian et al., 2009). When exposed to high nitrate, ethylene production is rapidly increased and lateral root growth is repressed, while lateral root growth in *etr1-3* and *ein2-1* mutants, both impaired in ethylene signaling, is insensitive to high nitrate. Interestingly, induction of *NRT1.1* and *NRT2.1* by nitrate in *etr1-3* and *ein2-1* are also attenuated, highlighting that ethylene likely regulates expression of nitrate transporters and consequently modulates lateral root development in high nitrate. In addition to phytohormones, transcription factors also participate in regulating the systemic response to high nitrate availability. By integrating genomics, systems biology and molecular genetics, the two bZIP transcription factors TGA1/TGA4 acting downstream of *NRT1.1* have been identified to bind to promoters of the two nitrate transporters *NRT2.1/NRT2.2* and to be essential for primary and lateral root growth under high nitrate (Alvarez et al., 2014). Whereas the *tga1/tga4* mutant shows strong reduction of both, primary root growth and lateral root density, the *nrt2.1/nrt2.2*

mutant only shows a partial reduction in lateral root density without any impact on primary root growth, indicating that *TGA1/TGA4* might employ different targets to regulate primary root versus lateral root development while *NRT2.1/NRT2.2* plays a minor role in lateral root initiation (Alvarez et al., 2014).

Ammonium has been also proposed as a signaling molecule regulating root growth (Lima et al., 2010; Li et al., 2014; Liu & von Wirén, 2017). Whenever ammonium is supplied to plants as sole N source, roots become shorter due to inhibited elongation of primary and lateral roots. It has been shown that the root apex is the primary site of ammonium sensing (Li et al., 2010), and ammonium inhibits primary root elongation primarily by inhibiting cell proliferation and expansion (Liu et al., 2013). Isolation of the *hsn1-1* mutant that is hypersensitive to ammonium has contributed to our understanding of ammonium-regulated root inhibition (Qin et al., 2008). *HSN1*, allelic to *VTC1*, encodes a GDP-mannose pyrophosphorylase (GMPase), which synthesizes GDP-mannose that is essential for L-ascorbic acid (AsA) and N-glycoprotein formation (Conklin et al., 1999). It has been shown that defective protein glycosylation in roots rather than decreased AsA synthesis causes root hypersensitivity to ammonium (Qin et al., 2008; Barth et al., 2010). In addition, ammonium inhibition of primary root elongation is also associated with elevated ammonium efflux in the elongation zone, which is more pronounced in the *vtc1-1* mutant (Li et al., 2010). These results suggest that the GMPase-dependent pathway participates in the regulation of futile ammonium cycling (Li et al., 2010). Regarding the role of phytohormones, the exact role of auxin in ammonium inhibition of root elongation is still unclear. In an earlier study, auxin has been shown to involve in ammonium-mediated inhibition of root elongation, because mutants impaired either in auxin transport (*aux1*) or signaling (*axr1* and *axr2*) are more resistant to ammonium (Cao et al., 1993). However, a more recent study showed that primary root elongation of *aux1* is still as sensitive as the wild type to root-supplied ammonium (Liu et al., 2013b).

Although elevated root-supplied ammonium represses lateral root elongation similar as in the primary root, ammonium stimulates lateral root branching. In contrast to nitrate that stimulates lateral root elongation, local availability of ammonium strongly

induces lateral root branching through AMT1;3-dependent transport or signaling (Lima et al., 2010). Unlike root-supplied ammonium, shoot-supplied ammonium likely acts as a systemic signal and strongly inhibits lateral root emergence (Li et al., 2011a; Li et al., 2014). The inhibitory role of shoot supplied ammonium on lateral root formation depends on AUX1-mediated shoot-to-root transport of auxin, because ammonium greatly represses *AUX1* expression in the shoot vasculature and consequently reduces the auxin level in roots (Li et al., 2011b). Moreover, shoot-supplied ammonium also triggers a burst of ethylene production, which is likely coupled with suppression of *AUX1* expression in shoot, thereby inhibiting acropetal auxin movement and hindering lateral root formation (Li et al., 2013).

External presence of very low concentration of L-glutamate (< 50 μ M) can also evoke distinct effects on root system architecture (Walch-Liu et al., 2006). When grown under L-glutamate, primary root growth was remarkably inhibited, whereas lateral roots appeared less sensitive to L-glutamate, consequently resulting in a shorter but more branched root system (Walch-Liu et al., 2006). Auxin appears to play a role in L-glutamate repression of the primary root tip. It has been shown that L-glutamate causes reduced *DR5-GFP* expression in the primary root tip, and auxin mutants (*aux1-7*, *axr1-3* and *axr1-12*) alter the sensitivity of primary root growth to L-glutamate (Walch-Liu et al., 2006). However, the exact role of auxin in this root system architectural change remains to be demonstrated. Using a chemical genetics approach, a role of the MAP signaling kinase MEKK1 has been implicated in glutamate signal transduction in the primary root tip (Forde et al., 2013). Very recently, QTL analysis using recombinant inbred lines derived from reciprocal crosses between the *Arabidopsis* accessions C24 and Col-0 mapped a major effect QTL, named *Glus1* (Walch-Liu et al., 2017). Future studies must prove whether one of the underlying genes will further extend our understanding on the mechanisms, by which L-glutamate inhibits primary root growth.

A comprehensive analysis of root system architecture under various nutrient deficiencies revealed that roots respond to N deficiency in a dual manner (Gruber et al., 2013). Whereas the elongation of primary and lateral roots as well as the emergence of new lateral roots is inhibited at severe low N, external N levels that

induce only mild deficiency stimulate the emergence of lateral roots (Ma et al., 2014) and especially the elongation of primary and lateral roots (Gruber et al., 2013; Giehl & von Wirén, 2014). The former root system architecture changes involve a role of NRT1.1-dependent auxin removal from lateral root primordia as well as a CLE/CLV1 peptide signaling module (Krouk et al., 2010; Araya et al., 2014a; Araya et al., 2014b; Araya et al., 2016). It has been shown that a set of *CLEs* (i.e. *CLE1*, *CLE3*, *CLE4*, and *CLE7*) are up-regulated in N-deficient roots, and their corresponding peptides are suggested to move from root pericycle cells to phloem companion cells, where they interact with CLV1 to inhibit the outgrowth and emergence of lateral roots (Araya et al., 2014a). Auxin appears to play an active role in RSA modification in response to mild N deficiency, as mild N deficiency induces the expression of the auxin biosynthesis gene *TAR2* in the pericycle and vasculature of roots, and the *tar2* mutant displays inhibited lateral root emergence under mild N deficiency (Ma et al., 2014). However, since the length of primary and lateral roots remained unaltered in *tar2* plants, the molecular mechanism underlying the elongation of roots under mild N deficiency still remains to be uncovered.

2.2.2 Root system architectural responses to other nutrients

Phosphate is another macronutrient that often limits plant growth and productivity. Under phosphate deficiency, plants establish a highly branched and shallow root system architecture by inhibiting primary root growth, but increasing initiation and emergence of lateral roots, and promoting root hair formation (Williamson et al., 2001; Lopez-Bucio et al., 2002; Gruber et al., 2013; Bates & Lynch, 1996). Inhibition of primary root growth by phosphate deficiency is a consequence of rapid reduction of cell elongation, followed by progressive loss of cell division and subsequent meristem exhaustion (Sanchez-Calderon et al., 2005; Balzergue et al., 2017). Phosphate deficiency is locally sensed at the root apex in an iron-dependent manner (Svistoonoff et al., 2007; Ward et al., 2008). The genes *PDR2* and *LPR1/2* have been identified through mutant screening and quantitative trait locus (QTL) analysis to play a central role in low phosphate-induced meristem exhaustion (Ticconi et al., 2004; Svistoonoff et al., 2007). Genetic analysis revealed that *lpr1lpr2* mutations are epistatic to *pdr2*, placing *PDR2* upstream of *LPR1* under phosphate deficiency conditions (Ticconi et al., 2009; Muller et al., 2015). Under phosphate deficiency, the

LPR1-PDR2 module facilitates apoplastic iron accumulation in cells of the elongation and meristematic zone of the primary root, which triggers production of reactive oxygen species (ROS) and callose deposition (Müller et al., 2015). The callose formation interferes with symplastic communication because it blocks the intercellular movement of SHR and thereby promotes cell differentiation in the apical meristem (Müller et al., 2015). Forward genetic screening revealed that the two genes *STOP1* and *ALMT1* play a critical role in primary root growth inhibition under low phosphate (Gutierrez-Alanis et al., 2017; Balzergue et al., 2017). Low phosphate post-translationally activates *STOP1*, whose activity is essential for *ALMT1*-dependent apoplastic malate exudation. Thereby, the *STOP1-ALMT1* module regulates iron accumulation and remobilization in the root apical meristem in an *LPR1*-dependent fashion (Gutierrez-Alanis et al., 2017; Balzergue et al., 2017). More recently, it has been found that low phosphate-induced iron remobilization is dependent on peptide signaling comprising of the *CLE14-CLV2/PEPR2* regulatory module (Gutierrez-Alanis et al., 2017). Iron accumulation causes meristem exhaustion by concomitant downregulation of *SHR/SCR* and *PIN*s leading to suppressed auxin signaling (Gutierrez-Alanis et al., 2017).

In the past decades, progress has been made also in our understanding of the roles of phytohormone synthesis, distribution or sensitivity in root system architectural changes upon phosphate limitation. While it has been proposed that modulation of meristematic activity by phosphate availability is independent of auxin (Lopez-Bucio et al., 2005; Jain et al., 2007), auxin is indispensable for lateral root formation upon phosphate limitation. Actually, phosphate deficiency enhances root sensitivity to auxin (Lopez-Bucio et al., 2002; Nacry et al., 2005). Low phosphate upregulates expression of the auxin receptor *TIR1*, which accelerates the degradation of *AUX/IAA* auxin repressors and releases *ARF* transcription factors, such as *ARF7* and *ARF19*, to induce genes involved in lateral root formation and emergence (Perez-Torres et al., 2008). In addition to *TIR1*, it has been found that the SUMO E3 ligase *SIZ1* promotes lateral root formation under low phosphate condition (Miura et al., 2005). The upregulation of several auxin-responsive genes in the *siz1* mutant suggests that *SIZ1* negatively regulates the reprogramming of lateral root development in response to low phosphate. However, *TIR1* is unlikely the direct target of *SIZ1*, since it lacks a

SUMOylation motif. Therefore, further research will be needed to understand how the SUMOylation pathway is integrated into auxin-regulated lateral root formation upon phosphate deficiency. More recently, *ARK2/PUB9* has been shown to play a role in lateral root formation under low phosphate. The double mutant *ark2pub9* exhibits severe reduction in lateral root development, which is likely owing to decreased auxin accumulation (Deb et al., 2014). Apart from lateral root formation, it has been shown that root hair elongation induced by low phosphate is also dependent on auxin. Phosphate deficiency elevates the auxin level in the root apex by increasing TAA1-dependent auxin synthesis and AUX1-dependent shootward auxin mobilization. An elevated auxin flow via the lateral root cap towards epidermal cells induces expression of *ARF19* and subsequently upregulates *RSL2* and *RSL4* in the differentiation zone to promote root hair formation (Bhosale et al., 2018).

Gibberellin signaling has also been implicated in plant responses to phosphate deficiency. GA promotes plant growth by triggering the degradation of growth-repressing DELLA proteins through the ubiquitin-dependent 26S proteasome pathway (Richards et al., 2001). Phosphate deficiency downregulates expression of GA biosynthesis genes, such as *GA3ox1* and *GA20ox1*, but concomitantly induces expression of the GA deactivation gene *GA2ox2* (Jiang et al., 2007). As a consequence, the resulting decreased bioactive GA levels in phosphate-starved plants allows the accumulation of DELLA proteins, for example RGA in roots (Jiang et al., 2007). In the same context, the Arabidopsis mutant *ga1-3* that is deficient of GA is hypersensitive to phosphate deficiency, developing a much shorter primary root, which can be rescued by exogenous application of GA. Conversely, plants with mutations in DELLA proteins, like *gai-t6 rga-t2 rgl1-1 rgl2-1*, are much more resistant to phosphate starvation (Jiang et al., 2007). Therefore, an appropriate level of bioactive GA is necessary for plants to maintain root growth under phosphate limitation. Interestingly, this study also showed that low phosphate-induced lateral root branching is independent of GA signaling, suggesting plants also modulate root system architecture via GA-independent signaling pathways.

A role for brassinosteroids (BRs) in regulating the developmental shift from deep to shallow root system formation in response to phosphate deficiency has emerged

recently by showing that an appropriate level of bioactive BRs is crucial for root growth in response to phosphate deficiency (Singh et al., 2014). Exogenous application of BR partially rescued root growth under low phosphate supply, whereas decreasing the endogenous BR level through application of the BR biosynthesis inhibitor brassinazole further decreased root elongation. In fact, the endogenous BR level is of crucial importance to switch on or off BR signaling by modulating nucleocytoplasmic shuttling of the transcription factors BZR1 and BES1 (Ryu et al., 2007). Consistent with this notion, phosphate deprivation reduces the expression levels of BR biosynthesis genes and the levels of bioactive BRs, which in turn promotes the cytoplasmic retention of BZR1/BES1 (Singh et al., 2014). More recently, it has been shown that BZR1 is able to bind to *LPR1* and transcriptionally repress its expression, thereby alleviating root growth repression by low phosphate (Singh et al., 2018).

Sulfur is another important macronutrient for plant growth, and plants take up sulfur from the soil in the form of sulfate. Whereas sulfate deprivation stimulates primary root elongation by increasing cell division and elongation (Dan et al., 2007; Gruber et al., 2013; Zhao et al., 2014), it is still controversial how it affects lateral root development. An early study reported that under sulfate-limiting growth conditions, lateral roots are formed closer to the tip resulting in a more branching root system (Kutz et al., 2002). In this context, *NITRILASE3* (*NIT3*), an enzyme that converts indole-3-acetonitrile to indole-3-acetic acid (IAA), is transcriptionally activated upon sulfate deprivation and thus links auxin biosynthesis to sulfate deficiency-induced root branching (Kutz et al., 2002). However, recently it was found that low sulfate decreases lateral root density, which correlates with decreased auxin accumulation and sensitivity (Dan et al., 2007; Gruber et al., 2013). Moreover, sulfate deprivation may affect stem cell niche maintenance by decreasing auxin biosynthesis and altering auxin distribution via PINs (Zhao et al., 2014).

Potassium (K) is the quantitatively most important cation for plant growth and is critically involved in cell expansion and various metabolic processes. Although moderate K deficiency decreases primary root growth, K deprivation additionally decreases lateral root growth, 1st order lateral root density, while increasing 2nd-order lateral root density and root hair elongation (Shin et al., 2007; Jung et al., 2009;

Gruber et al., 2013). Auxin appears to involve in K starvation-regulated lateral root density. Potassium deprivation represses expression of *MYB77* that controls lateral root development through interaction with *ARF7* upon potassium limitation (Shin et al., 2007). Moreover, it has been observed that the mutant *trh1* lacking proper potassium transport activity displays agravitropic root growth and impaired root hair formation most likely due to altered auxin transport or perception, since exogenous auxin supply can rescue *trh1* phenotypes (Vicente-Agullo et al., 2004). Potassium deficiency-induced inhibition of primary root growth and stimulation of root hair growth involves a regulatory role of ethylene (Jung et al., 2009). It has been reported that K deficiency induces the expression of a number of genes involved in ethylene biosynthesis, which coincides with increased ethylene production (Shin & Schachtman, 2004). Enhanced production of ethylene has a dual effect on root system architecture. On the one hand, elevated ethylene production inhibits primary root elongation (Jung et al., 2009). On the other hand, it promotes ROS formation in the root hair differentiation zone, which in turn stimulates root hair elongation and expression of the high-affinity potassium transporter *HAK5* to get plants acclimated to potassium deficiency (Shin & Schachtman, 2004; Jung et al., 2009). Ethylene inhibits root elongation through modulating auxin biosynthesis and basipetal transport towards elongation zone (Ruzicka et al., 2007; Swarup et al., 2007). Currently, it is intriguing whether auxin is acting downstream of ethylene in modifying root growth upon K starvation.

Root system architecture also responds to iron availability. Mild iron deficiency slightly but significantly increases the elongation of primary and lateral roots, whereas iron deprivation causes strong reduction of root elongation as well as lateral root density (Gruber et al., 2013; Leskova et al., 2017). Iron concentration and spatial availability have different impacts on hormone responses. Local high iron supply promotes lateral root elongation via upregulating *AUX1*-dependent rootward auxin movement, whereas homogenous iron deficiency modulates root elongation through brassinosteroids and gibberellin signaling, depending on the concentrations of iron supplied (Giehl et al., 2012; Wild et al., 2016; von Wirén & Bennett, 2016; Singh et al., 2018). When exposed to mild iron deficiency, root elongation is accelerated by enhancing meristem size and cell size, presumably through reduced stiffness of the

cell wall (Singh et al., 2018). Low iron accelerates root elongation by impinging translation efficiency of the BR signaling kinase BKI1, yielding lower level of BKI1 and higher levels of BZR1/BES1 activity and hence enhanced brassinosteroid signaling (Singh et al., 2018). Under severe iron deficiency, root elongation is greatly inhibited involving a role of GA signaling. Gibberellins play dual roles in root adaptation to iron deprivation in a root tissue-specific manner. When exposed to iron deprivation, plants accumulate DELLA proteins in the root meristem due to a decreased synthesis of GAs, which in turn restricts root elongation. At the same time, plants destabilize DELLA proteins in the epidermis of the root differentiation zone to release FIT from interaction with DELLAs and allow activation of the FIT-dependent iron uptake machinery (Wild et al., 2016, von Wirén & Bennett, 2016). Under excess supply of iron, primary root elongation and lateral root initiation are potently inhibited (Li et al., 2015a; Li et al., 2015b). The root apex appears to be the primary site of sensing high iron (Li et al., 2015a). AUX1 and PIN2-dependent auxin transport is indispensable for tolerance of lateral root formation to iron stress (Li et al., 2015a). Furthermore, iron stress stimulates the synthesis of ethylene, which plays a potent role in high iron-induced inhibition of primary root growth (Li et al., 2015b).

Regarding the remaining elements, such as boron, calcium, magnesium, manganese, copper and zinc, root systems also respond to changes in the external availability of these nutrients (Gruber et al., 2013). In general, root elongation is inhibited under either deprivation or excess levels of these elements, particularly of heavy metals (Richard et al., 2011; Jain et al., 2013; Gruber et al., 2013; Yuan et al., 2013; Leskova et al., 2017). Although an inhibitory effect on the primary root has been observed most frequently for several of these elements, it appears that the modulation on primary versus lateral root traits occurs in a nutrient-specific manner. For example, low calcium remarkably represses primary root elongation, whereas it has little impact on lateral root elongation (Gruber et al., 2013). These results suggest genetically uncoupled mechanisms regulating developmental processes in different orders of roots.

2.3.3 Interdependence of nutrient signals in shaping root system architecture

Although previous research has shed light on how roots respond to individual nutrient deficiencies, especially nitrogen and phosphorous, phenotypic changes in root traits depend not only on the supplied amount of the nutrient of interest but also on the supply level of other nutrients. Indeed, this is an expected scenario for plant roots growing in natural heterogeneous soils, where they are exposed to multiple facets of nutrient gradients at the same time. A quantitative approach to analyse such interactions has been made by monitoring root system architectural traits under a combination of nitrogen, phosphate, sulfur, potassium and light conditions. This approach found antagonistic, synergistic, or null effects of combined nutrient deficiencies as compared to single nutrient deficiencies (Kellermeier et al., 2014), suggesting an interdependence of nutrient signaling in shaping root system architecture. In fact, such nutrient interactions have been already manifested by monitoring the impact of iron on low phosphorous-induced primary root inhibition, by the impact of ammonium on the cessation of primary root growth under low potassium, or by the antagonistic effect of nitrate on L-glutamate-mediated inhibition of primary root elongation (Xu et al., 2006; Svistoonoff et al., 2007; Walch-Liu & Forde, 2008; Ward et al., 2008). Signaling mechanisms describing the crosstalk between nutrient signals in root development are just emerging. For instance, it has been shown that nitrate signaling mediated by *NRT1;1* could antagonize the inhibitory effect of L-glutamate on primary root growth (Walch-Liu & Forde, 2008), but the detailed mechanism is still unknown. Recently, the GRAS family transcription factors *HRS1* together with its paralog *HHO1* have been reported to be transcriptionally and post-translationally regulated by nitrate and phosphorous starvation and to coordinate a nitrate-dependent primary root response to phosphate deficiency (Medici et al., 2015). Additionally, brassinosteroid signaling has been demonstrated to coordinate the interdependence of iron and phosphate in primary root elongation (Singh et al., 2018). In this context, low phosphate-triggered iron accumulation in the elongation zone enhanced *BKI1* levels and lowered the activity of *BZR1/BES1*, which suppressed expression of *LPR1* and ultimately impeded primary root elongation (Singh et al., 2018). These examples show how nutrient-dependent signals can be integrated within a common signaling cascade.

2.3 Aim of the thesis

Plant root system architecture responds to a limiting dose of N in a dual manner (Gruber et al., 2013). While regulatory modules and hormones involve in arresting root elongation and branching under severe N deficiency (chapter 2.2.1), little is known about the regulation of RSA responses to mild N deficiency. Mild N deficiency expresses in an elongation of the primary and lateral roots, mediating a systemic foraging response and allowing the overall root system to explore a larger soil volume (Chun et al., 2005; Gruber et al., 2013; Ma et al., 2014; Sun et al., 2014; Melino et al., 2015). This foraging response is of particular interest for N uptake efficiency and thus for more efficient fertilizer use, as it promises to decrease future N fertilization doses by maintaining yield. A presumption to integrate such knowledge in plant breeding builds on knowledge of the molecular mechanisms underlying the N foraging response.

Against this background, this thesis aimed at identifying genetic components that regulate root elongation under low N availability. To achieve this goal, a forward genetics approach, i.e. a genome-wide association study (GWAS) has been conducted in combination with reverse genetics approaches, which allowed the identification of three genes involved in the phytohormonal regulation of root elongation under mild N deficiency. The central part of this thesis is devoted to the identification and characterization of candidate genes and elucidation of the underlying mechanisms. A prerequisite for performing GWAS is the existence of natural variation of the studied traits in a collection of genotyped accession lines. Therefore, this thesis starts with a description of the natural variation of individual root architectural traits and their responses to external N availability. Since root elongation is realized through coordinated processes involving cell division, cell differentiation and cell expansion, microscopic work was performed to probe cellular processes that contribute to N deficiency-induced root elongation. After a comprehensive phenotypic examination of the natural variation in morphological and cellular traits, the present study moves towards genome-wide association mapping of four root length-related traits and the characterization of candidate genes as well as their underlying mechanisms. Finally, the thesis closes with a discussion on the role of the identified genes in phytohormone metabolism and signaling and their relevance for shaping

root plasticity in response to N deficiency. The discussion further highlights the adaptive role of allelic variation in the identified candidate genes to environmental cues.

3. Materials and methods

3.1 Plant materials and growth conditions

Seeds were surface sterilized in 70% (v/v) ethanol and 0.05% (v/v) Triton X-100 and sown on modified half-strength MS medium (Gruber et al., 2013) supplemented with 11.4 mM N (1 mM NH₄NO₃ + 9.4 mM KNO₃), 0.5% (w/v) sucrose, 1% (w/v) Difco agar (Becton Dickinson) and 2.5 mM MES (pH 5.6). Agar plates containing seeds were kept in darkness at 4°C for two days to synchronize germination and then placed vertically in a growth cabinet (Percival Scientific) under a 22°C/19°C and 10h/14h light/dark regime with light intensity adjusted to 120 μmol photons m⁻² s⁻¹. Seven-day-old seedlings of similar sizes were transferred to new plates with identical sucrose, agar and nutrient composition as described above but supplied with either 11.4 mM (HN) or 0.55 mM (LN) N. For the temperature experiment, six-day-old seedlings were transferred to 29°C for 3 days growth, while half of the plants were maintained at 22°C as a control. If not indicated otherwise, plants were cultivated for 9 days on these conditions. The T-DNA knockout lines, SALK_096500C (N666828), SAIL_177_A05 (N862558), SALK_045890C (N659843), SALK_072016C (N671515), SALK_045930C (N657375), SALK_097452C (N673008), SALK_108536C (N653659), SALK_122041C (N658884), SALK_040968C (N662202), SALK_021829C (N682094), SALK_052744C (N678486), SALK_066478C (N698296), SALK_072882C (N675728), SALK_058980C (N678551), *eca2-1* (N666473), *eca2-2* (N662171), SALK_030563C (N674297), *bak1-1* (N6125), *bri1* (N678032), SALK_096110C (*yuc8-1*, N655757), SM_3.23299 (*yuc8-2*, N110939), SALK_077059C (N668516), SAIL_1286_E04C (N867481), GK-376G12 (*yuc3*, N436084), SAIL_116_C01 (*yuc5*, N860386), SALK_059832C (*yuc7*, N659416), SALK_006932 (*dwf1*, N506932), SAIL_882_F07 (*dwf4-44*, N839744), SALK_078291 (*cpd91*, N578291), *wei2-2* (N16398) and R2D2 (N2105637) were ordered from Nottingham Arabidopsis Stock Center (NASCC, Nottingham, United Kingdom). The *cbb1*, *bri1-5*, ProDIM1-GUS, DIM1-RNAi, DIM1 overexpression lines, *bsk3,4*, *bsk3,4,7*, *bsk3,4,8* and *bsk3,4,7,8*, proYUC8-GUS and *yucQ* have been described in previous studies (Schluter et al., 2002; Chung et al., 2011; Hossain et al., 2012; Sreeramulu et al., 2013; Hentrich et al., 2013; Chen et al., 2014). The accessions Col-0, Col-3 (N8846) and Ws-2 were used as corresponding wild types for mutant lines as indicated in the figure legends.

3.2 Root phenotyping, determination of dry mass, shoot N concentration and content

For root phenotyping, 200 accessions (Supplementary Table 1) were grown on HN and LN agar plates (4 individual plants per plate). The experiment was repeated three times so that a total of 12 plants were analyzed per accession on either N condition. To assess root system architecture, roots were separated until they were clearly distinguishable from each other on the agar and then scanned using an Epson Expression 10000XL scanner (Seiko Epson) with a resolution of 300 dots per inch. Root length (e.g. primary root length (PRL), length of the branching zone and total lateral root length (TLR) were quantified by WinRhizo Pro version 2009c (Regent Instruments) and the number of visible lateral roots (LRN) was manually counted. For calculating total lateral root length, only 1st-order lateral root were taken into account. The remaining root traits were calculated based on these measured traits. Total root length (TRL) was calculated by summing up the length of primary root and total lateral root length. The average lateral root length (aLR) was calculated by dividing the total lateral root length by the number of lateral roots. The lateral root density (LRD) was calculated by dividing the number of lateral roots by the length of the branching zone.

After scanning the root, shoot and root were separated and then subjected to freeze-drying for one week. Then, root and shoot dry mass were recorded to calculate root-to-shoot ratio (R/S). For the N analysis, freeze-dried shoot samples were ground using a ball mill, and ~1 mg of ground material was taken for analysis using an elemental analyzer (Euro-EA, HEKAtech, Wegberg, Germany). Shoot N concentration was then multiplied with shoot dry mass to calculate shoot N content used as a proxy for total N uptake.

3.3 Chemical treatments

Treatments with IAA, PPBO, BL or BRZ were performed by transferring seven-day-old seedlings to 1/2 MS medium supplemented with indicated concentrations of indole-3-acetic acid (IAA; I0901, Duchefa Biochemie), 4-Phenoxyphenylboronic acid (PPBo; CAS 51067-38-0, Sigma), 24-epibrassinolide (BL; CAS 78821-43-9, Sigma) or brassinazole (BRZ; CAS 280129-83-19, Sigma) were dissolved in pure ethanol or DMSO. Mock treatment was performed identically to the chemical treatment with the same amount of solvent.

3.4 GWA mapping and sequence mining

Average values of root traits from 12 plants were calculated for 200 accessions and used as phenotypic traits in GWAS. GWA mapping was performed using a mixed linear model algorithm implemented in the EMMA (Efficient Mixed-Model Association) package, as described by Kang et al. (2008), and vGWAS (variance-heterogeneity GWAS) package as described by (Shen et al., 2012) using ~250k SNP markers (Atwell et al., 2010; Horton et al., 2012). Only SNPs with minor allele frequency greater or equal to 10% were taken into account. The significant threshold was determined at a Benjamini and Hochberg false-discovery rate level of $q < 0.05$ (i.e. for the *YUC8* and *BSK3* locus) for correcting multiple testing or using an arbitrary cut-off $-\log_{10}P\text{-value} > 5$ (i.e. for the *DWF1* locus). The *BSK3* and *YUC8* protein haplogroups were analyzed using 139 genome re-sequenced accessions that were phenotyped in the current experiment. Coding sequence and predicted amino acid sequence were downloaded from the 1001 genome data center (<http://signal.salk.edu/atg1001/3.0/gebrowser.php>). Sequences were aligned with ClustalW2.1 (<http://bar.utoronto.ca>). Only polymorphisms with a minor allele frequency (MAF) $> 5\%$ were taken into account.

3.5 Cloning and plant transformation

For complementation of *BSK3*, *BSK3* promoter (1292bp) and open reading frame (2287 bp) fragments were amplified from genomic DNA of Col-0 using the primers listed in Supplementary Table 9. The amplified fragments were cloned into GreenGate entry modules (pGGA000 for promoter and pGGC000 for open reading frame) and assembled in a pGREEN-IIS-based binary vector following the instructions of (Lampropoulos et al., 2013). For allelic swapping, the promoter region of *BSK3* was amplified from genomic DNA of accessions Col-0 or Cvi-0 and the open reading frames carrying the L or P allele from Col-0 or Co, respectively. In the case of *YUC8*, the promoter region from genomic DNA of accessions Col-0, Co or Uod-1 and the open reading frames carrying the L or S allele from Col-0 or Co were amplified. All the fragments were cloned separately in GreenGate entry modules and assembled as described above. The *Agrobacterium tumefaciens* strain GV3101 containing the helper plasmid pSOUP was used to transform plants through the floral dip method (Clough & Bent, 1998). Positive transformants were selected on agar plates supplemented with either 40 mg/L kanamycin or hygromycin.

3.6 Histological and microscopic analysis

Tissue-specific localization of *BSK3*, *YUC8* and *DWF1* expression was investigated by histological staining of GUS activity in transgenic plants. In the case of *BSK3*, the GUS-dependent staining pattern was consistent in 12 independent lines. Thus, one representative line was used for detailed analysis. For the analysis of *YUC8* and *DWF1*, previously generated lines were used (Hossain et al., 2012; Hentrich et al., 2013). Root samples were stained in 20 mg ml⁻¹ (w/v) 5-bromo-4 chloro-3-indolyl-β-D-glucuronic acid (X-gluc), 100 mM NaPO₄, 0.5 mM K₃Fe(CN)₆, 0.5 mM K₄Fe(CN)₆ and 0.1% (v/v) Triton X-100 and incubated at 37°C for 30-60 min in the dark.

Samples were mounted in clearing solution (chloral hydrate:water:glycerol = 8:3:1) for 3 min and imaged using DIC optics on a light microscope (Axio Imager 2, Zeiss). For root meristem size and cortical cell length measurements, roots were stained with propidium iodide and imaged with a laser-scanning confocal microscope (LSM 780, Zeiss) using 561 nm and 650-710 nm as excitation and emission wavelengths, respectively. For *BSK3* protein localization, GFP was excited with a 488 nm Argon laser and emission detected between 505 nm and 530 nm. Quantifications were performed with ZEN software (Zeiss).

3.7 Quantitative real-time PCR

Root tissues were collected by excision and immediately frozen in liquid N. Total RNA was extracted with RNeasy Plant Mini Kit (QIAGEN GmbH, Hiden, Germany). qRT-PCR reactions were conducted with the CFX38TM Real-Time System and the SsoAdvancedTM Universal SYBR Green Supermix (Bio-Rad Laboratories) using the primers listed in Supplementary Table 9. Relative expression for all genes was normalized to internal reference *AtACT2* and *AtUBQ10*. Relative expression was calculated according to (Pfaffl, 2001).

3.8 Climate data

A subset of climate variables gathered by (Hancock et al., 2011) was prioritized in the present study. Raw data of 19 climate variables and latitude as well as longitude were downloaded for 115 accessions (Supplementary Table 8) from WorldClim Project (www.Worldclim.org).

3.9 Statistical analysis

For correlation analysis, the R function “cor.test” was used. Hierarchical-clustering was performed with “hclust” and visualized with “gplots” package. Root traits from several genotypes were compared by one-way ANOVA followed by post-hoc Tukey test at $P < 0.05$. Pairwise comparisons were carried out by Welch's t -test. Pearson correlation was used to test associations between climate variables and primary root length in the study of *BSK3*. In the case of *YUC8*, partial Mantel tests were conducted using the “Ecodist” package in R to calculate the Spearman correlation between a given SNP and climate variables while correcting the population structure with a kinship matrix as described by Hancock et al., (2011). The dependent variable in the model was either a distance matrix of the phenotype (Supplemental Table 6) or a distance matrix of genetic variant (Supplemental Table 7). To compare the difference between *BSK3* and *YUC8* variants, the trait value for each transgenic line was averaged and the difference among means of each construct was compared. For this purpose, the degree of freedom reflected the exact number of independent transgenic lines used for each variant in the experiment. All statistical analyses were performed in R.

4 Results

4.1 Natural variation of *Arabidopsis* root system architectural traits and biomass under two nitrogen conditions

Previously it has been shown that severe N limitation strongly inhibits root growth, while external N supply levels that induce mild deficiency stimulate the elongation of the primary root and lateral roots (Gruber et al., 2013). This stimulatory response is of particular interest as it reflects a foraging strategy, for which the underlying molecular mechanism still remains unknown. In order to identify genetic components that modulate root growth under mild nitrogen deficiency by using GWAS, the extent of the natural variation of root architectural traits for a diverse panel of 200 *Arabidopsis* accessions reflecting a wide geographic distribution was assessed (Figure 1; Supplemental Table 1). After one week of pre-culture with sufficient N (11.4 mM), plants were transferred to either 11.4 mM N (HN) or 0.55 mM N (LN), a concentration that strongly induces the systemic root foraging response in the accession Col-0 (Gruber et al., 2013). After 9 days on treatments, dry biomass of root and shoot as well as root morphological traits were measured. There was a very broad spectrum of variation of root traits and also their responses to N (Table 1 and Supplemental Table 1). More importantly, these responses were clearly dependent on genotypes as revealed by high broad-sense heritability (h^2) values with an average between 78.8% under HN and 84.8% under LN for all traits, ranging from 68.8% (FBR) to 91.3% (aLR) under HN and 68.5% (FBR) to 91.9% (LR/PR) under LN, respectively (Table 1). Then, two datasets collected from two N environments were pooled and ANOVA was used to estimate the effects of genotype, N treatment and interaction between genotype and N treatment. For all measured traits on average 40.4% of the observed variation could be attributed to genotype, while N treatment accounted on average for 33.1% variation (Figure 2; Supplemental Table 2), which is consistent with lower heritability (40.4% rather than 78.8% or 84.8 for individual N environment). Moreover, on average 5.9% of variation was attributed to genotype and N interaction as revealed by ANOVA (Figure 2). In addition, differential effects on the root traits were observed for genotype and N. Whereas genotype explained most of the variation for PRL, LRN, LRD, FBR, RB and SB, N treatment explained most of the variation for aLR, TLR, TRL, LR/PR as well as R/S, implying differential responses of root traits to N. In agreement with this, when all accessions were taken together, on average, PRL only

slightly increased by 16%, while the aLR increased by 100%, resulting in 70% and 100% increase of the TRL and TLR under LN compared with HN, respectively. By contrast, the LRN remained identical under two N conditions as the opposite responses were observed for different accessions, resulting in a slightly lower LRD under LN due to increased primary root length (Table 1). Overall, the population showed a stimulation (+35%) of root while a decrease (-14%) of shoot dry biomass production, resulting in an increased R/S from 0.31 at HN to 0.47 at LN (Table 1).

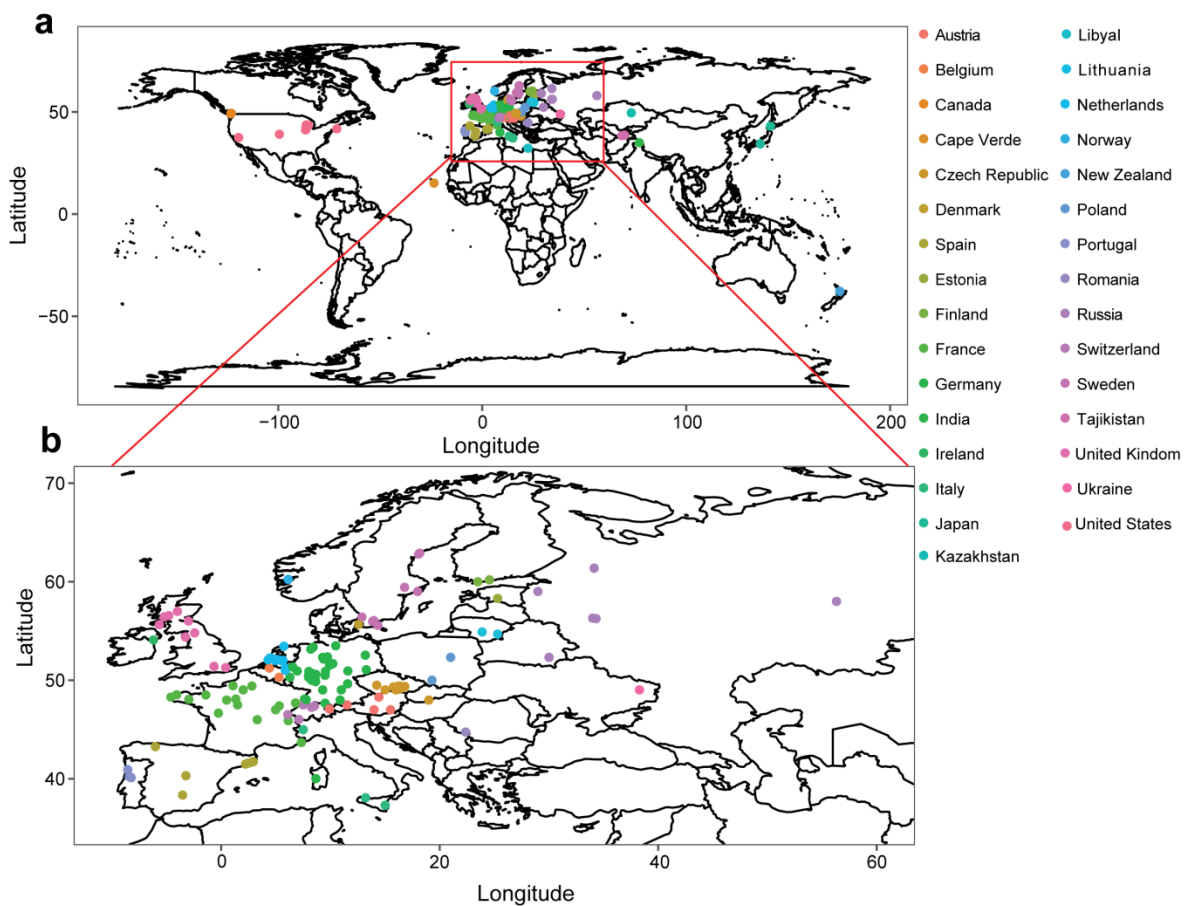


Figure 1. Geographic origin of the 200 accession lines used in the present study. Each dot represents the sampling site of an accession selected for the study. (A) The global map of 200 lines originating from 31 countries. (B) A high-resolution regional map for accessions contained within the area (-10° to 60° E and 35° to 70° N) highlighted by a red frame in (A). Dots represent the sampling site and color indicates the country of origin.

Table 1. Phenotypic description of 11 traits collected in two N environments. PRL, primary root length; aLR, average lateral root length; TRL, total root length; TLR, total lateral root length; FBR, fraction of lateral root branching zone (%); LRN, lateral root number; LRD, lateral root density; LR/PR, lateral root length/primary root length; RDB, root dry biomass; SDB, shoot dry biomass; R/S, root-to-shoot ratio.

Traits	HN				LN				LN/HN		
	Range	Mean	Ratio	$h^2(\%)$	Range	Mean	Ratio	$h^2(\%)$	Range	Mean	Ratio
PRL (cm)	2.95-10.76	8.45	3.6	88.8	3.48-12.52	10.64	3.6	85.7	1.03-1.42	1.17	1.38
TLR (cm)	4.99-29.79	14.38	6	89.0	12.73-57.86	33.22	4.5	89.4	1.75-3.58	2.08	2.05
TRL (cm)	9.72-39.85	22.81	4.1	88.8	16.21-69.53	43.65	4.3	88.5	1.45-2.43	1.72	1.67
LR/PR ($\text{cm}\cdot\text{cm}^{-1}$)	0.72-3.26	1.69	4.5	89.9	1.35-5.07	3.36	3.8	91.9	1.69-2.68	1.76	1.57
aLR(cm)	0.20-0.8	0.46	4	91.3	0.43-1.48	0.98	3.4	89.9	1.23-2.89	2.00	2.35
LRN	14.75-43.75	31.3	3	83.3	17.67-46.17	35.73	2.6	83.1	0.72-1.46	1.03	2.02
LRD (cm^{-1})	3.42-9.23	5.73	2.7	89.8	3.09-8.94	5.62	2.9	90.2	0.79-1.21	0.92	1.52
FBR (%)	0.58-0.76	0.66	1.3	68.8	0.56-0.74	0.65	1.3	68.5	0.88-1.09	0.96	1.24
RDB ($\mu\text{g}\cdot\text{plant}^{-1}$)	103.3-362.5	222.7	3.5	84.7	143.3-533.8	299.9	3.7	83.4	1.24-2.01	1.36	1.62
SDB ($\mu\text{g}\cdot\text{plant}^{-1}$)	324.2-1142.0	728.6	3.5	83.6	362.5-904.2	627.2	2.5	79.2	0.77-1.12	0.87	1.45
R/S	0.19-0.49	0.31	2.6	80.0	0.23-0.73	0.47	3.2	87.1	1.57-2.03	1.53	1.29

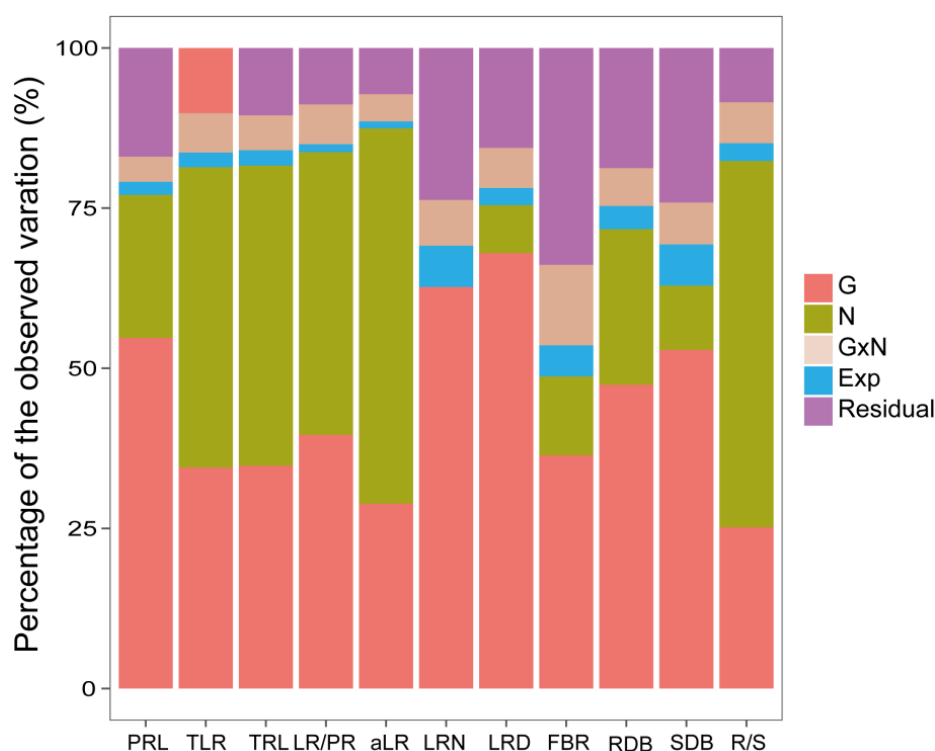


Figure 2. Variation in root and biomass parameters explained by genotype, N treatment and their interactions. Bars show the relative contribution to the variance as obtained by two-way ANOVA. Individually assessed root and biomass parameters are indicated on the x-axis. Variation is expressed as percentage of the total variation measured for each individual trait. G, genotype; N, nitrogen treatment; GxN; genotype x N interaction; Exp, experiment effect. Given traits were collected from 3 independent experiments, and ‘experiment’ was also considered as a factor in ANOVA.

4.2 Nitrogen independently modulates root system architectural traits

After getting the first-hand comprehensive atlas of root traits and their responsiveness to N, it was assessed how accessions respond to changing N

environments and what is the level of correlation or independence of root traits in different N environments. If responses of individual root traits to N environments are correlated, accessions should exhibit similar changes of a suite of traits in a distinct environment. Alternatively, if the trait responses are independent, it would be expected that genotypes with similar root traits in one N treatment should alter most root traits in a different N treatment. To address this, a hierarchical clustering of 11 traits collected from the two N conditions was performed. Different clusters grouping accessions with similar trait behavior under the respective N environment were identified (Figure 3A and B). Moreover, there was a dramatic rearrangement of accessions among clusters under the two distinct N conditions, as shown by dispersal of accessions within clusters formed under HN when they were projected to LN (Fig. 3A and B). Hence, these results clearly suggest a large degree of independence of root trait changes under LN.

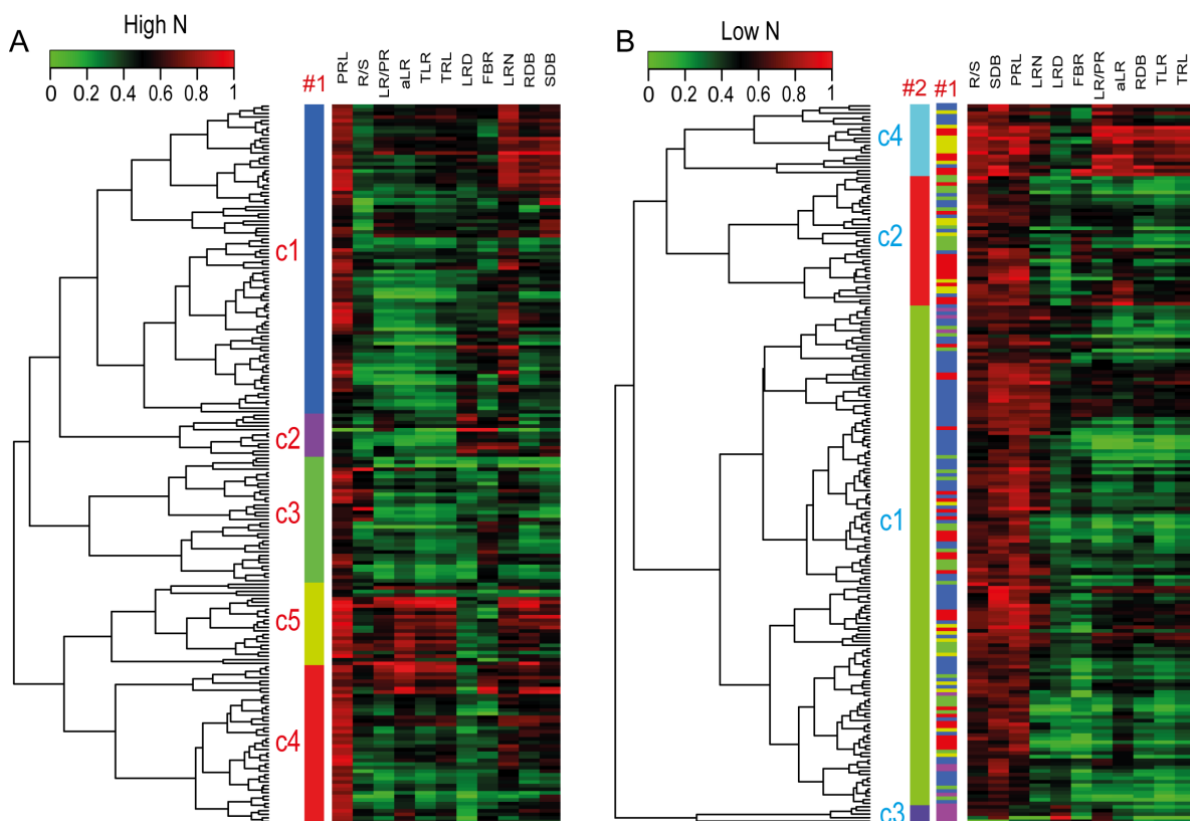
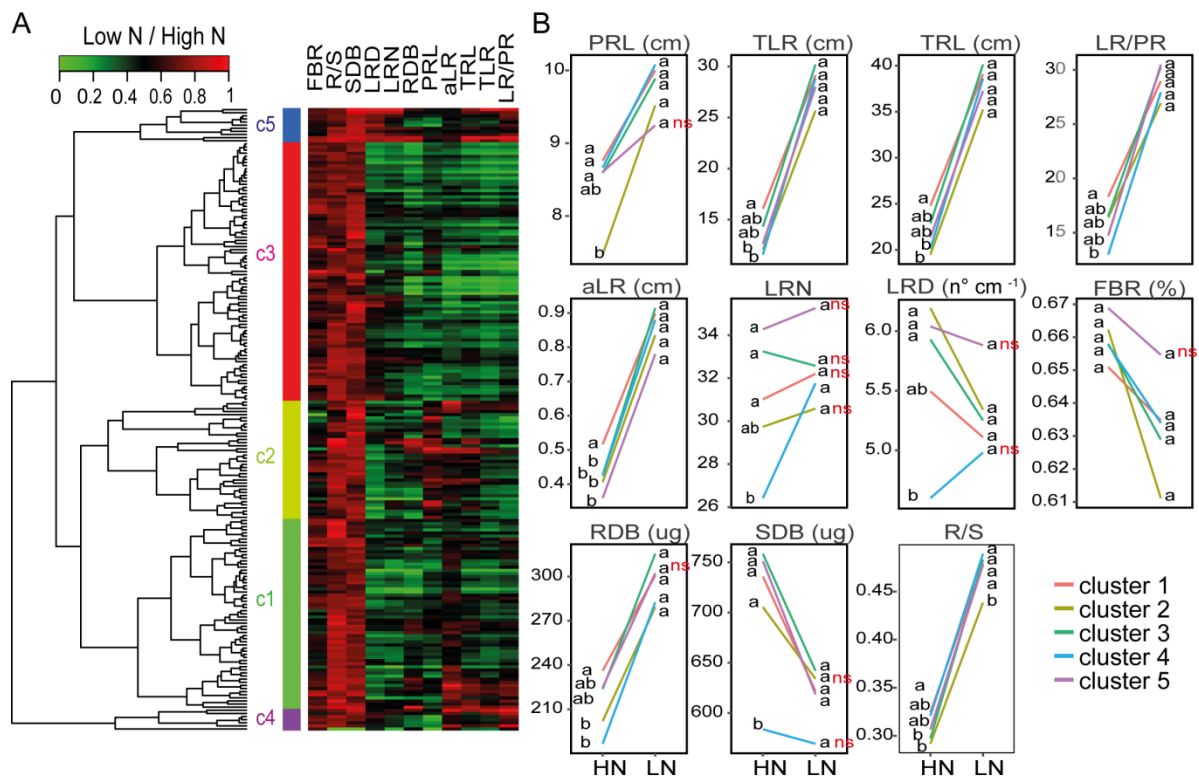


Figure 3. Clustering of 200 accessions grown on high or low N supply based on root traits and shoot dry biomass. (A) Clustering based on traits from high N (HN) yields 5 clusters (#1) as indicated by vertical bars next to the dendrogram; (B) Clustering based on traits from low N (LN) yields 4 clusters (#2). Bar #1 in the LN analysis represents the re-arrangement of clusters following the same color code as under HN. PRL, primary root length; aLR, average lateral root length; TRL, total root length; TLR, total lateral root length; FBR, fraction of the lateral root branching zone (%); LRN, lateral root number; LRD, lateral root density; LR/PR, lateral root length/ primary root length; RDB, root dry biomass; SDB, shoot dry biomass.

4.3 Low nitrogen-dependent root responses overcome inherent developmental differences

A further cluster analysis was carried out using the ratio of all the traits under LN versus HN to express variation in the responsiveness of the lines to the N treatment. 5 distinct clusters were identified (Figure 4A). The trait performance of each cluster of accessions was further analyzed, and trait responsiveness was expressed by reaction norms. In general, the independence of trait responsiveness to LN and cluster-specific responses were observed (Figure 4B). Whereas accessions in cluster 5 showed a sharp increase for lateral root-related traits (TLR, TRL, LR/PR and aLR), they were nearly unresponsive to LN for PRL, LRN, LRD, FBR, RDB and SDB, indicating that different accessions adopt different strategies to cope with LN. In cluster 4, the accessions displayed an increase of LRN under LN as opposed to those 4 remaining groups, whose LRN was not responsive to LN. Moreover, LN treatment shifted PRL, FBR and LRD of cluster 2 to a larger extent compared with others, while this difference appeared to be independent of the shoot response, because SDB in cluster 2 was even less responsive to LN than in the other clusters. Interestingly, whereas under HN there were significant differences among different clusters for root and shoot biomass traits, these differences disappeared under LN except for R/S, implying that a distinct responsiveness of accessions to LN could overcome inherent developmental differences.

Figure 4. Response of root traits to different N treatments in clustered accession lines. (A) Clustering of the ratios of root traits (including shoot dry biomass) from low versus high N (LN/HN) in 200 accession lines reveals 5 clusters indicated in different colors. **(B)** Reaction norms for root traits under HN and LN conditions in different clusters. Different letters indicate significant differences at $P < 0.05$ by Tukey's test among group means after one-way ANOVA within individual N treatments. Welch's t test was used to compare performance of each cluster between two N environments; only clusters showing no significant difference between two N environments were labeled with ns, not significant. If not indicated otherwise, there is a significant difference between the two N environments ($P < 0.05$).



→ Descriptions were shown on previous page.

4.4 Root response to low nitrogen positively correlates with shoot nitrogen content

Low N stimulates root growth, and in general a more exploratory root system is believed to be beneficial for plants as it may more efficiently capture resources. To address whether low N-stimulated root growth confers an advantage to plants growing under LN, N concentrations and content in the shoots were determined. On average, N concentration at LN decreased to 75% of that at HN ($60.3 \mu\text{g}\cdot\text{mg}^{-1}$ vs $80.2 \mu\text{g}\cdot\text{mg}^{-1}$; Figure 5A). Shoot N content was then calculated by multiplying shoot N concentration with shoot dry biomass and used as a proxy for total N uptake. Shoot N content ranged from $24.0 \mu\text{g}$ to $92.3 \mu\text{g}$ for HN and from $21.9 \mu\text{g}$ to $57.1 \mu\text{g}$ for LN, respectively (Figure 5B). To test whether a more extensive root system is beneficial for plant growth under low N condition, correlation analyses were carried out for the response of total root length (i.e. ratio of TRL under LN and HN) and shoot N content at HN or LN. Whereas in the HN treatment there was no significant correlation between the response of total root length and shoot N content, a significant and positive correlation was observed under LN, supporting the view that root plasticity increases N uptake and helps plants to better adapt to low N.

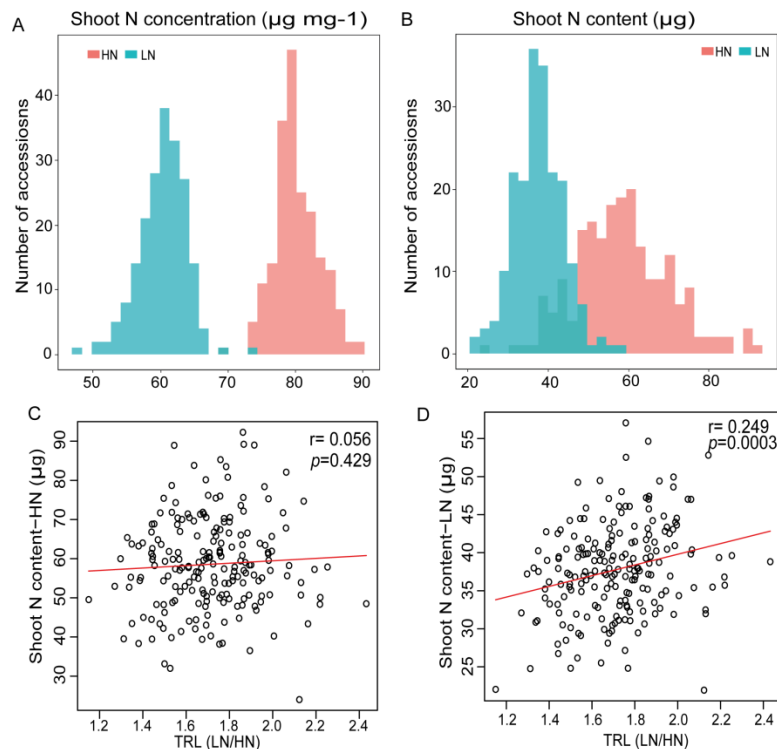


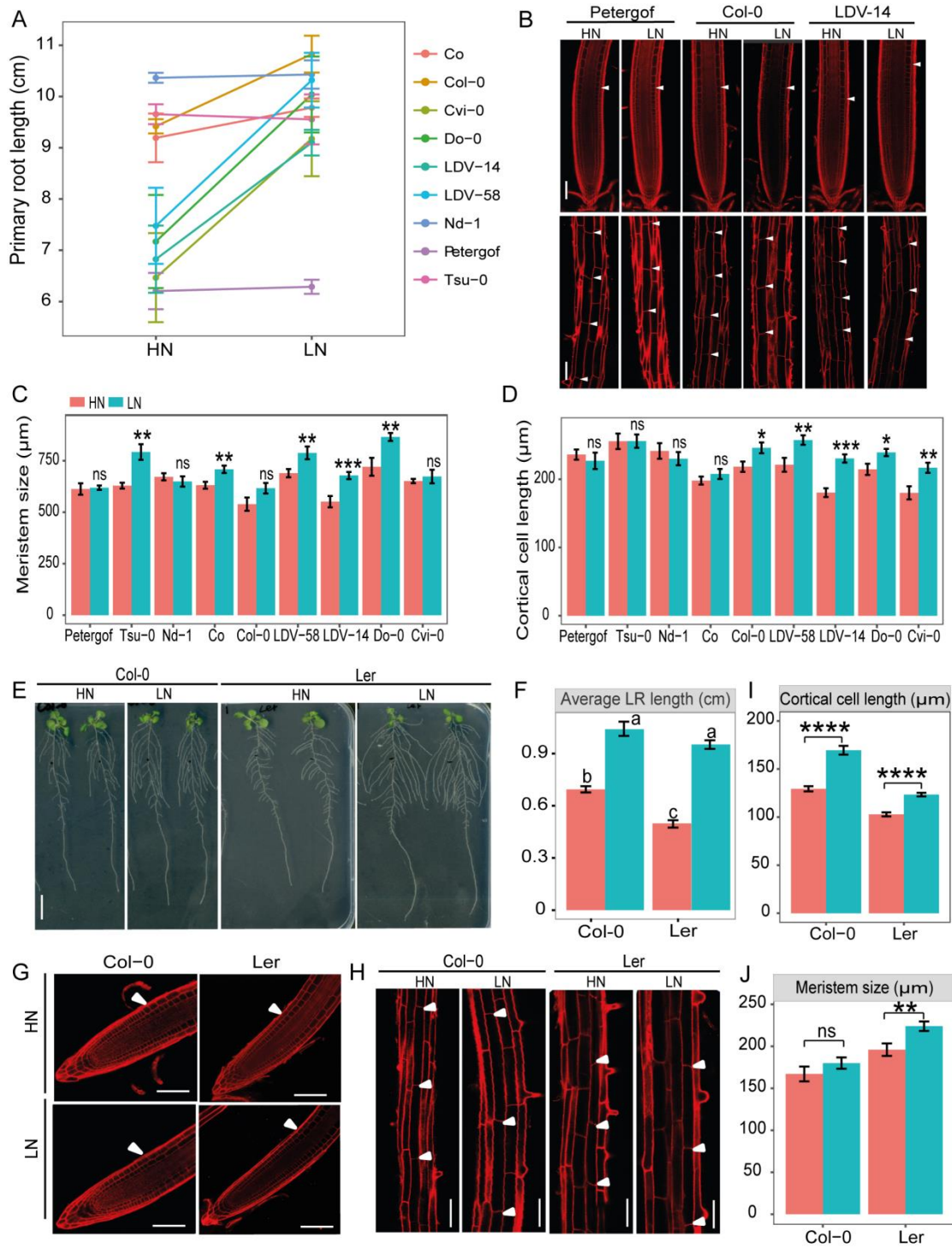
Figure 5. Phenotypic variation of shoot N concentration or content and correlation of shoot N content with the response of total root length to low N. (A-B) Distribution of shoot N concentration (A) and shoot N content (B) as measured in 200 accessions grown under HN or LN conditions. (C-D) Correlations between the response of total root length to low N (ratio of LN to HN) and the shoot N content at HN (C) or LN (D).

4.5 Low nitrogen promotes root elongation by stimulating cell elongation and cell division

Longitudinal root growth is a consequence of cell division, differentiation and elongation (Beemster & Baskin, 1998). To probe which cellular process contributes to the root elongation under LN, the meristem size as well as cortical cell length was measured in accessions exhibiting differential responses to LN. In case of the primary root, meristem size as well as cortical cell length were measured in accessions, in which the primary root exhibited weak (Ptergof, Tsu-0 and Nd-1), intermediate (Co and Col-0) or strong (LDV-14, LDV-58, Do-0 and Cvi-0) responses to LN (Figure 6A). Whereas under N deficiency all strong responders (LDV-14, LDV-58, Do-0 and Cvi-0) as well as one intermediate responder (Col-0) showed longer cortical cells than under HN, the meristem length was differentially affected in the different lines, irrespective of whether they showed a weak, intermediate or strong response to mild N deficiency (Figure 6B-D).

Similar results were also obtained for lateral roots. Two natural accessions, Col-0 and Ler, differed significantly in their response to LN. Although lateral root length of Ler was significantly shorter than that of Col-0 at HN, Ler was able to grow as long as Col-0 at LN, resulting in a stronger foraging response compared to Col-0 (92% vs 50% respectively; Figure 6E and F). Furthermore, LN significantly increased cortical cell length by 31% and 21% in Col-0 and Ler, respectively (Figure 6H and I). Root meristem size of elongated lateral roots was significantly increased by LN only in Ler, but not in Col-0 plants (Figure 6G and J). Altogether, these results suggest that LN promotes elongation of both primary and lateral root by increasing both, cell elongation and cell division, while the contribution of these two responses depends on the genotype.

Figure 6. Characterization of cellular root traits under high (HN) and low N (LN) supply in contrasting natural accessions. (A) Reaction norms of primary root response to LN for nine contrasting accessions. (B) Representative confocal images of root meristem (upper panel) and length of cortical cells (bottom panel) of three natural accessions grown under HN or LN. White arrowheads indicate the boundaries of the meristematic zone and elongation zone (upper panel) or two consecutive cortical cells (bottom panel). Scale bars, 50 μ m. (C-D) Meristem size (C) and length of cortical cells (D) of 9 natural accessions differing in their response to low N. Bars represent means \pm s.e. (n = 9-13 plants). (E) Appearance of Col-0 and Ler plants grown under HN and LN. (F) Average length of lateral roots for Col-0 and Ler grown under HN and LN. Different letters indicate significant differences at $P < 0.05$ according to one-way ANOVA and post-hoc Tukey test. Scale bar, 1 cm. (G-H) Representative confocal images of root meristem (G) and length of cortical cells (H) for lateral roots grown under HN or LN. White arrows indicate the boundary of meristematic zone and elongation zone (upper panel) or two consecutive cortical cells (bottom panel). Scale bars, 50 μ m. (I-J) Meristem size (I) and length of cortical cells (J) of lateral roots for Col-0 and Ler. Bars represent means \pm s.e. (n = 15). Asterisks indicate statistically significant differences between two N conditions within each genotype according to Welch's t test (* $P < 0.05$; ** $P < 0.01$; *** $P < 0.001$, **** $P < 0.0001$; ns, not significant).



→ Descriptions were shown on previous page.

4.6 Identification and characterization of BSK3 and its role in the primary root response to low nitrogen

4.6.1 GWAS maps primary root length variation under low N to BSK3

A diverse panel of 200 accessions of *A. thaliana* reflecting a wide geographic distribution (Fig. 1) was assessed for primary root length at sufficient N (11.4 mM, HN) or low N (0.55 mM, LN), a concentration that strongly induces the systemic root foraging response in the accession Col-0 (Gruber et al., 2013). After 9 days on treatments the primary root length of all accessions were measured. The primary root length showed a high degree of natural variation ranging from 3 cm to 10.8 cm at HN and from 3.5 cm to 12.5 cm at LN (Figure 7A; Supplementary Table 1). On average, primary roots of all examined accessions were 16% longer at LN than at HN ($P < 2.2e-16$; Figure 7A). The broad-sense heritability (h^2) for primary root length was estimated to 88.8% and 85.7% for HN and LN, respectively (Table 1).

To uncover genetic loci associated with the variation of primary root length in each N environment, GWA analysis using a mixed model that corrects for population structure was performed (Kang et al., 2008). At LN, the most significant locus associated with primary root length was detected on chromosome 4 with 7 SNPs above a threshold of 5% false discovery rate (FDR) and the the most significantly associated SNP explaining 11.7% of the phenotypic variation was located at position 386,519 (Figure 7B). Next, a confidence interval was estimated by computing the linkage disequilibrium (LD) with surrounding markers ($r^2 > 0.7$) starting from 292979 to 398078, a region that encompasses 31 genes (Supplemental Table 3). To identify the causal gene underlying this locus, T-DNA insertion lines were ordered for root phenotyping. However, for 15 genes no T-DNA insertion lines were available, so that primary root length in T-DNA insertion lines could be examined for 16 genes. Although the top SNP was located in the gene *AtECA2* (AT4G00900), phenotypic analysis of primary root length in two independent T-DNA insertion lines did not reveal any phenotype at either N condition (Figure 7C). An insertion mutant in the gene encoding for the GSK3/Shaggy-like kinase *ASKTHETA* (*ASKΘ*; AT4G00720) had shorter primary roots than its respective wild type, but this phenotype was independent of the N treatment (Figure 7D). Interestingly, an insertion mutant of *BSK3* (AT4G00710) specifically showed a shorter primary root at LN, although exhibiting primary root length similar to wild type at HN (Figure 7E). The primary root

lengths of the remaining insertion lines were indistinguishable from the wild type under either N condition (Figure 7F and G).

To further ascertain the causal gene for the associated locus, the expression of *ASKØ* and *BSK3* in 9 accessions that showed different primary root lengths was assessed. Transcript levels of *ASKØ* and *BSK3* did not correlate significantly with primary root length of the tested accessions in either N environment (Figure 7H and I), suggesting that either these genes are not causal for the identified marker-trait association or that polymorphisms in the coding region rather than expression variation contribute to the observed phenotypic variation. Next, the coding sequences (CDS) of 139 re-sequenced accessions were analyzed for SNPs that could potentially lead to changes in protein sequence. Whereas only one synonymous substitution (C774G) was detected in the CDS of *ASKØ*, two synonymous (G1353A and A1413G) and one non-synonymous (C956T) mutations were found in the CDS of *BSK3* (Figure 7J). This non-synonymous mutation results in a leucine (L) to proline (P) substitution in the predicted kinase domain of the protein. A protein haplotype analysis of *BSK3* showed that accessions with the *BSK3*-L allele had longer primary roots than those accessions carrying the *BSK3*-P allele (Figure 7K), suggesting that *BSK3* rather than *ASKØ* is the causal gene for this locus. In support to this assumption, it was found that the likely functional SNP (i.e., C956T) was in strong LD with the GWA SNP ($r^2 = 0.73$) and G1353A also showed a moderate association ($-\log_{10} P \text{ value} = 4.1$) with primary root length under LN in the 250 k GWA SNP array. Thus, these independent approaches strongly indicated that *BSK3* is the most likely candidate gene for the observed marker-trait association found on chromosome 4 (Figure 7B).

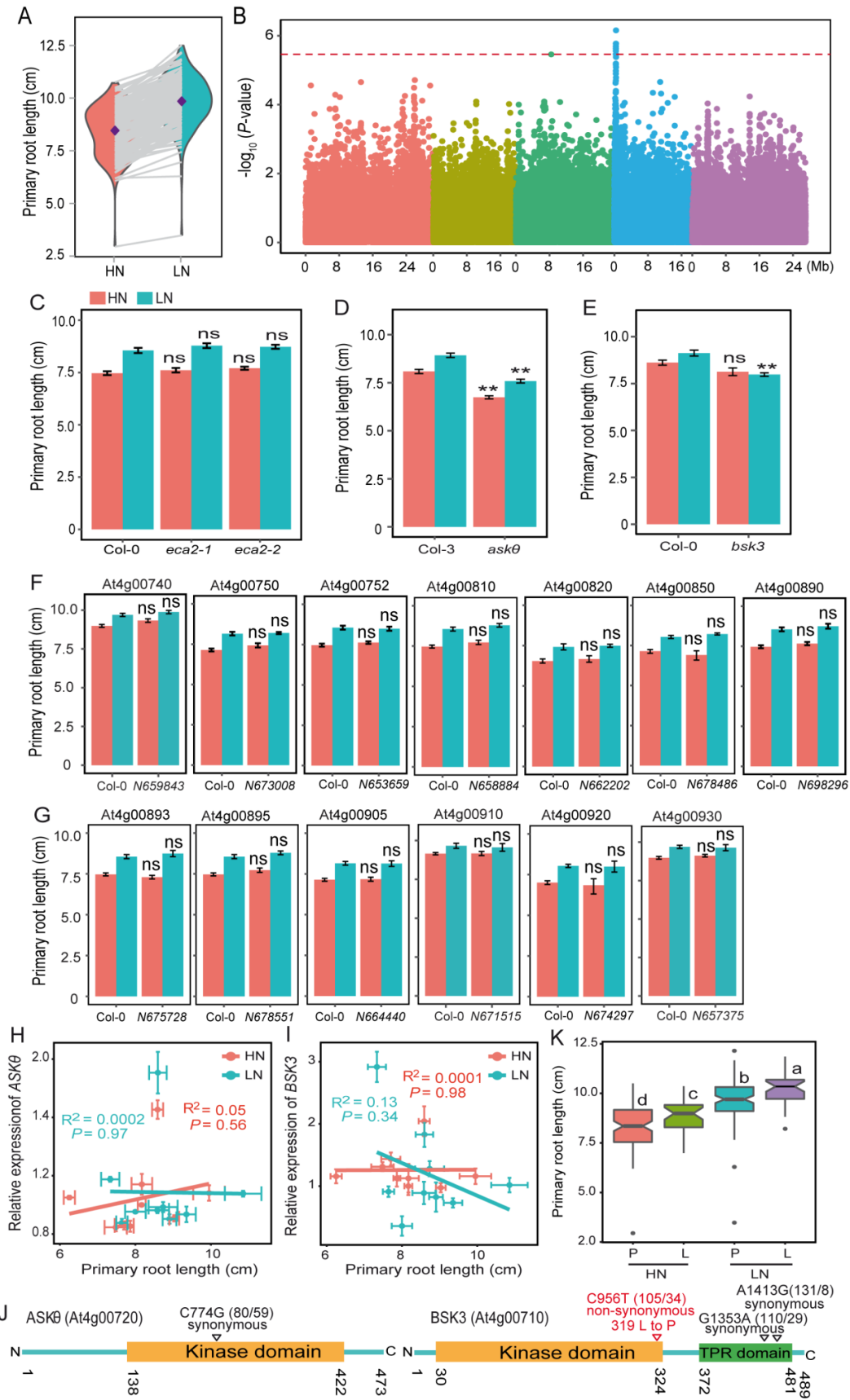


Figure 7. GWAS maps natural variation of primary root length under low N availability to a locus harbouring the *BSK3* gene. (A) Reaction norms and phenotypic variation of primary root

length of 200 natural accessions of *A. thaliana* under different N supplies. **(B)** Manhattan plot for the SNP associations to primary root length under low N performed with EMMA package. Negative \log_{10} -transformed *P* values from a genome-wide association scan were plotted against positions on each of the five chromosomes of *A. thaliana*. Chromosomes are depicted in different colors (I to V, from left to right). The red dashed line corresponds to the Benjamini and Hochberg false-discovery rate level of $q < 0.05$. **(C-G)** Primary root length of T-DNA knockout lines for *ECA2* **(C)**, *ASKθ* **(D)**, *BSK3* **(E)** and the remaining 13 genes **(F-G)**. Bars represent means \pm s.e. ($n = 9 - 10$ plants). Seven-day-old seedlings were pre-cultured on 11.4 mM N and then transferred to solid agar media containing either high N (11.4 mM N) or low N (0.55 mM N). Root system architecture was assessed after 9 days. Asterisks indicate statistically significant differences to wild-type according to Welch's *t* test (** $P < 0.01$; ns, not significant). **(H-I)** Correlation of *ASKθ* **(H)** or *BSK3* **(I)** transcript levels in roots with primary root length at two N conditions. Analysis was carried out in nine natural accessions with contrasting primary root length under HN or LN. **(J)** Schematic representation of *ASKθ* and *BSK3* protein sequences highlighting relevant protein domains. TPR, tetratricopeptide. Identification of SNPs in the coding sequence of *BSK3* and *ASKθ* according to genome sequencing data for 139 accession lines. Location, nucleotide polymorphism and effect at the amino acid level for each identified SNP are indicated. Numbers in brackets denote the number of lines carrying the corresponding allele. **(K)** Primary root length of natural accessions representing two *BSK3* protein haplotypes ($n = 105$ and 34 accessions for P and L haplotypes, respectively). Different letters indicate significant differences at $P < 0.05$ according to one-way ANOVA and post-hoc Tukey test.

4.6.2 *BSK3* and *BSK* homologs modulate root growth under low N

A more detailed analysis of the root system showed that, although unable to stimulate primary root elongation in response to LN, *bsk3* plants had only 13% shorter lateral roots and no differences in lateral root branching compared to wild-type plants at LN (Figure 8A-C and E). Nonetheless, as a consequence of the failed stimulation of primary root elongation and the partial loss of response of lateral roots to mild N deficiency, total root length of *bsk3* plants was only 78% of that of wild-type plants under LN (Figure 8C). Most importantly, the elongation of both primary root and lateral roots in response to LN could be largely rescued by introducing a genomic fragment containing the promoter and coding regions of *BSK3* into the *bsk3* mutant (Figure 8A-D).

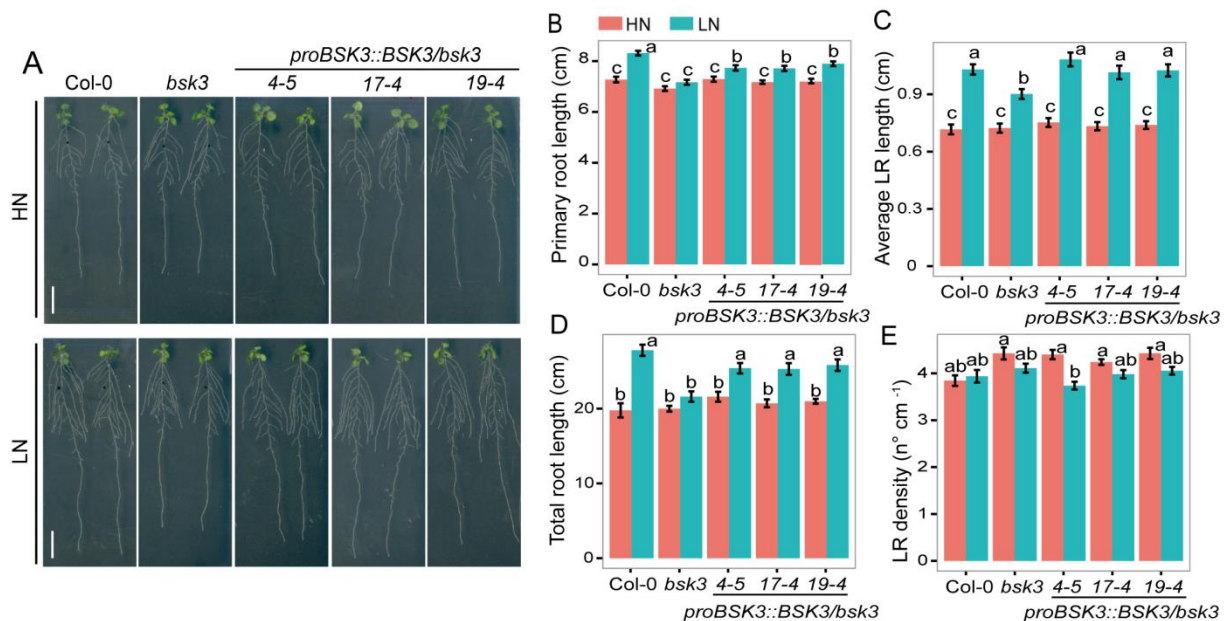
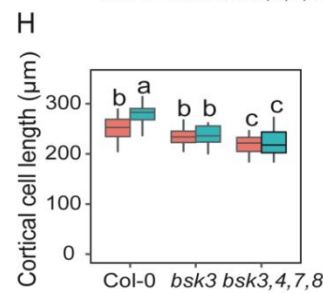
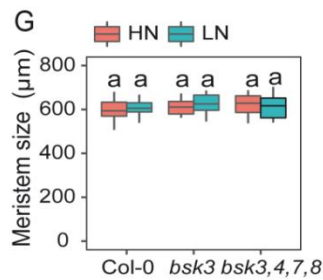
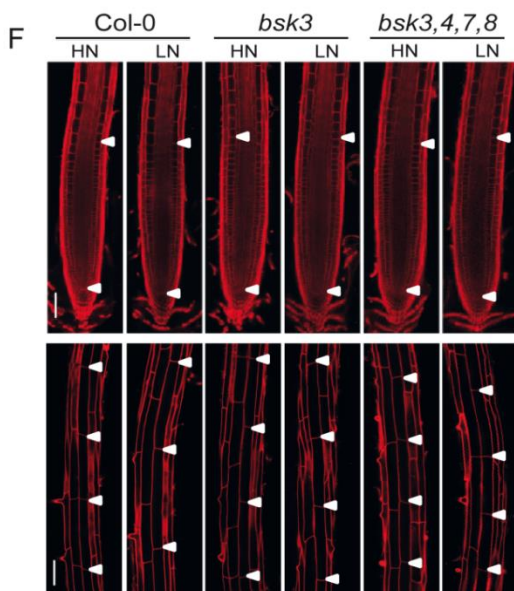
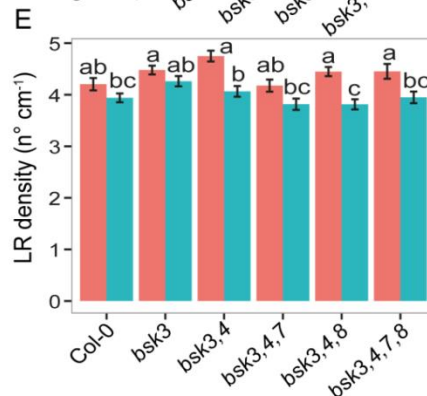
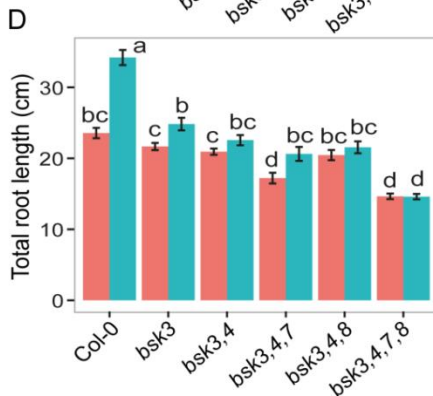
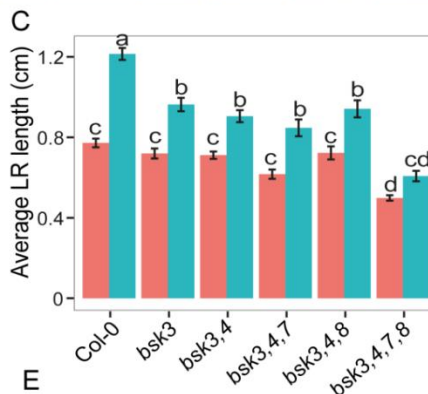
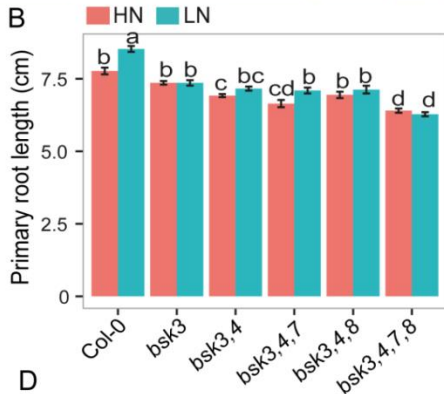
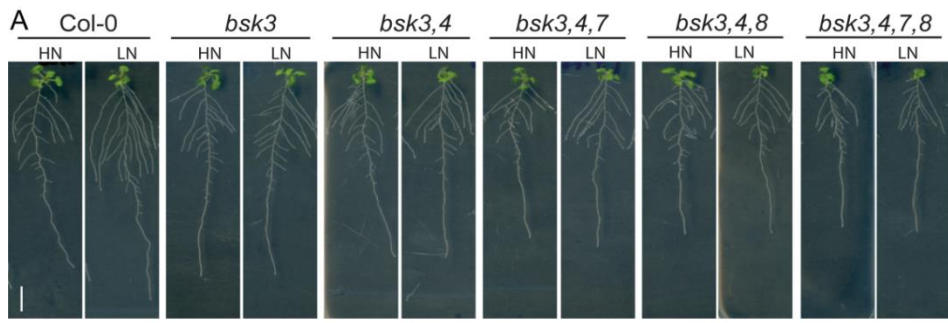


Figure 8. Root architecture of *bsk3* single mutant and recomplemented lines in response to low N availability. (A) Appearance of plants, (B) primary root length, (C) average lateral root length, (D) total root length and (E) lateral root density of wild-type (Col-0), *bsk3* plants and three independent T3 transformants complemented with *BSK3* of Col-0. Seven-day-old seedlings were pre-cultured on 11.4 mM N and then transferred to solid agar media containing either high N (11.4 mM N) or low N (0.55 mM N). Root system architecture was assessed after 9 days. Bars represent means \pm s.e. ($n = 18-22$ plants). Different letters indicate significant differences at $P < 0.05$ according to one-way ANOVA and post-hoc Tukey test. Scale bars, 1 cm.

Previously, it has been reported that *BSK3* functions in the BR signaling cascade and acts redundantly with other *BSK* family members in transducing the BR signal from the plasma membrane to the cytosol (Tang et al., 2008; Sreeramulu et al., 2013; Ren et al., 2019). To further assess the putative role of *BSK*-dependent BR signaling in the modulation of root architectural changes under mild N deficiency, the root system architecture of double, triple and quadruple mutants for *BSK3*, *BSK4*, *BSK7* and *BSK8* was analyzed under the same N treatments. In line with the partially redundant function of these most closely related *BSKs* (Sreeramulu et al., 2013), the *bsk3,4,7,8* quadruple mutant exhibited the strongest decrease in root length as compared to the *bsk3* single mutant, while no or only minor effects were observed for *bsk3,4* double, and *bsk3,4,7* or *bsk3,4,8* triple mutants (Figure 9). Notably, the primary root length response to LN was similarly attenuated in all tested mutants, except for *bsk3,4,7* (Figure 9A and B). The additive effect of all four *BSKs* was particularly relevant for average lateral root length, as *bsk3,4,7,8* plants failed to significantly induce lateral root elongation at LN (Figure 9C). As a consequence, these plants showed no increase in total root length under LN supply (Figure 9D). Compared to Col-0, no

significant changes in lateral root density were observed in the tested mutants (Fig. 9E). Microscopic analysis revealed the attenuated response of the primary root for *bsk3* and *bsk3,4,7,8* to LN was associated with decreased cell elongation (Figure 9F-H), suggesting a pivotal contribution of cell elongation to the LN-induced primary root elongation. Altogether, these results indicate that BSK3 plays a critical role in modulating cell elongation and consequential root elongation in response to LN and that this function is, at least in part, functionally redundant with BSK4, BSK7 and BSK8.

Figure 9. Root architecture of single and multiple *bsk* mutant plants in response to low N. (A) Appearance of plants, **(B)** primary root length, **(C)** average lateral root length, **(D)** total root length and **(E)** lateral root density of wild-type (Col-0) and single or multiple *bsk* mutant plants grown at high N (HN) or low N (LN) conditions. Bars represent means \pm s.e. ($n = 20-25$ plants). Scale bars, 1 cm. **(F)** Representative confocal images of the root apex including the apical meristem (upper panel) and length of cortical cells (bottom panel) of wild-type (Col-0), *bsk3* and *bsk3,4,7,8* grown under HN or LN. White arrowheads indicate the position of quiescent center (QC) and boundaries of meristematic zone and elongation zone (upper panel) and of two consecutive cortical cells (bottom panel). Bars = 100 μ m. **(G-H)** Meristem size **(G)** and cortical cell length **(H)** of wild-type (Col-0), *bsk3* and *bsk3,4,7,8* grown under HN versus low N ($n = 15$ plants). Seven-day-old seedlings were pre-cultured on 11.4 mM N and then transferred to solid agar media containing either high N (11.4 mM N) or low N (0.55 mM N). Root and cellular traits were assessed after 9 days. Different letters indicate significant differences at $P < 0.05$ according to one-way ANOVA and post-hoc Tukey test.

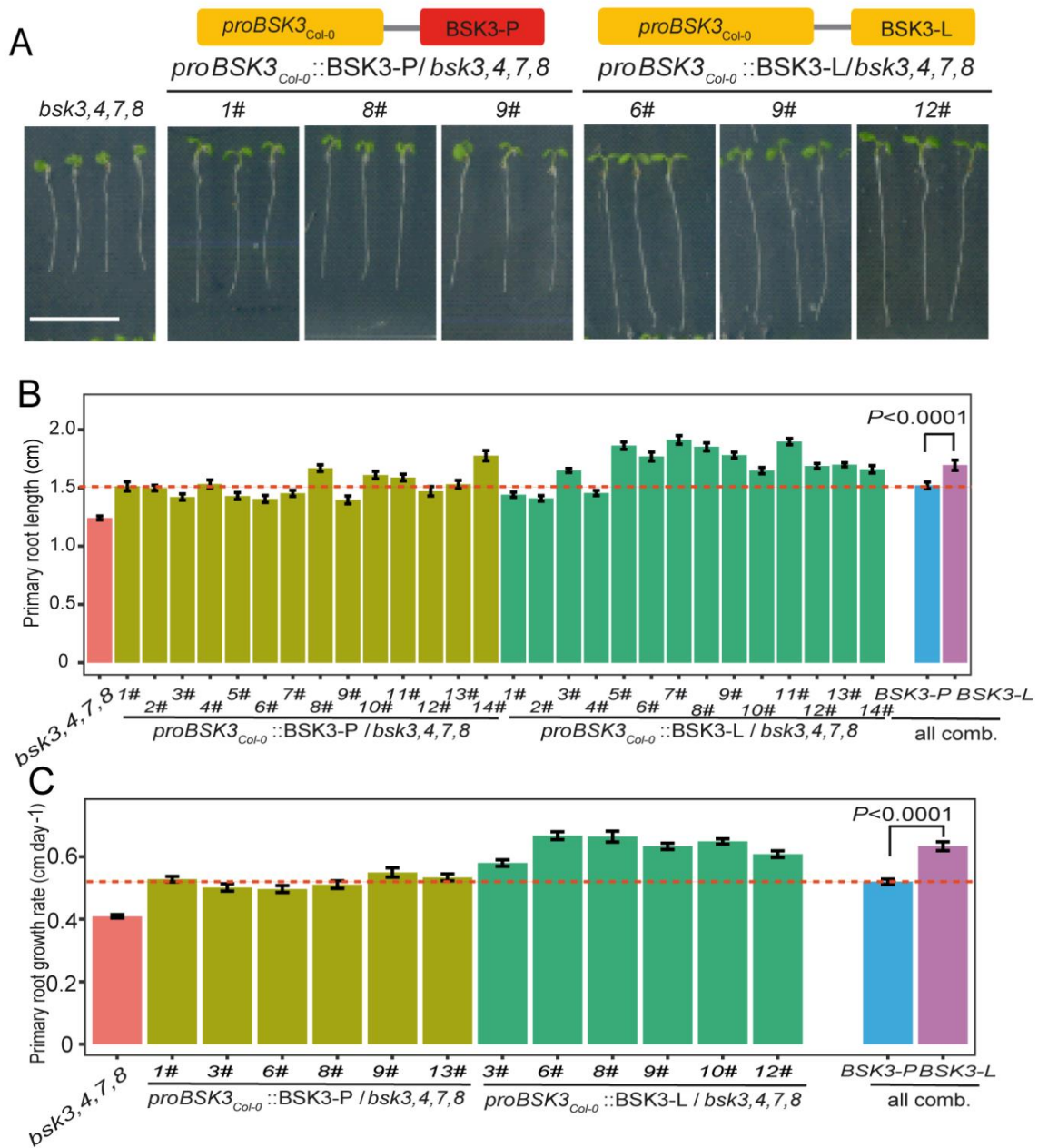


→ Descriptions were shown on previous page.

4.6.3 Allelic variation of *BSK3* determines root growth and BR sensitivity

Although initial data indicated that an L to P substitution at the position 319 in the predicted kinase domain of *BSK3* is causal for the observed natural variation of primary root length under LN (Figure 7K), this evidence remained mainly based on correlations. To test the relevance of this non-synonymous substitution, an allelic swapping approach was used, in which the *bsk3,4,7,8* mutant was transformed with the sequences coding for the P or L substitution to test the capacity of either *BSK3* allele in restoring primary root elongation of the quadruple mutant *bsk3,4,7,8*. Both *BSK3* alleles could recover primary root growth when expressed under the control of the *BSK3_{Col-0}* promoter (Figure 10A and B). However, transgenic lines carrying the *BSK3-L* allele exhibited significantly longer primary roots and faster growth rates than those complemented with the *BSK3-P* allele (Figure 10A-C).

Figure 10. Allelic variation of *BSK3* determines root growth. (A) Schematic of transgenic constructs used for complementation of the *bsk3,4,7,8* quadruple mutant and representative photographs of 6 day-old plants. Three representative lines for each construct are shown. Scale bar = 1 cm. (B) Primary root length of *bsk3,4,7,8* and 14 independent transgenic lines for each construct as well as all data combined for 14 independent lines of each construct. (C) Primary root growth rate of *bsk3,4,7,8* and of 6 independent transformants for each, the *BSK3-P* and *BSK3-L* variants as well as all data combined. Seeds were germinated on solid media containing 11.4 mM N. Primary root length was assessed 6 days after germination and growth rate was calculated by determining the primary root length of the same plants 6 and 8 days after germination. *P* values for indicated pairwise comparisons were calculated using Welch's *t* test.

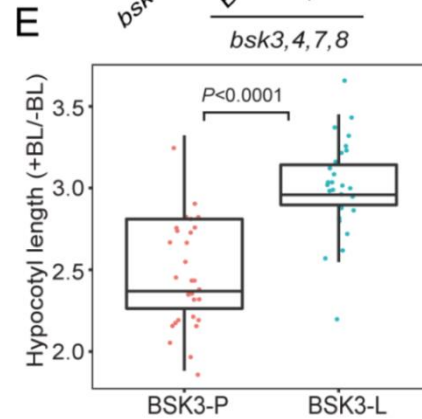
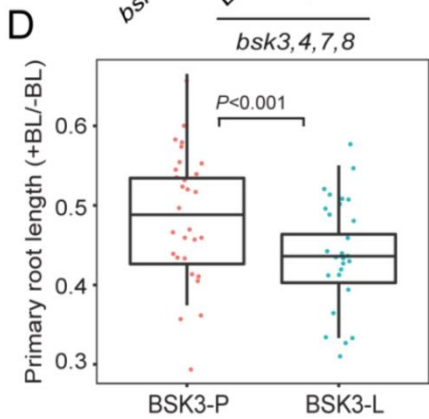
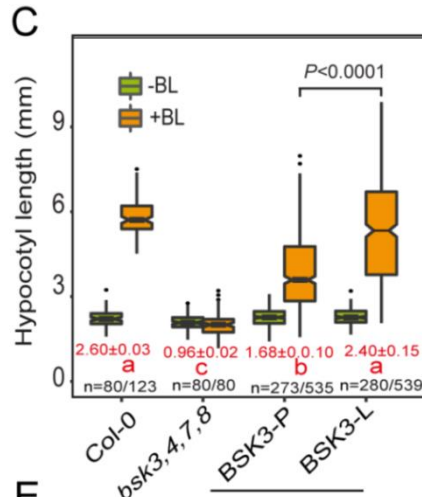
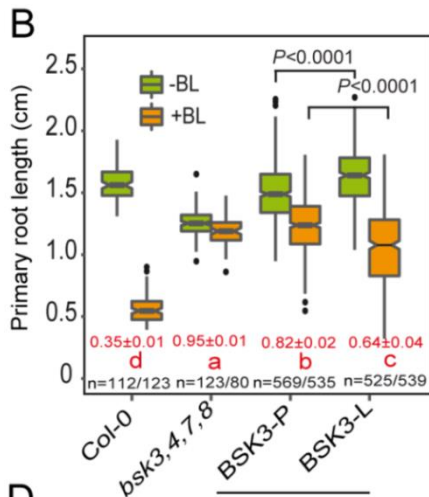
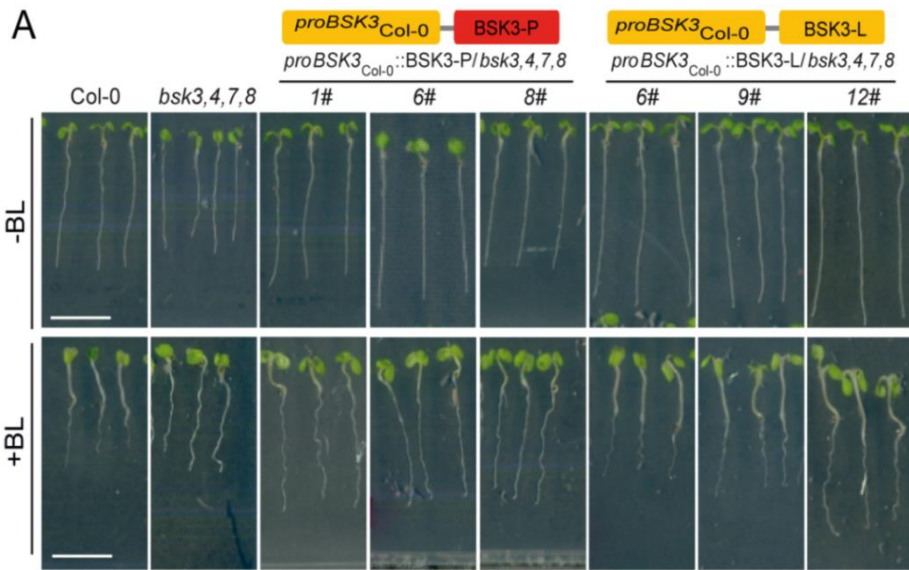


→ Descriptions were shown on previous page.

To further test whether the L to P substitution affects BR signaling, plant responses to the bioactive BR brassinolide (BL) were assessed *in vitro*. In agreement with previous studies (Tang et al., 2008; Sreeramulu et al., 2013; Ren et al., 2019), the exogenous supply of BL inhibited primary root length by 65% and stimulated hypocotyl elongation by 160% in wild-type plants (Figure 11A-C). As expected, in the *bsk3,4,7,8* quadruple mutant, these responses were strongly attenuated. Although

both BSK3 alleles could partially rescue the BR responsiveness of *bsk3,4,7,8* plants, expression of BSK3-L restored BR sensitivity to a larger extent than BSK3-P (Figure 11A-C). A further analysis of BR sensitivity in 56 natural accessions harboring either BSK3 variant revealed that genotypes carrying the BSK3-L variant were more sensitive to the exogenous supply of BR than those with the BSK3-P variant (Figure 11D-E). These results indicated that BSK3-L is more efficient than BSK3-P in mediating BR signaling.

Figure 11. Allelic variation of BSK3 determines plant sensitivity to brassinosteroids. (A-C) Brassinosteroid (BR) sensitivity of wild-type (Col-0), *bsk3,4,7,8* and independent transgenic lines expressing the sequences coding for either the BSK3-P or BSK3-L variant under control of the *BSK3_{Col-0}* promoter. **(A)** Appearance, **(B)** primary root length and **(C)** hypocotyl length of 6 day-old plants. For each construct, 14 independent transgenic T2 lines were germinated on solid 0.5x MS agar containing 1 μ M 24-epibrassinolide (+BL) or the equivalent amount of ethanol (-BL). Primary root length and hypocotyl length were assessed 6 days after germination. Scale bars, 1 cm. Numbers in red indicate relative root or hypocotyl length (+BL/-BL). Different letters indicate significant differences at $P < 0.05$ according to one-way ANOVA and post-hoc Tukey test. **(D-E)** Primary root **(D)** and hypocotyl **(E)** growth response to exogenous BR application for natural accessions carrying BSK3-P or BSK3-L, ($n = 29$ and 27 accessions for P and L haplotypes, respectively). Primary root length was assessed 6 days after germination. P values for indicated pairwise comparisons were calculated using Welch's t test.

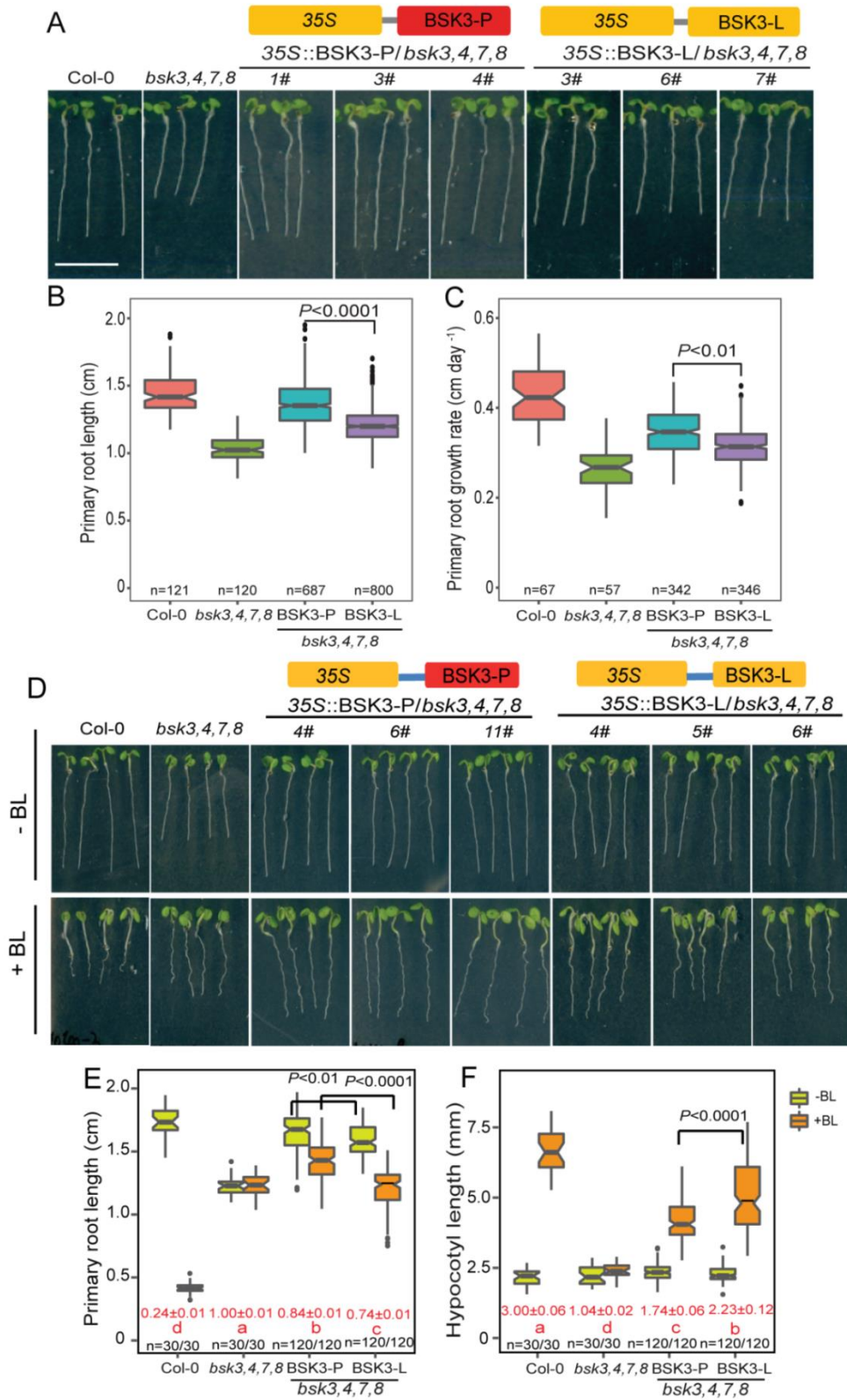


→ Descriptions were shown on previous page.

Previously, it has been shown that root elongation can be significantly impaired by genetically enhancing BR3 signaling (Gonzalez-Garcia et al., 2011). To test whether primary root length can be modulated by either BSK3-L or BSK3-P, two BSK3

variants were overexpressed in the *bsk3,4,7,8* mutant background. While both BSK3 variants could partially recover root growth of *bsk3,4,7,8* plants (Figure 12A), transgenic lines overexpressing BSK3-L showed significantly shorter and slower growing primary roots as compared to those expressing the BSK3-P variant (Figure 12B and C). In addition, transgenic lines overexpressing the BSK3-L variant exhibited significantly stronger BR sensitivity compared to those overexpressing the BSK3-P variant (Figure 12D-F). These results further demonstrated that the BSK3-L allele relays a stronger BR signaling output than the BSK3-P allele.

Figure 12. Overexpressing BSK3-L confers higher brassinosteroid sensitivity than BSK3-P. (A-C) Root growth of wild-type (Col-0), *bsk3,4,7,8* and independent transgenic lines expressing the sequences coding for either the BSK3-P or BSK3-L variant under control of the CaMV 35S promoter. **(A)** Appearance, **(B)** primary root length and **(C)** root growth rate of 6 day-old plants. For each construct, 17 independent transgenic T2 lines were germinated on solid 0.5x MS media containing 11.4 mM N. **(D-F)** Brassinosteroid sensitivity of wild-type (Col-0), *bsk3,4,7,8* and independent transgenic lines expressing the sequences coding for either the BSK3-P or BSK3-L variant under control of the CaMV 35S promoter. Appearance of 6-day-old plants **(D)**, primary root length **(E)** and hypocotyl length **(F)** grown under +BL versus -BL. For each construct, 12 independent transgenic T2 lines were germinated on solid 0.5x MS agar containing 1 μ M brassinolide (+BL) or the equivalent amount of ethanol (-BL). Primary root length and hypocotyl length were assessed 6 days after germination. *P* values for indicated pairwise comparisons were calculated using Welch's *t* test. Numbers in red indicate relative root or hypocotyl length (+BL/-BL). Different letters indicate significant differences at *P* < 0.05 according to one-way ANOVA and post-hoc Tukey test. Scale bars, 1 cm.



→ Descriptions were shown on previous page.

Initial expression analysis indicated that polymorphisms affecting the transcript level of *BSK3* are unlikely causal for the observed natural variation of root growth (Figure 7I). To further verify this assumption, the coding sequence of *BSK3* from Col-0 (a *BSK3-L* allele) was expressed under the control of *BSK3* promoters from Cvi-0 or Col-0, two accessions that exhibited contrasting primary root length and responsiveness to LN (Figure 13A). Both constructs were introduced into *bsk3,4,7,8* plants. If putative differences in *BSK3* expression determined the phenotypic variation between Cvi-0 and Col-0, it would be expected to detect different complementation efficiencies. However, both primary root growth (Figure 13B and C) and BR sensitivity (Figure 14A-C) were recovered to a similar extent in transgenic lines expressing either construct. Taken together, these results suggested that differential transcriptional regulation of *BSK3* is most likely not responsible for the natural variation of root growth and BR sensitivity.

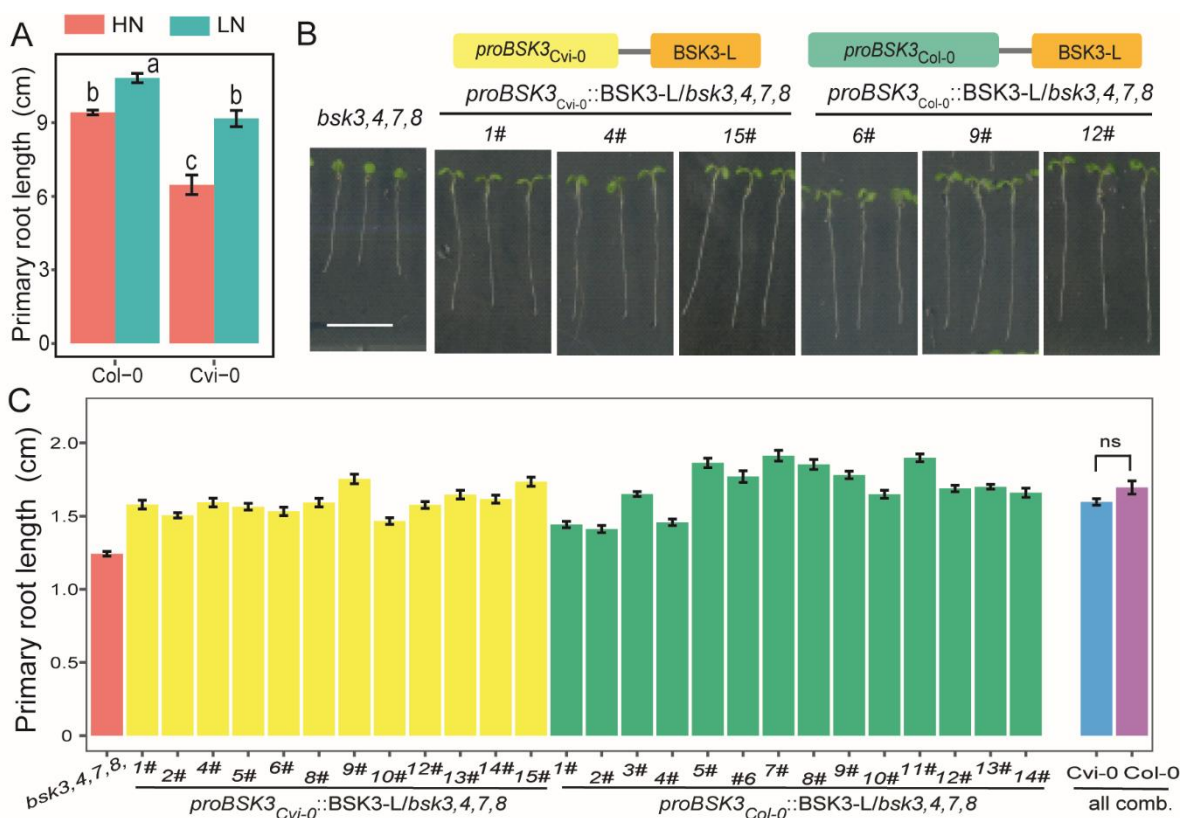


Figure 13. Natural variation of root length is not associated with expression variation of *BSK3*. (A) Primary root length of Col-0 and Cvi-0 showing differential responsiveness to low N. Seven day-old seedlings pre-cultured on 11.4 mM N were transferred to solid agar containing either high N (HN, 11.4 mM N) or low N (LN, 0.55 mM N). Primary root length was determined after 9 days. Bars represent means \pm s.e. ($n = 12$ plants). (B) Schematic of transgenic constructs used for complementation of the

bsk3,4,7,8 quadruple mutant and representative photographs of 6 day-old plants. Scale bar, 1 cm. **(C)** Primary root length of *bsk3*, and 12 or 14 independent lines complemented with the BSK3-L variant driven by the *BSK3* promoter from either *Cvi-0* or *Col-0* as well as all data combined for all examined independent lines of each construct. For a comparative analysis of the complementation efficiency of different BSK3 variants and promoters, values for BSK3-L lines driven by the *BSK3*_{*Col-0*} promoter are shown in Figure 10A-B. Seeds were germinated on solid media containing 11.4 mM N. Regarding root traits, no significant differences were detected between the two constructs, according to pairwise comparison using Welch's *t* test ($P > 0.05$; ns, not significant).

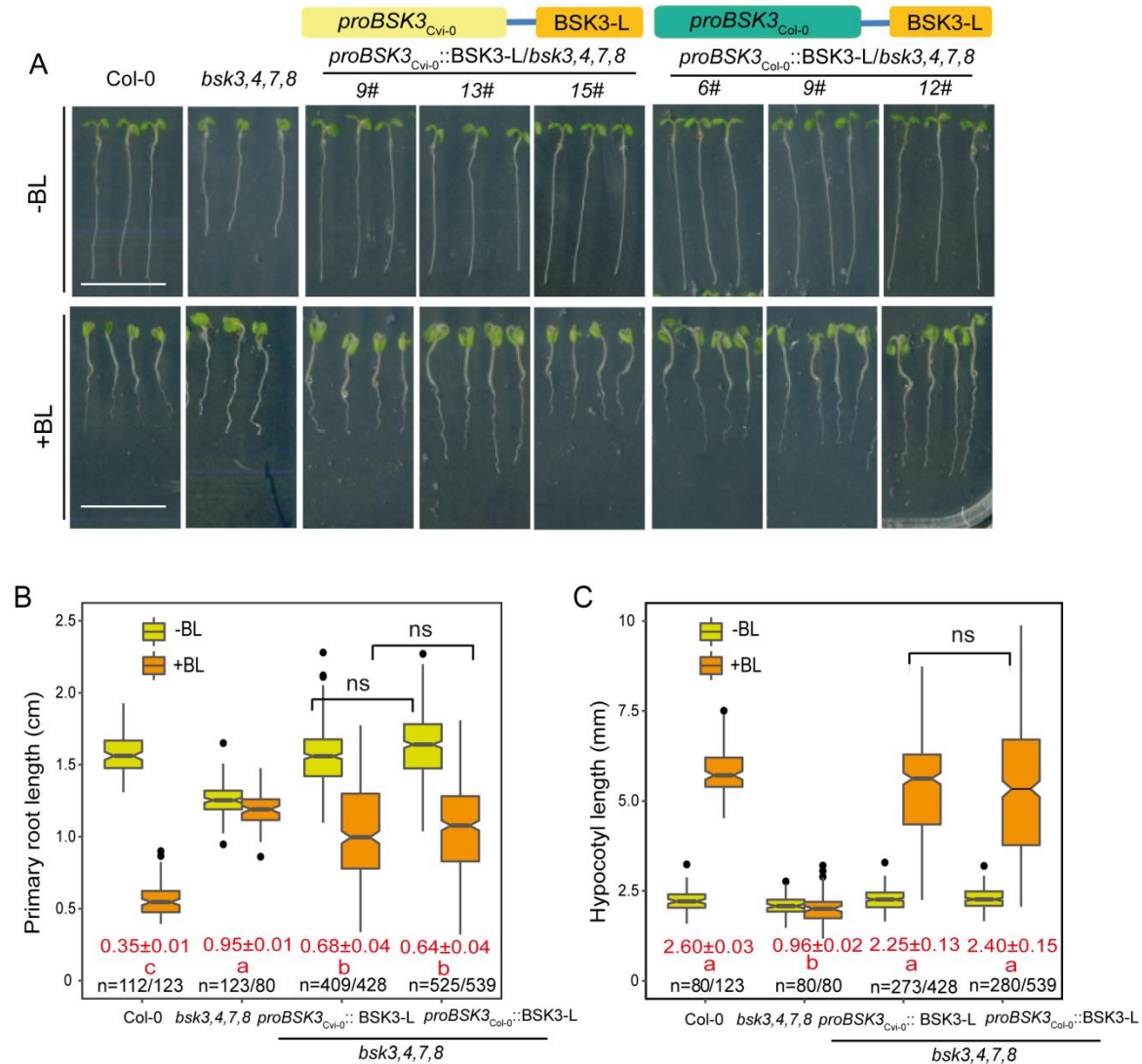


Figure 14. Genotypic variation in the *BSK3* promoter sequence is not associated with brassinosteroid sensitivity. (A-C) Brassinosteroid sensitivity of the wild-type (*Col-0*), *bsk3,4,7,8* quadruple mutant and independent transgenic *bsk3,4,7,8* lines expressing the sequence coding for the BSK3-L protein variant under control of either the *BSK3*_{*Col-0*} or *BSK3*_{*Cvi-0*} promoter. **(A)** Appearance, **(B)** primary root length and **(C)** hypocotyl length of 6-day-old plants. For each construct, 12 independent transgenic T2 lines were germinated on solid half-strength MS agar media containing 1 μ M 24-epibrassinolide (+BL) or the equivalent amount of ethanol (-BL). Regarding root traits, no significant differences were detected between the two constructs, according to pairwise comparison using Welch's *t* test ($P > 0.05$, ns, not significant). Scale bars, 1 cm.

4.6.4 BSK3-dependent brassinosteroid signaling fine-tunes root responsiveness to low nitrogen

Since natural allelic variation in *BSK3* modulated BR sensitivity and signaling, the question arose whether this variation also determines the root responsiveness to mild N deficiency? To answer this questions, wild-type, *bsk3,4,7,8* and 12 independent transgenic lines expressing either the BSK3-L or BSK3-P variant in the *bsk3,4,7,8* mutant background were assessed under HN and LN conditions. Since *bsk3,4,7,8* plants exhibit short primary and lateral roots already when grown on HN (Figure 9), relative root lengths (i.e. their ratio under LN to HN) were calculated to allow for direct comparison. In line with the initial experiment (Figure 9), the primary root of the *bsk3,4,7,8* quadruple mutant was largely insensitive to LN due to attenuated cell elongation (Figure 15A, E-G). Importantly, while complementation with BSK3-P could only partially recover the responsiveness of *bsk3,4,7,8* to LN, BSK3-L was able to fully rescue this response by significantly increasing cell elongation without altering meristem length (Figure 15A, E-G), suggesting that the BSK3-L variant confers a more pronounced response of the primary root to LN than the BSK3-P variant. Consistent with this notion, primary roots of natural accessions expressing the BSK3-L variant exhibited significantly stronger responses to LN than accessions carrying the BSK3-P variant (Figure 15J). BSK3-L was also able to more efficiently restore average lateral root length and total root length, while none of the *BSK3* alleles could recover the suppressed lateral root density of *bsk3,4,7,8* (Figure 15B-D). Furthermore, significant correlations were found between BR sensitivity, as determined by root length inhibition or hypocotyl elongation, and the responsiveness of the primary root (Figure 15H and K) or of average lateral root length (Figure 15I) to mild N deficiency. Together, these data provided further support for a specific role of BSK3 in root elongation and demonstrated that the BR sensitivity gained by L319P substitution in BSK3 is critical for the extent of the root foraging response to LN. Thus, it was concluded that BSK3-dependent modulation of BR signaling contributes significantly to the natural variation in root length responses to N availability.

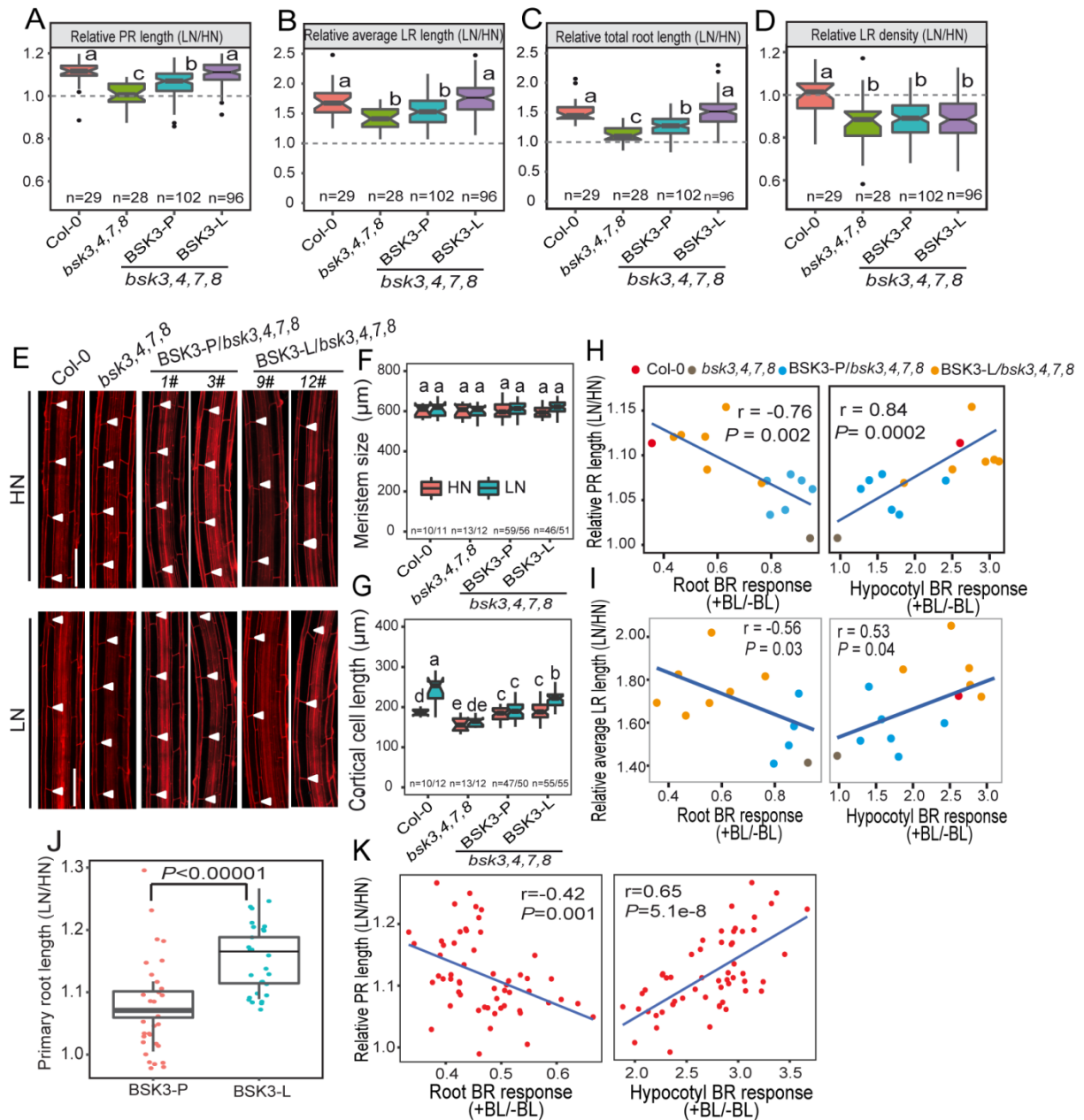


Figure 15. BSK3-dependent brassinosteroid sensitivity tunes root responses to low N. (A-D) Response to low N of Col-0, *bsk3,4,7,8* and independent transgenic plants expressing the sequences coding for either the BSK3-P or BSK3-L variant under control of the *BSK3_{Col-0}* promoter. **(A)** Relative change under low N of primary root length, **(B)** average lateral root length, **(C)** total root length and **(D)** lateral root density. Seven day-old seedlings were pre-cultured on 11.4 mM N and then transferred to solid agar containing either high N (HN, 11.4 mM N) or low N (LN, 0.55 mM N). Root system architecture was assessed after 9 days. Different letters indicate significant differences at $P < 0.05$ according to one-way ANOVA and post-hoc Tukey test. **(E)** Representative confocal images of the root meristem (upper panel) and length of cortical cells (bottom panel) of wild-type (Col-0), *bsk3,4,7,8* and complemented lines grown under HN or LN. White arrowheads indicate the position of the quiescent center (QC) and boundaries of the meristematic zone and elongation zone (upper panel) and two consecutive cortical cells (bottom panel). Bars = 100 μm . **(F-G)** Length of meristem size **(F)** and cortical cells **(G)** of wild-type (Col-0), *bsk3,4,7,8* and complemented lines grown under HN versus low N. **(H-I)** Correlation between BR-dependent root or hypocotyl elongation and the responsiveness to N of primary **(H)** and lateral roots **(I)**. **(J)** Primary root growth response to mild N deficiency for

natural accessions carrying BSK3-P or BSK3-L ($n = 29$ and 27 accessions for P and L haplotypes, respectively). **(K)** Correlation between BR-dependent root or hypocotyl elongation and the responsiveness to N of primary roots in natural accessions. The data used for the correlation analyses in Figure 15 H-I derived from experiments shown in Figure 11A-C and Figure 15A-B, data for correlations in Figure 15 K derived from Figure 11D-E and Figure 15J.

4.6.5 *BSK3* is strongly expressed in outer root cell layers but not regulated by nitrogen

Since experiments with *BSK3* insertion and complementation lines revealed N-dependent root growth phenotypes, the hypothesis was tested whether *BSK3* expression is regulated by external N supply. Initially, *BSK3* expression was monitored by qPCR in whole roots of Col-0 plants grown for 9 days on HN or LN and no significant alteration was found by N availability (Figure 16A). To investigate whether putative expression changes were confined to particular root zones, transgenic lines expressing GUS or a *BSK3*-GFP translational fusion under the control of the *BSK3* promoter from Col-0 were generated. Nine days after transferring plants to HN or LN, GUS activity was detected in all root tissues of both primary root and lateral root tips (Figure 16B, E-G). Confocal microscopy of plants expressing *proBSK3::BSK3-GFP* further revealed that the protein was present from the meristematic zone all the way through the elongation zone of epidermal, cortical and endodermal cells (Figure 16C). Confined localization at the cell border was in agreement with the recently confirmed binding of the myristoylated protein to the plasma membrane (Ren et al., 2019). External N supply had no effect on the pattern or intensity of *BSK3* expression. Moreover, also a time-course expression analysis and histological staining in roots did not reveal any significant differences in *BSK3* expression under progressing N deficiency (Figure 16D-F). For an in-depth understanding of the role of *BSK3* in root growth regulation, *BSK3* expression at different stages of lateral root development were monitored (Malamy & Benfey, 1997). Under both N conditions, *BSK3* promoter activity and *BSK3*-GFP fusion protein were only detected in lateral roots that had emerged from the parental root (Figure 16F). Overall, these data suggest that although *BSK3* expression is not regulated by N, it coincides spatially with developmental stages associated with cell elongation.

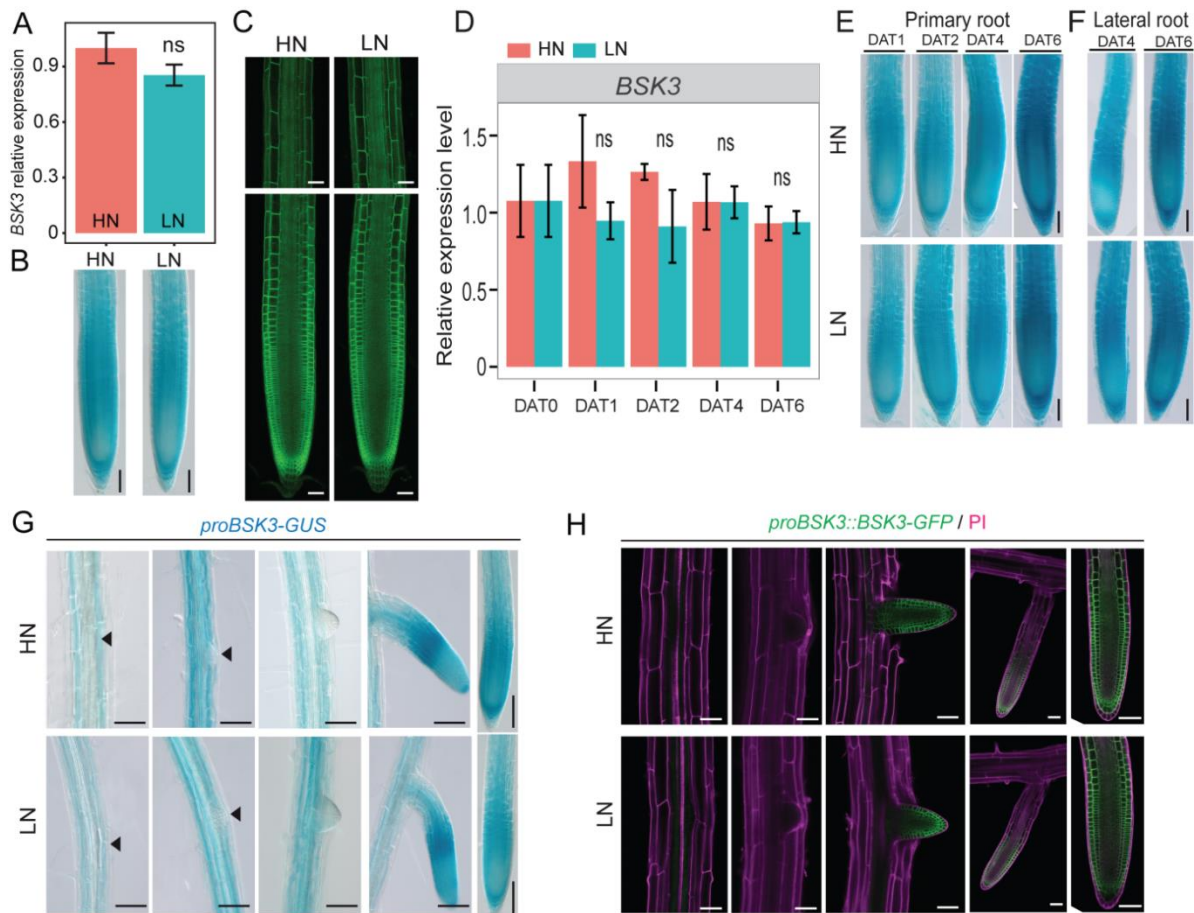


Figure 16. *BSK3* expression pattern and protein localization in response to N availability. (A) *BSK3* transcript level in response to high N (HN) or low N (LN) availability. **(B)** *proBSK3*-dependent GUS activity in response to high N (HN) or low N (LN) availability in the primary root. **(C)** *BSK3*-GFP localization in the primary root. **(D-F)** A time-course expression analysis of *BSK3* in the root **(D)** and GUS staining in the tips of primary root **(E)** and lateral roots **(F)**. **(G and H)** *proBSK3*-dependent GUS activity **(G)** and *BSK3*-GFP localization **(H)** in the lateral roots at several developmental stages. Seven day-old seedlings were pre-cultured on 11.4 mM N and then transferred to solid agar containing either high N (HN, 11.4 mM N) or low N (LN, 0.55 mM N). Samples for qPCR analysis and GUS activity assays were taken at indicated time points after transfer. *BSK3* expression levels **(A and D)** were assessed in whole roots by qPCR analysis and normalized to *ACT2* and *UBQ10*. Bars represent means \pm s.e. ($n = 4$ independent biological replicates) and ns denotes no significant difference to HN according to Welch's *t* test ($P > 0.05$). Arrowheads point to non-emerged lateral root buds. Representative images ($n > 15$) are shown. Scale bars, 100 μ m.

4.6.6 Low nitrogen interferes with brassinosteroid signaling by upregulating *BAK1*

In *Arabidopsis*, *BSK3* mediates BR signaling downstream of the BR receptors (Tang et al., 2008; Fàbregas et al., 2013). Since *BSK3* expression is not regulated by N (Figure 16), an N-dependent signal might enter BR signaling by interfering with BR perception upstream of *BSK3*. Therefore, time-course expression analysis was conducted to assess whether root expression of *BRI1* and *BAK1* respond to external

N. After 6 days of exposure to LN, *BAK1* transcript levels were significantly upregulated (Figure 17A). Notably, the response of primary and lateral roots to mild N deficiency was significantly attenuated in *bak1-1* mutant plants (Figure 17B-D). Furthermore, similar to *bsk3*, the attenuated response in primary root of *bak1-1* mutant was because of reduced cell elongation (Figure 17E-G).

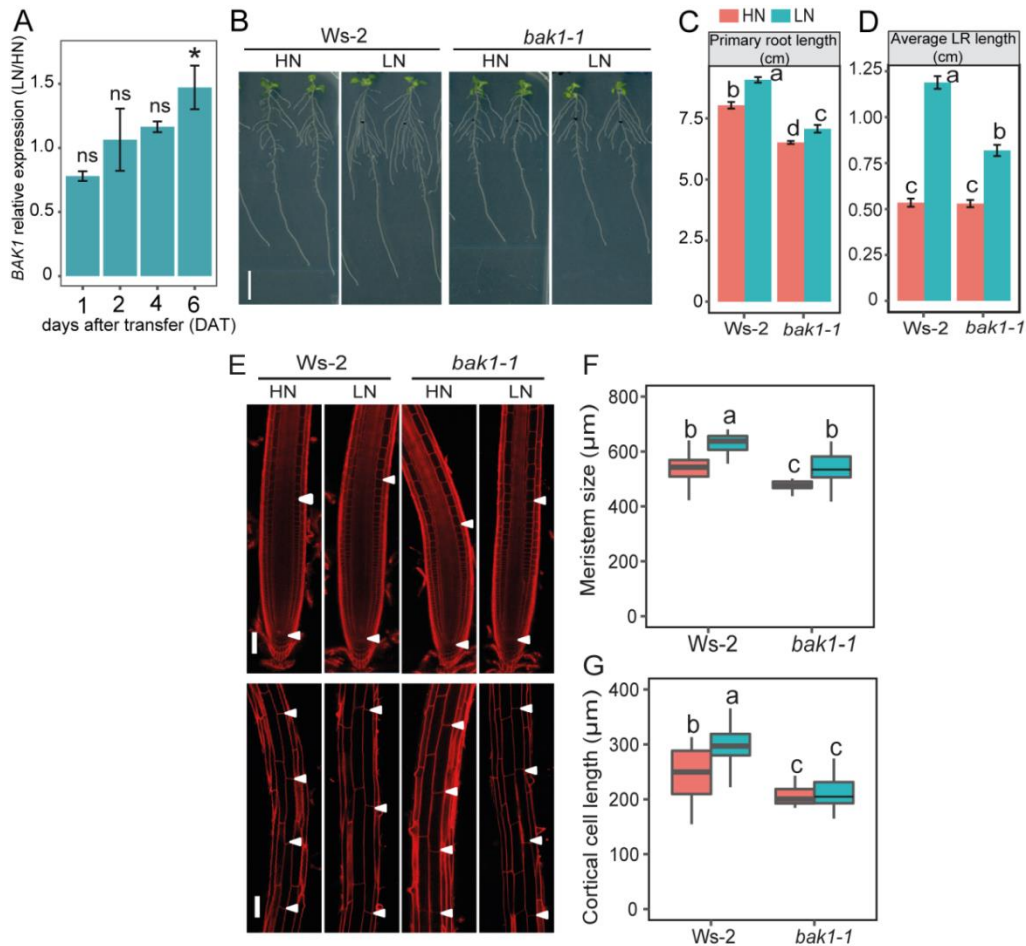
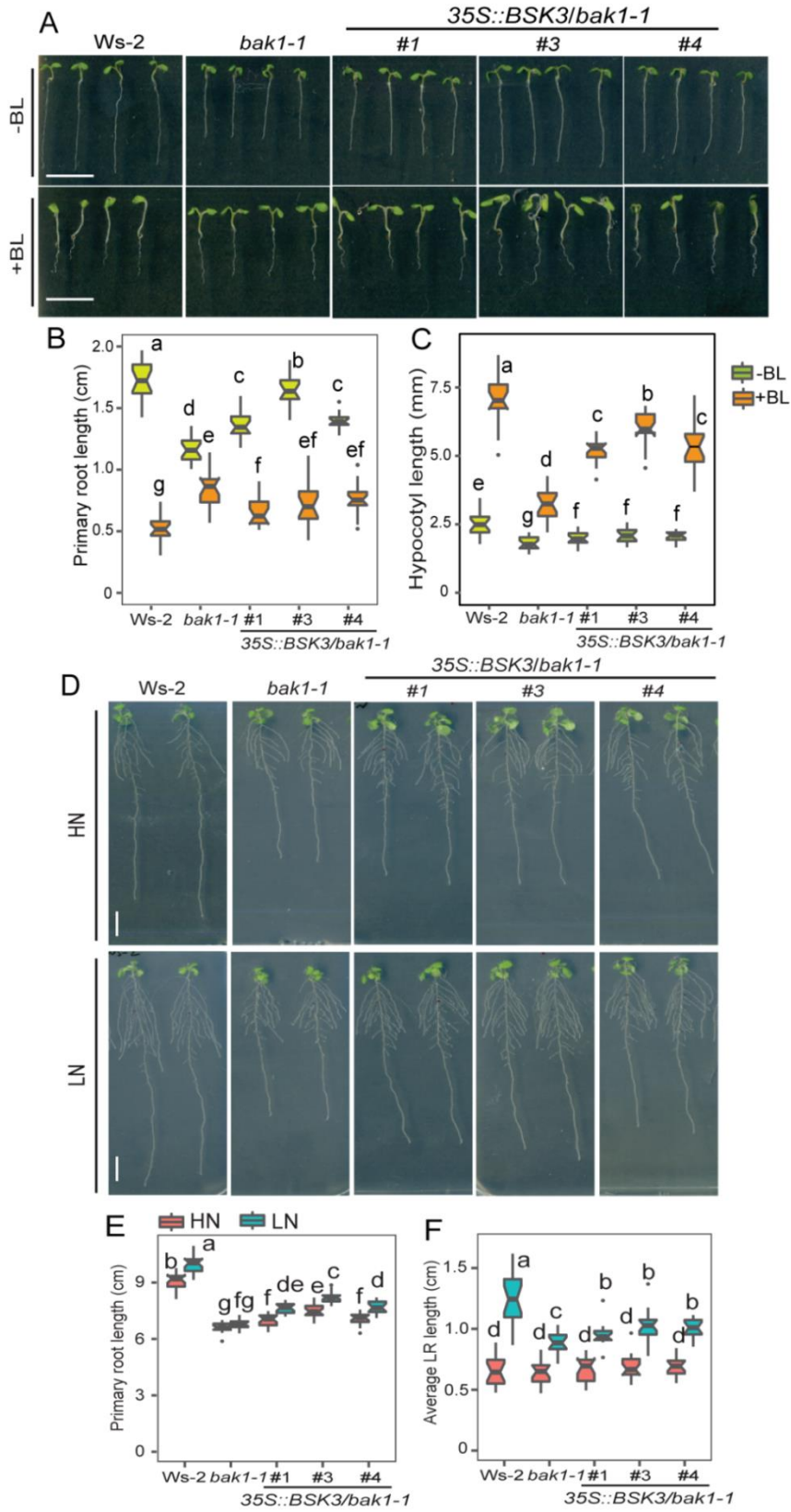


Figure 17. Transcriptional response of *BAK1* to low N and phenotypic analysis of *bak1* mutant plants. (A) *BAK1* transcript levels in roots during growth on low N. Seven day-old seedlings were pre-cultured on 11.4 mM N and then transferred to solid agar containing either high N (HN, 11.4 mM N) or low N (LN, 0.55 mM N). *BAK1* transcript levels were assessed in whole roots by qPCR analysis and normalized to *ACT2* and *UBQ10*. Bars represent means \pm s.e. ($n = 3$ independent biological replicates). Asterisks indicate significant differences to HN at each time point according to Welch's t test ($*P < 0.05$; ns, not significant). **(B-D)** Phenotypic analysis of *bak1-1* mutant plants. Appearance of plants **(B)**, primary root length **(C)**, average lateral root length **(D)** of wild-type (Col-0) and *bak1-1* plants grown under high N (HN) or low N (LN) conditions. Bars represent means \pm s.e. ($n = 16-18$ plants). Scale bar, 1 cm. **(E)** Representative confocal images of root meristem (upper panel) and length of cortical cells (bottom panel) of wild-type (Col-0) and *bak1-1* grown under HN or LN. White arrowheads indicate the position of quiescent center (QC) and boundaries of meristematic zone and elongation zone (upper panel) and two consecutive cortical cells (bottom panel). Bars = 100 μm . **(F-G)** Length of meristem size **(F)** and cortical cells **(G)** of wild-type (Col-0) and *bak1-1* grown under HN versus low N ($n = 15$ plants). Root system architecture and cellular traits were assessed after 9 days. Different letters indicate significant differences at $P < 0.05$ according to one-way ANOVA and post-hoc Tukey test.

BAK1 involves in multiple signaling pathways (Ma et al., 2016). To further verify the impaired response of *bak1-1* to LN was a consequence of perturbed BR signaling, the downstream BR signaling component *BSK3* was overexpressed in the *bak1-1* mutant. Ectopic expression of *BSK3* could significantly rescue sensitivity of *bak1-1* to exogenous BR supply (Figure 18A-C). Most importantly, overexpression of *BSK3* restored significantly both the primary and lateral root response of *bak1-1* to LN, suggesting that reduction in the root response of *bak1-1* to LN was due to impaired BR signaling (Figure 18D-F).

Figure 18. Overexpressing *BSK3* significantly rescues brassinosteroid sensitivity and the N response of the *bak1-1* mutant. (A-C) BR sensitivity of wild-type (*Ws-2*), *bak1-1* mutant and three independent *BSK3* overexpression lines (T2) in the *bak1-1* mutant background. Appearance of 6 day-old plants **(A)**, primary root length **(B)** and hypocotyl length **(C)**, (n=20 plants). Seeds were germinated on solid half-strength MS agar containing 1 μ M brassinolide (+BL) or the equivalent amount of ethanol (-BL). Primary root length and hypocotyl length were assessed 6 days after germination. **(D-F)** Phenotypic analysis of the *bak1-1* mutant and *BSK3* overexpression lines. Appearance of plants **(D)**, primary root length **(E)**, average lateral root length **(F)** of plants for wild-type (*Ws-2*), *bak1-1* and three independent T2 transgenic lines overexpressing *BSK3* in the *bak1-1* background grown under high N (HN) or low N (LN) conditions. Root system architecture was assessed after 9 days. (n = 16 plants). Different letters indicate significant differences at $P < 0.05$ according to one-way ANOVA and post-hoc Tukey test. Scale bars, 1 cm.



→ Descriptions were shown on previous page.

Unlike *BAK1*, expression of *BRI1* was not regulated by LN (Figure 19A). Although exhibiting shorter primary and lateral roots compared to wild-type plants under both N conditions, two independent *bri1* mutants were still able to stimulate primary root and lateral root growth under LN to a similar extent as the wild type (Figure 19B-F). Thus, these results indicate that mild N deficiency doesn't activate BR signaling upstream of BSK3 by upregulating *BRI1* expression.

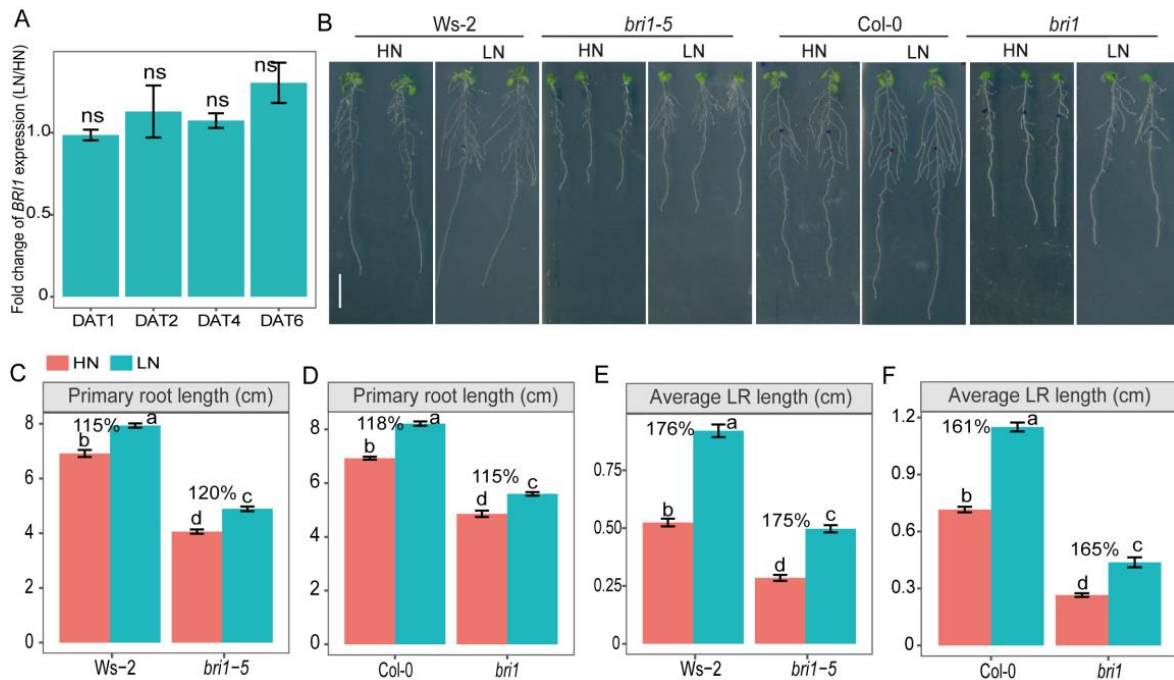


Figure 19. Transcriptional response of *BRI1* under progressing N deficiency and phenotypic analysis of *bri1* mutant plants. (A) Relative increase of *BRI1* transcript levels in roots during growth on low N. Seven day-old seedlings were pre-cultured on 11.4 mM N and then transferred to solid agar containing either high N (HN, 11.4 mM N) or low N (LN, 0.55 mM N). *BRI1* transcript levels were assessed in whole roots by qPCR analysis and normalized to *ACT2* and *UBQ10*. Bars represent means \pm s.e. ($n = 3$ independent biological replicates). No significant difference between two N treatments at each time points was detected according to Welch's t test ($P > 0.05$; ns, not significant). **(B-F)** Appearance of plants **(B)**, primary root length **(C-D)**, average lateral root length **(E-F)** of wild-type (Col-0 and Ws-2) and *bri1* mutant plants grown under high N (HN) or low N (LN) conditions. Seven day-old seedlings were pre-cultured on 11.4 mM N and then transferred to solid agar containing either high N (11.4 mM N) or low N (0.55 mM N). Root system architecture was assessed after 9 days. Bars represent means \pm s.e. ($n = 13-17$ plants). Different letters indicate significant differences at $P < 0.05$ according to one-way ANOVA and post-hoc Tukey test. Scale bar, 1 cm. Numbers above columns indicate percent changes under LN versus HN for primary and average lateral root length. No significant differences were detected between mutants and wild type (Col-0) according to Welch's t test ($P > 0.05$).

4.6.7 BSK3 variants are likely adaptive to selection pressure of precipitation

GWAS do not only shed light on the genetic architecture of phenotypic variation, but also allow identifying allelic variants that have undergone natural selection due to local stress factors and adaptations beneficial for competitiveness and survival in their natural environments (Rosas et al., 2013; Satbhai et al., 2017). To assess whether a longer primary root is associated with environmental adaptation, primary root lengths were correlated with climate data at the site where the accessions were collected. The only significant correlation found was between primary root length under low N and maximum precipitation in the wettest month (Figure 20A), suggesting that the natural variation for this trait was, at least in part, related to water availability. Interestingly, precipitation in the wettest month at sites where accessions carrying the BSK3-L-encoding allele were collected was significantly lower than those inhabited by accessions harboring the BSK3-P variant (Figure 20B). This indicates that precipitation likely exerts selection pressure on BSK3 variants.

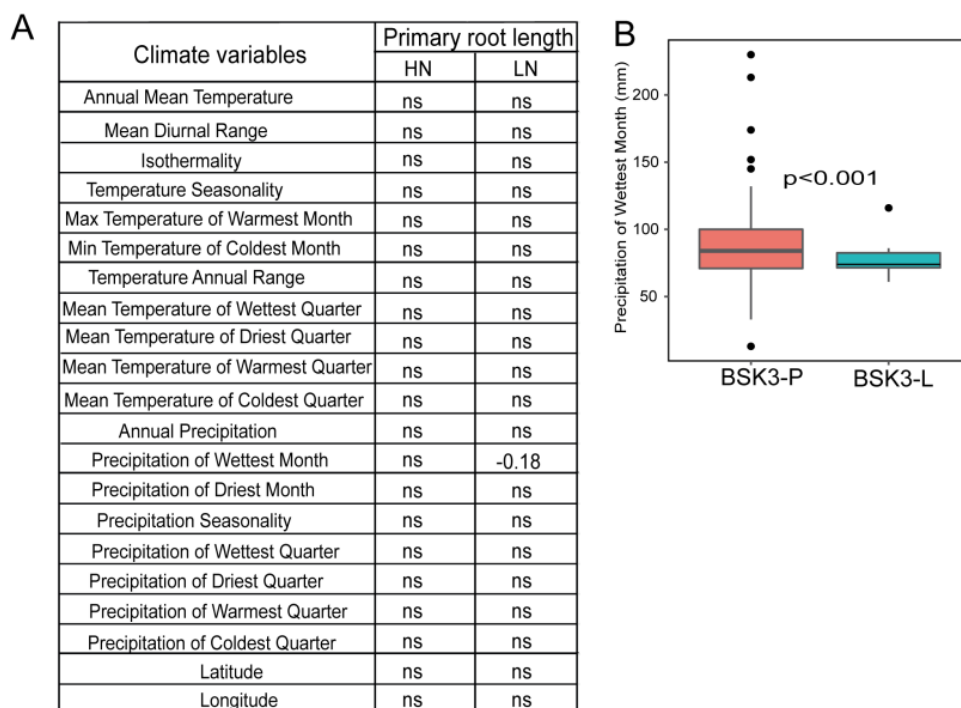


Figure 20. Precipitation pattern as selection factor for BSK3 variants. (A) Pearson correlation between primary root length and climate variables (19 climate scenarios, latitude and longitude). Only significant correlation coefficients ($P < 0.05$) are shown; otherwise non-significant correlations are denoted by “ns”. **(B)** Boxplot showing the association between BSK3-P or -L haplotypes and precipitation at the geographic location of the accession lines in terms of precipitation during wettest month. P values for pairwise comparisons were calculated using Welch’s t test ($n = 89$ and 26 accessions for P and L haplotypes, respectively).

4.7 Identification and characterization of *YUC8* in the lateral root response to low nitrogen

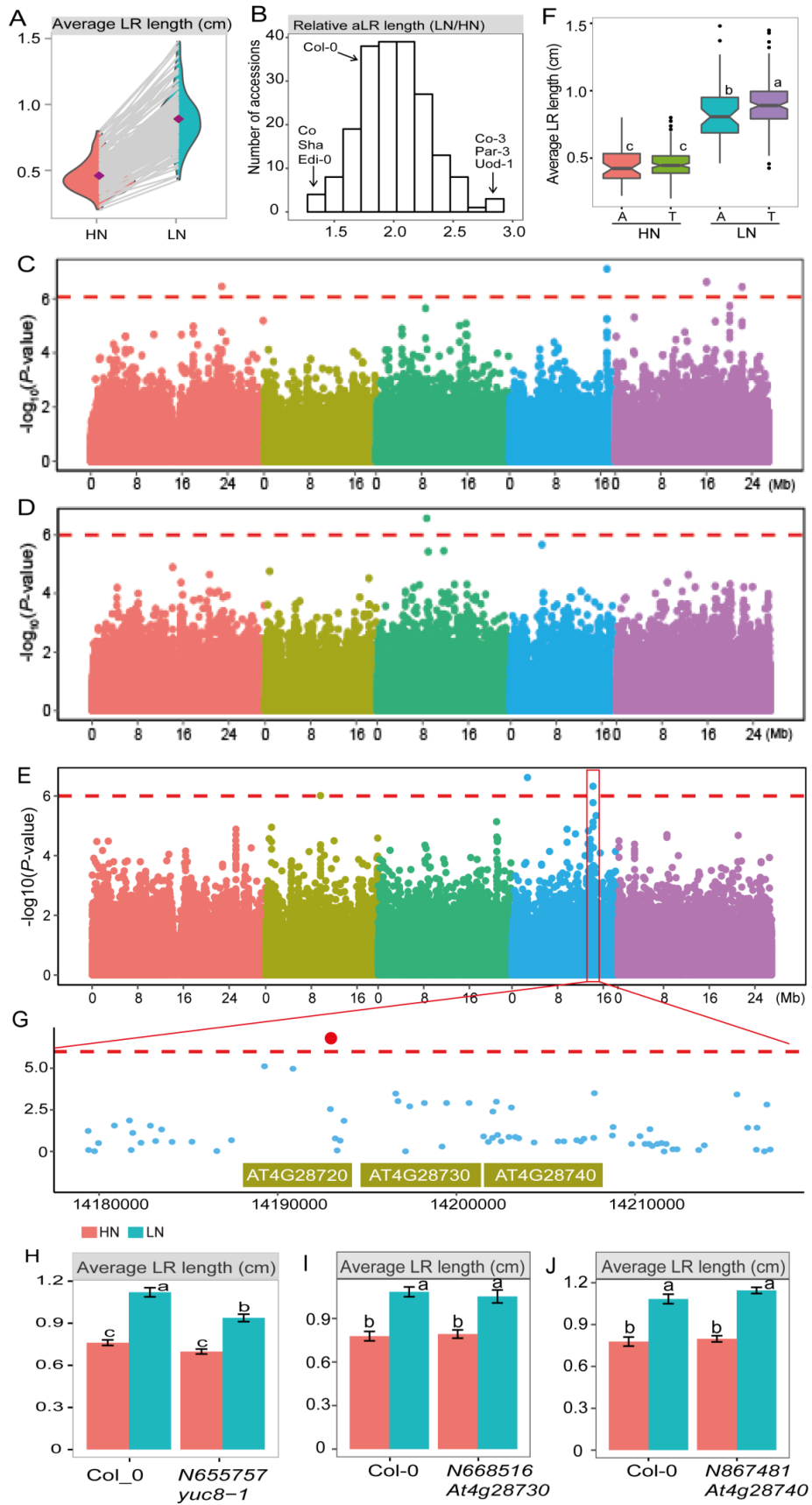
4.7.1 GWAS maps natural variation of lateral root response to *YUC8*

To gain insights into the regulation of lateral root foraging response to mild N deficiency, the same panel of 200 accessions of *A. thaliana* (Supplementary Table 1) as used above (Figure 1) was assessed also for lateral root length variation at HN and LN. There was a spectrum of phenotypic variation for average lateral root length, ranging from 0.2 cm to 0.8 cm at HN and from 0.43 cm to 1.48 cm at LN (Figure 21A; Table 1; Supplementary Table 1). On average, average length of lateral roots across all examined accessions increased by 100% when plants were grown on LN ($P < 2.2e-16$; Figure 21A). Although lateral root growth of all accessions increased at LN, there was significant variation in the extent of this response (Figure 21A and B). For instance, at LN average length of lateral roots of accessions Co, Sha and Edi-0 increased by 20-40% but by more than 180% in accessions Uod-1, Par-3 and Co-3 (Figure 21B). These observations indicated that the lateral root foraging response depends on the genotype. In line with this, the broad-sense heritability (h^2) for average length of lateral roots was estimated to 91.3% and 89.9% for HN and LN, respectively.

To uncover genetic factors controlling lateral root growth and its response to low N, GWAS was performed to associate the natural variation of lateral root length and its response to the genetic variation. In total, 7 genomic regions were identified corresponding to 39 genes within a 20 kb window centered around the most significant SNP (Supplemental Table 4). Of these 7 genomic regions, 4 and 1 loci were significantly associated with average lateral root length at HN and LN, respectively (Figure 21C and D). The two remaining loci were associated with the lateral root response to LN (i.e. LN/HN ratio; Figure 21E). Since identification of genes modulating lateral root response to LN was of particular interest in this study, a QTL on chromosome 4 (SNP_Chr4_14192732; Figure 21E) was chosen for further study. Even though at HN there was no difference for average lateral root length between A- and T-associated accessions, the average lateral root length at LN of accessions carrying the T allele was significantly higher than of those carrying the A allele (Figure 21F), indicating that this locus might specifically control lateral root

growth under LN. The identified SNP on chromosome 4 was located in At4g28720 (Figure 21G), which codes for the auxin biosynthesis protein YUCCA8 (YUC8). Nevertheless, phenotypic characterization of T-DNA insertion lines for all genes located within 20 kb interval centered on the GWA SNP was carried out to verify the role of these genes in regulating lateral root growth at given N conditions (Figure 21G). Whereas exhibiting similar average lateral root length at HN, the T-DNA insertion line *yuc8-1* for At4g28720 (*YUC8*) exhibited significantly decreased lateral root growth under LN (Figure 21H). The average lateral root length of the remaining insertion lines was similar to wild type plants at both N conditions (Figure 21I and J). Altogether, these results indicate that At4g28720 (*YUC8*) is most likely causal for the association between lateral root response and SNP_Chr4_14192732.

Figure 21. Genetic variation and GWAS of lateral root response to low N availability in natural accessions of *A. thaliana*. (A) Reaction norms and phenotypic variation of average lateral root length of 200 natural accessions of *A. thaliana* under different N supplies. Seven day-old seedlings pre-cultured on 11.4 mM N were transferred to solid agar media containing either high N (HN, 11.4 mM N) or low N (LN, 0.55 mM N). Average length of lateral roots was determined after 9 days. Purple diamonds represent means of average lateral root length for 200 accessions under each N treatment. (B) Frequency distribution of the lateral root response (LN/HN) for 200 natural accessions. Accessions with extreme responses and Col-0 are named. (C-E) Manhattan plots for the SNP associations to lateral root length at HN (C) or LN (D) or the lateral root response (E) performed with vGWAS package. Negative \log_{10} -transformed *P* values from a genome-wide scan were plotted against positions on each of the five chromosomes of *A. thaliana*. Chromosomes are depicted in different colors (I to V, from left to right). The red dashed line corresponds to the Benjamini and Hochberg false-discovery rate level of $q < 0.05$. (F) Average length of lateral roots for the accessions carrying A or T allele of the most significantly associated SNP at respective N treatment ($n = 50$ and 150 accessions for A and T alleles, respectively). (G) The 20 kb genomic region surrounding the lead GWA peak for lateral root response. dots represent $-\log_{10}$ (*P*-value) of association between the SNP and lateral root response. The most significantly associated SNP is given in red. Boxes stand for gene models in 20 kb genomic region. (H-J) Average length of LRs for T-DNA insertion lines of At4g28720 (H), At4g28730 (I) and At4g28740 (J). Bars represent means \pm s.e. ($n = 18-20$ plants). Different letters indicate significant differences at $P < 0.05$ according to one-way ANOVA and post-hoc Tukey test.



→ Descriptions were shown on previous page.

4.7.2 YUC8 and its homologs modulate root growth at low nitrogen

To further validate the role of *YUC8* in regulating lateral root elongation at LN, a second allelic insertion (*yuc8-2*, SM_3.23299) in *YUC8* was ordered and a more detailed analysis of the root system of *yuc8* mutant plants was conducted. Although at HN the average lateral root length of both *yuc8-1* and *yuc8-2* was similar as in the wild type, it decreased at LN by 25% and 18% compared to the wild type, respectively (Figure 22A and C). Whereas no significant decrease of primary root length was observed at either N condition, the responsiveness of the primary root length to mild N deficiency was also significantly decreased (Figures 22A and B, Figure 23A). In agreement with the minor effect of LN on lateral root branching (Gruber et al., 2013), no significant difference was observed for lateral root number (Figure 22E). Consequently, total root length of *yuc8* mutant plants was 16-20% lower than in wild-type plants at LN (Figure 22D).

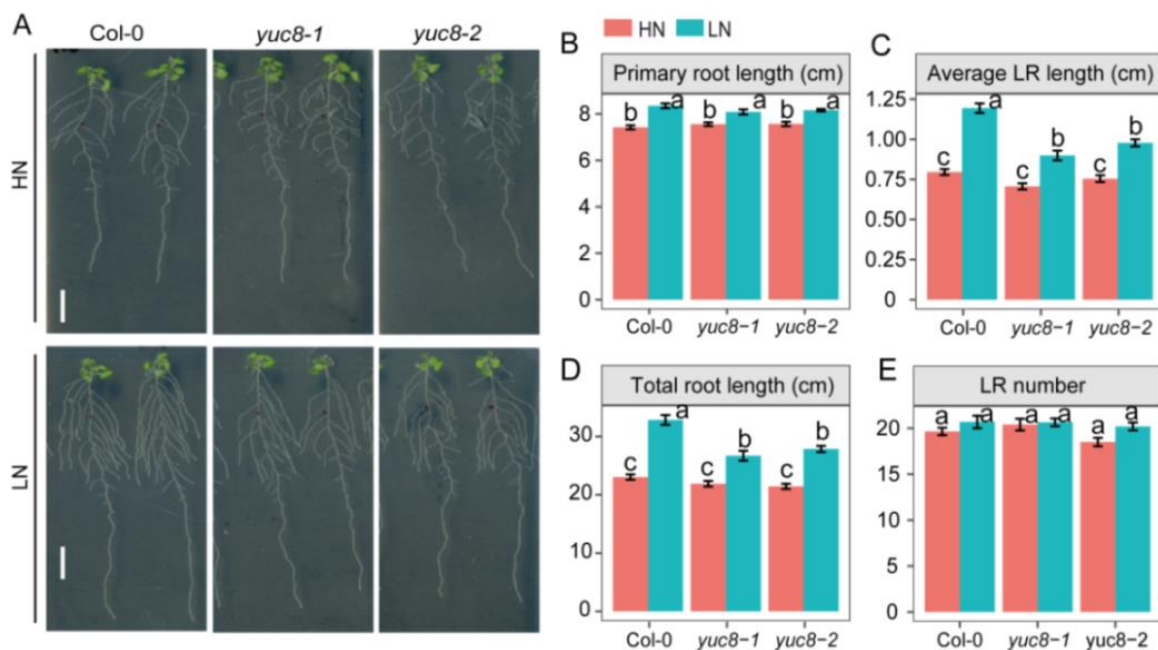


Figure 22. Root architecture of *yuc8* mutants in response to low N. (A) Appearance of plants, (B) primary root length, (C) average lateral root length, (D) total root length and (E) lateral root number of wild-type (Col-0) and two *yuc8* mutant alleles. Seven day-old seedlings were pre-cultured on 11.4 mM N and then transferred to solid agar media containing either high N (11.4 mM N) or low N (0.55 mM N). Root system architecture was assessed after 9 days. Bars represent means \pm s.e. ($n = 15-20$ plants). Different letters indicate significant differences at $P < 0.05$ according to one-way ANOVA and post-hoc Tukey test. Scale bars, 1 cm.

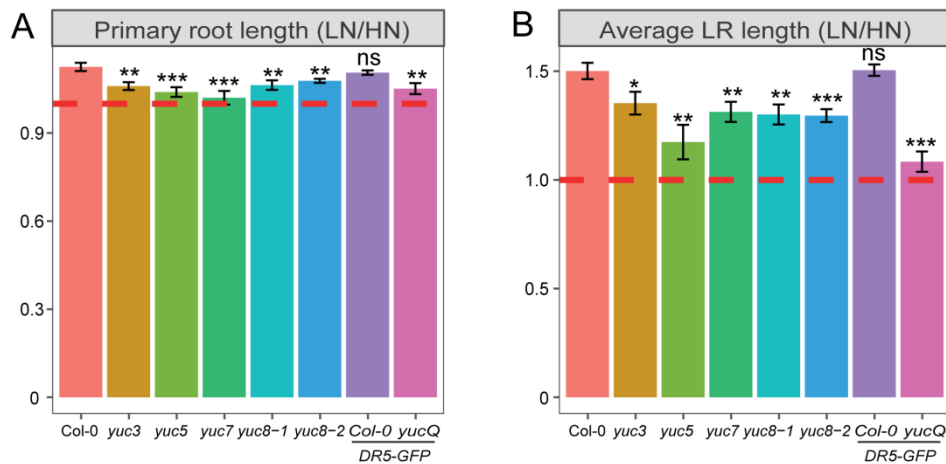


Figure 23. Root response of *yuc* mutants to low N. (A) Relative change of primary root length and **(B)** average lateral root length of wild type and *yuc* mutant plants. Seven day-old seedlings were pre-cultured on 11.4 mM N and then transferred to solid agar containing either high N (HN, 11.4 mM N) or low N (LN, 0.55 mM N). The dashed red line represents the reference line for the response to LN, namely LN/HN=1. Root system architecture was assessed after 9 days. Bars represent means \pm s.e. ($n = 15-20$ plants). Asterisks indicate significant differences between wild type and mutant plants according to Welch's *t* test (* $P < 0.05$, ** $P < 0.01$; *** $P < 0.001$; ns, not significant).

YUC8 has been shown previously to act redundantly with its close members and catalyze the rate-limiting step of auxin biosynthesis converting indole-3-pyruvic acid (IPyA) into the physiologically active plant hormone indole-3-acetic acid (IAA) (Won et al., 2011; Stepanova et al., 2011; Mashiguchi et al., 2011). Therefore, root architectural traits of *yuc3*, *yuc5*, *yuc7* single mutants and the *yucQ* (*yuc3,5,7,8,9/DR5-GFP*) quintuple mutant were analyzed to further investigate the role of YUCCA-dependent auxin biosynthesis in the regulation of the root foraging response under mild N deficiency. Consistent with the functional redundancy among YUCs (Chen et al., 2014), all *yuc* single mutants partially lost their response of the primary root and lateral roots to mild N deficiency (Figures 23 and 24).

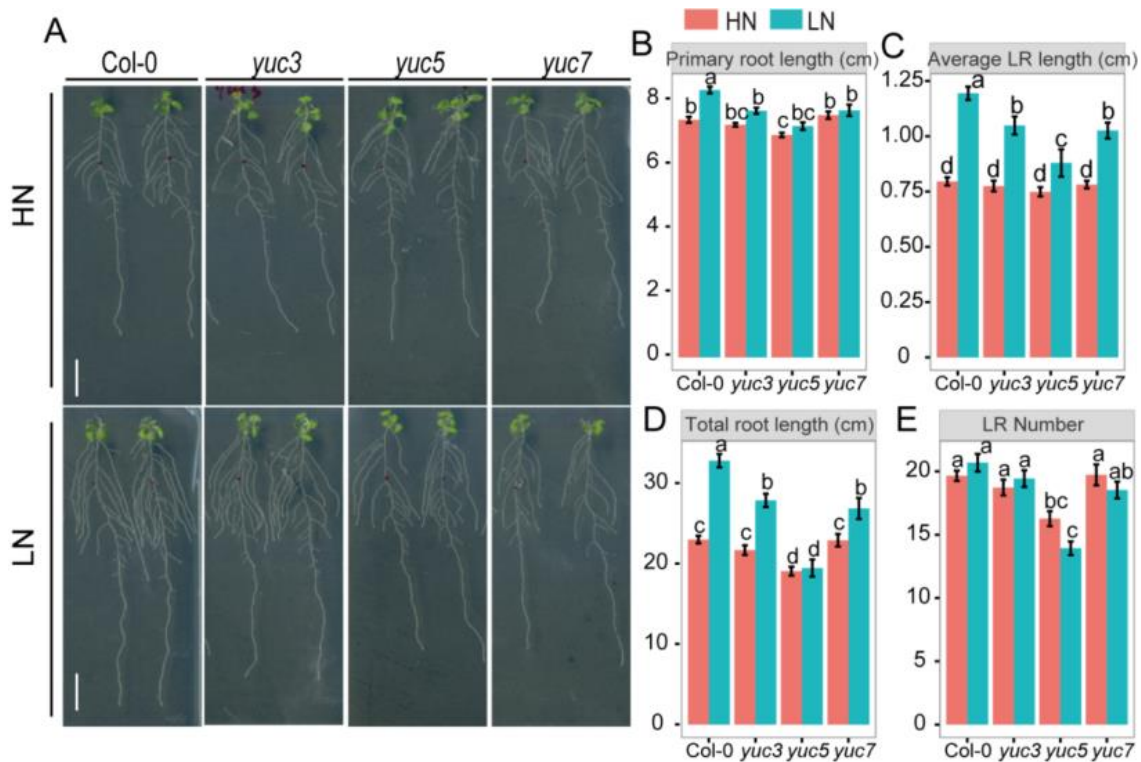


Figure 24. Root architecture of *yuc3*, *yuc5* and *yuc7* mutants in response to low N. (A) Appearance of plants, **(B)** primary root length, **(C)** average lateral root length, **(D)** total root length and **(E)** lateral root number of wild-type (Col-0) and *yuc* mutants. Seven day-old seedlings were pre-cultured on 11.4 mM N and then transferred to solid agar media containing either high N (HN, 11.4 mM N) or low N (LN, 0.55 mM N). Root system architecture was assessed after 9 days. Bars represent means \pm s.e. ($n = 14-20$ plants). Different letters indicate significant differences at $P < 0.05$ according to one-way ANOVA and post-hoc Tukey test. Scale bars, 1 cm.

More importantly, in *yucQ* plants the LN-induced primary root and lateral root elongation was completely abolished (Figure 25A-C). Apart from defective root elongation, *yuc5* and *yucQ* plants also formed less lateral roots irrespective of the N condition (Figures 24E and 25E). Consequently, the total root length of *yucQ* plants was significantly decreased, especially at LN (Figure 25D).

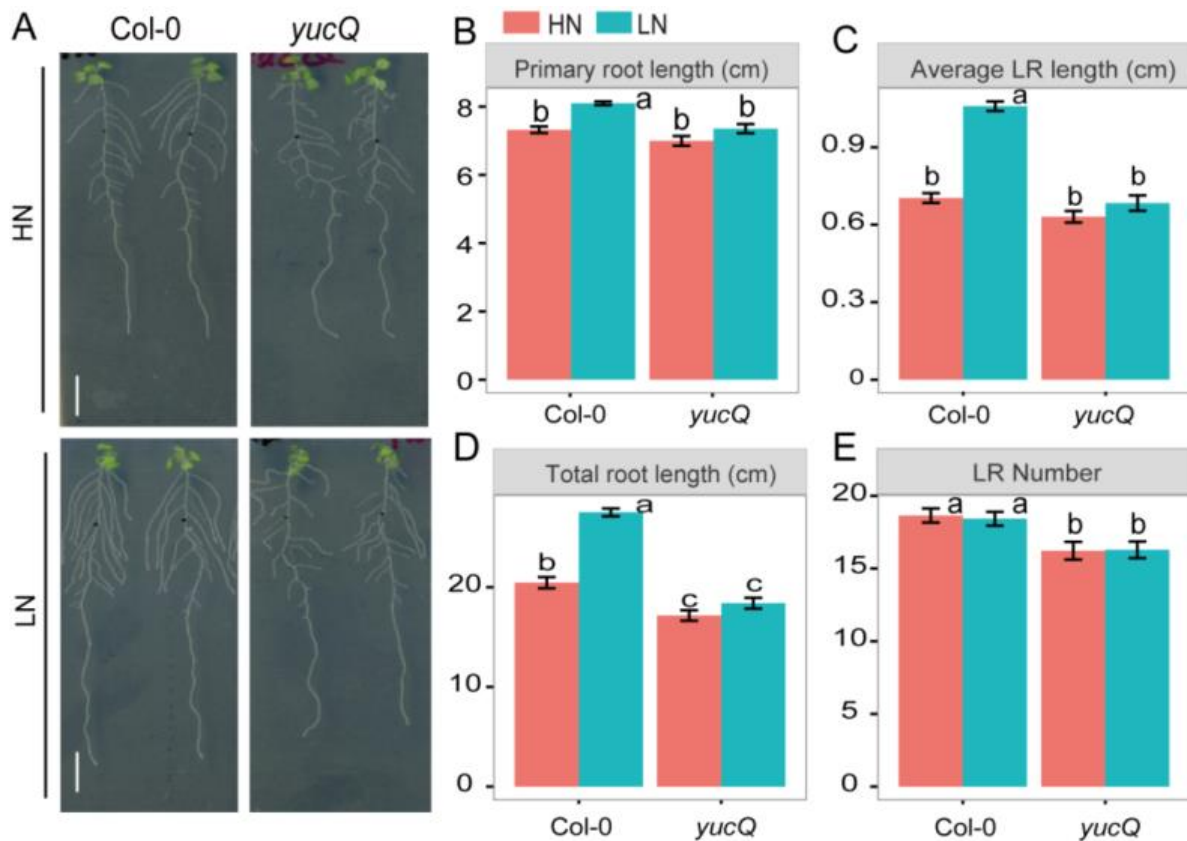


Figure 25. Root architecture of the quintuple *yucQ* (*yuc3,5,7,8,9/DR5-GFP*) mutant in response to low N. (A) Appearance of plants, **(B)** primary root length, **(C)** average lateral root length, **(D)** total root length and **(E)** lateral root number of wild-type (Col-0) and *yucQ* mutant plants grown at high N (HN) or low N (LN) conditions. Seven day-old seedlings were pre-cultured on 11.4 mM N and then transferred to solid agar media containing either high N (HN, 11.4 mM N) or low N (LN, 0.55 mM N). Root system architecture was assessed after 9 days. Bars represent means \pm s.e. ($n = 18-20$ plants). Different letters indicate significant differences at $P < 0.05$ according to one-way ANOVA and post-hoc Tukey test. Scale bars, 1 cm.

To further ascertain that a lack of auxin in *yucQ* plants caused loss of the root foraging response to mild N deficiency, exogenous IAA was supplied to the growth medium to test whether it can recover the root response to LN. Consistent with high concentrations of auxin inhibiting primary root growth (Evans et al., 1994), primary root length gradually decreased in wild type and *yucQ* plants with increasing concentrations of IAA (Figure 26A and B). However, most notably, the response of lateral root length, total root length as well as lateral root number of *yucQ* plants were fully recovered by supplying 50 nM IAA (Figure 26).

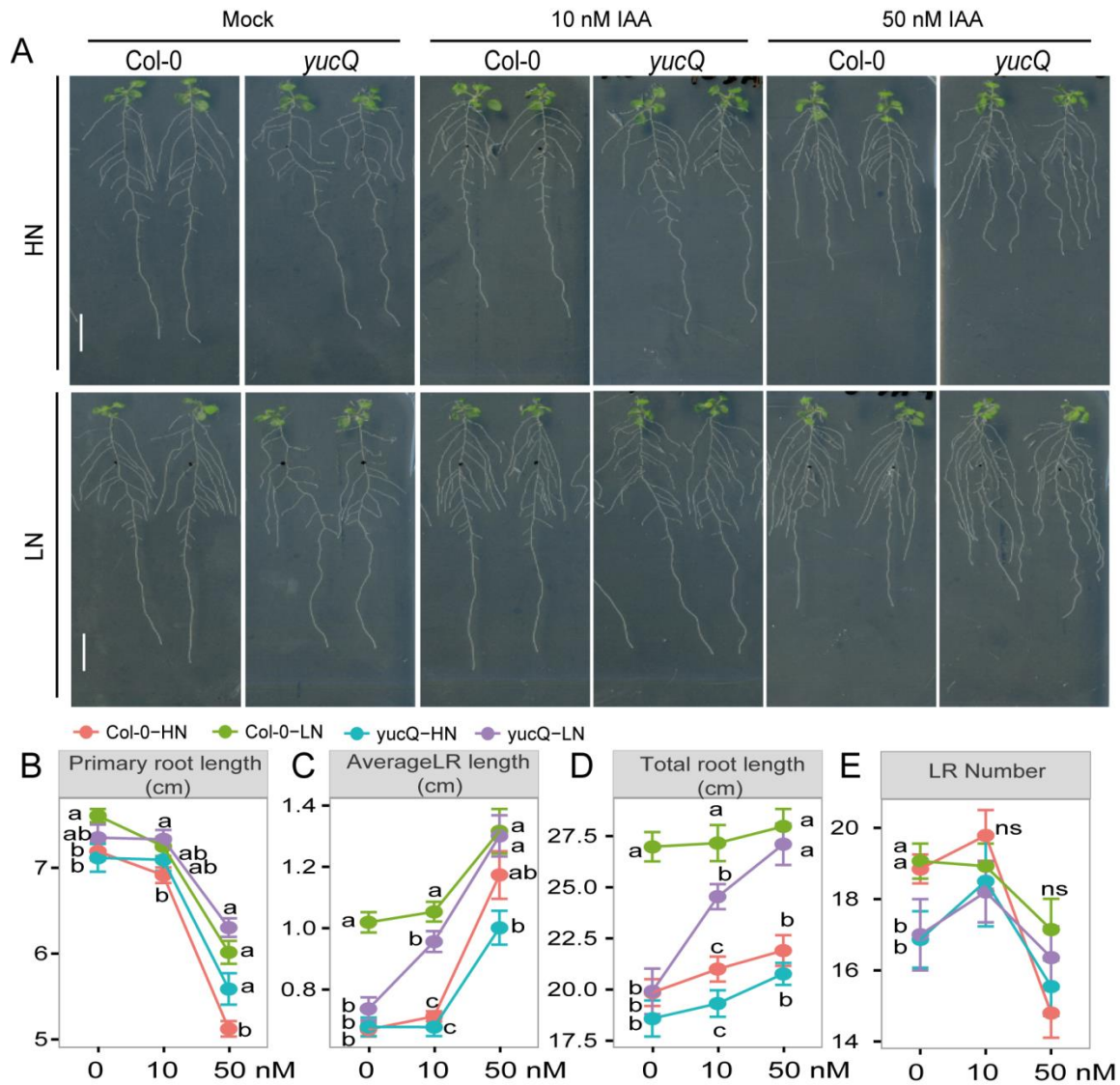


Figure 26. Influence of external auxin supplementation on root architecture of wild-type and *yucQ* mutant plants. (A) Appearance of plants, (B) primary root length, (C) average lateral root length, (D) total root length and (E) lateral root number of wild-type (*Col-0*) and *yucQ* mutant plants grown at high N (HN) or low N (LN) conditions in presence or absence of exogenously supplied IAA at the indicated concentrations. Dots represent means \pm s.e. ($n=13-15$). Different letters indicate significant differences at $P < 0.05$ according to one-way ANOVA and post-hoc Tukey test within each IAA treatment. Scale bars, 1 cm.

Conversely, when PPBo, an inhibitor of YUC protein activity (Kakei et al., 2015), was exogenously supplied to roots of wild-type plants, the mild N deficiency-induced elongation of both primary root and lateral roots was strongly reduced (Figure 27). Altogether, these results suggest that YUCCA-dependent auxin biosynthesis plays a critical role in modulating root elongation under mild N deficiency.

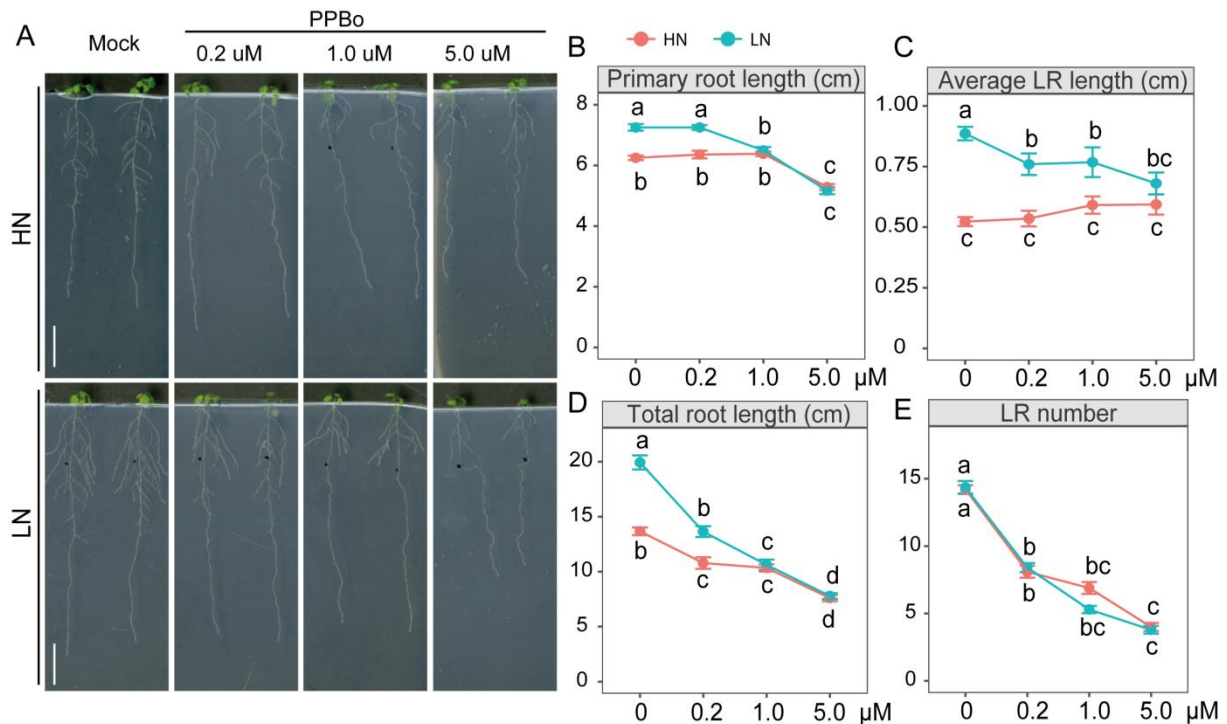


Figure 27. Exogenous application of a YUC inhibitor to roots blocks the root response to low N. (A) Appearance of plants, (B) primary root length, (C) average lateral root length, (D) total root length and (E) lateral root number of wild-type (Col-0) plants grown under various PPBo (4-phenoxyphenylboronic acid) concentrations. Seven day-old seedlings were pre-cultured on 11.4 mM N and then transferred to solid agar media containing either high N (HN, 11.4 mM N) or low N (LN, 0.55 mM N). Root system architecture was assessed after 9 days. Dots represent means \pm s.e. ($n = 14-20$ plants). Different letters indicate significant differences at $P < 0.05$ according to one-way ANOVA and post-hoc Tukey test. Scale bars, 1 cm.

4.7.3 The *yucQ* mutant reduces cell elongation under low nitrogen

Previous experiments with wild-type plants showed that the differential lateral root elongation of accessions under low N was a consequence of cell elongation and, in dependence of the genotype, also of cell division (Figure 6E-J). To understand which cellular process was affected by YUCCA-dependent auxin biosynthesis, meristem size and cortical cell length were measured in lateral roots of wild-type and *yucQ* plants. However, meristem size was not significantly altered by LN, neither in *yucQ* nor in Col-0 plants (Figure 28A and C). This was in agreement with the previous experiment, in which only the accession line Ler but not Col-0 enhanced meristem size under low N (Figure 6E-J). Relative to Col-0, *yucQ* mutant plants constitutively exhibited smaller meristem size and shorter cortical cell length (Figure 28A-D), whereas the LN-induced cell elongation observed in wild-type plants was completely lost in *yucQ* mutant plants (Figure 28B and D). Hence, it was concluded that YUCCA-

dependent auxin biosynthesis stimulates lateral root elongation by increasing cell elongation.

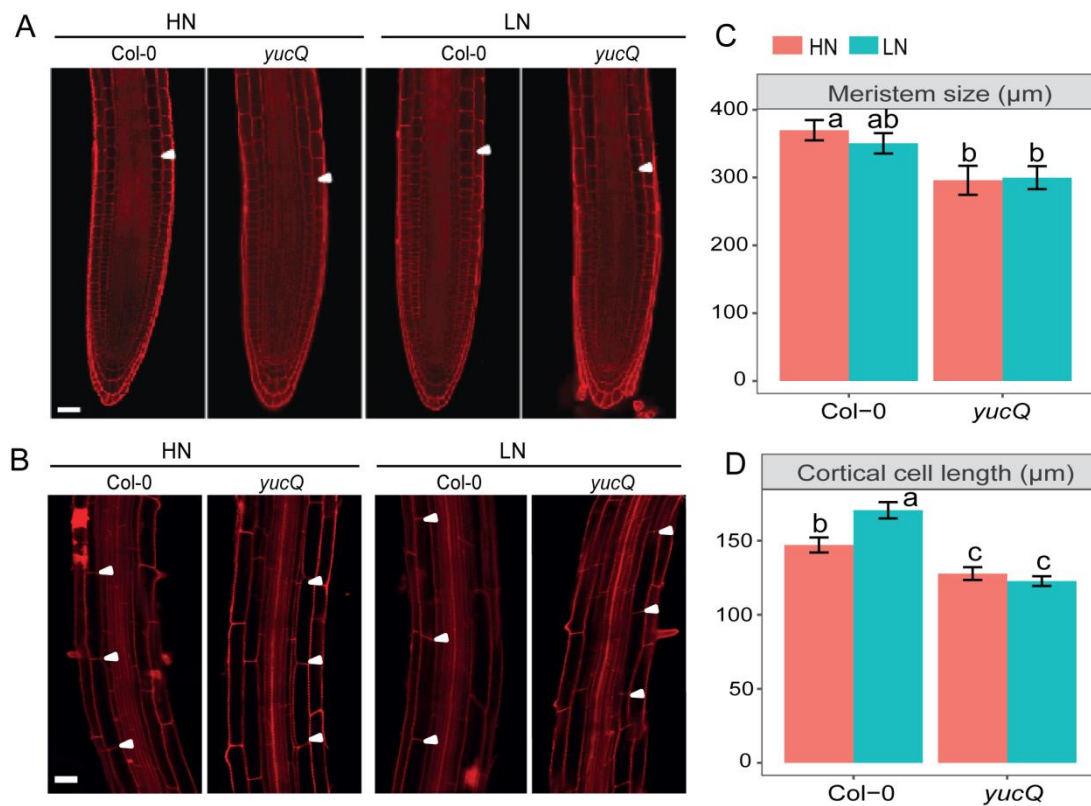


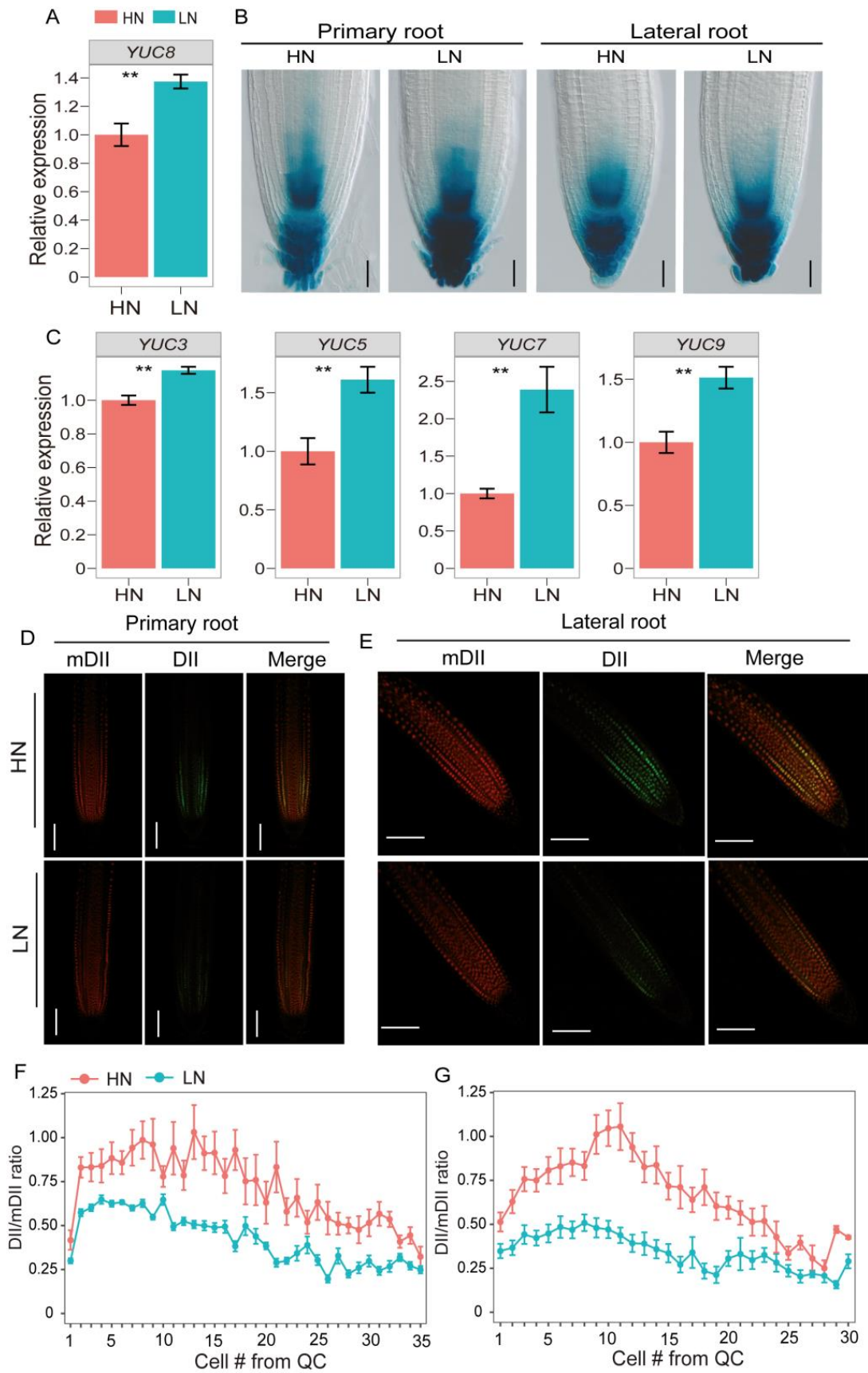
Figure 28. The *yucQ* mutant is defective in low N-induced cell elongation. (A-B) Representative confocal images of the root meristem (A) and of cortical cells (B) of Col-0 and *yucQ* plants grown under HN or LN. White arrows indicate the boundaries of the meristematic zone and elongation zone (A) or of two consecutive cortical cells (B). Scale bars, 50 μm. (C-D) Meristem size (C) and length of cortical cells (D) of Col-0 and *yucQ* mutant plants. Bars represent means ± s.e. (n = 13-16 plants). Different letters indicate significant differences at $P < 0.05$ according to one-way ANOVA and post-hoc Tukey test.

4.7.4 Low nitrogen increases auxin biosynthesis by upregulating gene expression of *YUC8* and some of its homologs

To investigate how *YUC8* and its homologous genes modulate root elongation in response to mild N deficiency, expression levels of *YUC* genes in roots were analyzed at varying external N availability. After exposure to HN or LN for 9 days, mRNA levels of *YUC8* were significantly higher under LN (Figure 29A). Consistent with up-regulation of *YUC8* gene expression at LN, a strong increase of *YUC8*-dependent GUS activity was observed in both primary and lateral root tips at LN compared to HN conditions (Figure 29B). Moreover, apart from *YUC8*, expression levels of *YUC3*, *YUC5*, *YUC7* and *YUC9* were also significantly up-regulated by LN

(Figure 29C), suggesting that low N enhances expression of *YUC8* and its homologs to increase auxin biosynthesis in the root. To test this assumption, local auxin concentrations were monitored by using the ratiometric auxin sensor R2D2, which expresses an auxin degradable reporter protein DII:n3xVenus along with an undegradable protein mDII:ntdTomato under the control of an *RPS5A* promoter and thus allows the quantitative assessment of relative auxin levels in the root (Liao et al., 2015). At LN, the auxin-insensitive mDII:ntdTomato signal remained stable, whereas DII-Venus-dependent fluorescence became much weaker in both primary and lateral root tips (Figure 29D-E). Compared to HN, DII-Venus fluorescence intensity, normalized to mDII tomato fluorescence, remarkably decreased at LN in the apices of both primary and lateral roots (Figure 29F-G), suggesting higher auxin accumulation at LN in the root apex. This matches the enhanced promoter activity of *YUC8* in the meristematic zone (Figure 28B). In summary, these results indicate that mild N deficiency induces expression of *YUC8* and its closely related genes to enhance auxin concentrations in the root meristematic zone, thereby stimulating root elongation.

Figure 29. The expression of *YUC8* and its closely related homologous genes is up-regulated by low N. (A-C) Transcript levels of *YUC8* (A), *proYUC8*-dependent GUS activity (B) and transcript levels of *YUC3*, *YUC5*, *YUC7*, *YUC9* (C) in response to high N (HN) or low N (LN) availabilities. Seven day-old seedlings were pre-cultured on 11.4 mM N and then transferred to solid agar containing either high N (HN, 11.4 mM N) or low N (LN, 0.55 mM N). Samples for qPCR analysis and GUS activity assays were taken 9 days after transfer. Transcript levels (A and C) were assessed in whole roots by qPCR analysis and normalized to *ACT2*. Bars represent means \pm s.e. ($n = 4$ independent biological replicates). Asterisks indicate statistically significant differences between two N conditions according to Welch's *t* test (** $P < 0.01$). (D-E) Representative images of apical root tips expression mDII-tomato (left), DII-Venus (middle), or both (merged; right) for primary (D) and lateral roots (E). (F-G) DII-Venus/mDII tomato fluorescence intensity ratio of epidermal cells in primary (F) and lateral roots (G). Bars represent means \pm s.e. ($n=10-12$ plants). Scale bars, 100 μ m.



→ Descriptions were shown on previous page.

4.7.5 Allelic variation of *YUC8* determines lateral root elongation under low nitrogen

To understand how *YUC8* affects phenotypic variation of average lateral root length, firstly transcript levels of *YUC8* were determined in nine representative accessions showing different lateral root responses to LN (Figure 30A). Although variation in *YUC8* mRNA levels was observed among different accessions, neither absolute transcript levels of *YUC8* at HN or LN nor their fold-change under LN relative to HN were significantly correlated with average lateral root length or the lateral root response (Figure 30B and C), indicating that *YUC8*-dependent natural variation under low N is likely not due to differences in gene expression. In the next step, predicted protein sequences of *YUC8* were examined in 139 re-sequenced lines that have been phenotyped in the current experiment to search for variation in the protein-coding sequence. Within the coding sequences of *YUC8* 17 SNPs (MAF>5%) were found, of which 15 led to synonymous substitutions and hence were unlikely causal for the phenotypic variation (Figure 30D). Interestingly, two SNPs (T41C and A42T) in LD with the detected GWA SNP (T45A) together resulted in a leucine (L) to serine (S) substitution at position 14 (Figure 30D). This non-synonymous mutation is 14 amino acids upstream of the FAD-binding motif, which is critical for enzyme activity (Hou et al., 2011; Dai et al., 2013). A significant association was observed between protein haplotypes and average lateral root length, as at low N L-haplotypes displayed longer average lateral root length than S-haplotypes, whereas they were similar at HN (Figure 30E). These results indicate that an L to S substitution in *YUC8* is causal for phenotypic variation of lateral root length at LN.

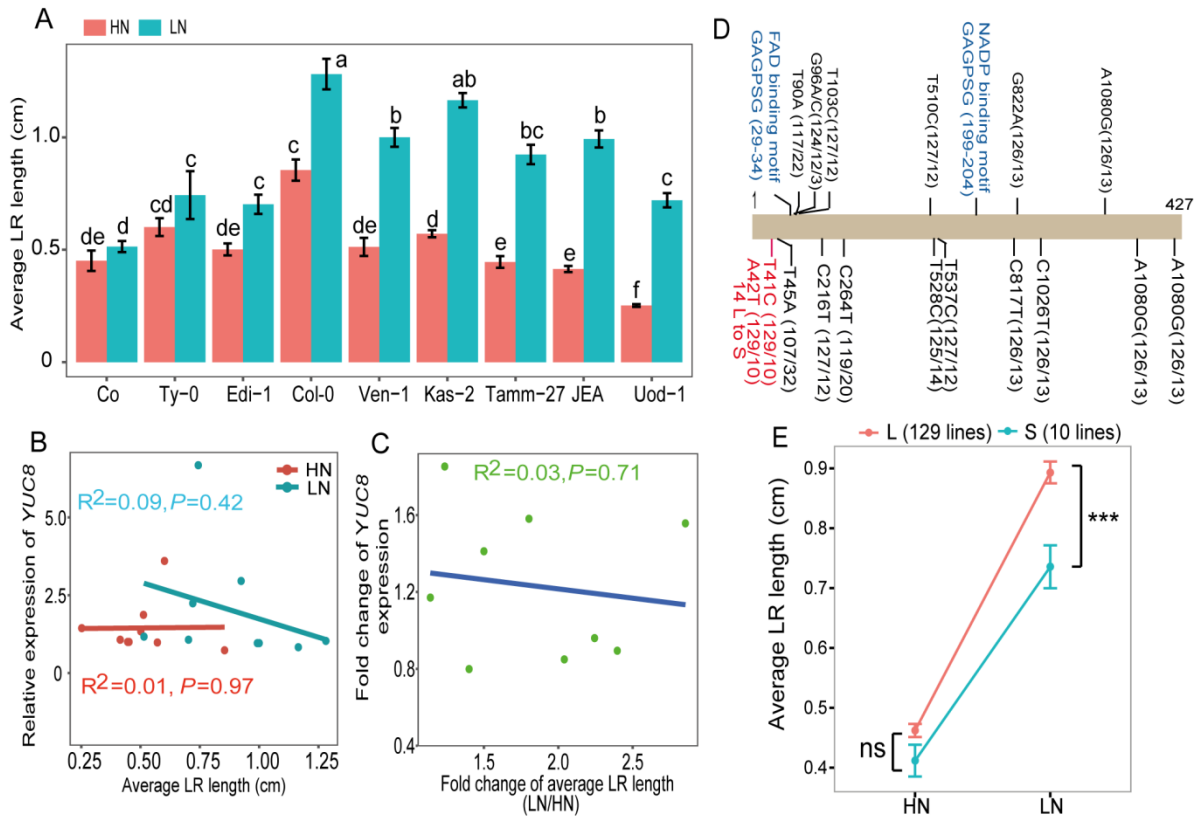


Figure 30. Allelic variants of *YUC8* associate with lateral root length. (A) Average length of lateral roots of nine natural accessions used for gene expression analysis under HN or LN. Seven day-old seedlings pre-cultured on 11.4 mM N were transferred to solid agar containing either high N (HN, 11.4 mM N) or low N (LN, 0.55 mM N). Average lateral root length was determined after 9 days. Bars represent means \pm s.e. ($n = 10-12$ plants). **(B)** Correlation between *YUC8* transcript levels in roots and average lateral root length under HN or LN. **(C)** Correlation between fold-change in *YUC8* transcript levels under LN versus HN with relative average lateral root length at two N conditions. Analysis was carried out in nine natural accessions with contrasting average lateral root length under high N or low N. **(D)** Schematic representation of SNPs identified in *YUC8* coding sequences according to genome sequencing data for 139 accession lines. Location, nucleotide polymorphism and critical function motif (in blue) are shown, with the non-synonymous substitution colored in red. Numbers in brackets denote the number of lines carrying the corresponding allele. **(E)** Average lateral root length of natural accessions representing two *YUC8* protein haplotypes ($n = 129$ and 10 accessions for L and S haplotypes, respectively). Asterisks indicate significant differences between two N conditions according to Welch's *t* test ($***P < 0.001$, ns, not significant).

To directly test whether the L/S substitution is causal for the phenotypic variation, an allele swapping approach was performed by introducing different suits of *YUC8* promoters and coding sequences into *yucQ* to test their efficacy to recover root growth of the quintuple mutant (*yucQ*). Three promoters, either from accession Uod-1 and Col-0 encoding the L-type protein, or from Co encoding the S-type protein were chosen, because they displayed a strong, intermediate or weak response of lateral root growth to low N. In addition, these lines differ in their expression levels of *YUC8* (Figure 31A and B). Initially, these transgenic lines were tested on high sucrose to

compare the complementation efficacy of different promoter and protein variants in rescuing *yucQ* root growth, as this high sucrose condition severely inhibits root growth of *yucQ* plants (Chen et al., 2014; Liu et al., 2016; Figures 31C-D).

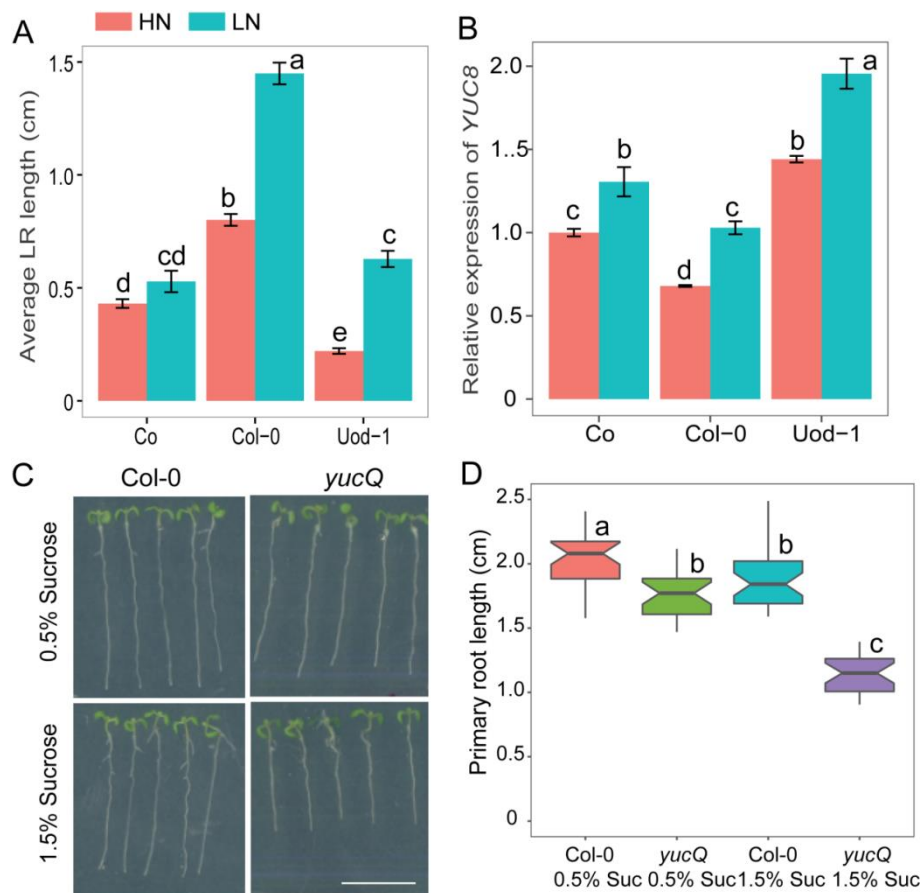


Figure 31. Lateral root length and expression of *YUC8* in natural accessions chosen for complementation and root growth analysis of *yucQ* under high sucrose. (A) Average lateral root length and **(B)** relative transcript levels of *YUC8* of three lines showing different lateral root lengths and responses to low N. Seven day-old seedlings pre-cultured on 11.4 mM N were transferred to solid agar containing either high N (HN, 11.4 mM N) or low N (LN, 0.55 mM N). Average length of lateral roots was determined after 9 days. Bars represent means \pm s.e. ($n = 10-12$ plants). Transcript levels were assessed in whole roots by *qPCR* analysis and normalized to *ACT2*. Bars represent means \pm s.e. ($n = 4$ independent biological replicates). **(C-D)** Appearance of plants **(C)** and primary root length **(D)** of Col-0 and *yucQ* plants. Seeds were germinated on solid media containing 11.4 mM N and either 0.5% or 1.5% sucrose. Primary root length was assessed 7 days after germination ($n=26-35$ plants). Different letters indicate significant differences at $P < 0.05$ according to one-way ANOVA and post-hoc Tukey test. Scale bar, 1 cm.

Transgenic lines expressing the *YUC8-L* allele rescued more efficiently primary root length and growth rate than lines expressing the *YUC8-S* allele (Figure 32A-C). Notably, this effect was independent of the promoter sequence used to drive *YUC8-L*

expression (Figure 32A-C). Since overproduction of auxin promotes hypocotyl elongation (Zhao et al., 2001; Chen et al., 2014), two YUC8 alleles were also overexpressed in either the wild-type or the *yucQ* background using the CaMV 35S promoter. Although overexpression of both variants could promote hypocotyl elongation compared to respective background, overexpression lines with the YUC8-L allele showed significantly longer hypocotyls than those expressing the YUC8-S allele (Figure 32D and E). These results suggested that the YUC8-L allele is more efficient in auxin biosynthesis than the YUC8-S allele.

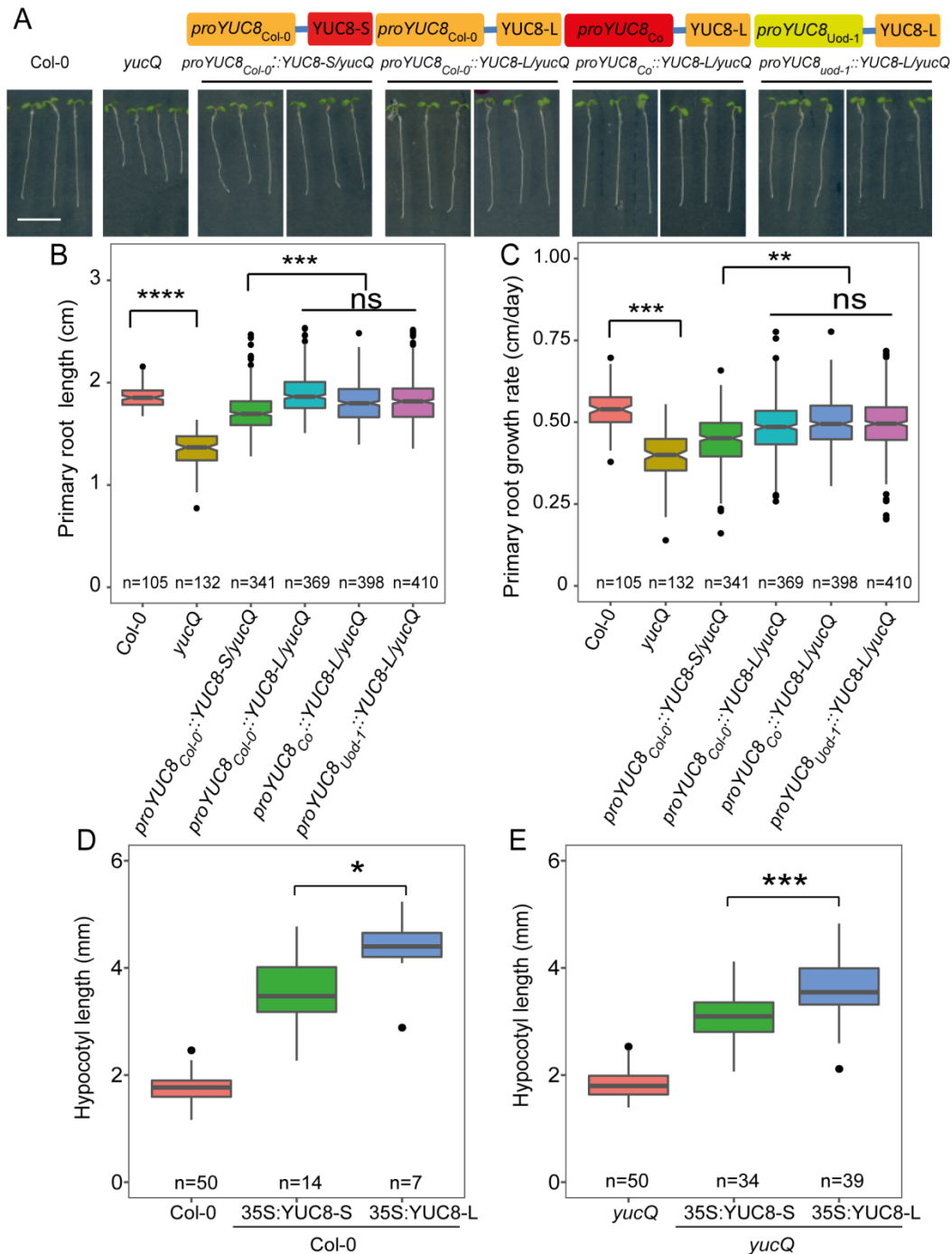


Figure 32. Allelic variation of *YUC8* determines root growth. (A) Schematic of transgenic constructs used to complement the *yucQ* mutant and photographs of representative 7 day-old plants. Scale bar, 1 cm. **(B-C)** Primary root length **(B)** and growth rate **(C)** of 20 independent transgenic T2 lines for each construct. Seeds were germinated on solid media containing 11.4 mM N and 1.5% sucrose. Primary root length was assessed 7 days after germination and growth rate was calculated by determining the primary root length of the same plants 7 and 9 days after germination. **(D-E)** Hypocotyl length of overexpression lines in the background of Col-0 **(D)** or *yucQ* **(E)** as determined in independent transgenic T1 lines. Here, numbers indicate independent T1 transgenic events for 35S::*YUC8*-S or 35S::*YUC8*-L in either the Col-0 or *yucQ* mutant background. For Col-0 and *yucQ*, 50 individuals were measured for hypocotyl length. Asterisks indicate significant differences according to Welch's *t* test (* $P < 0.05$, ** $P < 0.01$, *** $P < 0.001$, **** $P < 0.0001$, ns, not significant).

Previous experiments indicated that mild N deficiency enhances auxin biosynthesis to promote root growth (Figures 22-27). Therefore, plants were grown under N deficiency to verify whether allelic variation in *YUC8* is relevant for root growth. Root architectural traits of wild type (Col-0), *yucQ*, and 12 independent transgenic lines (6 for the YUC8-L allele and 6 for the YUC8-S allele) were examined under LN condition. Consistent with the initial experiments (Figure 25), *yucQ* plants displayed significantly shorter primary and LRs and formed less LRs, which finally resulted in strong reduction of total root length compared to the wild type (Figure 33). Whereas complementation with the YUC8-S allele could only partially rescue root growth of *yucQ* plants under LN, the expression of YUC8-L enabled full recovery of primary root and LR lengths, as well as LR number (Figure 33). Thus, it was concluded that allelic variation of *YUC8* contributes to the natural variation of root elongation under mild N deficiency.

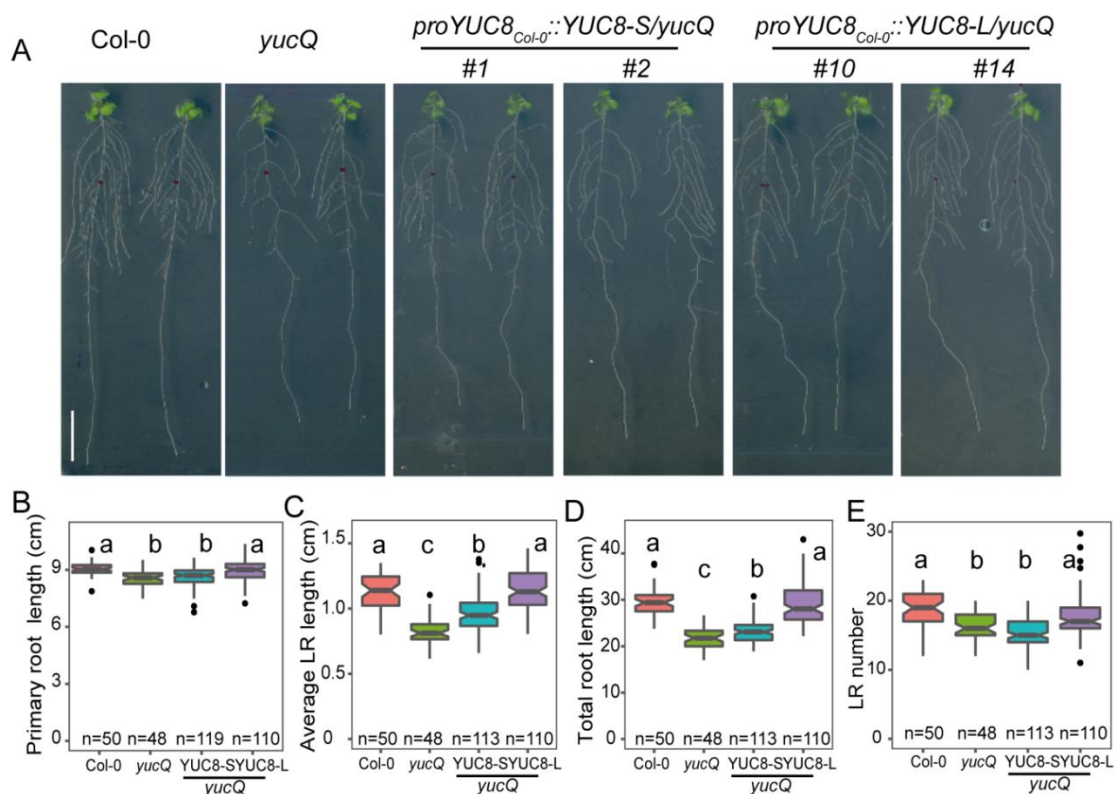


Figure 33. *YUC8* allelic variants associate with root length at low N. (A) Appearance of plants, **(B)** primary root length, **(C)** average lateral root length, **(D)** total root length and **(E)** lateral root number under LN of Col-0, *yucQ* and transgenic lines expressing sequences coding for either the YUC8-L (6 independent lines) or YUC8-S (6 independent lines) variant under control of the *YUC8*_{Col-0} promoter. Seven day-old seedlings were pre-cultured on 11.4 mM N and then transferred to low N (0.55 mM N). Root system architecture was assessed after 9 days. Different letters indicate significant differences at $P < 0.05$ according to one-way ANOVA and post-hoc Tukey test. Scale bar, 1 cm.

4.7.6 Growth responses of allelic variants of YUC8 associate with temperature variability

Arabidopsis colonizes a large range of environments and hence the genetic and related phenotypic variation likely reflects an adaptive response to the local environment. To investigate whether lateral root growth has a role in environmental adaption, correlations were calculated between the lateral root response and 19 climate variables as well as geographical locations, as expressed by longitude and latitude. Significant correlations were detected between the lateral root response and 9 temperature- and 5 precipitation-related variables (Supplemental Table 5). When performing a partial Mantel test to associate the GWA SNP with climate variables while accounting for population structure, it was found that the GWA SNP was significantly associated with several temperature- and precipitation-related parameters, in which the strongest association was observed for temperature seasonality (Supplemental Table 6). Surprisingly, a clear association between the allelic variation of YUC8 and temperature-related variables was observed, where accessions harboring the YUC8-L allele associated with a significantly higher mean diurnal temperature range, temperature seasonality, mean temperature of wettest quarter and annual temperature range as compared to accessions with the YUC8-S variant (Figure 34). These results suggest that allelic variants of YUC8 may play a role in the adaptation of Arabidopsis to locations with large temperature fluctuations.

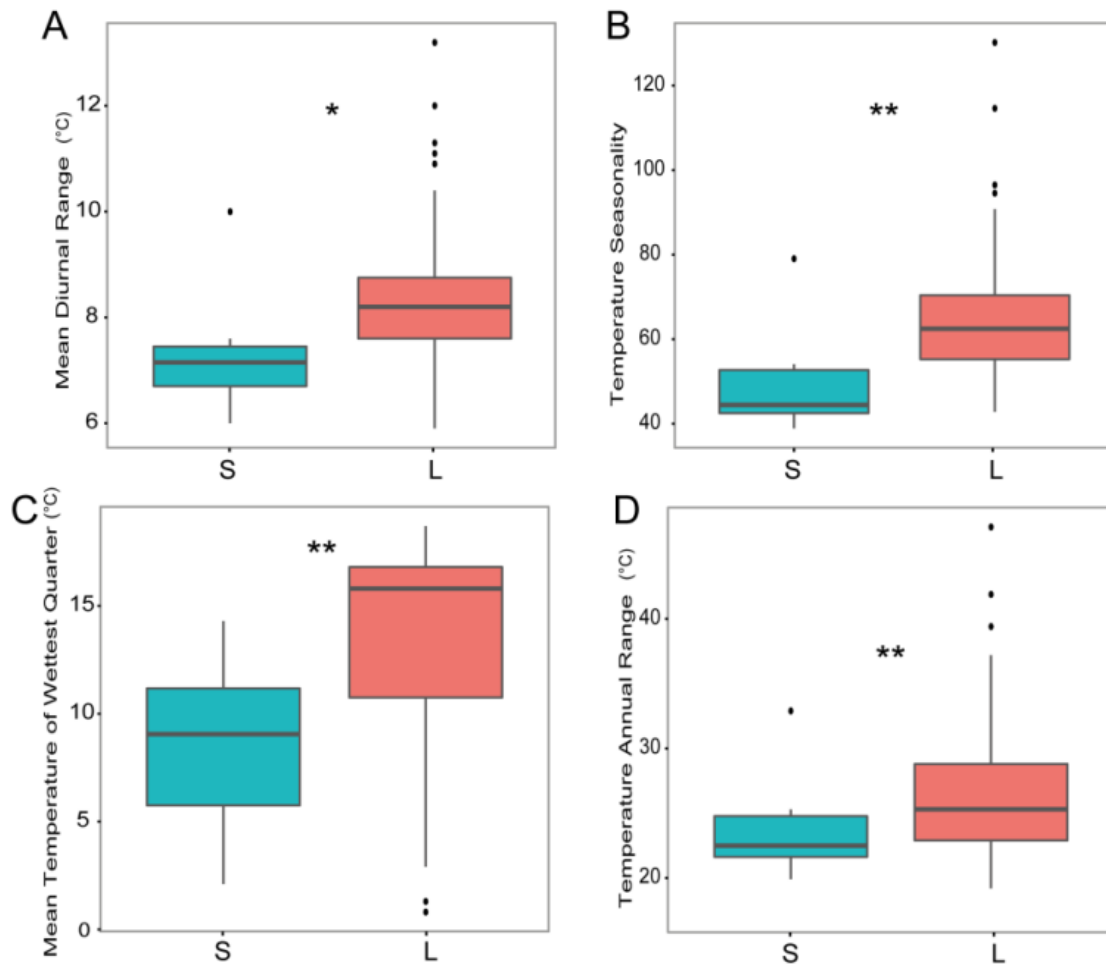


Figure 34. Temperature as putative selection factor for YUC8 variants. (A-D) Boxplot showing the association between YUC8-L or -S haplotypes and temperature variables in the geographic location of the accession lines in terms of mean diurnal temperature range (A), temperature seasonality (B), mean temperature of wettest quarter (C) and annual temperature range (D). Asterisks indicate significant differences according to Welch's *t*-test (* $P < 0.05$, ** $P < 0.01$), ($n = 107$ and 8 accessions for L and S haplotypes, respectively).

To test the hypothesis that YUC8 variants are associated with temperature variability, wild-type, *yucQ* and complementation lines expressing either the YUC8-L or -S allele were grown in a different diurnal temperature range, i.e. at a 19°C/ 22°C or 19°C/ 29°C temperature regime. Consistent with previous findings that high temperatures promote hypocotyl and petiole elongation in an auxin-dependent manner (Franklin et al., 2011; Sun et al., 2012; Lee et al., 2014), the hypocotyl and petiole elongation of wild-type plants were significantly increased by 60% and 80%, respectively, when grown at 19°C/29°C. However, these growth responses were largely attenuated in *yucQ* plants (20% and 33% for hypocotyl and petiole elongation, respectively; Figure 35A-C). At high temperature, complementation of the YUC8-S allele only led to a

partial rescue of hypocotyl and petiole elongation of *yucQ* plants, while expression of the YUC8-L allele was able to rescue hypocotyl as well as petiole elongation to a significantly larger extent than the YUC8-S variant (Figure 35B and C). These results suggest that S-to-L variation in YUC8 promotes growth responses and thus phenotypical adaptation to elevated temperature.

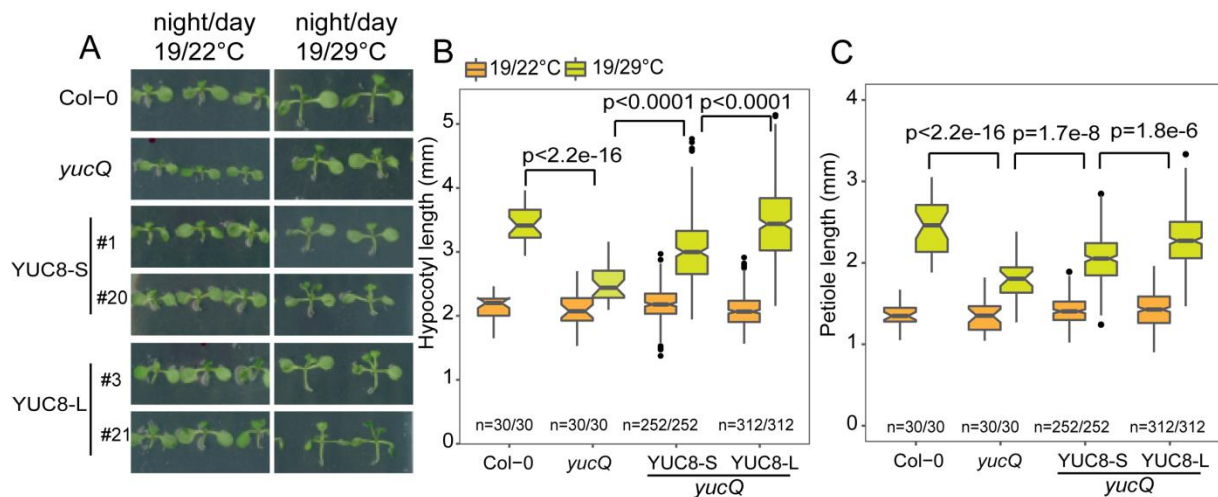


Figure 35. Phenotypic analysis of allelic variants of YUC8 under different temperature regimes. (A-C) Appearance of plants (A), hypocotyl length (B) and petiole length (C) of wild-type (Col-0), *yucQ* and T2 transgenic lines expressing the coding sequences for either the YUC8-L ($n=26$ independent lines) or YUC8-S ($n=21$ independent lines) variant under the control of the $YUC8_{Col-0}$ promoter. Plants were grown at high N (HN) at a 19°C/22°C or 19°C/29°C temperature and 10h/14h day/night regime. *P* values for indicated pairwise comparisons were calculated using Welch's *t*-test.

4.8 Identification of *DWF1* and characterization of its role in root responses to low nitrogen supply

4.8.1 Natural variation of total lateral root length and total root length under two N supply levels

Besides the primary root and average lateral root length, total lateral root length as well as total root length was also measured for the same diverse panel of 200 accessions of *A. thaliana* (Supplementary Table 1) at the two N concentrations described above. There was a wide range of phenotypic variation in both total lateral root length and total root length at the respective N environments (Figure 36A and B, Table 1 and Supplementary Table 1). Total lateral root lengths ranged from 4.9 cm to 29.7 cm at HN and from 12.7 cm to 57.9 cm at LN (Figure 36A; Table 1; Supplementary Table 1). Similarly, total root lengths ranged from 9.7 cm to 37.9 cm at HN and from 16.2 cm to 69.5 cm at LN (Figure 36B; Table 1; Supplementary Table 1). Although total lateral root length significantly correlated with total root length both within and across N treatments, correlations depended on N treatments (Figure 36C), suggesting a significant variation in the accession-dependent response to low N. In support of this view, the broad-sense heritability (h^2) was estimated, ranging from 88.5% to 89.4% (Table 1). On average, total lateral root length and total root length of all examined accessions increased by 100% and 70% at LN compared to HN, respectively ($P < 2.2e-16$; Figure 36A and B; Table 1).

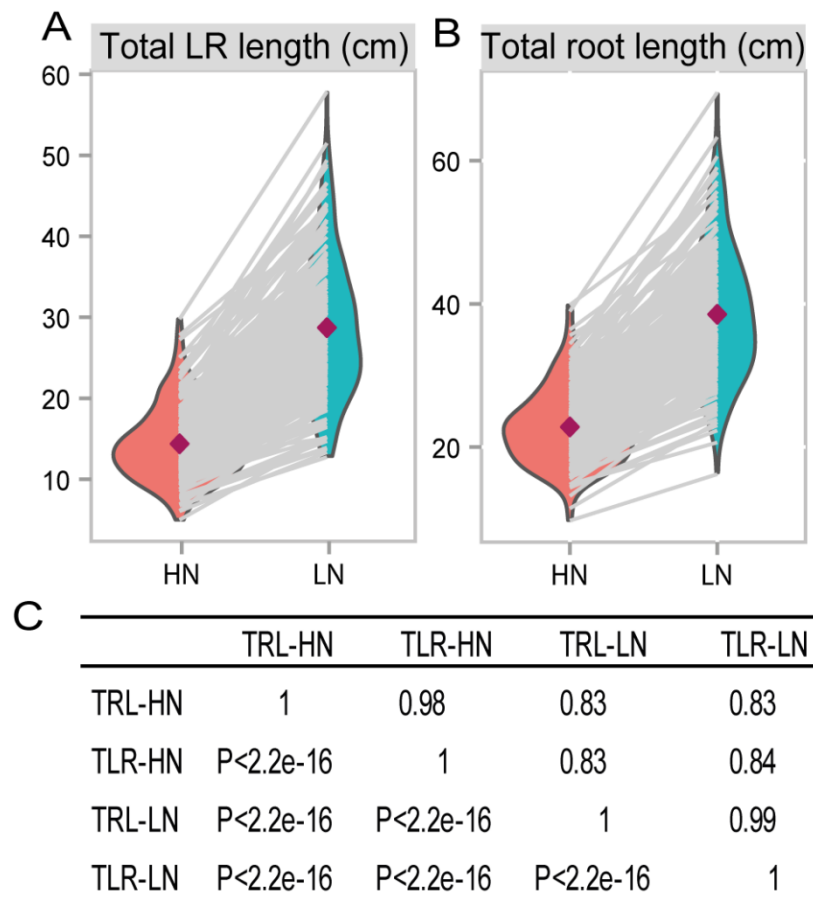


Figure 36. Natural variation of total lateral root length and total root length under two N environments. Seven day-old seedlings pre-cultured on 11.4 mM N were transferred to solid agar media containing either high N (HN, 11.4 mM N) or low N (LN, 0.55 mM N). Total LR length and total root length were determined after 9 days. **(A and B)** Reaction norms and phenotypic variation of total LR length and total root length of 200 natural accessions of *A. thaliana* under different N supplies. Purple diamonds represent means of total LR length and total root length for 200 accessions under each N treatment. **(C)** Correlations for total LR length and total root length within and across N environments. Upper right values show the coefficients of correlation, while lower left values indicate *P*-values of the correlations.

4.8.2 GWAS maps natural variation of total lateral root length and total root length under low nitrogen to *DWF1*

To identify genetic factors controlling total lateral root length and total root length, GWAS was performed to associate the phenotypic variation of total root length and total lateral root length to the genetic variation present in 200 accession lines. QTLs were detected using a mixed-linear model correcting for population structure (Kang et al., 2008). Unlike the GWAS outcome for primary root or average lateral root length, which detected prominent QTLs (Figures 7B and 21C-E), there were no genome-wide significant associations detected for either trait under any of the two N environments (Figure 37). However, as complex traits are usually controlled by

multiple genes with small to moderate effects (Kooke et al., 2016), GWAS cannot assure the identification of genome-wide significant associations. In support of this view, two groups of SNPs on chromosome 5 with $-\log_{10}(P\text{-value})$ of 4.85 and 4.89 were mapped in *ASA1/WEI2* (3 SNPs, position: 1720343 bp, 172166 bp and 1721826 bp) and close to *miRNA166* (2 SNPs, position: 16756603 bp and 16756753 bp). These genes are known to control root development (Sun et al., 2009, Carlsbecker et al., 2010; Figure 37A and C). In agreement with a previous study (Sun et al., 2009), the *wei2-2* mutant showed a significantly shorter primary root and formed less lateral roots, resulting in a significant reduction in total root length under either N environment (Figure 38). Despite this promising phenotype, investigations on *WEI2* were not pursued. For *miRNA166*, no deletion mutant was available. Nevertheless, these results suggested that more hidden but true associations could be uncovered by applying a lower significance threshold. When lowering the significant threshold to $-\log_{10}(P\text{-value})=5$, a total of 6 marker-trait associations was identified at low N, with 5 associations on chromosome 3 and 1 on chromosome 1 (Figure 37). The most significant association was repeatedly detected for both total lateral root length and total root length and located on chromosome 3 (position: 6869961bp). To identify candidate genes underlying this association, all annotated genes were inspected that centered in a 20-kb interval around this SNP. Among the genes in this region, *DWF1* (At3g19770) was identified, which is allelic to *DIM1/CBB1* and catalyzes an early step in BR synthesis (Klahre et al., 1998, Youn et al., 2018). Importantly, the known function of *DWF1* in cell elongation (Takahashi et al., 1995) is highly consistent with the growth effect at LN, which promotes root elongation through cell elongation. These results suggested *DWF1* as promising candidate underlying the marker-trait association on chromosome 3 (Chr 3_6869961, Figure 37B and D).

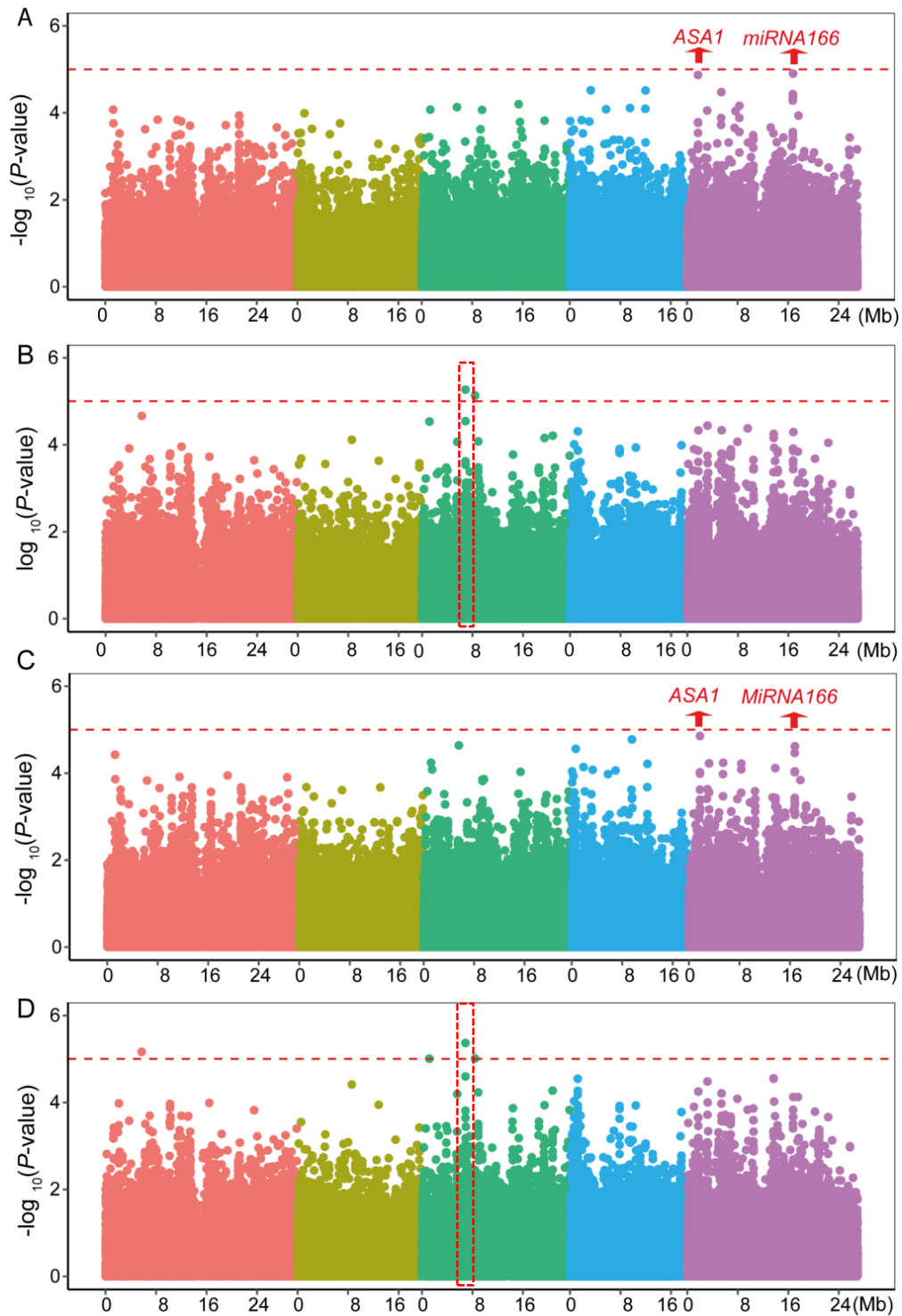


Figure 37. GWAS maps natural variation of total lateral root length and total root length under low N to *DWF1*. (A-D) Manhattan plots for SNP associations with total lateral root length under HN (A) or LN (B), or total root length under HN (C) or LN (D) performed with EMMA package. Negative \log_{10} -transformed P values from a genome-wide scan were plotted against positions on each of the five chromosomes of *A. thaliana*. Chromosomes are depicted in different colors (I to V, from left to right). The red dashed line corresponds to an arbitrary significance threshold value of $-\log_{10}(P\text{-value})=5$. The genomic region associated with the *DWF1* locus under LN is marked in a red frame. Two groups of SNPs on chromosome 5 associated with the two genes *ASA1* and *miRNA166* (marked in red).

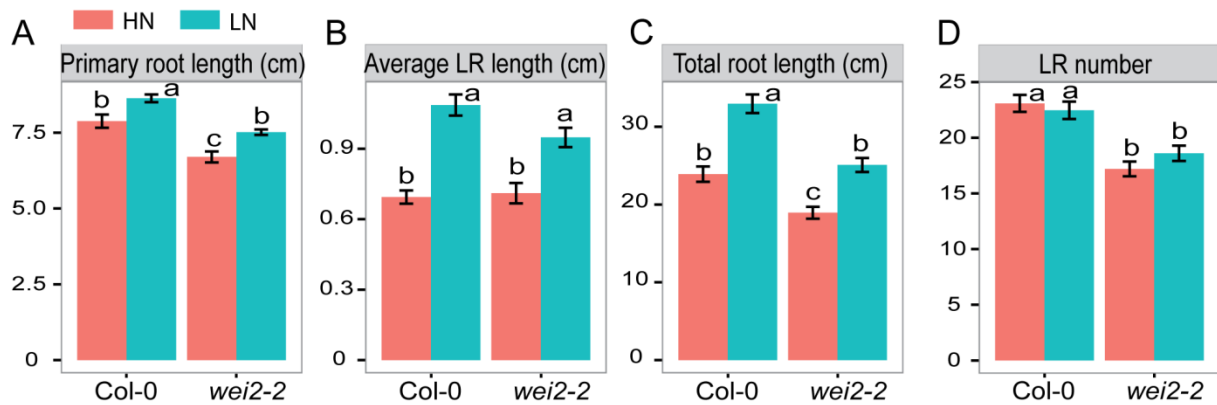


Figure 38. The *wei2-2* mutant exhibits shorter root length irrespective of N supply. Seven day-old seedlings were pre-cultured on 11.4 mM N and then transferred to solid agar media containing either high N (HN, 11.4 mM N) or low N (LN, 0.55 mM N). Root system architecture was assessed after 9 days. **(A)** Primary root length, **(B)** average lateral root length, **(C)** total root length and **(D)** lateral root number of wild-type (Col-0) and *wei2* mutant plants. Bars represent means \pm s.e. ($n = 10-13$ plants). Different letters indicate significant differences at $P < 0.05$ according to one-way ANOVA and post-hoc Tukey test.

To test the putative role of *DWF1* in regulating root responses to LN, root system architectural traits were characterized in two loss-of-function mutant alleles (*cbb1* and *dwf1*) and their respective wild types. Although *cbb1* and *dwf1* mutants showed significantly shorter primary and lateral roots under both N conditions, the response of lateral roots to LN was significantly attenuated by 24% and 28% for *cbb1* and *dwf1*, respectively (Figure 39A-E). As a consequence, total root length was significantly decreased by 20% and 25% compared to their respective wild types C24 and Col-0 (Figure 39F-G). However, none of mutants showed significant differences in lateral root density when compared to their wild types (Figure 39H-I). Thus, these results indicate that *DWF1* is involved in the root elongation response to LN.

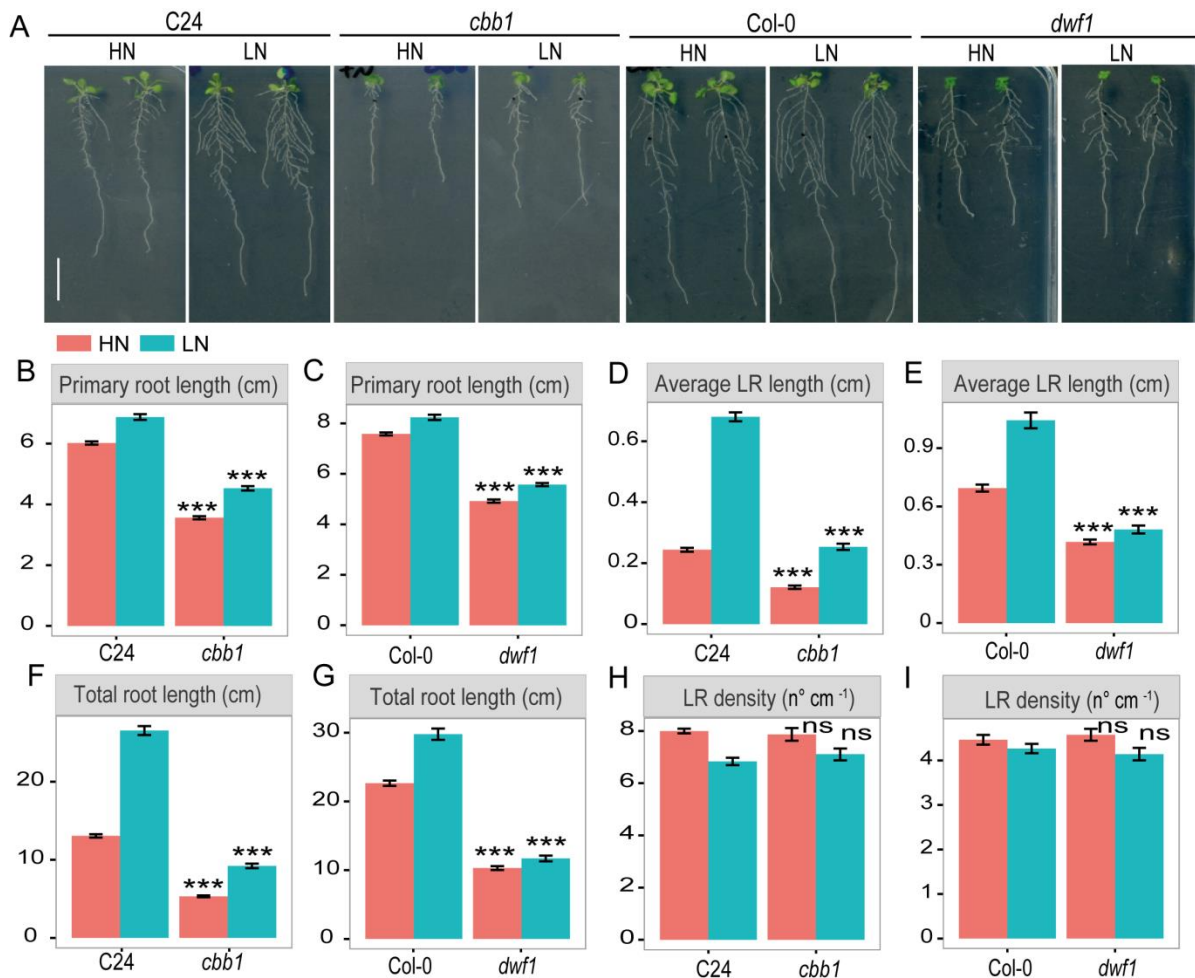


Figure 39. Root architecture of *dwarf1* mutants in response to low N. Seven day-old seedlings were pre-cultured on 11.4 mM N and then transferred to solid agar media containing either high N (HN, 11.4 mM N) or low N (LN, 0.55 mM N). Root system architecture was assessed after 9 days. **(A)** Appearance of plants, **(B-C)** primary root length, **(D-E)** average lateral root length, **(F-G)** total root length and **(H-I)** lateral root density of wild-type and two *dwarf1* mutant alleles. Bars represent means \pm s.e. ($n = 16-24$ plants). Asterisks indicate significant differences between mutants and corresponding wild types according to Welch's *t*-test (** $P < 0.001$, ns, not significant). Scale bar, 1 cm.

4.8.3 Low nitrogen upregulates gene expression of *DWF1*

To address how *DWF1* regulates the root growth response to LN, *qPCR* was carried out to investigate whether *DWF1* expression is regulated by N availability. After growing roots under HN or LN for 9 days, expression of *DWF1* was significantly up-regulated by LN (Figure 40A). This was also validated in a *proDWF1*-GUS reporter line, which revealed stronger intensities of GUS staining in the root apices of both primary and lateral roots grown under LN (Figure 40B). To better understand the role of *DWF1* in lateral root development, promoter activities of *DWF1* were monitored in lateral roots at different developmental stages (Malamy & Benfey, 1997). In a short-term staining, there was no detectable GUS staining in non-emerged and newly

emerged lateral root primordia. However, promoter activity of *DWF1* increased when lateral roots started elongation (Figure 40C-F). Intense GUS staining was observed in the elongation and maturation zone of lateral roots grown under LN compared to HN (Figure 40F-G). In summary, these data suggest that the expression level of *DWF1* is up-regulated by LN and spatially coincides with the root elongation zone, suggesting that *DWF1* contributes to cell elongation.

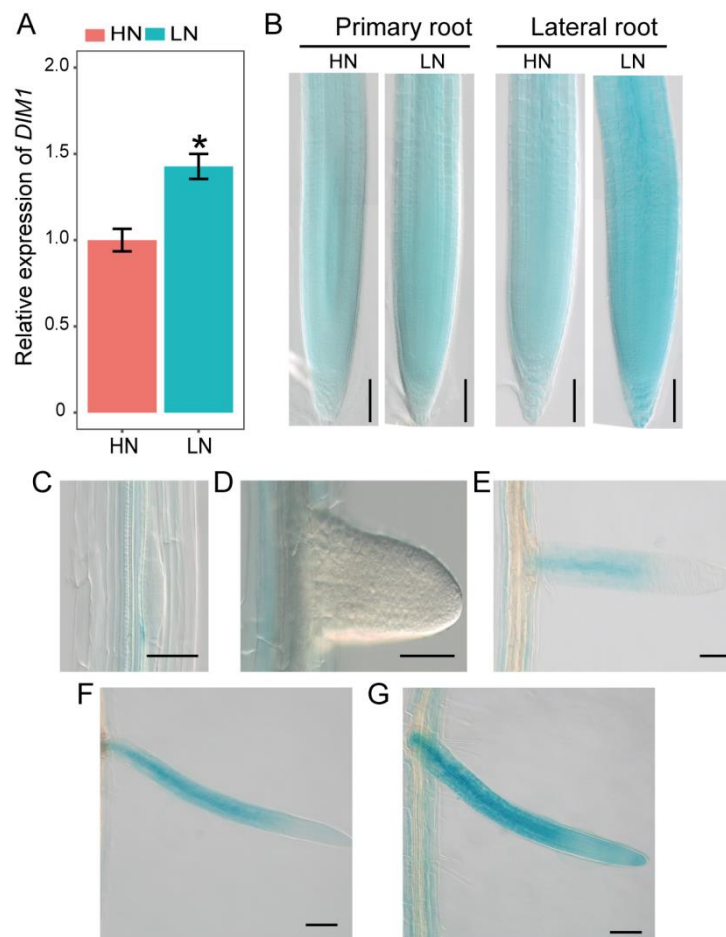


Figure 40. Low nitrogen up-regulates transcript levels and promoter activity of *DWF1*. Seven day-old seedlings were pre-cultured on 11.4 mM N and then transferred to solid agar containing either high N (HN, 11.4 mM N) or low N (LN, 0.55 mM N). Samples for qPCR analysis and GUS activity assays were taken 9 days after transfer. **(A)** *DWF1* transcript levels in response to high N (HN) or low N (LN) availabilities. *DWF1* expression levels were assessed in whole roots by qPCR analysis and normalized to *ACT2*. Bars represent means \pm s.e. ($n = 3$ independent biological replicates) and asterisks indicate significant differences between two N environments according to Welch's *t* test ($*P < 0.05$). **(B)** *proDWF1*-dependent GUS activity was assessed in primary and LR tips. **(C-E)** *proDWF1*-dependent GUS activity in lateral root primordia **(C)**, emerged lateral roots **(D)** and in elongated lateral roots **(E)**. **(F-G)** *proDWF1*-dependent GUS activity in elongated lateral roots grown under HN **(G)** or LN **(F)**. In this experiment, the GUS assay was conducted after 10 minutes incubation in X-gal. Scale bars, 100 μ m.

4.8.4 Low nitrogen enhances brassinosteroid biosynthesis to modulate root growth

Previous studies reported that *DWF1* encodes a C-24 reductase catalyzing the conversion of 24-methylenecholesterol to campesterol and (6-deoxo)dolichosterone to (6-deoxo)castasterone in BR synthesis (Klahre et al., 1998; Youn et al., 2018). To investigate whether the attenuation of the root response in *cbb1* and *dwf1* mutants is caused by perturbation of BR biosynthesis, the bioactive BR 24-epibrassinolide (BL) was exogenously supplied to plants. Irrespective of N treatments, the absolute length of the primary root of the wild type C24 continuously decreased with increasing BL concentrations. In contrast, the *cbb1* mutant was less sensitive to repression by BL and showed a continuous increase of primary root length, suggesting that *cbb1* plants were not able to maintain near-optimal endogenous BR levels for root growth (Figure 41A-B). Regarding average lateral root length, a promoting effect of exogenous BL was observed at 1 nM BL for both, wild type C24 and *cbb1* (Figure 41C-D). Notably, whereas total root length and average lateral root length of C24 at LN were significantly repressed at BL concentrations higher than 1 nM, they were maintained in the *cbb1* mutant as well as in C24 plants grown at HN (Figure 41C-D), suggesting that besides biosynthesis of BR, BR sensitivity is also enhanced at LN. Nonetheless, the response of average lateral root length to LN was almost completely rescued by application of 10 or 50 nM BL (Figure 41C). Consistent with a previous study (Bao et al., 2004), exogenous BL increased lateral root density of C24 under either N treatment, while there was no promoting effect observed in the *cbb1* mutant (Figure 41E). These results suggest that LN enhances BR biosynthesis and sensitivity to promote root growth.

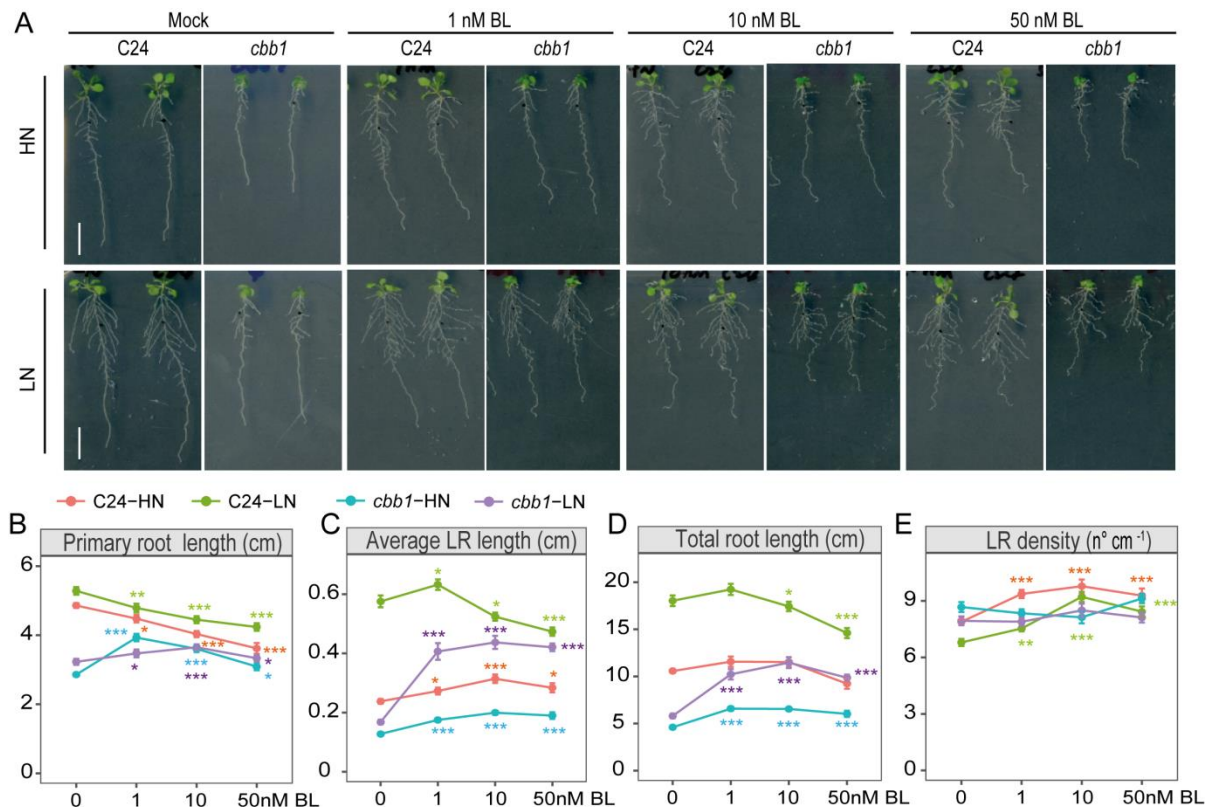


Figure 41. Exogenous BR supply rescues root responses of *cbb1* mutant plants to low nitrogen. Seven day-old seedlings were pre-cultured on 11.4 mM N and then transferred to solid agar media containing either high N (HN, 11.4 mM N) or low N (LN, 0.55 mM N) with or without 24-epibrassinolide (BL) at concentrations indicated. Root system architecture was assessed after 9 days. **(A)** Appearance of plants, **(B)** primary root length, **(C)** average lateral root length, **(D)** total root length and **(E)** lateral root density of wild-type C24 and *cbb1* mutant plants. Bars represent means \pm s.e. ($n = 15-20$ plants). Asterisks indicate significant differences between exogenous BR supply and mock treatment according to Welch's t test (* $P < 0.05$, ** $P < 0.01$, *** $P < 0.001$). Scale bars, 1 cm.

To strengthen the genetic evidence supporting that LN promotes BR biosynthesis and its role in stimulating root elongation under LN, transcript levels of *CPD*, *DWF4* and *BR6OX2* that play central roles in the biosynthetic pathway of BRs were analyzed by qPCR. Expression levels of all these three genes were significantly upregulated by LN in roots (Figure 42A). In agreement with a role of BR synthesis in root growth stimulation under LN, *cpd91* and *dwf4-44* mutants significantly attenuated the response of the primary root and lateral roots to LN (Figure 42B-D). Consequently, these mutant plants failed to significantly increase total root length at LN (Figure 42E). Compared to Col-0, there was no significant difference observed for lateral root density except for a significant reduction detected for *apd91* at HN (Figure 42F).

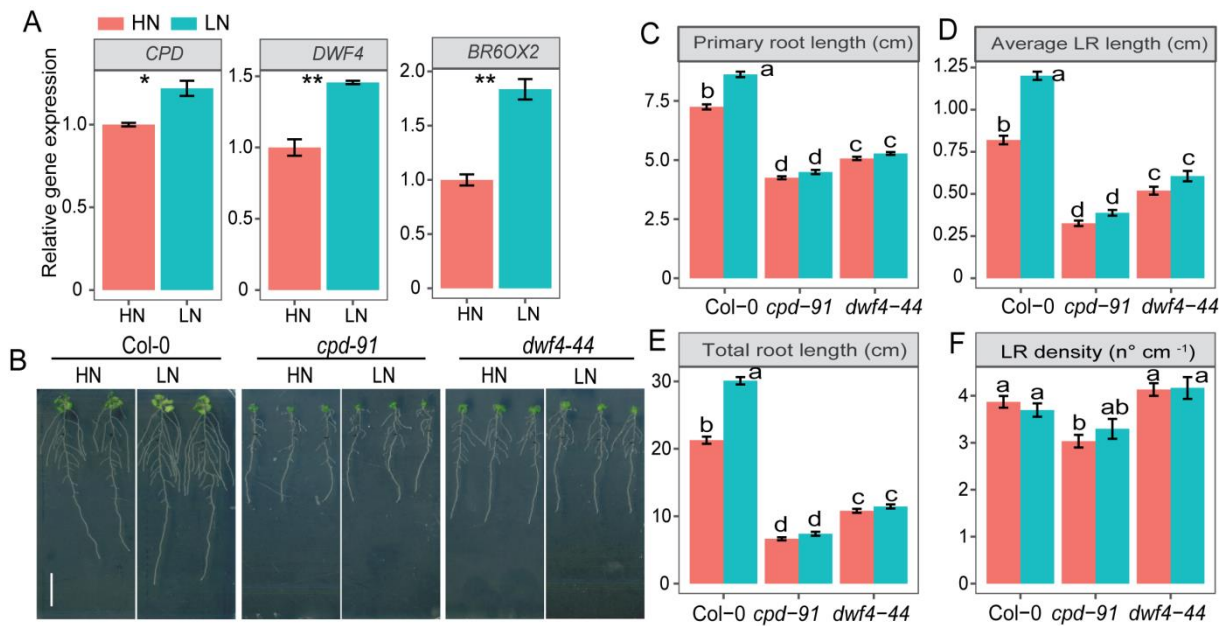


Figure 42. Expression levels of brassinosteroid biosynthesis genes and root architecture of their corresponding deletion mutants in response to low nitrogen. Seven day-old seedlings were pre-cultured on 11.4 mM N and then transferred to solid agar media containing either high N (HN, 11.4 mM N) or low N (LN, 0.55 mM N). Root system architecture was assessed after 9 days. **(A)** Transcript levels of *CPD*, *DWF4* and *BR6OX2* in response to HN or LN availabilities. Gene expression levels were assessed in whole roots by qPCR analysis and normalized to *ACT2*. Bars represent means \pm s.e. ($n = 3$ independent biological replicates) and asterisks indicate statistically significant differences between two N environments according to Welch's t test (* $P < 0.05$, ** $P < 0.01$). **(B)** Appearance of plants, **(C)** primary root length, **(D)** average lateral root length, **(E)** total root length and **(F)** lateral root density of wild-type (Col-0), *cpd91* and *dwf4-44* mutant plants. Bars represent means \pm s.e. ($n = 18-23$ plants). Different letters indicate significant differences at $P < 0.05$ according to one-way ANOVA and post-hoc Tukey test. Scale bar, 1 cm.

Consistent with the essential role of BR synthesis in modulating root responses to LN, exogenous supply of brassinazole (BRZ), an inhibitor of DWF4 that catalyzes the rate-limiting step in BR synthesis (Asami et al., 2000; Asami et al., 2001), significantly reduced the root growth response to LN (Figure 43). Taken together, these results indicate that LN promotes BR biosynthesis to stimulate root elongation.

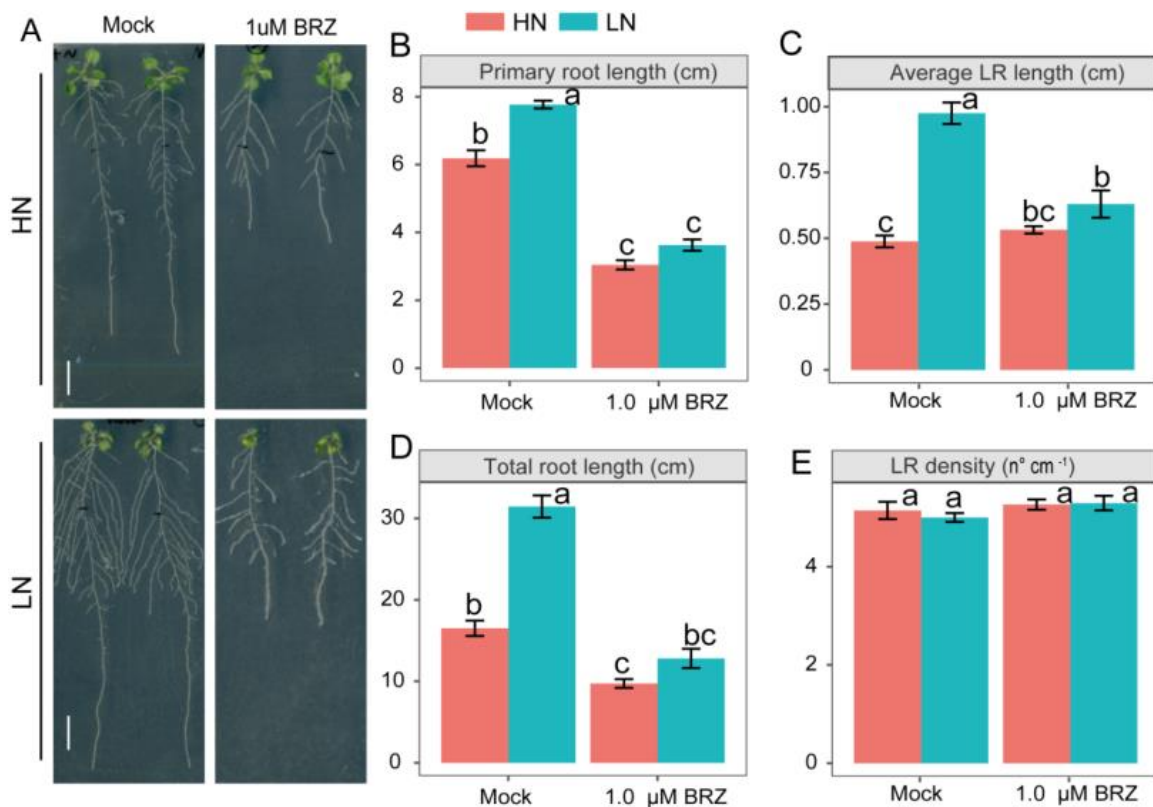


Figure 43. Inhibiting endogenous brassinosteroid biosynthesis blocks the root elongation response under low nitrogen. Seven day-old wild-type (Col-0) seedlings were pre-cultured on 11.4 mM N and then transferred to solid agar media containing either high N (HN, 11.4 mM N) or low N (LN, 0.55 mM N) in the presence or absence of 1 µM BR biosynthesis inhibitor brassinazole (BRZ). Root system architecture was assessed after 9 days. **(A)** Appearance of plants, **(B)** primary root length, **(C)** average lateral root length, **(D)** total root length and **(E)** lateral root density. Bars represent means \pm s.e. ($n = 13-15$ plants). Different letters indicate significant differences at $P < 0.05$ according to one-way ANOVA and post-hoc Tukey test. Scale bars, 1 cm.

4.8.5 Decreasing the endogenous brassinosteroid level attenuates the root response to low nitrogen in natural accessions

The previous results indicated that LN enhances BR biosynthesis and sensitivity to promote root elongation (Figures 39-43). To understand whether a natural variation in endogenous BR levels is associated with the phenotypic variation of root responses to LN, the BR biosynthesis inhibitor brassinazole (BRZ) was exogenously supplied to eight natural accessions that differed in their response to LN. The response of total root length, average lateral root length and primary root length were significantly and strongly reduced in 6 highly responsive lines, whereas exogenous BRZ supply had little impact on root responses to LN in the weaker responding lines Co and Kz-9 (Figure 44). Thus, it was concluded that natural variation in endogenous BR levels is associated with phenotypic variation in root responses to LN.

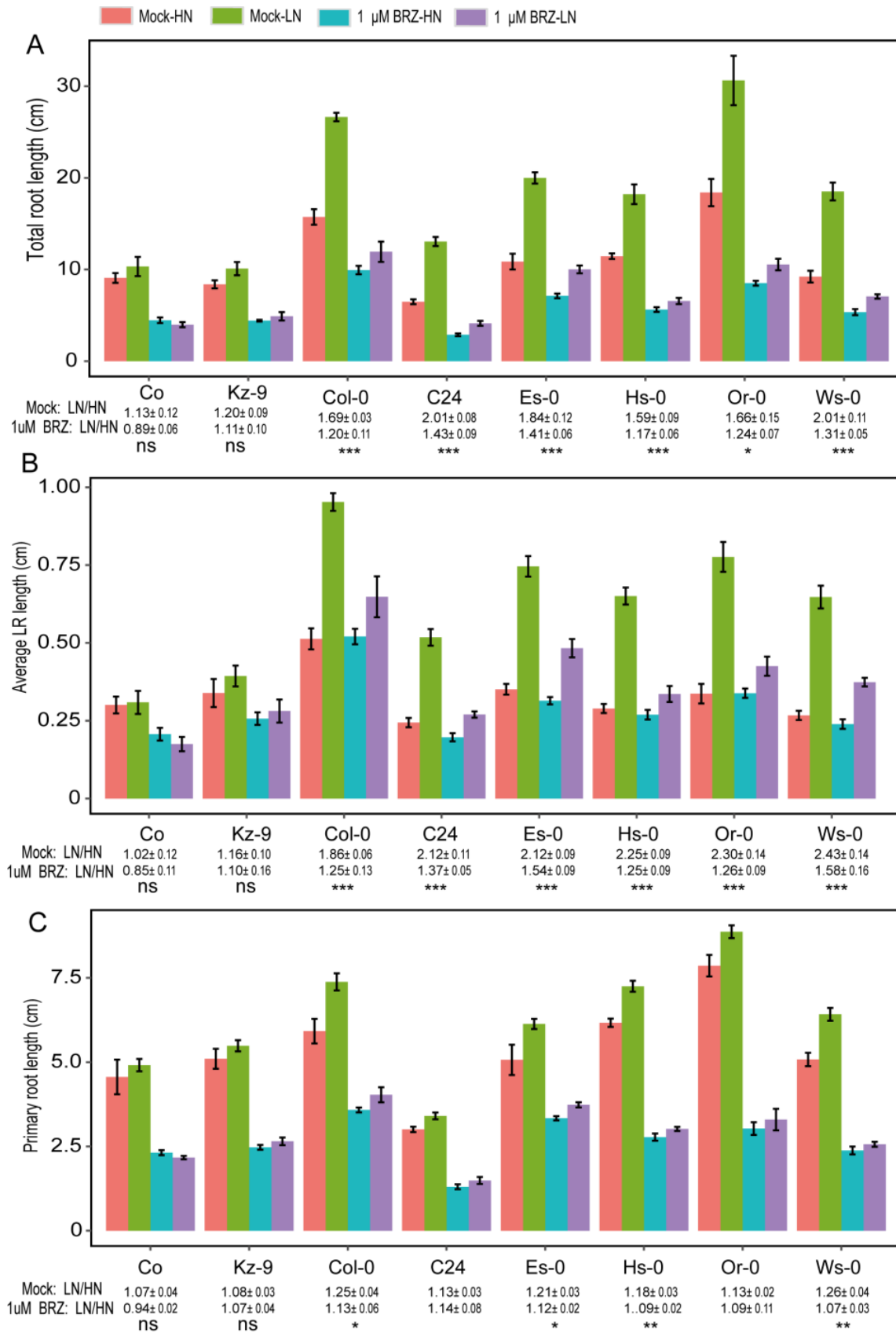


Figure 44. Reducing endogenous brassinosteroid levels inhibits the root elongation response to low nitrogen in natural accession lines. Seven day-old seedlings were pre-cultured on 11.4 mM N and then transferred to solid agar media containing either high N (HN, 11.4 mM N) or low N (LN,

0.55 mM N) in the absence or presence of 1 μ M BR biosynthesis inhibitor, brassinazole (BRZ). Root system architecture was assessed after 9 days. **(A)** Total root length, **(B)** average lateral root length and **(C)** primary root length for 2 weakly (Co, Kz-9) and 6 strongly N-responsive accessions. Bars represent means \pm s.e. ($n = 9-11$ plants). Asterisks indicate significant differences in relative root length (i.e. ratio of LN and HN) between BRZ and mock treatments according to Welch's t test (* $P < 0.05$, ** $P < 0.01$, *** $P < 0.001$, ns, not significant).

4.8.6 Variation in transcript levels of *DWF1* associates with natural variation of root length

Identification of *DWF1* by GWAS suggested that allelic variation in *DWF1* may associate with phenotypic variation of root length. To investigate how *DWF1* affects natural variation of total root length, the coding sequences of 139 natural accessions were analyzed to study whether there were non-synonymous amino acid substitutions that may alter protein function. Unlike BSK3 and YUC8, in which critical amino acid substitutions were found (Figures 7F and 30D), there was no non-synonymous substitution detected in the coding region, suggesting that *DWF1* protein functions were not likely causal for the observed phenotypic variation. Then, expression levels of *DWF1* were analyzed by q PCR in seven accession lines that differ significantly in their root length and response to low N (Figure 45A-B). While there was no significant correlation between transcript levels of *DWF1* and total root length, total lateral root length as well as average LR length at LN significantly correlated with *DWF1* transcript levels at HN ($R^2=0.58-0.60$, coefficient of determination of the linear regression) (Figure 45C-E). Interestingly, there was no significant correlation found between expression levels of *DWF1* and primary root length at either N condition (Figure 45F). These results suggest that expression variation of *DWF1* contributes to the natural variation only of lateral root length. At LN, the loss of correlation may be related to the higher BR sensitivity of roots that overrides the impact of elevated BR biosynthesis. In support of this hypothesis, at LN, root growth, in particular lateral roots, was more sensitive to exogenous 24-epibrassinolide supply (Figure 46).

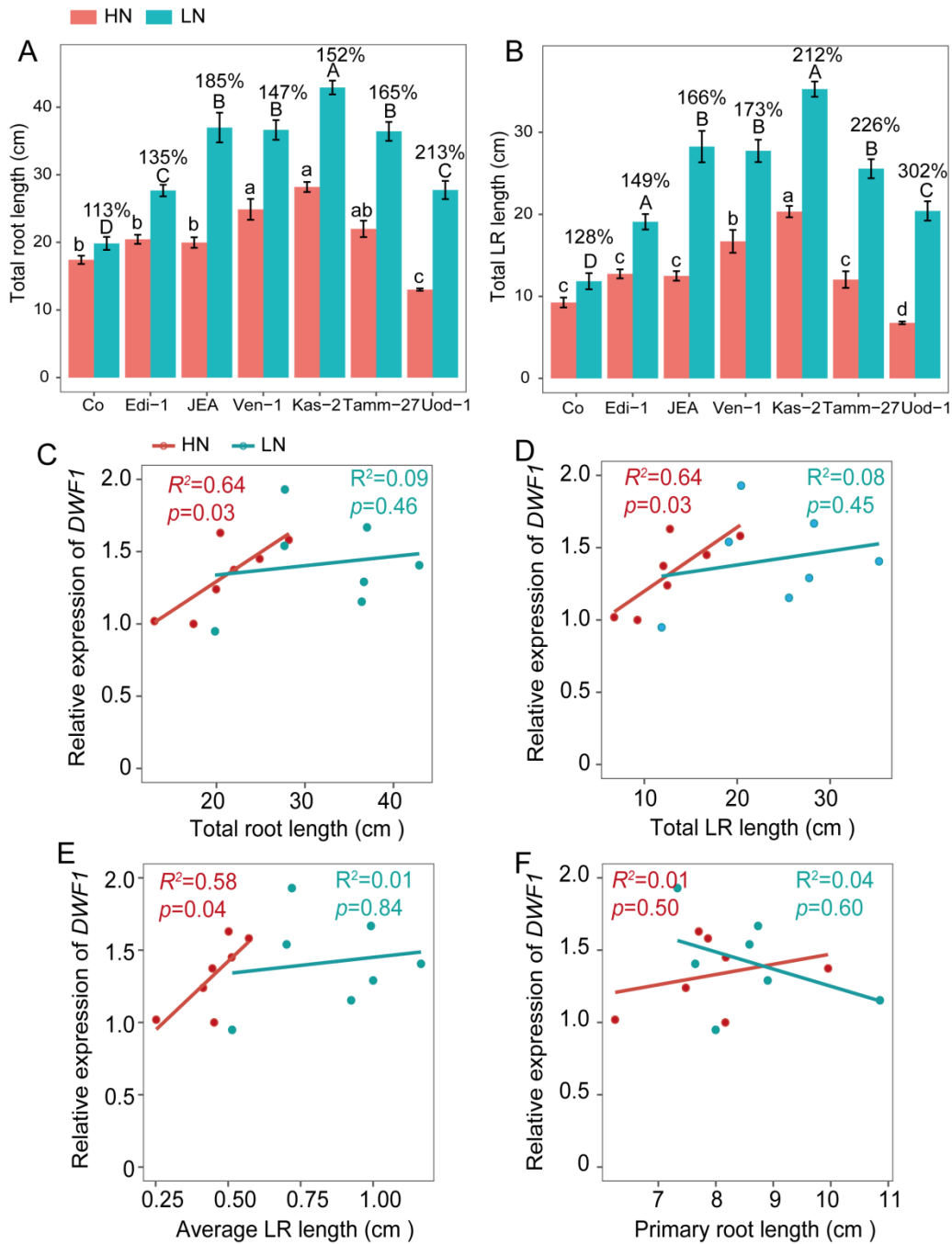


Figure 45. Expression levels of *DWF1* correlate with total root length and total lateral root length at high nitrogen. Seven day-old seedlings of accession lines were pre-cultured on 11.4 mM N and then transferred to solid agar media containing either high N (HN, 11.4 mM N) or low N (LN, 0.55 mM N). Total lateral root length and total root length were assessed after 9 days. **(A-B)** Total root length **(A)** and total lateral root length **(B)** of seven accession lines exhibiting wide variation in root length and response to low N. Bars represent means \pm s.e. ($n = 10-12$ plants). Different letters indicate significant differences at $P < 0.05$ according to one-way ANOVA and post-hoc Tukey test within individual N conditions. **(C-F)** Correlation of *DWF1* transcript levels with total root length **(C)**, total lateral root length **(D)**, average lateral root length **(E)** or primary root length **(F)** under either N condition. Transcript levels of *DWF1* were assessed in whole roots by qPCR analysis and normalized to *ACT2* ($n = 4$ independent biological replicates).

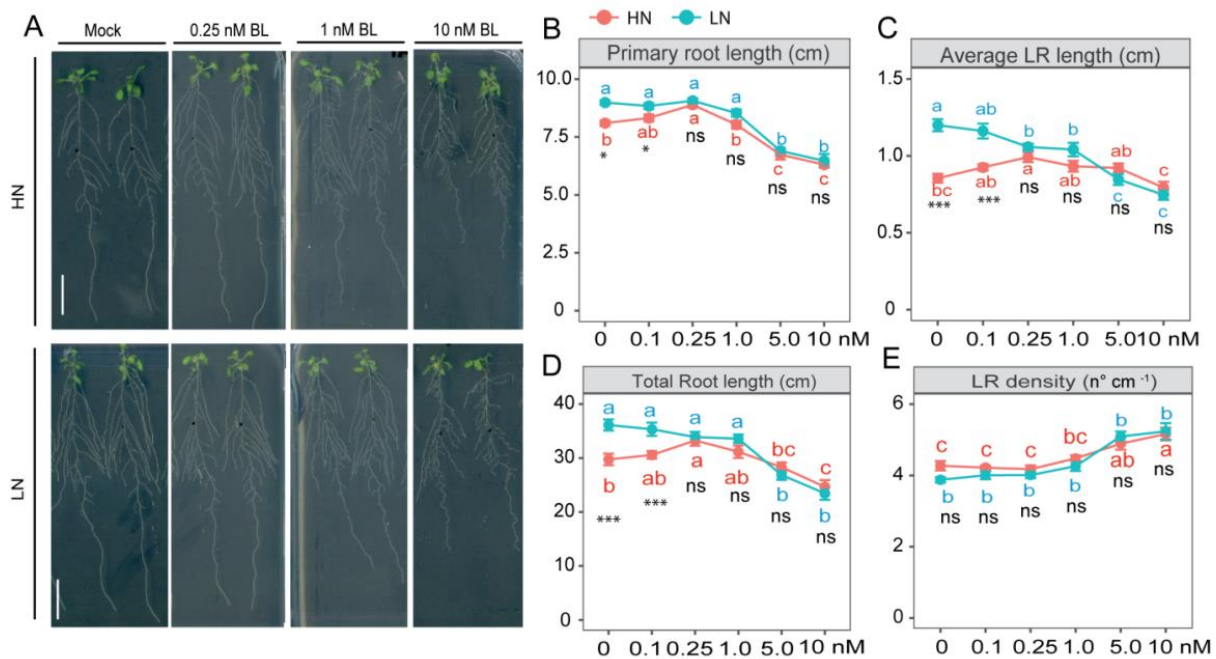


Figure 46. Root growth of Col-0 in response to exogenous BR supply under different N availabilities. Seven day-old seedlings were pre-cultured on 11.4 mM N and then transferred to solid agar media containing either high N (HN, 11.4 mM N) or low N (LN, 0.55 mM N). *DWF1* expression level and root system architecture were assessed after 9 days. **(A)** Appearance of plants, **(B)** primary root length, **(C)** average lateral root length, **(D)** total root length and **(E)** lateral root density of plants grown with supply of 24-epibrassinolide (BL) at the indicated concentrations. Bars represent means \pm s.e. ($n = 13-15$ plants). Different letters indicate significant differences at $P < 0.05$ according to one-way ANOVA and post-hoc Tukey test within the respective N treatment. Asterisks indicate significant differences between two N treatments at each BR concentration according to Welch's t test ($*P < 0.05$, $**P < 0.01$, $***P < 0.001$, ns, not significant). Scale bars, 1 cm.

To further validate the hypothesis that transcript levels of *DWF1* associate with root length variation, root system architectural traits were analyzed in *DWF1* RNA interference (RNAi) and overexpression lines (Figure 47A). At HN, *DWF1* knockdown lines showed shorter primary root and lateral roots compared to the wild type Col-0, whereas overexpression of *DWF1* significantly increased growth of the primary root and lateral roots (Figure 47B-D). At LN, shorter root length was also observed for *DWF1* knockdown lines, while the stimulatory effect of overexpression of *DWF1* was lost (Figure 47B-D). In addition, due to the decreased response of lateral roots to LN, the response of total root length to LN was reduced in both knockdown and overexpression lines (Figure 47E). Consistent with the initial experiment (Figure 39H and I), altering expression of *DWF1* had no impact on lateral root density (Figure 47F). Taken together, these results indicate that the gene expression level of *DWF1* is associated with the phenotypic variation in root elongation.

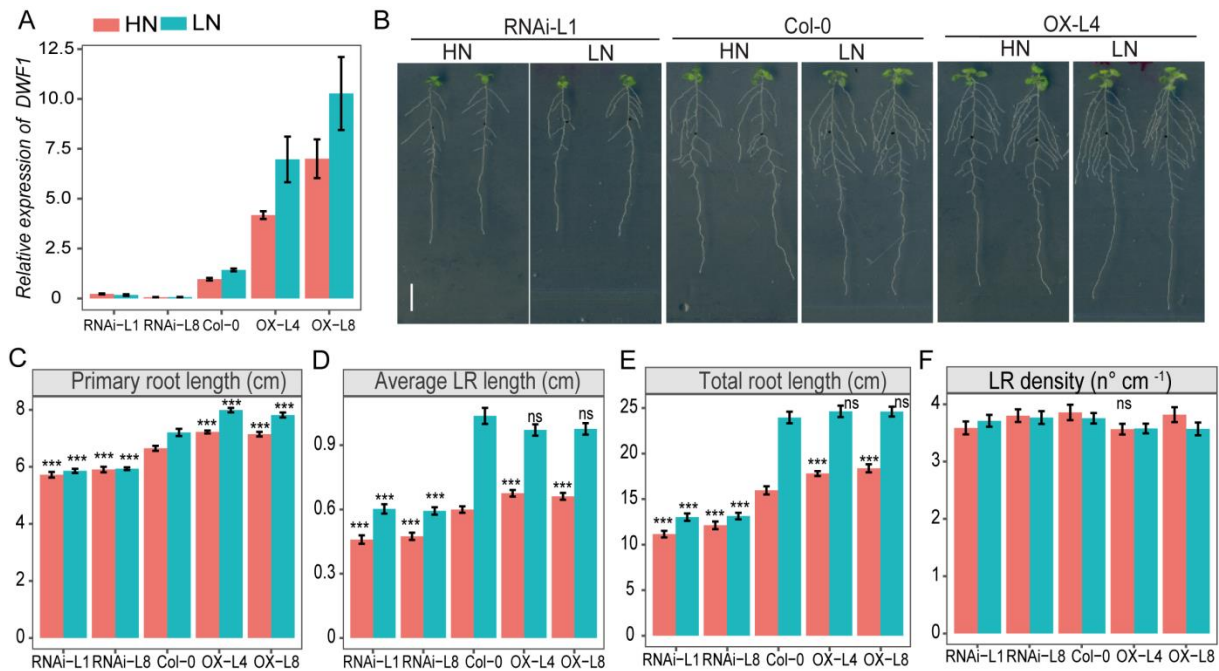


Figure 47. Root architecture of *DWF1* RNAi and overexpression lines in response to low nitrogen availability. Seven day-old seedlings were pre-cultured on 11.4 mM N and then transferred to solid agar media containing either high N (HN, 11.4 mM N) or low N (LN, 0.55 mM N). *DWF1* expression levels and root system architecture were assessed after 9 days. **(A)** Transcript levels of *DWF1* in Col-0 and transgenic lines with suppressed *DWF1* expression (RNAi-L1, -L8) or overexpressing *DWF1* under control of a *35SCaMV* promoter (OX-L1, -L8). Gene expression levels were assessed in whole roots by *qPCR* analysis and normalized to *ACT2*. Bars represent means \pm s.e. ($n = 3$ independent biological replicates). **(B)** Appearance of plants, **(C)** primary root length, **(D)** average lateral root length, **(E)** total root length and **(F)** lateral root density of wild-type (Col-0) and transgenic lines. Bars represent means \pm s.e. ($n = 18-24$ plants). Asterisks indicate significant differences between wild type and transgenic lines according to Welch's *t* test ($***P < 0.001$, ns, not significant). Scale bar, 1 cm.

4.8.7 Overexpression of *DWF1* improves shoot growth and N uptake

Initial correlation analyses indicated that increased root size contributes to enhanced N uptake, especially at LN (Figure 5C and D). To verify whether altered root size affects N uptake, shoot growth and N contents of *DWF1* transgenic lines were analyzed. Knockdown lines of *DWF1* exhibited a significant reduction in shoot growth by 17% and 22% at HN, respectively (Figure 48). By contrast, shoot biomass accumulation of *DWF1* RNAi lines decreased 32% and 35% at LN compared to the wild type (Figure 48A), suggesting an important role of *DWF1* in plant growth adaptation to LN. Overexpression of *DWF1* significantly increased shoot growth by 18-22% and 15-20% compared to the wild type Col-0 at either N treatment (Figure 48A). However, altered expression of *DWF1* had no impact on shoot N concentrations at either N supply level. Hence, the shoot N contents, which were

significantly lower in the RNAi and higher in the overexpression lines (Figure 48B and C), just reflected the differences in biomass formation among the lines. Thus, direct evidence for the role of *DWF1*-dependent root elongation in N uptake efficiency at LN could not be shown, due to the dominant impact of BR on overall biomass formation.

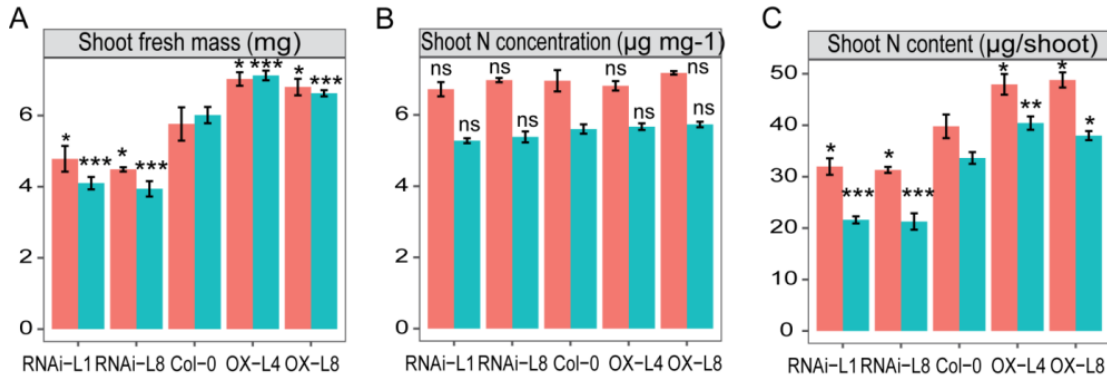


Figure 48. Influence of de-regulated *DWF1* expression on shoot growth and N content. Seven day-old seedlings were pre-cultured on 11.4 mM N and then transferred to solid agar media containing either high N (HN, 11.4 mM N) or low N (LN, 0.55 mM N). Shoot biomass and N concentrations were assessed after 9 days. **(A)** Shoot fresh mass, **(B)** shoot N concentration and **(C)** shoot N content of wild-type (Col-0) and transgenic lines with suppressed *DWF1* expression (RNAi-L1, -L8) or overexpressing *DWF1* under control of a 35SCaMV promoter (OX-L1, -L8). Bars represent means \pm s.e. ($n = 4$ replicates). Asterisks indicate statistically significant differences between wild type and transgenic lines according to Welch's *t*-test (* $P < 0.05$, ** $P < 0.01$, *** $P < 0.001$, ns, not significant).

5 Discussion

Root developmental plasticity is crucial for optimizing nutrient capture in continuously changing or nutrient-depleted soils. Due to the high enrichment of N in the plant body, N is required in largest amounts among all mineral elements for proper plant development and productivity. However, because of complex N transformation processes in soils and heterogeneity of soil N pools over time and space, agroecosystems do often not provide sufficient N to meet the plant N demand. When facing N limitation, most plant species have evolved sophisticated mechanisms to enlarge their root systems by developing longer primary and lateral roots (Chun et al., 2005; Gruber et al., 2013; Ma et al., 2014; Sun et al., 2014; Melino et al., 2015). More expanded root systems enable plants to forage larger soil volumes and to facilitate the acquisition of water and nutrients from deeper soil layers. Although this systemic foraging response has been recognized and described for a long time (Chun et al., 2005; Gruber et al., 2013; Ma et al., 2014; Sun et al., 2014; Melino et al., 2015), it is still largely unknown how plants perceive N deficiency and translate their N nutritional status in a root foraging response.

The work in the present thesis exploited the natural variation of *Arabidopsis* accessions and allowed the identification of three key genes involved in phytohormone synthesis and signaling. As these genes modulate brassinosteroid and auxin signaling, this thesis sheds new light on how the N nutritional status interacts with endogenous developmental signals to modulate root system architecture. Furthermore, functional quantitative trait nucleotides (QTNs) in *BSK3* and *YUC8* have been revealed by sequence mining and confirmed by haplotype analysis and via transgenic allelic complementation. Thus, this work paves the way to unlock the genetic potential of plants building more expanded root systems for higher nutrient efficiency.

5.1 Root size relates to plant performance and N accumulation

Considering that plants are sessile, plants must continuously adjust their root system to cope with fluctuating soil factors. Such developmental plasticity is of prime importance for plants getting acclimated to ever-changing edaphic conditions. For example, local proliferation of lateral roots into nutrient-enriched soil patches contributes significantly to plant nitrogen or iron nutrition (Hodge et al., 1999; Robinson et al., 1999; Giehl et al., 2012), while a shallower but more branched root system favours topsoil foraging and phosphorous acquisition on P-limiting sites (Nielsen et al., 2001). Developing longer primary and lateral roots to increase root size is commonly observed in many plant species that are suffering from N limitation or depletion in soils (Chun et al., 2005; Gruber et al., 2013; Ma et al., 2014; Sun et al., 2014; Melino et al., 2015). Whether such an enlarged root system is indeed beneficial for N acquisition by roots is not well documented. By assessing root architectural traits and aerial N accumulation as proxy for total N uptake, experiments performed in this thesis found that changes in the root system size under low N are significantly and positively correlated with above-ground N accumulation (Figure 5), suggesting that an extensive root system confers an advantage for N uptake, in particular at low N. An attempt was made to genetically verify an association of root size and above-ground N accumulation by altering the expression of *DWF1* that is involved in brassinosteroid biosynthesis (Klahre et al., 1998; Youn et al., 2018). Here, experiments showed that knock-down of *DWF1* expression significantly decreased whereas over-expression enhanced N accumulation under both, high and low N conditions (Figure 48C). However, the impact of *DWF1* expression on N accumulation was mainly brought about by enhanced biomass accumulation, while N concentration was not altered (Figures 48A and B). Thus, it cannot be unambiguously concluded whether the impact of BRs on plant biomass formation per se or on enhanced root formation boosted overall shoot N contents. Previous whole genome-wide profiling of targets of the transcription factor BZR1 revealed that BZR1 is able to bind to promoters of the nitrogen transporters *NRT1;1* and *AMT1;1* (Sun et al., 2010). Moreover, it has been shown that application of brassinosteroids is able to enhance the expression of *AMTs* and of the transcription factor *ABI3/VP1-Like 1 (RAVL1)* involved in BR homeostasis that directly binds to the promoter and activates expression of *AMT1;2* and subsequent ammonium uptake in rice (Xuan et al., 2017).

Collectively, these studies link brassinosteroid signaling to N uptake. As suggested by the higher accumulation of N in the shoot of *DWF1* overexpression lines, it would be highly interesting in the future to study how overexpressing *DWF1* impacts on root N uptake. More recently, root engineering by driving expression of *CKX* encoding a cytokinin oxidase that degrades cytokinin under control of a root-specific promoter significantly yielded improved root functions and conferred drought tolerance in barley (Ramireddy et al., 2018). Likewise, overexpression of the auxin biosynthesis gene *TaTAR2.1* in wheat greatly improved root growth as well as above-ground N accumulation and grain yield (Shao et al., 2017). Considering that overexpressing *DWF1* significantly increased root growth at high N and maintained root growth at low N (Figure 47), *DWF1* may be an interesting target for molecular breeding approaches. For the sake of enhanced nitrogen fertilizer use efficiency, uncoupling suppression of *DWF1* by high nitrogen doses e.g. by overexpression may allow growing crops with more extensive root systems even in intensive agriculture, where large amounts of nitrogen fertilizer are supplied. Thus, it can be expected that the *DWF1*-related phenotype identified here is a useful target for future improvement of crop N uptake.

5.2 Employing natural variation enables identification of key regulators in hormonal pathways modulating the root foraging response

Plant root development is under tight genetic control and highly responsive to external factors (Malamy, 2005). Amongst the most critical environmental factors, nutrient availability provokes profound root system architectural changes by interfering with endogenous developmental programs (López-Bucio et al., 2003; Forde, 2014; Giehl et al., 2014; Giehl & von Wirén, 2014). When exploring root architectural plasticity under nutrient deficiencies, it has been observed that plants of the *A. thaliana* accession Col-0 adopt a “foraging strategy” by increasing the length of primary and lateral roots under external N concentrations that induce mild N deficiency in shoots (Gruber et al., 2013). There is mounting evidence that root architectural responses to nutrients underlie large natural genetic variation (Ristova & Busch, 2014). For instance, natural variation of RSA in response to severe N deficiency has been described in diverse *Arabidopsis* collections, in which a substantial variation was observed for distinct root traits (De Pessemier et al., 2013; Gifford et al., 2013). Also in the present work, a wide range of natural variation for root traits has been observed under mild N deficiency (Figures 7A, 21A-B, 36A-B,

Table 1 and Supplemental Table 1). In addition, it has been also found that the foraging response to mild N deficiency is conserved across accessions that capture a large fraction of the genetic variation in Arabidopsis, as the length of both types of roots, i.e. primary and lateral roots, increased in 200 accessions (Figures 7A, 21A-B; 35A-B, Supplemental Table 1). At the cellular level, low N-induced elongation of both primary and lateral roots in Col-0 can be primarily attributed to cell elongation (Figures 6, 9F-H, 15E-G and 28). In case of P deficiency, repression of primary root growth has been assigned to rapid reduction in cell expansion and meristem exhaustion, while suboptimal iron and sulfur nutrition promote cell elongation and cell division (Sanchez-Calderon et al., 2005; Dan et al., 2007; Zhao et al., 2014; Balzergue et al., 2017; Singh et al., 2018). These results indicate that nutrient deficiencies may target different cellular processes to ultimately achieve repressive or stimulatory effects on root growth. When looking at the whole set of natural accessions, Col-0 is a line that only stimulates cell elongation, while other accessions either only increase meristem size or even enhance both cellular processes (Figures 6 and 17E-G). This suggests that low N stimulates root growth by increasing cell expansion as well as cell division, while the contribution of either mechanism varies depending on genotype. Such variation in these cellular processes provides an explanation for the different extent, by which accessions respond to low N.

Although the overall root system appears increased by low N, individual root traits vary in direction and extent of their response to low N. Hierarchical cluster analyses that characterized the pattern of root traits changing under low N identified and separated groups of accessions sharing similar or diverse responses to N deficiency (Figures 4 and 5). This suggested that different accessions employ different strategies to achieve extensive root systems. For example, a group of accessions in cluster 4 is able to increase lateral root outgrowth by increasing lateral root number, compared to other lines that only increase root elongation (Figure 5). In this regard, the identified accessions are useful for choosing parents to build RILs (recombinant inbred lines) allowing to generate new combinations of root trait responses but also enabling quantitative trait mapping of novel alleles responsible for total root enhancement. In addition, the independence of the response of root traits to low N suggests that certain genes target specific root developmental processes while

responding to extrinsic factors. For instance, an increased expression of *ARF8* at high N supply decreased lateral root growth but increased lateral root initiation (Gifford et al., 2008).

Natural variation is a powerful resource for identifying and characterizing molecular functions of genes as well as understanding their roles in environmental adaptation (Ogura & Busch, 2016; Bazakos et al., 2017). Traditionally, the genetic basis of complex traits has been characterized using a linkage mapping approach in biparental populations, such as in RILs, which have a high power to detect quantitative trait loci (QTLs) (Mouchel et al., 2004). However, constraints such as the low recombination frequency and a limited number of alternative alleles make it difficult to identify causal genes and detect important minor alleles (Zhu et al., 2008). As an alternative, genome-wide association studies (GWAS) link historically generated DNA polymorphisms to phenotypic variation, allowing mapping at a more refined scale (Zhu et al., 2008; Ogura & Busch, 2015). Recently, natural genetic variation followed by GWAS has been successfully exploited to uncover novel genes or alleles regulating root growth under nutrient-deficient conditions (Satbhai et al., 2017; Bouain et al., 2018). Here, by applying GWAS three critical genes involved in auxin biosynthesis (*YUC8*) or brassinosteroid synthesis and signaling (*DWF1* and *BSK3*) were identified, suggesting essential roles of these two growth-promoting phytohormones in the root foraging response to mild N deficiency. In a previous study, GWAS, transcriptome analysis and reverse genetics found among two genes regulating lateral root length in N-starved plants the jasmonate-responsive gene *JR1* (Gifford et al., 2013). Collectively, these independent studies emphasize the crucial role of phytohormones in modulating root development under nutrient deficiencies.

5.3 Brassinosteroid synthesis and signaling regulate root foraging responses to low nitrogen

Brassinosteroids (BRs) are a class of naturally occurring polyhydroxy steroidal hormones that are of crucial importance for several physiological and developmental processes in plants (Wang et al., 2012). It has been shown that these plant steroid hormones play a critical role in the transcriptional regulation of N uptake (Sun et al., 2010; Xuan et al., 2017). Regarding root growth, BRs modulate the elongation of differentiated cells (Fridman et al., 2014) and the size of meristems (Gonzalez-Garcia

et al., 2011; Hacham et al., 2011; Chaiwanon & Wang, 2015). Consequently, mutants deficient of BRs or impaired in BR signal transduction exhibit shorter root length (Gonzalez-Garcia et al., 2011; Hacham et al., 2011; Chaiwanon & Wang, 2015). Recently, emerging evidence has been obtained that BRs are involved in nutrient- and ambient temperature-dependent root growth (Singh et al., 2014; Martins et al., 2017; Singh et al., 2018). BRs are mostly considered as growth-promoting phytohormones, as suggested e.g. by light-grown seedlings subjected to exogenous application of BL or by genotypes with enhanced BR signaling that produce longer hypocotyls (Wang et al., 2012). However, it does not hold true for root growth in some specific cases. For example, it has been shown that low iron induces root growth by activating BR signaling, whereas ambient temperature downregulates BR signaling to promote root elongation (Martins et al., 2017; Singh et al., 2018), suggesting a complex role of BRs in the regulation of root growth responses to different environmental cues. Nonetheless, both studies suggest that low iron- and ambient temperature-dependent root elongation is hormone ligand-independent, since mutants impaired in BR biosynthesis (i.e., *det2*, *cpd* and *dwf4*) are still responsive to iron deficiency or ambient temperature (Martins et al., 2017; Singh et al., 2018). In contrast, phosphate deficiency concomitantly downregulates BR synthesis as well as BR signaling, which in turn inhibits root elongation (Singh et al., 2014). In this thesis, several lines of evidence suggest that BR synthesis is necessary for the root foraging response under low N. Firstly, through genome-wide association mapping *DWF1* was detected to associate with total lateral root length and total root length at low N (Figures 37B and D). In addition, phenotypic characterization of null *dwf1* alleles and also of RNAi lines indicated that the function of *DWF1* is necessary for root elongation in response to mild N deficiency (Figures 39 and 42). *DWF1* encodes a Ca²⁺-dependent calmodulin-binding protein, initially demonstrated to be a sterol C-24 reductase that converts 24-methylelecholesterol to campesterol, which is the first precursor for C₂₈-BR formation (Klahre et al., 1998; Du & Poovaiah, 2005). More recently, *DWF1* has been shown to possess enzyme activity not only as a sterol C-24 reductase, but also as BR C-24 reductase, catalyzing C-24 reduction of 6-deoxodolichosterone to 6-deoxocastasterone and dolichosterone to castasterone in *Arabidopsis* (Youn et al., 2018). Accordingly, profiling BRs in *dwf1* null plants shows a significant reduction in the bioactive BR

species castasterone (Youn et al., 2018). Secondly, exogenous application of the biologically active BR 24-epibrassinolide could successfully revert the root response of the *ccb1* mutant (allelic to *dwf1*) to low N (Figure 41). Thirdly, lowering endogenous BR levels either by mutation of central BR biosynthesis genes (*CPD* and *DWF4*) or exogenous supply of the BR biosynthesis inhibitor brassinazole (BRZ) could significantly attenuate low N-induced root elongation (Figures 42, 43 and 44). At low N, it was found that transcript levels of *DWF1*, *CPD*, *DWF4* and *BR6OX2* were significantly upregulated (Figures 40 and 42A), indicating that several steps in BR biosynthesis are enhanced. Although analytical approaches for the measurement of BR concentrations in plant tissues still need to be taken, it has been shown that in *Arabidopsis* expression levels of *DWF4* and *BR6OX2*, whose corresponding proteins catalyze the rate-limiting and farthest downstream step of BR synthesis, respectively, correlate with endogenous levels of BRs (Shimada et al., 2003; Kim et al., 2006). Taken together, these results suggest that low N upregulates the expression of several genes in the biosynthetic pathway of BRs to stimulate BR biosynthesis, thereby promoting root elongation.

Notably, it turned out that root growth at low N is more sensitive to exogenous supply of BR, provided here in the form of 24-epibrassinolide (Figures 41 and 46). For example, when exogenous BR was supplied to high N-grown wild-type plants, the root growth, in particular lateral roots, was significantly enhanced with increasing concentrations of BRs, while root growth at low N was repressed even at concentrations showing a stimulatory effect on root growth at high N (Figures 41 and 46). This suggests that apart from enhanced BR synthesis, low N also increases root sensitivity to BRs. Consistent with this assumption, GWAS mapped natural variation of primary root length at low N to *BSK3*, which is central for relaying a BR-dependent signal from the plasma membrane to the cytosol (Tang et al., 2008; Figure 7B). Subsequent phenotypic characterization of *bsk3* mutants confirmed an essential role of *BSK3* in modulating root responses to low N (Figures 7E and 8). Interestingly, *bsk3* deletion alone is sufficient to prevent low N-dependent elongation of the primary root, while strong suppression of N-responsive lateral root elongation required the absence of other closely related *BSK3* homologs (Figures 7E, 8 and 9). These results indicate the existence of multiple levels of redundancy among *BSKs* in the regulation of primary and lateral root responses. Indeed, redundancy is common for these

proteins, as clear growth phenotypes were so far only detected in multiple knockout lines (Sreeramulu et al., 2013).

It was observed that BSK3 is present mainly in the epidermis, cortex and endodermis of the primary root and emerged lateral roots (Figure 16C and H). Thus, it largely overlaps with the expression of *BRI1* and *BAK1* (Fàbregas et al., 2013; Dressano et al., 2017). Intriguingly, although N-dependent root growth phenotypes were observed for *bsk3* plants, *BSK3* expression was not regulated by N (Figure 16). This observation suggested that an N-derived signal likely interferes with BR signaling events upstream of BSK3. In agreement with this assumption, *BAK1* but not *BRI1* was found to be significantly upregulated after prolonged exposure to mild N deficiency (Figures 17A and 19A), and *bak1-1* plants exhibited attenuated root responses to low N (Figure 17B-D). Although BAK1 involves in multiple signaling pathways (Ma et al., 2016), for example PSK-dependent peptide signaling cascades that can impact on root growth, genetic augmentation downstream of BR signaling could successfully recover root responses of *bak1-1* to low N (Figure 18), reinforcing the conclusion that perturbation of BR signaling is responsible for the weaker root response of *bak1-1* to low N. Furthermore, it was found that low N-induced cell elongation was absent in *bsk3*, *bsk3,4,7,8* as well as *bak1-1* (Figures 9F-H, 15E-G and 17E-G), suggesting that BRs regulate low N-dependent root elongation by accelerating cell elongation. Recently, it has been shown that prolonged exposure to high temperature or iron deficiency promotes primary root elongation in a *BRI1*-dependent manner (Martins et al., 2017; Singh et al., 2018). Here, *BRI1* expression and the root phenotype of *bri1* mutants indicated a *BRI1*-independent mechanism for the root foraging response under N deficiency (Figure 19), suggesting that at low N plants may activate other receptors, such as BRL1 and BRL3 that have been shown to employ conserved signaling components (.i.e BAK1 and BSK3) to promote root growth (Fabregas et al., 2013).

Natural phenotypic variation can arise from polymorphisms in the *cis*-regulatory region, leading to altered transcript levels, or in the coding sequence, which can potentially modify protein function (Chao et al., 2012; Meijon et al., 2014; Chao et al., 2014; Hu et al., 2015). In the case of *DWF1*, it was found that transcript levels of *DWF1* in different accessions highly correlated with root length variation (Figure 45),

indicating that expression variation of *DWF1* likely caused variation in endogenous BR levels and in the corresponding phenotypic responses to low N. Consistent with this, root foraging responses of lines with strong responses to low N were largely compromised, when endogenous BR biosynthesis was blocked by exogenous BRZ supply (Figure 44). This could also be confirmed by altering *DWF1* expression, since root growth is positively associated with *DWF1* expression levels (Figure 47). Interestingly, this association disappeared at low N (Figures 45 and 47). As low N also increases root sensitivity to BR, and supra-optimal BR levels have a repressive role in root growth (Figure 46), it is likely that a stimulatory effect of enhanced BR production can be compromised by enhanced BR sensitivity.

Unlike *DWF1*, several lines of evidence indicate that non-coding sequence variation at the *BSK3* locus is not responsible for the variation in primary root length under mild N deficiency, since i) there was no correlation between *BSK3* transcript levels and primary root length (Figure 7I), and ii) promoters of accessions exhibiting differential responses to LN complemented primary root length and BR sensitivity of *bsk3,4,7,8* at similar efficiency (Figures 13 and 14). This is in contrast with growth responses to severe N deficiency, in which root elongation correlated significantly with the expression levels of *JR1* and *PhzC* or of the signaling peptide *CLE3* (Gifford et al., 2013; Araya et al., 2014a). Instead, one non-synonymous mutation (C956T) was identified in the coding region of *BSK3* that causes a leucine (L) to proline (P) substitution at position 319 (Figure 7J). Since accessions with the L allele had longer primary roots than those carrying the P allele (Figure 7K), the C956T polymorphism in the coding sequence is most likely the determining quantitative trait nucleotide (QTN) underlying this phenotypic variation. Supporting this notion, natural accessions carrying the *BSK3*-L variant or expression of *BSK3*-L in the *bsk3,4,7,8* quadruple mutant more effectively promoted root growth and BR sensitivity than *BSK3*-P (Figures 10, 11 and 12).

BSK3 is a plasma membrane-anchored protein belonging to a subfamily of 12 receptor-like cytoplasmic kinases (RLCK-XII) (Tang et al., 2008). Several BSKs, including *BSK3*, can interact with BR receptors upon BR binding (Tang et al., 2008; Sreeramulu et al., 2013; Fabregas et al., 2013; Ren et al., 2019). For instance, it has been shown that *BRI1*-dependent phosphorylation activates BSKs, since in their

phosphorylated form these proteins are released from the BRI1/BAK1 receptor complex and can interact with the Kelch-repeats-containing phosphatase BSU1 (Kim et al., 2009; Zhang et al., 2016), which in turn dephosphorylates and inactivates the GS3/Shaggy-like kinases BIN2 and BIL2 (Kim et al., 2011). How BSKs activate BSU1 still remains unclear. All BSKs contain a putative N-terminal kinase domain and C-terminal tetratricopeptide repeats (Tang et al., 2008). However, consistent kinase activity has not been detected for any BSK protein (Shi et al., 2013; Grutter et al., 2013; Zhang et al., 2016; Ren et al., 2019), even though weak Mn²⁺-dependent kinase activity was recorded in some instances (Shi et al., 2013; Zhang et al., 2016). It has therefore been proposed that kinase activity of BSKs may rely on activation by another yet unknown binding partner. Alternatively, rather than being *bona fide* kinases, BSKs may function as scaffolds that facilitate the interaction between BSU1 and BIN2/BIL2 (Sreeramulu et al., 2013; Grutter et al., 2013; Ren et al., 2019). Notably, mutating two invariable amino acids considered critical for the putative kinase activity of OsBSK3 made the protein non-functional (Zhang et al., 2016). Furthermore, it has been shown very recently that three ethyl methanesulfonate-induced missense mutations in the kinase domain of BSK3 result in loss-of-function or reduced BR responses (Ren et al., 2019). However, the amino acid substitution found in BSK3 does not relate to the phosphorylation site targeted by BRI1 or the sites assessed by Zhang et al. (2016) or Ren et al. (2019). This is conceivable as alleles with deleterious consequences would likely not be present at a detectable frequency in natural accessions due to negative selection.

Well in agreement with the role of BR signaling in modulating root growth in response to mild N deficiency, it was found that L319P substitution in BSK3 is also critical for the extent of the cell elongation and hence the root foraging response to mild N deficiency (Figures 15A-G and J). In support of the existence of a tight coupling of BSK3-dependent BR signaling and natural variation in root foraging responses, increased sensitivity to BR conferred by BSK3-L was also accompanied by increased capacities to elongate roots in response to low N (Figures 15H, I and K).

Based on these results, it is proposed that low N on the one hand upregulates expression of BR synthesis genes to increase BR biosynthesis; on the other hand, it directly upregulates expression of *BAK1*, thereby activating the BR signaling cascade.

Downstream of *BAK1*, the amplitude of BR signaling is modulated as a result of allelic variation in *BSK3*, which tunes downstream processes, in particular the root foraging response through differential cell elongation (Figure 49).

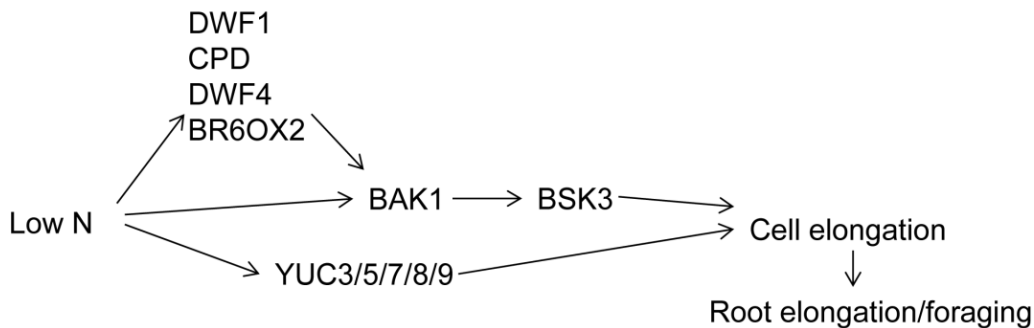


Figure 49. Working model summarizing the role of brassinosteroids and auxin in regulating the root foraging response to low nitrogen.

5.4 Role of auxin in regulating root responses to low nitrogen

For a long time, auxin has been demonstrated to play a pivotal role in plant development and plant adaptability to fluctuating environments. It has been reported that several root architectural responses to nutrient availability relate to changes in auxin distribution or signaling (Krouk et al., 2010; Vidal et al., 2010; Giehl et al., 2012, Bhosale et al., 2018). Although early experimental evidences suggested that low N availability increases root auxin content (Walch-Liu et al., 2006; Tian et al., 2008; Caba et al., 2010), it remained unknown whether this increase is required to stimulate root elongation at mild N deficiency. By assessing root responses to low N in natural accessions, a considerable natural variation in the lateral root response to low N was detected, which enabled mapping allelic variants in *YUC8*, encoding an enzyme catalyzing the rate-limiting step in the IPyA-dependent route of auxin biosynthesis (Figure 21). Single deletion mutants of *YUC8* or its closest homologs *YUC3*, *YUC5*, *YUC7* and *YUC9* partially disrupted lateral root elongation under low N (Figures 21H, 22, 23 and 24). Most importantly, simultaneous inactivation of all five *YUC* genes (*yucQ* mutant) completely suppressed the root response to low N (Figure 25), while exogenous application of IAA could fully restore the response of this mutant to low N (Figure 26). These results collectively indicate that low N drives YUCCA-dependent auxin biosynthesis to stimulate root elongation. Consistent with this conclusion, exogenous supply of an inhibitor for the enzymatic activity of YUCCA proteins, PPBo, largely suppressed root elongation responses to low N (Figure 27). Although it was

reported that low N enhances *TAR2* expression and consequently increases auxin biosynthesis, *TAR2*-dependent auxin synthesis is not sufficient for lateral root elongation while being crucial for lateral root emergence under low N (Ma et al., 2014). This is presumably due to the spatially confined expression of *TAR2* in the vasculature in the basal root zone. Unlike *TAR2*, *YUC8* and its closest homologs are strongly expressed in the root apex (Figure 29A-C; Chen et al., 2014; Hentrich et al., 2013), thus overlapping with the expression domain of *TAA1* (Tao et al., 2008; Stepanova et al., 2008). These results suggest that low N increases auxin synthesis presumably in the root apex. Consistent with this notion, it was observed that the auxin response is remarkably enhanced in low N-grown root tips (Figure 29D-G). It has been shown that low phosphate availability or toxic levels of aluminum can locally induce *TAA1*-dependent auxin synthesis to promote root hair elongation (Bhosale et al., 2018) or inhibit root elongation (Yang et al., 2014), respectively. These studies implicate that plants can spatially regulate auxin levels in a root zone-specific manner by targeting various steps in the auxin biosynthetic pathway to reprogram root system architecture and adapt to nutrient availability. Microscopic analyses indicate that low N not only accelerates cell elongation but also enlarges the meristem size in a genotype-dependent manner, while genetic perturbation of auxin synthesis largely disturbs cell elongation (Figure 6E-J and 28). More recently, it has been found that in rapeseed the abundance of proteins involved in cell wall biosynthesis and organization was significantly enriched in N-deficient roots (Qin et al., 2018). Since auxin triggers apoplastic acidification by promoting the plasma membrane ATPase (Hager, 2003), it thereby activates cell wall-loosening enzymes that enable cell elongation (Barbez et al., 2017). Further analysis of apoplastic pH and characterization of mutants of cell wall-remodeling enzymes will elucidate the relation of auxin, apoplastic acidification and cell wall remodeling in the low N-induced reprogramming of root development. Altogether, it is concluded that low N upregulates expression of *YUC8* and its closest homologs to enhance auxin biosynthesis, which accelerates cell elongation and subsequent root elongation (Figure 49).

Expression analyses further demonstrate that non-coding regulatory variation is not responsible for the natural variation observed for the lateral root response to mild N deficiency, because neither steady-state expression levels of *YUC8* nor the fold-

change of its expression correlated with lateral root length (Figure 30A-C). In addition, promoters of accessions exhibiting different levels of expression complemented *yucQ* root elongation with similar efficiency (Figures 31 and 32A-C). However, two mutations ($T_{41}A_{42} \rightarrow C_{41}T_{42}$) were identified in the coding region of *YUC8*, resulting in the non-synonymous substitution of leucine (L) to serine (S) at position 14. This amino acid substitution differentiates the lateral root response to low N (Figures 30D-E), suggesting that these two SNPs are the most informative quantitative trait nucleotides (QTNs). This assumption is supported by the fact that expression of the *YUC8*-L variant in various genetic backgrounds confers an overall improved root and hypocotyl growth under different conditions (Figures 32, 33 and 35). *YUC8* belongs to the family of flavin-containing monooxygenases (FMOs), which use NADPH as the electron donor and FAD as a cofactor to convert IPyA to IAA (Dai et al., 2013). EMS mutagenesis of *yuc4* and selection of mutants for YUCCA-specific phenotypes in vascular and floral development has demonstrated that two conserved glycine residues in the FAD- and NADPH-binding motifs of *YUC1* (GXGXXG) are critical for the *in vivo* function of the protein (Hou et al., 2011). The L14S substitution found here lies outside of these conserved residues, suggesting the existence of other regulatory sites putatively regulating *YUC8* function. Indeed, mutations in other non-conserved regions of FMOs close to the FAD-binding domain have been shown to compromise the catalytic activity of FMOs (Zhang et al., 2003; Hou et al., 2011). In future approaches, enzymatic activity assays and crystal structural analyses of *YUC8* will be required to address whether and how the L14S substitution affects the IPyA to IAA conversion by this enzyme.

5.5 Allelic variation in genes shaping phytohormone signaling pathways associates with local environmental adaptation

Arabidopsis colonizes a wide range of environments, therefore a part of the genetic variation and the resulting phenotypic variation is likely an adaptive response to the local environment. As a result, GWA studies do not only shed light on the genetic architecture of traits underlying the phenotypic variation, but also allow identifying allelic variants that have undergone natural selection due to local stress factors and adaptations beneficial for competitiveness and survival in their natural environments (Rosas et al., 2013; Satbhai et al., 2017). Root traits highly relevant to plant survival

and productivity might provide plants an adaptive role in colonizing special local environments. In support of this notion, primary root length under low N is significantly but negatively correlated with maximum precipitation in the wettest month (Figure 20A), suggesting that longer primary roots are generated by accessions originating from areas with less soil moisture. Likewise, lateral root growth is significantly correlated with temperature- and precipitation-related variables (Supplemental Table 5). These results suggest that the natural variation for root growth was, at least in part, related to water availability and temperature.

Relating BSK3 protein haplotypes to precipitation in the geographic location where the accession were collected indicates that the BSK3-L variant is associated with lower precipitation in the wettest month (Figure 20B), suggesting that BSK3 variants were potentially selected by precipitation. An extensive linkage disequilibrium (LD) at the *BSK3* locus is indicative of a selective sweep, suggesting fixation of the beneficial *BSK3* allele due to natural selection. In accordance with this hypothesis, genome-wide estimation of selection in *A. thaliana* revealed a strong selection signal in the *BSK3* gene (Horton et al., 2012). Interestingly, precipitation in the wettest month at sites, where accessions carrying the BSK3-L-encoding allele were collected, is significantly lower than at those inhabited by accessions harboring the BSK3-P variant (Figure 20B). This observation supports the hypothesis that Arabidopsis may have been adapted to topsoil drought by selection of the stronger *BSK3* allele allowing for longer primary roots. When the topsoil dries out under low precipitation, longer primary roots most likely confer an adaptive advantage as water can be acquired from deep soil layers (Uga et al., 2013). In fact, also *A. thaliana* plants respond to topsoil drought by developing steeper root systems as a result of enhanced primary root elongation and narrower lateral root angles (Rellan-Alvarez et al., 2015). Future research will be necessary to test whether *A. thaliana* accessions may have adapted to topsoil drought by selection of the stronger *BSK3* allele allowing for longer primary roots.

Unlike BSK3, YUC8 allelic variants are clearly associated with temperature-related variables, because accessions expressing the YUC8-L variant colonize in sites with a higher mean diurnal temperature range, temperature seasonality, mean temperature of wettest quarter and annual temperature range compared to lines expressing

YUC8-S (Figure 34 and Supplemental Table 6). These results indicate that YUC8 allelic variants may take in an adaptive role in temperature fluctuation. In fact, previous studies have shown that YUC8-dependent auxin synthesis is indispensable for plants to increase hypocotyl and petiole elongation in response to increased air temperatures (Sun et al., 2012; Lee et al., 2014), which improves leaf cooling capacity by shifting the meristematic and photosynthetically active tissues away from the heat-absorbing soil surface and by increasing the distance between leaves for better air circulation (Crawford et al., 2012; Quint et al., 2016). In accordance, it was found that YUC8-L can more efficiently complement the temperature response of *yucQ* plants when exposed to large day-night temperature fluctuations (Figure 35). Although reciprocal transplant experiments will be necessary to validate this result, there is additional evidence suggesting that the *YUC8* locus is related to local temperature adaptation. For instance, a genome-wide study of thermal responses in the bi-parental population Cvi-0 x Col-0 identified a QTL, which includes *YUC8* (Sanchez-Bermejo et al., 2015). Consistent with this conclusion, additional evidence from recent environmental GWAS reveals that *YUC8* is underlying a major temperature-adaptive locus (Tabas-Madrid et al., 2018). Furthermore, “auxin biosynthesis process” has been found among significantly enriched genes associated with temperature seasonality (Hancock et al., 2011). Taken together, the present identification of allelic variation in *YUC8* and its role in shaping root length, gains additional importance when considering the association of YUC8 variants with temperature-related growth conditions. Elucidating whether YUC8-dependent root elongation has an immediate impact on temperature-dependent plant growth and survival or relates indirectly to temperature, e.g. via altered water regimes, paves the way to unlock novel aspects in the importance of root traits in plant fitness.

6 References

- Achard P, Gusti A, Cheminant S, *et al.*, 2009. Gibberellin signaling controls cell proliferation rate in *Arabidopsis*. *Curr Biol* **19**, 1188-1193.
- Aida M, Beis D, Heidstra R, *et al.*, 2004. The PLETHORA genes mediate patterning of the *Arabidopsis* root stem cell niche. *Cell* **119**, 109-120.
- Alvarez JM, Riveras E, Vidal EA, *et al.*, 2014. Systems approach identifies *TGA1* and *TGA4* transcription factors as important regulatory components of the nitrate response of *Arabidopsis thaliana* roots. *Plant J* **80**, 1-13.
- Amano Y, Tsubouchi H, Shinohara H, Ogawa M, Matsubayashi Y, 2007. Tyrosine-sulfated glycopeptide involved in cellular proliferation and expansion in *Arabidopsis*. *Proc Natl Acad Sci U S A* **104**, 18333-18338.
- Araya T, Miyamoto M, Wibowo J, *et al.*, 2014a. CLE-CLAVATA1 peptide-receptor signaling module regulates the expansion of plant root systems in a nitrogen-dependent manner. *Proc Natl Acad Sci U S A* **111**, 2029-2034.
- Araya T, von Wirén N, Takahashi H, 2014b. CLE peptides regulate lateral root development in response to nitrogen nutritional status of plants. *Plant Signal Behav* **9**.
- Araya T, von Wirén N, Takahashi H, 2016. CLE peptide signaling and nitrogen interactions in plant root development. *Plant Mol Biol* **91**, 607-615.
- Asami T, Min YK, Nagata N, *et al.*, 2000. Characterization of brassinazole, a triazole-type brassinosteroid biosynthesis inhibitor. *Plant Physiol* **123**, 93-99.
- Asami T, Mizutani M, Fujioka S, *et al.*, 2001. Selective interaction of triazole derivatives with DWF4, a cytochrome P450 monooxygenase of the brassinosteroid biosynthetic pathway, correlates with brassinosteroid deficiency *in Planta*. *J Biol Chem* **276**, 25687-25691.
- Atwell S, Huang YS, Vilhjalmsón BJ, *et al.*, 2010. Genome-wide association study of 107 phenotypes in *Arabidopsis thaliana* inbred lines. *Nature* **465**, 627-631.
- Balzergue C, Dartevielle T, Godon C, *et al.*, 2017. Low phosphate activates STOP1-ALMT1 to rapidly inhibit root cell elongation. *Nat Commun* **8**, 15300.
- Bao F, Shen J, Brady SR, Muday GK, Asami T, Yang Z, 2004. Brassinosteroids interact with auxin to promote lateral root development in *Arabidopsis*. *Plant Physiol* **134**, 1624-1631.

Barbez E, Dunser K, Gaidora A, Lendl T, Busch W, 2017. Auxin steers root cell expansion via apoplastic pH regulation in *Arabidopsis thaliana*. *Proc Natl Acad Sci USA* **114**, 4884-4893.

Barth C, Gouzd ZA, Steele HP, Imperio RM, 2010. A mutation in GDP-mannose pyrophosphorylase causes conditional hypersensitivity to ammonium, resulting in *Arabidopsis* root growth inhibition, altered ammonium metabolism, and hormone homeostasis. *J Exp Bot* **61**, 379-394.

Bates TR, Lynch JP, 1996. Stimulation of root hair elongation in *Arabidopsis thaliana* by low phosphorus availability. *Plant Cell Environ* **19**, 529-538.

Bazakos C, Hanemian M, Trontin C, Jimenez-Gomez JM, Loudet O, 2017. New strategies and tools in quantitative genetics: how to go from the phenotype to the genotype. *Annu Rev Plant Biol* **68**, 435-455.

Beemster GTS, Baskin TI, 1998. Analysis of cell division and elongation underlying the developmental acceleration of root growth in *Arabidopsis thaliana*. *Plant Physiol* **116**, 1515-1526.

Benkova E, Michniewicz M, Sauer M, *et al.*, 2003. Local, efflux-dependent auxin gradients as a common module for plant organ formation. *Cell* **115**, 591-602.

Bergonci T, Ribeiro B, Ceciliato PH, Guerrero-Abad JC, Silva-Filho MC, Moura DS, 2014. *Arabidopsis thaliana* RALF1 opposes brassinosteroid effects on root cell elongation and lateral root formation. *J Exp Bot* **65**, 2219-2230.

Bhalerao RP, Eklof J, Ljung K, Marchant A, Bennett M, Sandberg G, 2002. Shoot-derived auxin is essential for early lateral root emergence in *Arabidopsis* seedlings. *Plant J* **29**, 325-332.

Bhosale R, Giri J, Pandey BK, *et al.*, 2018. A mechanistic framework for auxin dependent *Arabidopsis* root hair elongation to low external phosphate. *Nat Commun* **9**, 1409.

Bielach A, Podlesakova K, Marhavy P, *et al.*, 2012. Spatiotemporal regulation of lateral root organogenesis in *Arabidopsis* by cytokinin. *Plant Cell* **24**, 3967-3981.

Bishopp A, Bennett MJ, 2014. Hormone crosstalk: directing the flow. *Curr Biol* **24**, 366-368.

Blilou I, Xu J, Wildwater M, *et al.*, 2005. The PIN auxin efflux facilitator network controls growth and patterning in *Arabidopsis* roots. *Nature* **433**, 39-44.

Bouain N, Satbhai SB, Korte A, *et al.*, 2018. Natural allelic variation of the *AZI1* gene controls root growth under zinc-limiting condition. *PLoS Genet* **14**, e1007304.

Bouguyon E, Brun F, Meynard D, *et al.*, 2015. Multiple mechanisms of nitrate sensing by Arabidopsis nitrate transceptor NRT1.1. *Nat Plants* **1**, 15015.

Bouguyon E, Perrine-Walker F, Pervent M, *et al.*, 2016. Nitrate controls root development through posttranscriptional regulation of the NRT1.1/NPF6.3 transporter/sensor. *Plant Physiol* **172**, 1237-1248.

Brady SM, Sarkar SF, Bonetta D, Mccourt P, 2003. The *ABSCISIC ACID INSENSITIVE 3 (ABI3)* gene is modulated by farnesylation and is involved in auxin signaling and lateral root development in Arabidopsis. *Plant J* **34**, 67-75.

Brumos J, Robles LM, Yun J, *et al.*, 2018. Local auxin biosynthesis is a key regulator of plant development. *Dev Cell* **47**, 306-318.

Cano-Delgado A, Yin Y, Yu C, *et al.*, 2004. BRL1 and BRL3 are novel brassinosteroid receptors that function in vascular differentiation in Arabidopsis. *Development* **131**, 5341-5351.

Cao YW, Glass ADM, Crawford NM, 1993. Ammonium inhibition of Arabidopsis root growth can be reversed by potassium and by auxin resistance mutations *aux1*, *axr1*, and *axr2*. *Plant Physiol* **102**, 983-989.

Carlsbecker A, Lee JY, Roberts CJ, *et al.*, 2010. Cell signalling by *microRNA165/6* directs gene dose-dependent root cell fate. *Nature* **465**, 316-321.

Casimiro I, Beeckman T, Graham N, *et al.*, 2003. Dissecting Arabidopsis lateral root development. *Trends Plant Sci* **8**, 165-171.

Casimiro I, Marchant A, Bhalerao RP, *et al.*, 2001. Auxin transport promotes Arabidopsis lateral root initiation. *Plant Cell* **13**, 843-852.

Celenza JL, Jr., Grisafi PL, Fink GR, 1995. A pathway for lateral root formation in *Arabidopsis thaliana*. *Genes Dev* **9**, 2131-2142.

Chaiwanon J, Wang ZY, 2015. Spatiotemporal brassinosteroid signaling and antagonism with auxin pattern stem cell dynamics in Arabidopsis roots. *Curr Biol* **25**, 1031-1042.

Chao DY, Chen Y, Chen J, *et al.*, 2014. Genome-wide association mapping identifies a new arsenate reductase enzyme critical for limiting arsenic accumulation in plants. *PLoS Biol* **12**, e1002009.

Chao DY, Silva A, Baxter I, *et al.*, 2012. Genome-wide association studies identify heavy metal ATPase3 as the primary determinant of natural variation in leaf cadmium in *Arabidopsis thaliana*. *PLoS Genet* **8**, e1002923.

Chen Q, Dai X, De-Paoli H, *et al.*, 2014. Auxin overproduction in shoots cannot rescue auxin deficiencies in Arabidopsis roots. *Plant Cell Physiol* **55**, 1072-1079.

Cho H, Ryu H, Rho S, *et al.*, 2014. A secreted peptide acts on BIN2-mediated phosphorylation of ARFs to potentiate auxin response during lateral root development. *Nat Cell Biol* **16**, 66-76.

Chun L, Mi GH, Li JS, Chen FJ, Zhang FS, 2005. Genetic analysis of maize root characteristics in response to low nitrogen stress. *Plant Soil* **276**, 369-382.

Chung Y, Maharjan PM, Lee O, *et al.*, 2011. Auxin stimulates *DWARF4* expression and brassinosteroid biosynthesis in Arabidopsis. *Plant J* **66**, 564-578.

Clough SJ, Bent AF, 1998. Floral dip: a simplified method for Agrobacterium-mediated transformation of *Arabidopsis thaliana*. *Plant J* **16**, 735-743.

Conklin PL, Norris SR, Wheeler GL, Williams EH, Smirnoff N, Last RL, 1999. Genetic evidence for the role of GDP-mannose in plant ascorbic acid (*vitamin C*) biosynthesis. *Proc Natl Acad Sci USA* **96**, 4198-4203.

Crawford AJ, Mclachlan DH, Hetherington AM, Franklin KA, 2012. High temperature exposure increases plant cooling capacity. *Curr Biol* **22**, 396-397.

Cui H, Levesque MP, Vernoux T, *et al.*, 2007. An evolutionarily conserved mechanism delimiting SHR movement defines a single layer of endodermis in plants. *Science* **316**, 421-425.

Dai X, Mashiguchi K, Chen Q, *et al.*, 2013. The biochemical mechanism of auxin biosynthesis by an arabidopsis YUCCA flavin-containing monooxygenase. *J Biol Chem* **288**, 1448-1457.

Dan H, Yang G, Zheng ZL, 2007. A negative regulatory role for auxin in sulphate deficiency response in *Arabidopsis thaliana*. *Plant Mol Biol* **63**, 221-235.

De Pessemier J, Chardon F, Juraniec M, Delaplace P, Hermans C, 2013. Natural variation of the root morphological response to nitrate supply in *Arabidopsis thaliana*. *Mech Dev* **130**, 45-53.

De Rybel B, Vassileva V, Parizot B, *et al.*, 2010. A novel aux/IAA28 signaling cascade activates GATA23-dependent specification of lateral root founder cell identity. *Curr Biol* **20**, 1697-1706.

De Smet I, Lau S, Voss U, *et al.*, 2010. Bimodular auxin response controls organogenesis in Arabidopsis. *Proc Natl Acad Sci USA* **107**, 2705-2710.

De Smet I, Signora L, Beeckman T, Inze D, Foyer CH, Zhang H, 2003. An abscisic acid-sensitive checkpoint in lateral root development of Arabidopsis. *Plant J* **33**, 543-555.

De Smet I, Tetsumura T, De Rybel B, *et al.*, 2007. Auxin-dependent regulation of lateral root positioning in the basal meristem of Arabidopsis. *Development* **134**, 681-690.

De Smet I, Vassileva V, De Rybel B, *et al.*, 2008. Receptor-like kinase ACR4 restricts formative cell divisions in the Arabidopsis root. *Science* **322**, 594-597.

Deb S, Sankaranarayanan S, Wewala G, Widdup E, Samuel MA, 2014. The S-domain receptor kinase Arabidopsis Receptor Kinase 2 and the U Box/Armadillo Repeat-Containing E3 Ubiquitin Ligase 9 module mediates lateral root development under phosphate starvation in Arabidopsis. *Plant Physiol* **165**, 1647-1656.

Dello Ioio R, Linhares FS, Scacchi E, *et al.*, 2007. Cytokinins determine Arabidopsis root-meristem size by controlling cell differentiation. *Curr Biol* **17**, 678-682.

Dello Ioio R, Nakamura K, Moubayidin L, *et al.*, 2008. A genetic framework for the control of cell division and differentiation in the root meristem. *Science* **322**, 1380-1384.

Dewitte W, Murray Ja H, 2003. The plant cell cycle. *Annu Rev Plant Biol* **54**, 235-264.

Dilaurenzio L, Wysockadiller J, Malamy JE, *et al.*, 1996. The SCARECROW gene regulates an asymmetric cell division that is essential for generating the radial organization of the Arabidopsis root. *Cell* **86**, 423-433.

Dodd AN, Kudla J, Sanders D, 2010. The language of calcium signaling. *Annu Rev Plant Biol* **61**, 593-620.

Dressano K, Ceciliato PHO, Silva AL, *et al.*, 2017. BAK1 is involved in AtRALF1-induced inhibition of root cell expansion. *PLoS Genet* **13**, e1007053.

Drew MC, 1975. Comparison of effects of a localized supply of phosphate, nitrate, ammonium and potassium on growth of seminal root system, and shoot, in barley. *New Phytol* **75**, 479-490.

Du L, Poovaiah BW, 2005. Ca²⁺/calmodulin is critical for brassinosteroid biosynthesis and plant growth. *Nature* **437**, 741-745.

Evans ML, Ishikawa H, Estelle MA, 1994. Responses of Arabidopsis roots to auxin studied with high temporal resolution-comparison of wild-type and auxin-response mutants. *Planta* **194**, 215-222.

Fabregas N, Li N, Boeren S, *et al.*, 2013. The BRASSINOSTEROID INSENSITIVE1-LIKE3 signalosome complex regulates Arabidopsis root development. *Plant Cell* **25**, 3377-3388.

Fiers M, Golemiec E, Xu J, *et al.*, 2005. The 14-amino acid CLV3, CLE19, and CLE40 peptides trigger consumption of the root meristem in Arabidopsis through a CLAVATA2-dependent pathway. *Plant Cell* **17**, 2542-2553.

Forde BG, 2014. Nitrogen signalling pathways shaping root system architecture: an update. *Curr Opin Plant Biol* **21**, 30-36.

Forde BG, Cutler SR, Zaman N, Krysan PJ, 2013. Glutamate signalling via a *MEKK1* kinase-dependent pathway induces changes in Arabidopsis root architecture. *Plant J* **75**, 1-10.

Franklin KA, Lee SH, Patel D, *et al.*, 2011. *PHYTOCHROME-INTERACTING FACTOR 4* (PIF4) regulates auxin biosynthesis at high temperature. *Proc Natl Acad Sci USA* **108**, 20231-20235.

Fridman Y, Elkouby L, Holland N, Vragovic K, Elbaum R, Savaldi-Goldstein S, 2014. Root growth is modulated by differential hormonal sensitivity in neighboring cells. *Genes Dev* **28**, 912-20.

Frigerio M, Alabadi D, Perez-Gomez J, *et al.*, 2006. Transcriptional regulation of gibberellin metabolism genes by auxin signaling in Arabidopsis. *Plant Physiol* **142**, 553-563.

Fu X, Harberd NP, 2003. Auxin promotes Arabidopsis root growth by modulating gibberellin response. *Nature* **421**, 740-743.

Fukaki H, Nakao Y, Okushima Y, Theologis A, Tasaka M, 2005. Tissue-specific expression of stabilized SOLITARY-ROOT/IAA14 alters lateral root development in Arabidopsis. *Plant J* **44**, 382-395.

Fukaki H, Tameda S, Masuda H, Tasaka M, 2002. Lateral root formation is blocked by a gain-of-function mutation in the SOLITARY-ROOT/IAA14 gene of Arabidopsis. *Plant J* **29**, 153-168.

Fukaki H, Tasaka M, 2009. Hormone interactions during lateral root formation. *Plant Mol Biol* **69**, 437-449.

Galinha C, Hofhuis H, Luijten M, *et al.*, 2007. PLETHORA proteins as dose-dependent master regulators of Arabidopsis root development. *Nature* **449**, 1053-1057.

Gamuyao R, Chin JH, Pariasca-Tanaka J, *et al.*, 2012. The protein kinase Pstol1 from traditional rice confers tolerance of phosphorus deficiency. *Nature* **488**, 535-539.

Giehl RF, Gruber BD, von Wirén N, 2014. It's time to make changes: modulation of root system architecture by nutrient signals. *J Exp Bot* **65**, 769-778.

Giehl RF, Lima JE, von Wirén N, 2012. Localized iron supply triggers lateral root elongation in Arabidopsis by altering the AUX1-mediated auxin distribution. *Plant Cell* **24**, 33-49.

Giehl RF, von Wirén N, 2014. Root nutrient foraging. *Plant Physiol* **166**, 509-517.

Giehl RF, von Wirén N, 2015. Nitrate signalling: functions of a nitrate transceptor. *Nat Plants* **1**, 15021.

Gifford ML, Banta JA, Katari MS, *et al.*, 2013. Plasticity regulators modulate specific root traits in discrete nitrogen environments. *PLoS Genet* **9**, e1003760.

Gifford ML, Dean A, Gutierrez RA, Coruzzi GM, Birnbaum KD, 2008. Cell-specific nitrogen responses mediate developmental plasticity. *Proc Natl Acad Sci USA* **105**, 803-808.

Gonzalez-Garcia MP, Vilarrasa-Blasi J, Zhiponova M, *et al.*, 2011. Brassinosteroids control meristem size by promoting cell cycle progression in Arabidopsis roots. *Development* **138**, 849-859.

Gruber BD, Giehl RFH, Friedel S, von Wirén N, 2013. Plasticity of the Arabidopsis root system under nutrient deficiencies. *Plant Physiol* **163**, 161-179.

Grutter C, Sreeramulu S, Sessa G, Rauh D, 2013. Structural characterization of the RLCK family member BSK8: a pseudokinase with an unprecedented architecture. *J Mol Biol* **425**, 4455-4467.

Guan P, Wang R, Nacry P, *et al.*, 2014. Nitrate foraging by Arabidopsis roots is mediated by the transcription factor TCP20 through the systemic signaling pathway. *Proc Natl Acad Sci USA* **111**, 15267-15272.

Gutierrez-Alanis D, Yong-Villalobos L, Jimenez-Sandoval P, *et al.*, 2017. Phosphate starvation-dependent iron mobilization induces *CLE14* expression to trigger root meristem differentiation through CLV2/PEPR2 signaling. *Dev Cell* **41**, 555-570.

Hacham Y, Holland N, Butterfield C, *et al.*, 2011. Brassinosteroid perception in the epidermis controls root meristem size. *Development* **138**, 839-848.

Hager A, 2003. Role of the plasma membrane H⁺-ATPase in auxin-induced elongation growth: historical and new aspects. *J Plant Res* **116**, 483-505.

Hancock AM, Brachi B, Faure N, *et al.*, 2011. Adaptation to climate across the *Arabidopsis thaliana* genome. *Science* **334**, 83-86.

Haruta M, Sabat G, Stecker K, Minkoff BB, Sussman MR, 2014. A peptide hormone and its receptor protein kinase regulate plant cell expansion. *Science* **343**, 408-411.

Hemerly AS, Ferreira P, Engler JD, Vanmontagu M, Engler G, Inze D, 1993. *Cdc2a* expression in *Arabidopsis* is linked with competence for cell division. *Plant Cell* **5**, 1711-1723.

Hentrich M, Bottcher C, Duchting P, *et al.*, 2013. The jasmonic acid signaling pathway is linked to auxin homeostasis through the modulation of *YUCCA8* and *YUCCA9* gene expression. *Plant J* **74**, 626-637.

Heyman J, Cools T, Vandenbussche F, *et al.*, 2013. *ERF115* controls root quiescent center cell division and stem cell replenishment. *Science* **342**, 860-863.

Himanen K, Boucheron E, Vanneste S, Engler JD, Inze D, Beeckman T, 2002. Auxin-mediated cell cycle activation during early lateral root initiation. *Plant Cell* **14**, 2339-2351.

Hirota A, Kato T, Fukaki H, Aida M, Tasaka M, 2007. The auxin-regulated *AP2/EREBP* gene *PUCHI* is required for morphogenesis in the early lateral root primordium of *Arabidopsis*. *Plant Cell* **19**, 2156-2168.

Hobe M, Muller R, Grunewald M, Brand U, Simon R, 2003. Loss of *CLE40*, a protein functionally equivalent to the stem cell restricting signal *CLV3*, enhances root waving in *Arabidopsis*. *Dev Genes Evol* **213**, 371-381.

Hodge A, Robinson D, Griffiths BS, Fitter AH, 1999. Why plants bother: root proliferation results in increased nitrogen capture from an organic patch when two grasses compete. *Plant Cell Environ* **22**, 811-820.

Hong JH, Seah SW, Xu J, 2013. The root of ABA action in environmental stress response. *Plant Cell Rep* **32**, 971-983.

Horton MW, Hancock AM, Huang YS, *et al.*, 2012. Genome-wide patterns of genetic variation in worldwide *Arabidopsis thaliana* accessions from the RegMap panel. *Nature Genet* **44**, 212-216.

Hossain Z, Mcgarvey B, Amyot L, Gruber M, Jung J, Hannoufa A, 2012. *DIMINUTO 1* affects the lignin profile and secondary cell wall formation in *Arabidopsis*. *Planta* **235**, 485-98.

Hou X, Liu S, Pierri F, Dai X, Qu LJ, Zhao Y, 2011. Allelic analyses of the *Arabidopsis* YUC1 locus reveal residues and domains essential for the functions of YUC family of flavin monooxygenases. *J Integr Plant Biol* **53**, 54-62.

Hu B, Wang W, Ou SJ, *et al.*, 2015. Variation in NRT1.1B contributes to nitrate-use divergence between rice subspecies. *Nature Genet* **47**, 834-838.

Ishida T, Fujiwara S, Miura K, *et al.*, 2009. SUMO E3 ligase HIGH PLOIDY2 regulates endocycle onset and meristem maintenance in *Arabidopsis*. *Plant Cell* **21**, 2284-2297.

Ito Y, Nakanomyo I, Motose H, *et al.*, 2006. Dodeca-CLE peptides as suppressors of plant stem cell differentiation. *Science* **313**, 842-845.

Ivanchenko MG, Muday GK, Dubrovsky JG, 2008. Ethylene-auxin interactions regulate lateral root initiation and emergence in *Arabidopsis thaliana*. *Plant J* **55**, 335-547.

Jain A, Poling MD, Karthikeyan AS, *et al.*, 2007. Differential effects of sucrose and auxin on localized phosphate deficiency-induced modulation of different traits of root system architecture in *Arabidopsis*. *Plant Physiol* **144**, 232-247.

Jain A, Sinilal B, Dhandapani G, Meagher RB, Sahi SV, 2013. Effects of deficiency and excess of zinc on morphophysiological traits and spatiotemporal regulation of zinc-responsive genes reveal incidence of crosstalk between micro- and macronutrients. *Environ Sci Technol* **47**, 5327-5335.

Jiang CF, Gao XH, Liao L, Harberd NP, Fu XD, 2007. Phosphate starvation root architecture and anthocyanin accumulation responses are modulated by the gibberellin-DELLA signaling pathway in *Arabidopsis*. *Plant Physiol* **145**, 1460-1470.

Jung JY, Shin R, Schachtman DP, 2009. Ethylene mediates response and tolerance to potassium deprivation in *Arabidopsis*. *Plant Cell* **21**, 607-621.

Kakei Y, Yamazaki C, Suzuki M, *et al.*, 2015. Small-molecule auxin inhibitors that target YUCCA are powerful tools for studying auxin function. *Plant J* **84**, 827-837.

Kang HM, Zaitlen NA, Wade CM, *et al.*, 2008. Efficient control of population structure in model organism association mapping. *Genetics* **178**, 1709-1723.

Kellermeier F, Armengaud P, Seditas TJ, Danku J, Salt DE, Amtmann A, 2014. Analysis of the root system architecture of *Arabidopsis* provides a quantitative readout of crosstalk between nutritional signals. *Plant Cell* **26**, 1480-1496.

Kemmerling B, Schwedt A, Rodriguez P, *et al.*, 2007. The BRI1-associated kinase 1, BAK1, has a brassinolide-independent role in plant cell-death control. *Curr Biol* **17**, 1116-1122.

Kim HB, Kwon M, Ryu H, *et al.*, 2006. The regulation of *DWARF4* expression is likely a critical mechanism in maintaining the homeostasis of bioactive brassinosteroids in *Arabidopsis*. *Plant Physiol* **140**, 548-557.

Kim TW, Guan S, Burlingame AL, Wang ZY, 2011. The CDG1 kinase mediates brassinosteroid signal transduction from BRI1 receptor kinase to BSU1 phosphatase and GSK3-like kinase BIN2. *Mol Cell* **43**, 561-571.

Kim TW, Guan S, Sun Y, *et al.*, 2009. Brassinosteroid signal transduction from cell-surface receptor kinases to nuclear transcription factors. *Nat Cell Biol* **11**, 1254-1260.

Kim TW, Lee SM, Joo SH, *et al.*, 2007. Elongation and gravitropic responses of *Arabidopsis* roots are regulated by brassinolide and IAA. *Plant Cell Environ* **30**, 679-689.

Klahre U, Noguchi T, Fujioka S, *et al.*, 1998. The *Arabidopsis* *DIMINUTO/DWARF1* gene encodes a protein involved in steroid synthesis. *Plant Cell* **10**, 1677-1690.

Kooke R, Kruijer W, Bours R, *et al.*, 2016. Genome-wide association mapping and genomic prediction elucidate the genetic architecture of morphological traits in *Arabidopsis*. *Plant Physiol* **170**, 2187-2203.

Krouk G, Lacombe B, Bielach A, *et al.*, 2010. Nitrate-regulated auxin transport by NRT1.1 defines a mechanism for nutrient sensing in plants. *Dev Cell* **18**, 927-937.

Kumpf RP, Shi CL, Larrieu A, *et al.*, 2013. Floral organ abscission peptide IDA and its HAE/HSL2 receptors control cell separation during lateral root emergence. *Proc Natl Acad Sci USA* **110**, 5235-5240.

Kutz A, Muller A, Hennig P, Kaiser WM, Piotrowski M, Weiler EW, 2002. A role for *nitrilase 3* in the regulation of root morphology in sulphur-starving *Arabidopsis thaliana*. *Plant J* **30**, 95-106.

Lampropoulos A, Sutikovic Z, Wenzl C, Maegele I, Lohmann JU, Forner J, 2013. GreenGate - A novel, versatile, and efficient cloning system for plant transgenesis. *Plos One* **8**.

Laplaze L, Benkova E, Casimiro I, *et al.*, 2007. Cytokinins act directly on lateral root founder cells to inhibit root initiation. *Plant Cell* **19**, 3889-3900.

Lark RM, Milne AE, Addiscott TM, Goulding KWT, Webster CP, O'flaherty S, 2004. Scale- and location-dependent correlation of nitrous oxide emissions with soil properties: an analysis using wavelets. *Eur J Soil Sci* **55**, 611-627.

Laskowski MJ, Williams ME, Nusbaum HC, Sussex IM, 1995. Formation of lateral root meristems is a two-stage process. *Development* **121**, 3303-3310.

Lavenus J, Goh T, Roberts I, *et al.*, 2013. Lateral root development in Arabidopsis: fifty shades of auxin. *Trends Plant Sci* **18**, 450-458.

Lee HJ, Jung JH, Llorca LC, *et al.*, 2014. FCA mediates thermal adaptation of stem growth by attenuating auxin action in Arabidopsis. *Nature Commun* **5**.

Lee HW, Kim NY, Lee DJ, Kim J, 2009. LBD18/ASL20 regulates lateral root formation in combination with LBD16/ASL18 downstream of ARF7 and ARF19 in Arabidopsis. *Plant Physiol* **151**, 1377-1389.

Leran S, Edel KH, Pervent M, *et al.*, 2015. Nitrate sensing and uptake in Arabidopsis are enhanced by *ABI2*, a phosphatase inactivated by the stress hormone abscisic acid. *Sci Signal* **8**.

Leskova A, Giehl RFH, Hartmann A, Fargasova A, von Wirén N, 2017. Heavy metals induce iron deficiency responses at different hierarchic and regulatory levels. *Plant Physiol* **174**, 1648-1668.

Lewis DR, Negi S, Sukumar P, Muday GK, 2011. Ethylene inhibits lateral root development, increases IAA transport and expression of *PIN3* and *PIN7* auxin efflux carriers. *Development* **138**, 3485-3495.

Li B, Li G, Kronzucker HJ, Baluska F, Shi W, 2014. Ammonium stress in Arabidopsis: signaling, genetic loci, and physiological targets. *Trends Plant Sci* **19**, 107-114.

Li B, Li Q, Kronzucker HJ, Shi W, 2011a. Roles of abscisic acid and auxin in shoot-supplied ammonium inhibition of root system development. *Plant Signal Behav* **6**, 1451-1453.

Li BH, Li Q, Su YH, *et al.*, 2011b. Shoot-supplied ammonium targets the root auxin influx carrier *AUX1* and inhibits lateral root emergence in Arabidopsis. *Plant Cell Environ* **34**, 933-946.

-
- Li GJ, Li BH, Dong GQ, Feng XY, Kronzucker HJ, Shi WM, 2013. Ammonium-induced shoot ethylene production is associated with the inhibition of lateral root formation in Arabidopsis. *J Exp Bot* **64**, 1413-1425.
- Li GJ, Song HY, Li BH, Kronzucker HJ, Shi WM, 2015a. *Auxin Resistant 1* and *PIN-FORMED2* protect lateral root formation in Arabidopsis under iron stress. *Plant Physiol* **169**, 2608-2623.
- Li GJ, Xu WF, Kronzucker HJ, Shi WM, 2015b. Ethylene is critical to the maintenance of primary root growth and Fe homeostasis under Fe stress in Arabidopsis. *J Exp Bot* **66**, 2041-2054.
- Li Q, Li BH, Kronzucker HJ, Shi WM, 2010. Root growth inhibition by NH_4^+ in Arabidopsis is mediated by the root tip and is linked to NH_4^+ efflux and GMPase activity. *Plant Cell Environ* **33**, 1529-1542.
- Li X, Mo X, Shou H, Wu P, 2006. Cytokinin-mediated cell cycling arrest of pericycle founder cells in lateral root initiation of Arabidopsis. *Plant Cell Physiol* **47**, 1112-1123.
- Liao CY, Smet W, Brunoud G, Yoshida S, Vernoux T, Weijers D, 2015. Reporters for sensitive and quantitative measurement of auxin response. *Nat Methods* **12**, 207-210.
- Lima JE, Kojima S, Takahashi H, von Wirén N, 2010. Ammonium triggers lateral root branching in Arabidopsis in an AMMONIUM TRANSPORTER1;3-dependent manner. *Plant Cell* **22**, 3621-3633.
- Liu G, Gao S, Tian H, Wu W, Robert HS, Ding Z, 2016. Local transcriptional control of *YUCCA* regulates auxin promoted root growth inhibition in response to aluminium stress in Arabidopsis. *PLoS Genet* **12**, e1006360.
- Liu Y, Lai N, Gao K, Chen F, Yuan L, Mi G, 2013. Ammonium inhibits primary root growth by reducing the length of meristem and elongation zone and decreasing elemental expansion rate in the root apex in *Arabidopsis thaliana*. *PLoS One* **8**, e61031.
- Liu Y, von Wirén N, 2017. Ammonium as a signal for physiological and morphological responses in plants. *J Exp Bot* **68**, 2581-2592.
- Liu Y, Xu M, Liang N, Zheng Y, Yu Q, Wu S, 2017. Symplastic communication spatially directs local auxin biosynthesis to maintain root stem cell niche in Arabidopsis. *Proc Natl Acad Sci USA* **114**, 4005-4010.

Lohar DP, Schaff JE, Laskey JG, Kieber JJ, Bilyeu KD, Bird DM, 2004. Cytokinins play opposite roles in lateral root formation, and nematode and Rhizobial symbioses. *Plant J* **38**, 203-214.

López-Bucio J, Cruz-Ramírez A, Herrera-Estrella L, 2003. The role of nutrient availability in regulating root architecture. *Curr Opin Plant Biol* **6**, 280-287.

Lopez-Bucio J, Hernandez-Abreu E, Sanchez-Calderon L, Nieto-Jacobo MF, Simpson J, Herrera-Estrella L, 2002. Phosphate availability alters architecture and causes changes in hormone sensitivity in the Arabidopsis root system. *Plant Physiol* **129**, 244-256.

Lopez-Bucio J, Hernandez-Abreu E, Sanchez-Calderon L, *et al.*, 2005. An auxin transport independent pathway is involved in phosphate stress-induced root architectural alterations in Arabidopsis. Identification of BIG as a mediator of auxin in pericycle cell activation. *Plant Physiol* **137**, 681-691.

Lucas M, Kenobi K, Von Wangenheim D, *et al.*, 2013. Lateral root morphogenesis is dependent on the mechanical properties of the overlaying tissues. *Proc Natl Acad Sci USA* **110**, 5229-5234.

Lynch J, 1995. Root architecture and plant productivity. *Plant Physiol* **109**, 7-13.

Ma W, Li J, Qu B, *et al.*, 2014. Auxin biosynthetic gene *TAR2* is involved in low nitrogen-mediated reprogramming of root architecture in Arabidopsis. *Plant J* **78**, 70-79.

Ma X, Xu G, He P, Shan L, 2016. SERKING coreceptors for receptors. *Trends Plant Sci* **21**, 1017-1033.

Malamy JE, 2005. Intrinsic and environmental response pathways that regulate root system architecture. *Plant Cell Environ* **28**, 67-77.

Malamy JE, Benfey PN, 1997. Organization and cell differentiation in lateral roots of *Arabidopsis thaliana*. *Development* **124**, 33-44.

Marchant A, Bhalerao R, Casimiro I, *et al.*, 2002. AUX1 promotes lateral root formation by facilitating indole-3-acetic acid distribution between sink and source tissues in the Arabidopsis seedling. *Plant Cell* **14**, 589-597.

Marhavy P, Bielach A, Abas L, *et al.*, 2011. Cytokinin modulates endocytic trafficking of PIN1 auxin efflux carrier to control plant organogenesis. *Dev Cell* **21**, 796-804.

Marhavy P, Duclercq J, Weller B, *et al.*, 2014. Cytokinin controls polarity of PIN1-dependent auxin transport during lateral root organogenesis. *Curr Biol* **24**, 1031-1037.

Martins S, Montiel-Jorda A, Cayrel A, *et al.*, 2017. Brassinosteroid signaling-dependent root responses to prolonged elevated ambient temperature. *Nature Commun* **8**.

Mashiguchi K, Tanaka K, Sakai T, *et al.*, 2011. The main auxin biosynthesis pathway in Arabidopsis. *Proc Natl Acad Sci USA* **108**, 18512-18517.

Mason MG, Mathews DE, Argyros DA, *et al.*, 2005. Multiple type-B response regulators mediate cytokinin signal transduction in Arabidopsis. *Plant Cell* **17**, 3007-3018.

Matsubayashi Y, 2012. MBSJ MCC Young Scientist Award 2010. Recent progress in research on small post-translationally modified peptide signals in plants. *Genes Cells* **17**, 1-10.

Matsuzaki Y, Ogawa-Ohnishi M, Mori A, Matsubayashi Y, 2010. Secreted peptide signals required for maintenance of root stem cell niche in Arabidopsis. *Science* **329**, 1065-1067.

Medici A, Marshall-Colon A, Ronzier E, *et al.*, 2015. AtNIGT1/HRS1 integrates nitrate and phosphate signals at the Arabidopsis root tip. *Nature Commun* **6**.

Meijon M, Satbhai SB, Tsuchimatsu T, Busch W, 2014. Genome-wide association study using cellular traits identifies a new regulator of root development in Arabidopsis. *Nature Genet* **46**, 77-81.

Melino VJ, Fiene G, Enju A, Cai JH, Buchner P, Heuer S, 2015. Genetic diversity for root plasticity and nitrogen uptake in wheat seedlings. *Funct Plant Biol* **42**, 942-956.

Miura K, Rus A, Sharkhuu A, *et al.*, 2005. The Arabidopsis SUMO E3 ligase SIZ1 controls phosphate deficiency responses. *Proc Natl Acad Sci USA* **102**, 7760-7765.

Moubayidin L, Perilli S, Dello Iorio R, Di Mambro R, Costantino P, Sabatini S, 2010. The rate of cell differentiation controls the Arabidopsis root meristem growth phase. *Curr Biol* **20**, 1138-1143.

Mouchel CF, Briggs GC, Hardtke CS, 2004. Natural genetic variation in Arabidopsis identifies *BREVIS RADIX*, a novel regulator of cell proliferation and elongation in the root. *Genes Dev* **18**, 700-714.

Mouchel CF, Osmont KS, Hardtke CS, 2006. *BRX* mediates feedback between brassinosteroid levels and auxin signalling in root growth. *Nature* **443**, 458-461.

Muller J, Toev T, Heisters M, *et al.*, 2015. Iron-dependent callose deposition adjusts root meristem maintenance to phosphate availability. *Dev Cell* **33**, 216-230.

Murphy E, Smith S, De Smet I, 2012. Small signaling peptides in Arabidopsis development: how cells communicate over a short distance. *Plant Cell* **24**, 3198-3217.

Mussig C, Shin GH, Altmann T, 2003. Brassinosteroids promote root growth in Arabidopsis. *Plant Physiol* **133**, 1261-1271.

Nacry P, Canivenc G, Muller B, *et al.*, 2005. A role for auxin redistribution in the responses of the root system architecture to phosphate starvation in Arabidopsis. *Plant Physiol* **138**, 2061-2074.

Negi S, Ivanchenko MG, Muday GK, 2008. Ethylene regulates lateral root formation and auxin transport in Arabidopsis thaliana. *Plant J* **55**, 175-187.

Nielsen KL, Eshel A, Lynch JP, 2001. The effect of phosphorus availability on the carbon economy of contrasting common bean (*Phaseolus vulgaris* L.) genotypes. *J Exp Bot* **52**, 329-339.

Ogura T, Busch W, 2015. From phenotypes to causal sequences: using genome wide association studies to dissect the sequence basis for variation of plant development. *Curr Opin Plant Biol* **23**, 98-108.

Ogura T, Busch W, 2016. Genotypes, networks, phenotypes: moving toward plant systems genetics. *Annu Rev Cell Dev Biol* **32**, 103-26.

Okushima Y, Fukaki H, Onoda M, Theologis A, Tasaka M, 2007. ARF7 and ARF19 regulate lateral root formation via direct activation of *LBD/ASL* genes in Arabidopsis. *Plant Cell* **19**, 118-130.

Ortega-Martinez O, Pernas M, Carol RJ, Dolan L, 2007. Ethylene modulates stem cell division in the Arabidopsis thaliana root. *Science* **317**, 507-510.

Ou Y, Lu XT, Zi QN, *et al.*, 2016. RGF1 INSENSITIVE 1 to 5, a group of LRR receptor-like kinases, are essential for the perception of root meristem growth factor 1 in Arabidopsis thaliana. *Cell Res* **26**, 686-698.

Pallakies H, Simon R, 2014. The CLE40 and CRN/CLV2 signaling pathways antagonistically control root meristem growth in Arabidopsis. *Mol Plant* **7**, 1619-1636.

Pearce G, Moura DS, Stratmann J, Ryan CA, Jr., 2001. RALF, a 5-kDa ubiquitous polypeptide in plants, arrests root growth and development. *Proc Natl Acad Sci USA* **98**, 12843-12847.

Peret B, De Rybel B, Casimiro I, *et al.*, 2009. Arabidopsis lateral root development: an emerging story. *Trends Plant Sci* **14**, 399-408.

Peret B, Li G, Zhao J, *et al.*, 2012. Auxin regulates aquaporin function to facilitate lateral root emergence. *Nat Cell Biol* **14**, 991-998.

Peret B, Middleton AM, French AP, *et al.*, 2013. Sequential induction of auxin efflux and influx carriers regulates lateral root emergence. *Mol Syst Biol* **9**.

Perez-Torres CA, Lopez-Bucio J, Cruz-Ramirez A, *et al.*, 2008. Phosphate availability alters lateral root development in Arabidopsis by modulating auxin sensitivity via a mechanism involving the TIR1 auxin receptor. *Plant Cell* **20**, 3258-3272.

Petricka JJ, Winter CM, Benfey PN, 2012. Control of Arabidopsis root development. *Annu Rev Plant Biol* **63**, 563-590.

Pfaffl MW, 2001. A new mathematical model for relative quantification in real-time RT-PCR. *Nucleic Acids Res* **29**, e45.

Qin C, Qian WQ, Wang WF, *et al.*, 2008. GDP-mannose pyrophosphorylase is a genetic determinant of ammonium sensitivity in *Arabidopsis thaliana*. *Proc Natl Acad Sci USA* **105**, 18308-18313.

Qin L, Walk TC, Han P, *et al.*, 2018. Adaption of roots to nitrogen deficiency revealed by 3-D quantification and proteomic analysis. *Plant Physiol*.

Quint M, Delker C, Franklin KA, Wigge PA, Halliday KJ, Van Zanten M, 2016. Molecular and genetic control of plant thermomorphogenesis. *Nat Plants* **2**, 15190.

Ramireddy E, Hosseini SA, Eggert K, *et al.*, 2018. Root engineering in barley: increasing cytokinin degradation produces a larger root system, mineral enrichment in the shoot and improved drought tolerance. *Plant Physiol* **177**, 1078-1095.

Rellan-Alvarez R, Lobet G, Lindner H, *et al.*, 2015. GLO-Roots: an imaging platform enabling multidimensional characterization of soil-grown root systems. *Elife* **4**.

Remans T, Nacry P, Pervent M, *et al.*, 2006. The Arabidopsis NRT1.1 transporter participates in the signaling pathway triggering root colonization of nitrate-rich patches. *Proc Natl Acad Sci USA* **103**, 19206-19211.

Ren H, Willige BC, Jaillais Y, *et al.*, 2019. BRASSINOSTEROID-SIGNALING KINASE 3, a plasma membrane-associated scaffold protein involved in early brassinosteroid signaling. *PLoS Genet* **15**, e1007904.

Richard O, Pineau C, Loubet S, *et al.*, 2011. Diversity analysis of the response to Zn within the *Arabidopsis thaliana* species revealed a low contribution of Zn translocation to Zn tolerance and a new role for Zn in lateral root development. *Plant Cell Environ* **34**, 1065-1078.

Richards DE, King KE, Ait-Ali T, Harberd NP, 2001. How gibberellin regulates plant growth and development: a molecular genetic analysis of gibberellin signaling. *Annu Rev Plant Physiol Plant Mol Bio* **52**, 67-88.

Riefler M, Novak O, Strnad M, Schmulling T, 2006. Arabidopsis cytokinin receptor mutants reveal functions in shoot growth, leaf senescence, seed size, germination, root development, and cytokinin metabolism. *Plant Cell* **18**, 40-54.

Ristova D, Busch W, 2014. Natural variation of root traits: from development to nutrient uptake. *Plant Physiol* **166**, 518-527.

Riveras E, Alvarez JM, Vidal EA, Oses C, Vega A, Gutierrez RA, 2015. The calcium ion is a second messenger in the nitrate signaling pathway of Arabidopsis. *Plant Physiol* **169**, 1397-1404.

Robinson D, Hodge A, Griffiths BS, Fitter AH, 1999. Plant root proliferation in nitrogen-rich patches confers competitive advantage. *Proc R Soc Lond B Biol Sci*. **266**, 431-435.

Rogg LE, Lasswell J, Bartel B, 2001. A gain-of-function mutation in IAA28 suppresses lateral root development. *Plant Cell* **13**, 465-480.

Rosas U, Cibrian-Jaramillo A, Ristova D, *et al.*, 2013. Integration of responses within and across Arabidopsis natural accessions uncovers loci controlling root systems architecture. *Proc Natl Acad Sci USA* **110**, 15133-15138.

Ruzicka K, Ljung K, Vanneste S, *et al.*, 2007. Ethylene regulates root growth through effects on auxin biosynthesis and transport-dependent auxin distribution. *Plant Cell* **19**, 2197-2212.

Ruzicka K, Simaskova M, Duclercq J, *et al.*, 2009. Cytokinin regulates root meristem activity via modulation of the polar auxin transport. *Proc Natl Acad Sci USA* **106**, 4284-4289.

Ryu H, Kim K, Cho H, Park J, Choe S, Hwang I, 2007. Nucleocytoplasmic shuttling of BZR1 mediated by phosphorylation is essential in Arabidopsis brassinosteroid signaling. *Plant Cell* **19**, 2749-2762.

Sabatini S, Beis D, Wolkenfelt H, *et al.*, 1999. An auxin-dependent distal organizer of pattern and polarity in the Arabidopsis root. *Cell* **99**, 463-472.

Sabatini S, Heidstra R, Wildwater M, Scheres B, 2003. SCARECROW is involved in positioning the stem cell niche in the Arabidopsis root meristem. *Genes Dev* **17**, 354-358.

Sanchez-Bermejo E, Zhu WS, Tasset C, *et al.*, 2015. Genetic architecture of natural variation in thermal responses of *Arabidopsis*. *Plant Physiol* **169**, 647-659.

Sanchez-Calderon L, Lopez-Bucio J, Chacon-Lopez A, *et al.*, 2005. Phosphate starvation induces a determinate developmental program in the roots of *Arabidopsis thaliana*. *Plant Cell Physiol* **46**, 174-184.

Satbhai SB, Setzer C, Freynschlag F, Slovak R, Kerdaffrec E, Busch W, 2017. Natural allelic variation of *FRO2* modulates *Arabidopsis* root growth under iron deficiency. *Nature Commun* **8**, 15603.

Scacchi E, Osmont KS, Beuchat J, *et al.*, 2009. Dynamic, auxin-responsive plasma membrane-to-nucleus movement of *Arabidopsis* BRX. *Development* **136**, 2059-2067.

Schluter U, Kopke D, Altmann T, Mussig C, 2002. Analysis of carbohydrate metabolism of *CPD* antisense plants and the brassinosteroid-deficient *cbb1* mutant. *Plant Cell Environ* **25**, 783-791.

Shahzad Z, Amtmann A, 2017. Food for thought: how nutrients regulate root system architecture. *Curr Opin Plant Biol* **39**, 80-87.

Shao A, Ma W, Zhao X, *et al.*, 2017. The auxin biosynthetic TRYPTOPHAN AMINOTRANSFERASE RELATED *TaTAR2.1-3A* increases grain yield of wheat. *Plant Physiol* **174**, 2274-2288.

Shen X, Pettersson M, Ronnegard L, Carlborg O, 2012. Inheritance beyond plain heritability: variance-controlling genes in *Arabidopsis thaliana*. *PLoS Genet* **8**, e1002839.

Shi H, Shen Q, Qi Y, *et al.*, 2013. BR-SIGNALING KINASE1 physically associates with FLAGELLIN SENSING2 and regulates plant innate immunity in *Arabidopsis*. *Plant Cell* **25**, 1143-1157.

Shimada Y, Goda H, Nakamura A, Takatsuto S, Fujioka S, Yoshida S, 2003. Organ-specific expression of brassinosteroid-biosynthetic genes and distribution of endogenous brassinosteroids in *Arabidopsis*. *Plant Physiol* **131**, 287-297.

Shin R, Burch AY, Huppert KA, *et al.*, 2007. The *Arabidopsis* transcription factor MYB77 modulates auxin signal transduction. *Plant Cell* **19**, 2440-2453.

Shin R, Schachtman DP, 2004. Hydrogen peroxide mediates plant root cell response to nutrient deprivation. *Proc Natl Acad Sci USA* **101**, 8827-8832.

Shinohara H, Mori A, Yasue N, Sumida K, Matsubayashi Y, 2016. Identification of three LRR-RKs involved in perception of root meristem growth factor in Arabidopsis. *Proc Natl Acad Sci USA* **113**, 3897-3902.

Shkolnik-Inbar D, Bar-Zvi D, 2010. ABI4 mediates abscisic acid and cytokinin inhibition of lateral root formation by reducing polar auxin transport in Arabidopsis. *Plant Cell* **22**, 3560-3573.

Signora L, De Smet I, Foyer CH, Zhang H, 2001. ABA plays a central role in mediating the regulatory effects of nitrate on root branching in Arabidopsis. *Plant J* **28**, 655-662.

Simaskova M, O'brien JA, Khan M, *et al.*, 2015. Cytokinin response factors regulate PIN-FORMED auxin transporters. *Nat Commun* **6**, 8717.

Singh AP, Fridman Y, Friedlander-Shani L, Tarkowska D, Strnad M, Savaldi-Goldstein S, 2014. Activity of the brassinosteroid transcription factors BRASSINAZOLE RESISTANT1 and BRASSINOSTEROID INSENSITIVE1-ETHYL METHANESULFONATE-SUPPRESSOR1/BRASSINAZOLE RESISTANT2 blocks developmental reprogramming in response to low phosphate availability. *Plant Physiol* **166**, 678-688.

Singh AP, Fridman Y, Holland N, *et al.*, 2018. Interdependent nutrient availability and steroid hormone signals facilitate root growth plasticity. *Dev Cell* **46**, 59-72.

Sozzani R, Maggio C, Giordo R, *et al.*, 2010. The E2FD/DEL2 factor is a component of a regulatory network controlling cell proliferation and development in Arabidopsis. *Plant Mol Biol* **72**, 381-395.

Sreeramulu S, Mostizky Y, Sunitha S, *et al.*, 2013. BSKs are partially redundant positive regulators of brassinosteroid signaling in Arabidopsis. *Plant J* **74**, 905-919.

Stahl Y, Grabowski S, Bleckmann A, *et al.*, 2013. Moderation of Arabidopsis root stemness by CLAVATA1 and ARABIDOPSIS CRINKLY4 receptor kinase complexes. *Curr Biol* **23**, 362-371.

Stepanova AN, Hoyt JM, Hamilton AA, Alonso JM, 2005. A link between ethylene and auxin uncovered by the characterization of two root-specific ethylene-insensitive mutants in Arabidopsis. *Plant Cell* **17**, 2230-2242.

Stepanova AN, Robertson-Hoyt J, Yun J, *et al.*, 2008. TAA1-mediated auxin biosynthesis is essential for hormone crosstalk and plant development. *Cell* **133**, 177-191.

-
- Stepanova AN, Yun J, Robles LM, *et al.*, 2011. The Arabidopsis YUCCA1 flavin monooxygenase functions in the indole-3-pyruvic acid branch of auxin biosynthesis. *Plant Cell* **23**, 3961-3973.
- Sun HW, Tao JY, Liu SJ, *et al.*, 2014. Strigolactones are involved in phosphate- and nitrate-deficiency-induced root development and auxin transport in rice. *J Exp Bot* **65**, 6735-6746.
- Sun JQ, Qi LL, Li YN, Chu JF, Li CY, 2012. PIF4-mediated activation of YUCCA8 expression integrates temperature into the auxin pathway in regulating Arabidopsis hypocotyl growth. *Plos Genet* **8**.
- Sun JQ, Xu YX, Ye SQ, *et al.*, 2009. Arabidopsis ASA1 is important for jasmonate-mediated regulation of auxin biosynthesis and transport during lateral root formation. *Plant Cell* **21**, 1495-1511.
- Sun Y, Fan XY, Cao DM, *et al.*, 2010. Integration of brassinosteroid signal transduction with the transcription network for plant growth regulation in Arabidopsis. *Dev Cell* **19**, 765-777.
- Svistoonoff S, Creff A, Reymond M, *et al.*, 2007. Root tip contact with low-phosphate media reprograms plant root architecture. *Nature Genet* **39**, 792-796.
- Swarup K, Benkova E, Swarup R, *et al.*, 2008. The auxin influx carrier LAX3 promotes lateral root emergence. *Nat Cell Biol* **10**, 946-954.
- Swarup R, Perry P, Hagenbeek D, *et al.*, 2007. Ethylene upregulates auxin biosynthesis in Arabidopsis seedlings to enhance inhibition of root cell elongation. *Plant Cell* **19**, 2186-2196.
- Tabas-Madrid D, Mendez-Vigo B, Arteaga N, *et al.*, 2018. Genome-wide signatures of flowering adaptation to climate temperature: regional analyses in a highly diverse native range of *Arabidopsis thaliana*. *Plant Cell Environ* **41**, 1806-1820.
- Takahashi T, Gasch A, Nishizawa N, Chua NH, 1995. The *DIMINUTO* gene of Arabidopsis is involved in regulating cell elongation. *Genes Dev* **9**, 97-107.
- Tang J, Han ZF, Sun YD, Zhang HQ, Gong XQ, Chai JJ, 2015. Structural basis for recognition of an endogenous peptide by the plant receptor kinase PEPR1. *Cell Res* **25**, 110-120.
- Tang W, Kim TW, Oses-Prieto JA, *et al.*, 2008. BSKs mediate signal transduction from the receptor kinase BRI1 in Arabidopsis. *Science* **321**, 557-560.

Tao Y, Ferrer JL, Ljung K, *et al.*, 2008. Rapid synthesis of auxin via a new tryptophan-dependent pathway is required for shade avoidance in plants. *Cell* **133**, 164-176.

Tian QY, Sun P, Zhang WH, 2009. Ethylene is involved in nitrate-dependent root growth and branching in *Arabidopsis thaliana*. *New Phytol* **184**, 918-931.

Ticconi CA, Delatorre CA, Lahner B, Salt DE, Abel S, 2004. *Arabidopsis pdr2* reveals a phosphate-sensitive checkpoint in root development. *Plant J* **37**, 801-814.

Ticconi CA, Lucero RD, Sakhonwasee S, *et al.*, 2009. ER-resident proteins PDR2 and LPR1 mediate the developmental response of root meristems to phosphate availability. *Proc Natl Acad Sci USA* **106**, 14174-14179.

To JPC, Haberer G, Ferreira FJ, *et al.*, 2004. Type-A *Arabidopsis* response regulators are partially redundant negative regulators of cytokinin signaling. *Plant Cell* **16**, 658-671.

Ubeda-Tomas S, Federici F, Casimiro I, *et al.*, 2009. Gibberellin signaling in the endodermis controls *Arabidopsis* root meristem size. *Curr Biol* **19**, 1194-1199.

Ubeda-Tomas S, Swarup R, Coates J, *et al.*, 2008. Root growth in *Arabidopsis* requires gibberellin/DELLA signalling in the endodermis. *Nat Cell Biol* **10**, 625-628.

Uga Y, Sugimoto K, Ogawa S, *et al.*, 2013. Control of root system architecture by DEEPER ROOTING 1 increases rice yield under drought conditions. *Nature Genet* **45**, 1097-1102.

Vanneste S, De Rybel B, Beemster GTS, *et al.*, 2005. Cell cycle progression in the pericycle is not sufficient for SOLITARY ROOT/IAA14-mediated lateral root initiation in *Arabidopsis thaliana*. *Plant Cell* **17**, 3035-3050.

Vaseva II, Qudeimat E, Potuschak T, *et al.*, 2018. The plant hormone ethylene restricts *Arabidopsis* growth via the epidermis. *Proc Natl Acad Sci USA* **115**, 4130-4139.

Vermeer JEM, Von Wangenheim D, Barberon M, *et al.*, 2014. A spatial accommodation by neighboring cells is required for organ initiation in *Arabidopsis*. *Science* **343**, 178-183.

Vicente-Agullo F, Rigas S, Desbrosses G, Dolan L, Hatzopoulos P, Grabov A, 2004. Potassium carrier *TRH1* is required for auxin transport in *Arabidopsis* roots. *Plant J* **40**, 523-535.

Vidal EA, Araus V, Lu C, *et al.*, 2010. Nitrate-responsive *miR393/AFB3* regulatory module controls root system architecture in *Arabidopsis thaliana*. *Proc Natl Acad Sci USA* **107**, 4477-4482.

Vidal EA, Moyano TC, Riveras E, Contreras-Lopez O, Gutierrez RA, 2013. Systems approaches map regulatory networks downstream of the auxin receptor *AFB3* in the nitrate response of *Arabidopsis thaliana* roots. *Proc Natl Acad Sci USA* **110**, 12840-12845.

Vilarrasa-Blasi J, Gonzalez-Garcia MP, Frigola D, *et al.*, 2014. Regulation of plant stem cell quiescence by a brassinosteroid signaling module. *Dev Cell* **30**, 36-47.

von Wirén N, Bennett MJ, 2016. Crosstalk between gibberellin signaling and iron uptake in plants: an achilles' heel for modern cereal varieties? *Dev Cell* **37**, 110-111.

Walch-Liu P, Forde BG, 2008. Nitrate signalling mediated by the NRT1.1 nitrate transporter antagonises L-glutamate-induced changes in root architecture. *Plant J* **54**, 820-828.

Walch-Liu P, Liu LH, Remans T, Tester M, Forde BG, 2006. Evidence that L-glutamate can act as an exogenous signal to modulate root growth and branching in *Arabidopsis thaliana*. *Plant Cell Physiol* **47**, 1045-1057.

Walch-Liu P, Meyer RC, Altmann T, Forde BG, 2017. QTL analysis of the developmental response to L-glutamate in *Arabidopsis* roots and its genotype-by-environment interactions. *J Exp Bot* **68**, 2919-2931.

Wang HJ, Tang J, Liu J, *et al.*, 2018. Abscisic acid signaling inhibits brassinosteroid signaling through dampening the dephosphorylation of BIN2 by ABI1 and ABI2. *Mol Plant* **11**, 315-325.

Wang L, Hua DP, He JN, *et al.*, 2011. Auxin Response Factor 2 (ARF2) and its regulated homeodomain gene HB33 mediate abscisic acid response in *Arabidopsis*. *Plos Genetics* **7**.

Wang ZY, Bai MY, Oh E, Zhu JY, 2012. Brassinosteroid signaling network and regulation of photomorphogenesis. *Annu Rev Genet* **46**, 701-724.

Ward JT, Lahner B, Yakubova E, Salt DE, Raghothama KG, 2008. The effect of iron on the primary root elongation of *Arabidopsis* during phosphate deficiency. *Plant Physiol* **147**, 1181-1191.

Werner T, Motyka V, Laucou V, Smets R, Van Onckelen H, Schmulling T, 2003. Cytokinin-deficient transgenic *Arabidopsis* plants show multiple developmental

alterations indicating opposite functions of cytokinins in the regulation of shoot and root meristem activity. *Plant Cell* **15**, 2532-2550.

Werner T, Motyka V, Strnad M, Schmulling T, 2001. Regulation of plant growth by cytokinin. *Proc Natl Acad Sci USA* **98**, 10487-10492.

Wild M, Daviere JM, Regnault T, *et al.*, 2016. Tissue-specific regulation of gibberellin signaling fine-tunes Arabidopsis iron-deficiency responses. *Dev Cell* **37**, 190-200.

Williamson LC, Ribrioux SPCP, Fitter AH, Leyser HMO, 2001. Phosphate availability regulates root system architecture in Arabidopsis. *Plant Physiol* **126**, 875-882.

Won C, Shen X, Mashiguchi K, *et al.*, 2011. Conversion of tryptophan to indole-3-acetic acid by TRYPTOPHAN AMINOTRANSFERASES OF *ARABIDOPSIS* and YUCCAs in Arabidopsis. *Proc Natl Acad Sci USA* **108**, 18518-18523.

Wu G, Lewis DR, Spalding EP, 2007. Mutations in Arabidopsis multidrug resistance-like ABC transporters separate the roles of acropetal and basipetal auxin transport in lateral root development. *Plant Cell* **19**, 1826-1837.

Xu J, Li HD, Chen LQ, *et al.*, 2006. A protein kinase, interacting with two calcineurin B-like proteins, regulates K⁺ transporter AKT1 in Arabidopsis. *Cell* **125**, 1347-60.

Xuan YH, Duan FY, Je BI, *et al.*, 2017. Related to *ABI3/VP1-Like 1 (RAVL1)* regulates brassinosteroid-mediated activation of *AMT1;2* in rice (*Oryza sativa*). *J Exp Bot* **68**, 727-737.

Xue LW, Du JB, Yang H, Xu F, Yuan S, Lin HH, 2009. Brassinosteroids counteract abscisic acid in germination and growth of Arabidopsis. *Z. Naturforsch., C, J. Biosci* **64**, 225-230.

Yang ZB, Geng XY, He CM, *et al.*, 2014. TAA1-regulated local auxin biosynthesis in the root-apex transition zone mediates the aluminum-induced inhibition of root growth in Arabidopsis. *Plant Cell* **26**, 2889-2904.

Youn JH, Kim TW, Joo SH, *et al.*, 2018. Function and molecular regulation of DWARF1 as a C-24 reductase in brassinosteroid biosynthesis in Arabidopsis. *J Exp Bot* **69**, 1873-1886.

Yuan HM, Xu HH, Liu WC, Lu YT, 2013. Copper regulates primary root elongation through PIN1-mediated auxin redistribution. *Plant Cell Physiol* **54**, 766-778.

Zhang B, Wang X, Zhao Z, *et al.*, 2016. OsBRI1 activates BR signaling by preventing binding between the TPR and kinase domains of OsBSK3 via phosphorylation. *Plant Physiol* **170**, 1149-1161.

-
- Zhang H, Han W, De Smet I, *et al.*, 2010. ABA promotes quiescence of the quiescent centre and suppresses stem cell differentiation in the *Arabidopsis* primary root meristem. *Plant J* **64**, 764-774.
- Zhang HM, Forde BG, 1998. An *Arabidopsis* MADS box gene that controls nutrient-induced changes in root architecture. *Science* **279**, 407-409.
- Zhang HM, Jennings A, Barlow PW, Forde BG, 1999. Dual pathways for regulation of root branching by nitrate. *Proc Natl Acad Sci USA* **96**, 6529-6534.
- Zhang HM, Rong HL, Pilbeam D, 2007. Signalling mechanisms underlying the morphological responses of the root system to nitrogen in *Arabidopsis thaliana*. *J Exp Bot* **58**, 2329-2338.
- Zhang J, Tran Q, Lattard V, Cashman JR, 2003. Deleterious mutations in the flavin-containing monooxygenase 3 (FMO3) gene causing trimethylaminuria. *Pharmacogenetics* **13**, 495-500.
- Zhao Q, Wu Y, Gao L, Ma J, Li CY, Xiang CB, 2014. Sulfur nutrient availability regulates root elongation by affecting root indole-3-acetic acid levels and the stem cell niche. *J Integr Plant Biol* **56**, 1151-1163.
- Zhao Y, Christensen SK, Fankhauser C, *et al.*, 2001. A role for flavin monooxygenase-like enzymes in auxin biosynthesis. *Science* **291**, 306-309.
- Zhu C, Gore M, Buckler ES, Yu J, 2008. Status and prospects of association mapping in plants. *Plant Genome* **1**, 5.

7 Appendix

Supplemental Table 1. Geo-referenced Arabidopsis ecotypes with their root lengths and allelic status of BSK3 and YUC8.

Genotype	Latitude	Longitude	Country	Primary root length (cm)		Average LR length (cm)		Total LR root length (cm)		Total root length (cm)		BSK3(L319P)	YUC8(L14S)
				HN	LN	HN	LN	HN	LN	HN	LN		
Aa-0	50.92	9.571	Germany	9.3234	10.42	0.489	0.9	9.49	17.5	18.82	27.89	L	L
Ak-1	48.07	7.626	Germany	10.063	12.15	0.333	0.79	11.4	31.1	21.3	43.29	P	L
Alc-0	40.31	-3.22	Spain	8.3422	9.908	0.39	0.79	9.62	21.8	17.96	31.72	P	L
Alst-1	54.8	-2.43	United Kindom	9.62	10.9	0.352	0.7	13.2	24.8	22.83	35.67	P	S
Amel-1	53.45	5.73	Netherlands	7.0823	9.103	0.416	0.7	10.4	20.7	17.45	29.5	P	L
An-1	51.22	4.4	Belgium	8.9647	9.675	0.569	1	14.5	27	23.5	36.68	P	L
An-2	51.22	4.4	Belgium	9.4162	11.03	0.458	0.89	14	30.6	23.44	41.66	NA	NA
Ang-0	50.3	5.3	Belgium	7.1532	8.671	0.359	0.83	9.48	23.2	16.64	31.88	P	L
Ann-1	45.9	6.13	France	7.7621	9.174	0.419	0.89	11.5	22.3	19.26	31.52	P	L
Arby-1	59.43	16.8	Sweden	9.7402	11	0.496	0.83	18	29.5	26.59	40.51	NA	NA
Ba-1	56.55	-4.8	United Kindom	8.1122	9.121	0.34	0.71	12.7	24.7	20.78	33.87	P	L
Ba1-2	56.4	12.9	Sweden	8.6395	9.991	0.455	0.82	15.6	29	24.27	39.02	NA	NA
Bay-0	49	11	Germany	8.5375	9.307	0.529	0.97	18	30.4	25.51	39.74	NA	NA
Bla-1	41.68	2.8	Spain	9.0801	9.528	0.331	0.76	10.7	21.3	19.78	30.85	P	L
Blh-1	48	19	Czech Republic	8.4641	10.74	0.387	0.87	10.4	36.5	18.87	45.43	P	L
Boot-1	54.4	-3.27	United Kindom	7.5241	8.881	0.364	0.73	13	25.4	20.55	34.28	P	L
Bor-1	49.4	16.23	Czech Republic	9.3441	10.21	0.58	1.02	18.4	33.2	27.76	43.39	P	L
Bor-4	49.4	16.23	Czech Republic	7.1416	7.659	0.575	0.92	13	23.3	20.18	30.99	P	L
Br-0	49.2	16.62	Czech Republic	8.2692	10.07	0.398	0.84	11.7	26.5	19.99	36.56	P	L
Bs-1	47.5	7.5	Switzerland	9.1978	9.798	0.463	0.79	12.7	22	21.85	31.81	P	L
Bs-2	47.5	7.5	Switzerland	10.475	11.61	0.55	1.02	18	38.9	28.46	50.56	NA	NA
Bsch-0	40.02	8.667	Germany	9.2935	11.17	0.322	0.75	11.9	27.3	21.22	38.5	P	L
Bu-0	50.5	9.5	Germany	9.1053	9.604	0.54	0.95	12.6	21.3	21.67	30.91	L	L

Bur-0	54.1	-6.2	Ireland	9.3077	9.354	0.416	0.88	11.8	25.3	21.14	34.65	P	S
Ca-0	50.3	8.266	Germany	10.318	11.86	0.631	1.18	22.6	43.8	32.89	55.69	L	L
CAM-16	48.27	-4.58	France	7.7174	9.597	0.381	0.68	10.5	20	18.22	29.57	NA	NA
Cha-0	46.03	7.117	Switzerland	9.9542	11.79	0.691	1.36	23	51.5	32.96	63.29	NA	NA
Chat-1	48.07	1.339	France	7.7526	9.689	0.326	0.67	11.5	22.7	19.23	32.36	L	L
CIBC-17	51.41	-0.64	United Kindom	8.2643	9.746	0.676	1.25	20.4	43.9	28.63	53.75	P	L
CIBC-5	51.41	-0.64	United Kindom	7.4132	8.972	0.363	0.72	14.8	29.5	22.23	38.52	P	L
Co	40.21	-8.43	Portugal	9.1932	9.782	0.43	0.53	12.6	15.1	21.79	24.85	P	S
Co-2	40.12	-8.25	Portugal	8.7617	9.659	0.669	1.48	22.6	48.6	31.38	58.3	NA	NA
Co-3	40.12	-8.25	Portugal	6.9345	8.185	0.326	0.92	10.9	29.4	17.87	37.54	NA	NA
Co-4	40.12	-8.25	Portugal	8.8041	10.27	0.4	0.75	16.3	28.4	25.1	38.65	NA	NA
Col-0	38.3	-92.3	Germany	9.4186	10.83	0.801	1.45	25	45.9	34.42	56.72	L	L
Com-1	49.42	2.823	France	7.0213	9.411	0.287	0.62	10	25.9	17.06	35.31	P	L
Ct-1	37.3	15	Italy	8.2839	10.12	0.497	1.08	17.7	40.7	25.93	50.87	P	L
Cvi-0	15.11	-23.6	Cape Verde	6.4659	9.176	0.353	0.88	9.46	23.2	15.93	32.39	P	S
Da-0	49.87	8.651	Germany	8.8931	10.92	0.291	0.61	9.97	24.4	18.87	35.32	NA	NA
Di-1	47	5	France	8.857	10.5	0.405	1	11.7	27.7	20.52	38.18	NA	NA
Do-0	50.72	8.237	Germany	7.171	10.04	0.495	0.84	11.9	22	18.88	32.01	P	L
Dra-0	49.42	16.27	Czech Republic	7.2622	8.663	0.404	0.72	10.6	20.4	17.85	29.02	P	L
DralV1-14	49.41	16.28	Czech Republic	8.4261	9.26	0.504	0.86	15.8	30.7	24.25	39.75	NA	NA
Duk	49.1	16.2	Czech Republic	9.8894	10.66	0.318	0.76	12.9	32.1	22.76	42.74	P	L
Ede-1	52.03	5.667	Netherlands	7.974	9.772	0.471	0.97	15.3	31.5	23.26	41.29	NA	NA
Eden-1	62.88	18.18	Sweden	7.9646	9.665	0.269	0.63	8.71	22.1	16.68	31.79	P	L
Edi-0	56	-3	United Kindom	9.4042	11.18	0.454	0.63	14.4	22.4	24.11	33.57	L	S
Ei-2	50.3	6.3	Germany	9.3732	10.21	0.5	1.03	17.1	37.2	26.5	47.43	L	L
En-1	50	8.5	Germany	9.0904	9.702	0.535	0.92	20.3	35.5	29.35	45.35	P	L
Ep-0	50.17	8.389	Germany	8.5473	9.809	0.452	0.91	17.1	32.9	25.6	42.68	NA	NA
Es-0	60.2	24.57	Finland	7.9743	9.103	0.64	0.92	18.9	31.1	26.84	40.16	P	L
Est-0	58.3	25.3	Estonia	10.503	11.67	0.776	1.45	29.8	57.9	38.95	69.53	P	L

Est-1	58.3	25.3	Estonia	8.8846	10.28	0.487	0.88	18.6	36.1	27.46	46.36	L	L
Fei-0	40.92	-8.54	Portugal	8.2785	8.98	0.364	0.79	12.1	23	20.37	31.97	P	L
Fi-1	50.5	8.017	Germany	9.4115	10.06	0.409	0.95	16	29.4	25.4	39.42	NA	NA
Ga-0	50.3	8	Germany	8.8676	10.33	0.427	0.89	13.1	28.5	21.96	38.83	P	L
Gd-1	53.5	10.5	Germany	10.021	11.25	0.448	0.95	16.4	38.1	26.38	49.36	NA	NA
Ge-1	46.5	6.08	Switzerland	8.9459	10.66	0.335	0.82	10.2	23.9	19.15	34.58	NA	NA
Gel-1	51.02	5.867	Netherlands	9.1594	10.15	0.392	0.7	13.3	26.5	22.46	36.65	L	L
Gie-0	50.58	8.678	Germany	7.9985	9.902	0.602	1.19	18.4	34.7	26.42	44.64	P	L
GOT-7	51.53	9.936	Germany	7.5152	10.53	0.538	0.98	14.9	30.9	22.37	41.44	P	L
Gr-1	47	15.5	Austria	7.4783	9.013	0.399	0.8	9.21	24.3	16.69	33.29	P	L
Gu-0	50.3	8	Germany	7.8128	9.278	0.401	0.82	11.5	25.8	19.28	35.05	L	L
Gy-0	49	2	France	7.5494	8.609	0.358	0.81	11.1	24.2	18.65	32.77	P	L
Ha-0	52.37	9.736	Germany	7.2851	8.817	0.517	0.97	15.4	32.6	22.68	41.39	L	L
Hau-0	55.68	12.57	Denmarkmark	7.2793	8.632	0.39	0.78	11.8	25	18.03	33.59	P	L
Hey-1	51.25	5.9	Netherlands	9.0755	11.5	0.476	1.02	13.7	30.6	22.78	42.06	L	L
Hi-0	52	5	Netherlands	7.9508	9.488	0.408	0.91	12.8	31.1	20.76	40.61	P	L
HI-3	52.14	9.378	Germany	6.876	7.697	0.422	0.84	15	27.9	21.89	35.57	NA	NA
HOG	38.72	69.71	Tajikistan	6.065	6.964	0.433	0.65	12.9	20	18.99	26.95	NA	NA
HR-10	51.41	-0.64	United Kindom	7.2656	8.565	0.402	0.83	11.6	24	18.84	32.61	NA	NA
HR-5	51.41	-0.64	United Kindom	7.2913	9.314	0.436	0.74	11.7	22.7	19.01	32.02	NA	NA
Hs-0	52.24	9.44	Germany	9.7237	9.964	0.449	0.98	17.8	36.7	27.55	46.69	L	L
HSm	49.33	15.76	Czech Republic	6.8405	8.172	0.482	1.01	13.3	28.4	20.15	36.61	NA	NA
In-0	47.5	11.5	Austria	7.8172	9.186	0.502	1.1	16.8	41.2	24.66	50.4	P	L
Je-0	50.93	11.59	Germany	9.5658	10.99	0.443	0.83	15.1	32.4	24.65	43.38	P	L
JEA	43.68	7.333	France	8.5638	10.29	0.451	1.1	13.7	33.7	22.29	43.94	P	L
Jl-3	49.31	16.61	Czech Republic	9.2082	10.14	0.578	1.28	20.1	48.9	29.35	59.06	P	L
Jm-1	49	15	Czech Republic	8.0286	9.164	0.39	0.83	13.5	28.3	21.53	37.43	NA	NA
Kä-0	47	14	Austria	9.2773	11.05	0.465	0.81	12.2	28.1	21.44	39.14	NA	NA
Kas-2	35	77	India	8.5906	9.101	0.535	1.25	23.1	46.6	31.66	55.72	P	L

Kelsterbach-2	50.07	8.533	Germany	8.4591	9.875	0.463	0.95	13.3	30.5	21.76	40.27	NA	NA
Kil-0	55.64	-5.66	United Kindom	8.8981	10.4	0.343	0.83	12.1	31.3	20.96	41.68	L	L
Kin-0	43.36	-85.3	United states of America	9.1202	9.602	0.473	1.04	14.8	25.7	23.92	35.33	P	L
KI-5	50.95	6.967	Germany	8.8748	10.53	0.433	0.88	14.8	34	23.71	44.57	L	L
Kn-0	54.9	23.89	Lithuania	9.0507	10.27	0.448	0.92	16.1	32.6	25.12	42.61	P	L
Kno-18	41.28	-86.6	United states of America	10.09	11.47	0.401	0.76	13.8	25.2	23.9	36.63	NA	NA
Kr-0	51.33	6.559	Germany	10.76	11.83	0.696	1.19	27.8	43.3	39.85	55.08	NA	NA
Krot-2	49.63	11.57	Germany	7.6324	9.637	0.498	0.96	15.1	31.5	22.71	41.14	NA	NA
Kz-1	49.5	73.1	Kazakhstan	9.3411	10.85	0.431	0.89	18.8	43.5	28.16	54.49	NA	NA
Kz-9	49.5	73.1	Kazakhstan	9.3176	11.32	0.628	1.37	17.7	49.4	26.98	60.61	P	L
LAC-5	47.7	6.817	France	6.1859	7.449	0.385	0.81	12.5	24.3	18.69	32.85	NA	NA
Lc-0	57	-4	United Kindom	6.6599	8.24	0.323	0.65	4.99	15.2	11.43	23.47	NA	NA
LDV-14	48.52	-4.07	France	6.826	9.099	0.323	0.77	10.2	26.2	16.99	35.33	NA	NA
LDV-58	48.52	-4.07	France	7.4763	10.32	0.359	0.69	11	24.2	18.51	34.57	NA	NA
Ler-1	47.98	10.87	Germany	7.856	9.583	0.61	1.13	21	44.1	28.81	53.67	P	L
Li-3	50.38	8.067	Germany	9.6592	10.9	0.694	1.14	21.5	41.8	31.12	52.72	NA	NA
Li-7	50.38	8.067	Germany	8.5786	10.48	0.436	0.86	13.2	32.1	21.74	42.61	NA	NA
Lip-0	50	19.3	Poland	8.6644	11.38	0.53	1.09	16.2	42.1	24.9	53.52	P	L
LL-0	41.59	2.49	Spain	7.4816	9.313	0.46	0.79	9.11	16.4	16.59	25.74	P	L
Lm-2	48	0.5	France	9.5833	11.05	0.536	1.02	13.5	27.6	23.44	38.63	P	L
Löv-5	62.8	18.08	Sweden	7.2342	9.118	0.401	0.95	9.29	21.3	16.52	30.45	NA	NA
Lp2-2	49.38	16.81	Czech Republic	8.2129	9.284	0.388	0.79	11.3	24.4	19.5	33.68	P	L
Lp2-6	49.38	16.81	Czech Republic	6.8662	8.463	0.428	0.86	10.6	20.4	17.5	28.84	P	L
Lz-0	46	3.3	France	9.8916	10.64	0.652	1.16	21.2	35.9	31.12	46.53	NA	NA
Mh-0	50.95	7.5	Poland	8.1704	10.38	0.371	0.81	12.9	28.9	21.03	39.3	L	L
Mh-1	50.95	7.5	Poland	9.9256	12.19	0.359	0.83	14.8	36.4	24.77	48.56	NA	NA
MIB-28	47.38	5.317	France	8.9077	10.48	0.328	0.73	11.6	25	20.47	35.52	NA	NA
MNF-Pot-48	43.6	-86.3	United states of America	7.5839	9.667	0.329	0.79	9.22	22.3	16.81	32	NA	NA

Mnz-0	50	8.267	Germany	9.9269	10.82	0.392	0.67	13.8	24.4	23.7	35.2	L	L
Mrk-0	49	9.3	Germany	7.0733	9.442	0.391	0.8	11	23.5	18.06	32.92	NA	NA
Mt-0	32.34	22.46	Libya	8.6841	10.94	0.477	0.82	16.2	32.3	24.9	43.26	P	L
Mz-0	50.3	8.3	Germany	8.1009	9.615	0.575	1.09	19.9	37.3	28.01	46.88	L	L
N13	61.36	34.15	Russia	7.5442	8.625	0.326	0.57	9.5	17	17.05	25.65	P	L
Na-1	47.5	1.5	France	7.3216	9.804	0.514	0.89	14.6	26.7	21.91	36.48	NA	NA
Nd-1	50	10	Switzerland	10.365	10.43	0.691	1.27	21.1	36.7	31.44	47.18	L	L
NFA-10	51.41	-0.64	United Kindom	8.6382	10.02	0.625	1.19	18.1	33.2	26.77	43.22	P	L
NFA-8	51.41	-0.64	United Kindom	9.7466	11.46	0.576	1.08	16.3	32.1	26.05	43.55	P	L
No-0	51.06	13.3	Germany	9.0429	10.97	0.492	0.91	15.6	37.9	24.59	48.84	P	L
Nok-1	52.24	4.45	Netherlands	7.3685	8.079	0.484	0.9	13.4	19.5	20.75	27.55	NA	NA
Nw-0	50.5	8.5	Germany	6.9875	8.85	0.44	0.96	9.92	20.8	16.9	29.61	L	L
Nz-1	-37.79	175.3	New Zealand	8.3246	9.771	0.391	0.84	8.42	21.9	16.55	31.64	P	L
Old-1	53.17	8.2	Germany	9.3535	10.33	0.495	0.92	15.5	31.6	24.82	41.98	L	L
Or-0	50.38	8.012	Germany	9.593	10.85	0.431	1.05	14.8	43.2	24.39	54.21	P	L
Ors-1	44.72	22.4	Romania	10.41	11.85	0.638	1.12	21.7	38.7	32.13	50.6	NA	NA
Ors-2	44.72	22.4	Romania	9.2366	11.14	0.503	0.94	14.8	32.6	24.07	43.71	NA	NA
Ove-0	53.34	8.423	Germany	9.378	10.37	0.583	1	21	37.7	30.41	48.06	L	L
Oy-0	60.23	6.13	Norway	9.7548	10.64	0.427	0.82	13.7	27.4	22.35	38.01	L	L
Pa-1	38.07	13.22	Italy	6.6461	8.258	0.328	0.72	9.18	19.9	15.83	28.14	NA	NA
PAR-3	46.65	-0.25	France	6.7566	8.179	0.297	0.86	8.79	22.5	15.55	30.69	NA	NA
Per-1	58	56.32	Russia	7.6594	8.744	0.733	1.27	25.1	37.2	32.75	45.91	P	L
Petergof	59	29	Russia	6.2042	6.287	0.478	0.85	14	23.7	20.19	29.94	P	L
PHW-10	51.29	0.409	United Kindom	6.6155	8.525	0.597	0.97	14.4	24.1	21.05	32.67	NA	NA
PHW-33	52.25	4.567	Netherlands	9.8348	12.52	0.39	0.93	14.7	35.8	24.56	48.33	NA	NA
Pla-0	41.5	2.25	Spain	9.5478	11.28	0.488	0.91	18.2	34.3	27.76	45.6	P	L
Pn-0	48.07	-2.97	France	6.9245	9.026	0.371	0.76	13.6	28.2	20.55	37.25	NA	NA
Pna-10	42.09	-86.3	United states of America	8.7509	10.7	0.325	0.59	12.1	22.7	22.18	33.44	L	L
Pog-0	49.27	-123	Canada	7.8451	9.928	0.233	0.58	6.91	18.7	14.76	28.61	P	L

Pr-0	50.14	8.607	Germany	7.2652	8.441	0.359	0.67	9.34	18.5	16.61	26.99	NA	NA
Pro-0	43.25	-6	Spain	8.6565	10	0.46	1.01	14.3	24.2	22.92	34.21	P	L
Pu2-23	49.42	16.36	Czech Republic	7.6157	9.511	0.362	0.72	10	20.6	17.02	30.12	P	L
Pu2-7	49.42	16.36	Czech Republic	9.2397	10.17	0.346	0.74	10.8	18.5	20.01	28.65	NA	NA
Ra-0	46	3.3	France	8.5973	10.13	0.225	0.46	7.53	13.8	16.13	23.88	P	L
Rak-2	49	16	Czech Republic	9.7132	10.64	0.535	1.06	14.3	24.9	23.98	35.31	P	L
Ren-1	48.5	-1.41	France	8.2651	9.69	0.2	0.43	6.04	13.3	14.31	23.02	L	L
Rhen-1	51.97	5.567	Netherlands	8.5359	9.554	0.38	0.76	8.44	16.6	16.97	26.17	L	S
Ri-0	49.16	-123	Canada	9.6783	9.975	0.402	0.98	14.5	24.9	24.17	34.91	P	L
RLD-2	56.25	34.32	Russia	9.9166	10.94	0.563	1.02	20.8	32.7	30.7	43.63	NA	NA
Rmx-A02	42.04	-86.5	United states of America	10.028	11.09	0.361	0.69	13.3	19.1	23.31	30.24	P	L
Rmx-A180	42.04	-86.5	United states of America	8.8372	10.02	0.349	0.6	9.75	15.2	18.59	25.25	P	L
Rou-0	49.44	1.098	France	6.8746	8.246	0.35	0.69	10.6	19.5	17.52	27.73	P	L
RRS-10	41.56	-86.4	United states of America	8.2322	9.811	0.288	0.46	7.5	14.7	15.73	24.54	L	L
RRS-7	41.56	-86.4	United states of America	8.7662	10.19	0.296	0.65	9.85	22.2	18.61	32.42	P	S
Rsch-4	56.3	34	Russia United	10.082	11.25	0.514	0.84	16.9	26.5	27.01	37.56	P	L
Rubeszhnoe	49	38.28	Kindomraine	9.5434	10.62	0.594	0.9	15.7	25.4	24.07	36.06	NA	NA
S96	NA	NA	Netherlands	9.1334	10.69	0.486	1.01	15.9	36.4	25.19	45.47	NA	NA
Sap-0	49.49	14.24	Czech Republic	7.8625	9.722	0.441	0.97	12.3	29	20.13	38.76	P	L
Sapporo-0	43.06	141.3	Japan	8.3919	9.12	0.423	0.77	11.7	21	20.08	30.07	NA	NA
Se-0	38.33	-3.53	Spain	7.2972	8.973	0.443	0.77	12.7	22.1	19.95	31.06	P	L
Sg-1	47.67	9.5	Germany	8.1261	9.524	0.263	0.55	7.71	15.2	15.83	24.73	P	L
Sh-0	51.68	10.21	Germany	9.9432	10.73	0.389	0.79	12.4	27.1	22.33	37.84	NA	NA
Shahdara	38.35	68.48	Tajikistan	9.0171	9.625	0.705	0.98	20.5	30	29.5	39.63	P	L
Si-0	50.87	8.023	Germany	7.109	7.941	0.425	0.71	10.9	17.5	18.02	25.39	P	L
Sorbo	38.35	68.48	Tajikistan	7.3041	7.823	0.498	0.68	16	21.9	23.35	29.67	P	L
Sp-0	52.53	13.18	Germany	7.325	8.562	0.403	0.73	12.5	24.3	19.87	32.89	P	L

Sq-1	51.41	-0.64	United Kindom	6.4509	8.408	0.297	0.52	8.02	13.9	14.47	22.31	P	L
Sq-8	51.41	-0.64	United Kindom	9.4559	11.02	0.584	0.8	20	28	28.42	37.31	L	L
St-0	59	18	Sweden	8.4831	10.01	0.443	0.89	13.8	29	22.32	38.99	P	L
TAMM-2	60	23.5	Finland	9.0162	10.77	0.474	0.74	12.2	19.6	21.26	30.33	P	L
Tamm-27	60	23.5	Finland	9.7931	11.18	0.442	0.71	12.5	21	22.28	32.18	P	S
Tha-1	52.08	4.3	Netherlands	9.4202	10.47	0.387	0.79	15	27	24.42	37.5	L	S
Tottarp-2	55.95	13.85	Sweden	7.843	9.284	0.504	0.9	14.9	27.8	22.72	37.11	P	L
Ts-1	41.72	2.931	Spain	6.6935	8.347	0.424	0.92	13.2	26.7	19.86	35	P	L
Ts-5	41.72	2.931	Spain	9.6264	11.19	0.543	0.95	19.1	33.7	28.64	44.92	P	L
Tscha-1	47.07	9.904	Austria	8.0776	8.767	0.541	0.97	18.5	32	26.59	40.76	P	L
Tsu-0	34.43	136.3	Japan	9.6546	9.553	0.412	0.89	15.1	33.3	24.79	42.83	P	L
Tsu-1	34.43	136.3	Japan	9.4417	10.01	0.437	0.92	16.4	37.3	26.61	47.28	P	L
Tu-0	45	7.5	Italy	9.5424	10.06	0.456	0.87	17.7	34.5	27.23	44.58	P	L
Ty-0	56.43	-5.23	United Kindom	8.3517	9.285	0.607	0.83	16.3	21.8	24.68	30.19	P	S
Uk-1	48.03	7.767	Germany	2.9449	3.479	0.347	0.73	6.78	12.7	9.722	16.21	P	L
UII2-3	56.06	13.97	Sweden	8.7253	9.213	0.547	1	21.2	36.4	29.97	45.63	P	L
UII-2-5	56.06	13.97	Sweden	7.5288	8.214	0.37	0.58	7.79	14.7	14.8	20.64	L	L
Uod-1	48.3	14.45	Austria	7.0615	8.557	0.22	0.63	6.1	19.8	13.16	28.33	P	L
Uod-7	48.3	14.45	Austria	7.8081	9.133	0.293	0.61	9.49	19	17.3	28.1	P	L
Utrecht	52.09	5.115	Netherlands	9.1362	10.63	0.466	0.99	18.3	36.6	27.45	47.27	P	L
Van-0	49.3	-123	Canada	9.3399	10.38	0.802	1.23	25.1	36.9	35.58	47.32	P	L
Var-2-1	55.58	14.33	Sweden	9.4989	12.14	0.469	0.93	10.4	23.8	18.66	35.94	NA	NA
Ven-1	52.03	5.55	Netherlands	8.3529	10.26	0.35	0.92	11.2	30.1	19.56	40.34	L	L
Wa-1	52.3	21	Poland	9.1777	9.444	0.739	1.32	22.4	46.5	30.87	57.12	P	L
Wa-1	52.3	21	Poland	8.4979	10.58	0.774	1.28	21.1	39.9	30.23	49.35	P	L
WAR	41.73	-71.3	United states of America	8.8529	10.04	0.379	0.85	14.2	32.6	23.05	42.65	L	L
Wei-0	47.25	8.26	Switzerland	6.9973	8.875	0.542	1.08	16.7	32.4	23.7	41.26	P	L
Wil-2	54.68	25.32	Lithuania	9.1676	10.29	0.712	1.14	27.2	41.1	36.4	51.42	P	L
Ws-0	52.3	30	Russia	8.1831	9.144	0.462	0.73	17.3	26.7	25.52	35.84	P	L

Ws-2	52.3	30	Russia	9.6197	11.24	0.713	1.43	23.7	45.4	33.29	58.44	L	L
Wt-5	52.3	9.3	Germany	6.8159	9.172	0.323	0.83	9.25	26.5	16.06	35.7	P	L
Yo-0	37.45	-119	United states of America	8.4837	10.87	0.549	0.98	19	37.2	27.46	48.11	L	L
Zdr-1	49.39	16.25	Czech Republic	8.7217	9.276	0.656	0.97	21	30.5	29.7	39.73	P	L
Zdr-6	49.39	16.25	Czech Republic	6.944	8.387	0.521	1.05	15.4	32.7	22.36	41.05	NA	NA
Zü-1	47.37	8.55	Switzerland	8.9988	10.32	0.464	1.04	14.4	30.7	23.36	41.02	P	L

Supplemental Table 2. Variance components assessed by two-way ANOVA for each trait.

Values represent the variance of each factor expressed as percentage of the total variance explained.

Trait	Genotype	Nitrogen	Experiment	GenotypexNitrogen	Residuals
PRL	54.736437	22.33936	2.0430935	3.916891112	16.96422
TLRL	34.517194	46.88255	2.28158041	6.140370938	10.1783
TRL	34.776664	46.85253	2.40934873	5.458067457	10.50339
LR/PR	39.613725	44.14424	1.22251901	6.215327717	8.804191
MLR	28.85439	58.61884	1.05995717	4.250535332	7.216274
LRN	62.695864	0.452555	5.99270073	7.145985401	23.7129
LRD	67.983348	7.483784	2.68176977	6.263917127	15.58718
FBR	36.394903	12.34213	4.8488949	12.57329725	33.84078
RB	47.438035	24.28404	3.60456241	5.931171906	18.74219
SB	52.86725	10.05043	6.41505938	6.559050143	24.10821
R/S	25.158919	57.21069	2.76480049	6.395037145	8.470552

Supplemental Table 3. Candidates genes residing in the LD region ($r^2=0.7$) of the locus associated with primary root length at low N. For each gene in the LD region of the representative SNP start and end positions are given together with the gene annotation.

Representative SNP	Genes in LD ($r^2>0.7$)	Start of gene	End of gene	Annotation
SNP_Chr4_386519	AT4G00710	290048	293453 150	BSK3

SNP_Chr4_386519	AT4G00720	293641	297314	ASKØ
SNP_Chr4_386519	AT4G00730	299359	304508	AHDP
SNP_Chr4_386519	AT4G00740	307431	310482	QUA3
SNP_Chr4_386519	AT4G00750	314353	317657	
SNP_Chr4_386519	AT4G00752	317564	320895	
SNP_Chr4_386519	AT4G00755	324982	327008	
SNP_Chr4_386519	AT4G00760	327025	333477	
SNP_Chr4_386519	AT4G00770	331157	333477	TRM9
SNP_Chr4_386519	AT4G00780	334732	336344	
SNP_Chr4_386519	AT4G00790	336945	340602	
SNP_Chr4_386519	AT4G00800	336945	345714	SETH5
SNP_Chr4_386519	AT4G00810	345952	347199	
SNP_Chr4_386519	AT4G00820	349116	351550	IQD17
SNP_Chr4_386519	AT4G00830	352016	355233	LIF2
SNP_Chr4_386519	AT4G00840	355258	357279	
SNP_Chr4_386519	AT4G00850	357551	359194	GIF3
SNP_Chr4_386519	AT4G00860	359315	360495	ATOZI1
SNP_Chr4_386519	AT4G00870	362169	363691	
SNP_Chr4_386519	AT4G00872	364147	364736	
SNP_Chr4_386519	AT4G00880	366373	367274	SAUR31
SNP_Chr4_386519	AT4G00885	369856	369991	MIR165B
SNP_Chr4_386519	AT4G00890	373960	375350	
SNP_Chr4_386519	AT4G00891	377481	377908	
SNP_Chr4_386519	AT4G00893	379793	381455	
SNP_Chr4_386519	AT4G00895	381788	382643	
SNP_Chr4_386519	AT4G00900	382663	386529	ATECA2
SNP_Chr4_386519	AT4G00905	387865	389113	
SNP_Chr4_386519	AT4G00910	389370	391287	
SNP_Chr4_386519	AT4G00920	393767	395382	

SNP_Chr4_386519

AT4G00930

396558

400734

CIP4.1

Supplemental Table 4. Candidate genes residing in the LD region (20 kb interval) of the locus associated with average lateral root length.

Trait	Associated SNP	p-value	$-\log_{10}P$	Candidate gene	Start of gene	End of gene	Annotation and description
HN	Chr4_17094057	7.67E-08	7.11	AT5G42640	17088695	17089597	GAL2
				AT5G42645	17090938	17095801	transposable_element_gene
				AT5G42650	17097564	17099565	ALLENE OXIDE SYNTHASE
				AT5G42655	17102027	17102896	Disease resistance-responsive
				AT5G42660	17102924	17106103	DNA-directed RNA polymerase subunit beta
	Chr5_16016322	2.35E-07	6.63	AT5G39990	16004253	16006823	GLCAT14A
				AT5G39995	16007835	16009651	pseudogene P-loop containing nucleoside triphosphate
				AT5G40000	16010869	16012559	hydrolases superfamily protein
				AT5G40010	16020058	16021916	ATPASE-IN-SEED-DEVELOPMENT Pathogenesis-related thaumatin superfamily
				AT5G40020	16022579	16024316	protein
	Chr1_23007100	3.44E-07	6.46E	AT1G62260	22997755	22999829	MEF9
				AT1G62262	23000157	23002096	SLAH4 F-box and associated interaction domains-
				AT1G62270	23004499	23005650	containing protein
				AT1G62280	23007044	23008621	SLAH1
				AT1G62290	23009895	23013601	ATPASPA2

				AT1G62300	23016569	23019494	ATWRKY6
	Chr5_22247425	3.57E-07	6.45	AT5G54740	22238358	22239187	SEED STORAGE ALBUMIN 5
				AT5G54745	22240256	22241233	DEG16
				AT5G54750	22241478	22243721	Transport protein particle (TRAPP) component
				AT5G54760	22243800	22245810	Translation initiation factor SUI1 family protein
				AT5G54770	22246519	22248332	THI1
				AT5G54780	22248369	22252191	Ypt/Rab-GAP domain of gyp1p superfamily protein
				AT5G54790	22253986	22255663	VUP4
LN	Chr3_8658699	2.68E-07	6.57E	AT3G23940	8648669	8652605	DHAD
				AT3G23950	8652908	8654164	F-box family protein
				AT3G23955	8655023	8657439	F-box family protein
				AT3G23960	8657736	8658580	F-box and associated interaction domains- containing protein
				AT3G23970	8660447	8661688	F-box family protein
				AT3G23980	8662413	8668040	BLI
LN/HN	Chr4_2724898	2.43E-07	6.61	AT4G05310	2714765	2716012	Ubiquitin-like superfamily protein POLYUBIQUITIN 10. UBI10. UBIQUITIN 10.
				AT4G05320	2717977	2720308	UBQ10
				AT4G05330	2720493	2723214	ARF-GAP DOMAIN 13
				AT4G05340	2725690	2726065	P-loop containing nucleoside triphosphate hydrolases superfamily protein
				AT4G05350	2726910	2727530	RING/U-box superfamily protein
				AT4G05360	2728204	2732337	Zinc knuckle (CCHC-type) family protein
	Chr4_14192732	4.74E-07	6.32	AT4G28720	14192569	14194302	YUC8
				AT4G28730	14199043	14200903	GLUTAREDOXIN C5
				AT4G28740	14200903	14202776	LOW PSII ACCUMULATION-like protein

Supplemental Table 5. Correlation analyses between lateral root response and climate variables.

A partial Mantel test with kinship correction for population structure was used to test correlations between each of the variables and the root length phenotype.

Climate variables	<i>r</i>	<i>p</i>-value
Annual Mean Temperature (bio1)	0.1	0.005
Mean Diurnal Range (bio2)	0.06	0.03
Isothermality (bio3)	0.07	0.02
Temperature Seasonality (bio4)	0.09	0.009
Max Temperature of Warmest Month (bio5)	0.09	0.01
Min Temperature of Coldest Month (bio6)	0.07	0.03
Temperature Annual Range (bio7)	0.06	0.05
Mean Temperature of Wettest Quarter (bio8)	0.02	0.28
Mean Temperature of Driest Quarter (bio9)	0.13	0.001
Mean Temperature of Warmest Quarter (bio10)	0.1	0.008
Mean Temperature of Coldest Quarter (bio11)	0.08	0.01
Annual Precipitation (bio12)	0.05	0.08
Precipitation of Wettest Month (bio13)	0.04	0.11
Precipitation of Driest Month (bio14)	0.009	0.008
Precipitation Seasonality (bio15)	0.09	0.002
Precipitation of Wettest Quarter (bio16)	0.03	0.22
Precipitation of Driest Quarter (bio17)	0.08	0.01
Precipitation of Warmest Quarter (bio18)	0.08	0.02
Precipitation of Coldest Quarter (bio19)	0.07	0.04
Latitude	0.13	0.001
Longitude	0.11	0.002

Supplemental Table 6. Correlation analyses between the SNP identified by GWAS and climate variables.

A partial Mantel test with kinship correction for population structure was used to test correlations between each of the variables and the root length phenotype.

Climate variables	<i>r</i>	<i>p-value</i>
Annual Mean Temperature (bio1)	0.14	0.001
Mean Diurnal Range (bio2)	0.12	0.001
Isothermality (bio3)	0.2	0.001
Temperature Seasonality (bio4)	0.31	0.001
Max Temperature of Warmest Month (bio5)	0.09	0.013
Min Temperature of Coldest Month (bio6)	0.2	0.001
Temperature Annual Range (bio7)	0.3	0.001
Mean Temperature of Wettest Quarter (bio8)	0.06	0.039
Mean Temperature of Driest Quarter (bio9)	0.2	0.001
Mean Temperature of Warmest Quarter (bio10)	0.08	0.034
Mean Temperature of Coldest Quarter (bio11)	0.19	0.001
Annual Precipitation (bio12)	0.07	0.034
Precipitation of Wettest Month (bio13)	0.06	0.05
Precipitation of Driest Month (bio14)	0.07	0.03
Precipitation Seasonality (bio15)	0.08	0.007
Precipitation of Wettest Quarter (bio16)	0.06	0.06
Precipitation of Driest Quarter (bio17)	0.09	0.007
Precipitation of Warmest Quarter (bio18)	0.07	0.06
Precipitation of Coldest Quarter (bio19)	0.06	0.001
Latitude	0.16	0.001
Longitude	0.28	0.001

Supplemental Table 7. List of 19 climate variables, latitude and longitude for 115 natural accessions used in the study.

Genotype	ID	bio1	bio2	bio3	bio4	bio5	bio6	bio7	bio8	bio9	bio10	bio11	bio12	bio13	bio14	bio15	bio16	bio17	bio18	bio19	Latitue	Longitude
Aa-0	7000	79	82	32	6299	216	-37	253	158	6	158	-3	736	83	46	18	229	144	229	161	50.92	9.571
Bu-0	8271	78	85	32	6402	216	-42	258	158	4	158	-6	756	84	46	16	230	152	230	167	50.5	9.5
Ca-0	7062	91	80	31	6290	231	-21	252	172	50	172	10	644	64	40	15	190	127	190	148	50.3	8.266
Chat-1	7071	106	88	36	5544	241	1	240	44	68	177	34	642	63	47	9	178	145	152	166	48.07	1.339
Edi-0	6914	83	74	38	4239	189	-4	193	117	48	138	30	743	73	45	16	218	146	192	178	55.95	-3.16
Ei-2	6915	72	68	30	5701	192	-30	222	8	33	144	-1	1043	116	69	15	305	225	280	290	50.3	6.3
Est-1	6916	52	66	21	8290	210	-92	302	63	-16	159	-53	637	74	28	30	214	98	183	129	58.3	25.3
Gel-1	7143	100	77	34	5539	224	-1	225	170	58	170	29	766	74	50	12	220	160	220	177	51.02	5.867
Gu-0	6922	81	77	31	6091	214	-29	243	158	39	158	2	750	73	48	13	213	154	213	188	50.3	8
Ha-0	7163	88	82	33	6089	222	-22	244	165	42	165	10	666	73	39	18	211	134	211	147	52.37	9.736
Hey-1	7166	99	77	34	5586	222	-3	225	170	57	170	27	768	74	50	12	219	159	219	181	51.25	5.9
Hs-0	8310	84	79	32	5999	215	-25	240	160	40	160	7	760	80	48	16	233	155	233	178	52.24	9.44
KI-5	7199	101	83	34	5943	235	-8	243	176	59	176	24	778	83	52	17	244	157	244	177	50.95	6.967
Mh-0	7255	87	77	32	5835	215	-19	234	161	45	161	12	872	86	57	13	249	183	249	220	50.95	7.5
Mnz-0	7244	98	83	32	6390	240	-18	258	179	57	179	15	553	61	33	20	177	102	177	118	50	8.267
Mz-0	6940	84	79	31	6249	222	-27	249	164	42	164	4	716	69	45	13	204	145	204	172	50.3	8.3
Nd-1	6942	89	89	32	6718	238	-34	272	174	14	174	1	636	74	38	18	198	128	198	139	50	10
Nw-0	7258	87	80	31	6322	227	-25	252	153	45	168	6	735	70	46	11	206	156	201	175	50.5	8.5
Old-1	7280	87	75	32	5748	212	-17	229	161	42	161	14	775	80	44	17	236	146	236	176	53.17	8.2
Ove-0	7287	88	75	32	5800	213	-16	229	161	41	161	14	761	81	39	18	233	141	233	168	53.34	8.423
Ren-1	6959	112	78	38	4621	225	22	203	63	103	171	54	735	83	47	18	230	154	158	207	48.5	-1.41
Rhen-1	7316	91	76	34	5410	212	-8	220	62	49	160	22	800	76	49	14	221	159	220	196	51.97	5.567
Sq-8	6967	98	79	34	5234	225	-3	228	40	61	166	31	701	71	43	14	207	150	160	182	51.41	-0.64
Tha-1	7353	96	60	29	5227	206	3	203	110	50	161	31	775	85	44	20	237	147	203	185	52.08	4.3
UII-2-5	6974	76	61	26	6234	204	-30	234	152	22	159	1	640	71	36	21	198	113	185	151	56.06	13.97
Ven-1	7384	93	76	34	5452	214	-7	221	159	50	162	24	784	74	47	14	218	154	217	191	52.03	5.55

Ak-1	6987	101	85	32	6366	246	-12	258	182	31	182	18	725	92	40	28	250	130	250	130	48.07	7.626
Alc-0	6988	127	111	36	6632	304	2	302	84	216	216	48	457	55	13	33	153	58	58	127	40.31	-3.22
Alst-1	6989	69	71	36	4522	177	-18	195	21	88	128	12	1064	112	67	18	332	206	240	297	54.8	-2.43
Amel-1	6990	87	59	28	5267	199	-7	206	102	38	154	24	804	87	45	22	250	142	215	191	53.45	5.73
An1	6898	101	74	33	5476	221	-1	222	72	60	169	31	778	77	49	12	217	166	199	188	51.22	4.4
Ang-0	6992	92	79	34	5646	219	-12	231	164	53	164	20	888	83	62	9	241	193	241	218	50.3	5.3
Ann-1	6994	101	97	33	6594	259	-28	287	108	14	185	14	927	96	66	10	251	218	233	218	45.9	6.13
Ba-1	7014	76	67	34	4573	180	-12	192	29	98	138	20	1824	230	92	30	636	286	330	591	56.55	-4.8
Bla-1	8256	68	64	26	6325	193	-51	244	143	12	151	-9	805	88	41	24	256	138	238	184	56.4	12.9
Blh-1	8265	84	93	30	7536	243	-63	306	161	-1	176	-18	677	84	40	24	221	125	215	138	48	19
Boot-1	7026	85	69	35	4525	190	-2	192	59	105	144	28	995	107	56	23	318	184	227	263	54.4	-3.27
Bor-4	6903	72	86	30	6981	221	-59	280	159	-7	159	-20	626	88	30	40	251	93	251	97	49.4	16.23
Bs-1	8270	96	84	33	6226	241	-11	252	176	30	176	17	816	101	52	22	271	162	271	165	47.5	7.5
Bsch-0	7031	98	89	33	6474	246	-22	268	180	26	180	13	653	71	41	16	202	133	202	142	50.02	8.667
Bur-0	6905	93	68	39	3889	190	17	173	74	106	144	47	942	98	61	16	277	191	224	255	54.1	-6.2
CIBC-17	6907	98	79	34	5234	225	-3	228	40	61	166	31	701	71	43	14	207	150	160	182	51.41	-0.64
CIBC-5	6730	98	79	34	5234	225	-3	228	40	61	166	31	701	71	43	14	207	150	160	182	51.41	-0.64
Co	7081	162	100	44	4257	289	62	227	107	215	217	107	914	128	9	53	367	60	65	367	40.21	-8.43
Com-1	7092	105	86	36	5518	235	0	235	110	68	175	34	622	59	42	10	170	131	162	150	49.42	2.823
Ct-1	6910	175	102	40	5457	316	61	255	155	245	247	111	503	108	4	72	241	23	50	183	37.3	15
Do-0	7102	81	75	31	6064	213	-27	240	13	39	157	2	849	85	55	12	233	182	225	219	50.72	8.237
Dra-0	7104	70	85	30	6953	217	-61	278	156	-10	156	-23	640	89	31	40	256	96	256	100	49.42	16.27
Duk	6008	83	90	31	7168	237	-52	289	172	2	172	-12	594	82	29	38	232	92	232	95	49.1	16.2
Eden-1	6009	33	83	25	8592	205	-126	331	134	-33	146	-76	655	74	38	24	207	117	184	148	62.88	18.18
En-1	8290	97	87	32	6552	243	-22	265	180	25	180	12	606	66	37	18	192	118	192	130	50	8.5
Es-0	7126	51	68	22	8034	212	-90	302	145	-16	158	-48	637	78	31	31	220	99	199	129	60.2	24.57
Est-0	7128	52	66	21	8290	210	-92	302	63	-16	159	-53	637	74	28	30	214	98	183	129	58.3	25.3
Fei-0	8215	137	94	41	4445	263	39	224	89	193	195	81	1205	174	13	53	484	81	85	484	40.5	-8.32
Ga-0	6919	81	77	31	6091	214	-29	243	158	39	158	2	750	73	48	13	213	154	213	188	50.3	8

Gie-0	7147	93	82	31	6426	235	-23	258	159	50	174	9	693	70	42	13	199	150	187	158	50.58	8.678
Gr-1	8300	85	101	31	7651	252	-66	318	181	-17	181	-17	863	123	31	43	354	108	354	108	47	15.5
Gy-0	8214	105	83	35	5439	234	3	231	110	67	173	34	646	61	44	9	176	141	159	160	49	2
Hau-0	7164	84	62	27	6175	210	-19	229	158	31	165	10	618	67	33	20	191	111	182	140	55.68	12.57
Hi-0	8304	94	73	33	5320	213	-3	216	67	50	161	27	800	81	46	16	230	158	213	193	52	5
In-0	8311	33	80	31	6208	166	-90	256	110	-48	110	-48	1101	152	58	34	420	188	420	188	47.5	11.5
Je-0	7181	87	84	33	6219	229	-24	253	167	17	167	8	561	77	31	29	200	103	200	103	50.93	11.59
Jea	91	152	83	37	5097	269	45	224	128	217	219	90	808	119	17	42	317	90	117	231	43.68	7.333
Jl-3	7424	90	91	30	7321	246	-49	295	180	7	180	-8	518	75	23	42	209	73	209	76	49.2	16.62
Kas-2	8424	-73	109	27	9650	126	-268	394	46	-172	47	-200	66	13	2	52	29	9	26	11	35	77
Kn-0	7186	67	79	26	8071	225	-77	302	167	-32	167	-39	613	77	28	28	217	99	217	112	54.9	23.89
Kz-9	6931	26	113	23	13022	270	-201	471	169	-129	187	-143	297	38	17	28	104	53	94	57	49.5	73.1
Lip-0	8325	86	91	29	7755	244	-67	311	180	-6	180	-21	720	102	33	40	290	105	290	109	50	19.3
LL-0	6933	148	69	31	5347	268	47	221	159	218	219	84	752	99	36	24	244	152	178	160	41.59	2.49
Lm-2	8329	106	91	38	5391	241	2	239	46	175	175	37	692	69	50	11	203	154	154	192	48	0.5
Lp2-2	7520	68	85	30	7002	216	-64	280	155	-12	155	-25	648	93	31	40	262	95	262	102	49.38	16.81
Lp2-6	7521	68	85	30	7002	216	-64	280	155	-12	155	-25	648	93	31	40	262	95	262	102	49.38	16.81
Mt-0	6939	175	109	48	4491	286	60	226	116	227	230	116	132	33	0	93	83	0	1	83	32.34	22.46
N13	7438	19	78	21	9455	204	-154	358	125	-95	141	-104	644	91	26	35	235	96	223	109	61.36	34.15
NFA-10	6943	98	79	34	5234	225	-3	228	40	61	166	31	701	71	43	14	207	150	160	182	51.41	-0.64
NFA-8	6944	98	79	34	5234	225	-3	228	40	61	166	31	701	71	43	14	207	150	160	182	51.41	-0.64
No-0	7275	81	76	29	6730	221	-38	259	166	3	166	-6	627	79	36	26	221	113	221	121	51.06	13.3
Or-0	7282	93	80	32	6184	229	-18	247	171	51	171	13	652	65	41	14	192	130	192	153	50.38	8.012
Per-1	8354	20	82	19	11462	234	-185	419	163	-51	163	-132	609	78	25	34	218	86	218	105	58	56.32
Petergof	7296	45	73	22	8954	219	-107	326	144	-63	161	-69	678	85	30	32	240	104	235	121	59	29
Pla-0	7300	154	70	31	5313	273	53	220	164	90	224	90	660	86	32	26	221	133	165	133	41.5	2.25
Pro-0	8213	121	98	44	4280	246	24	222	99	176	178	69	840	114	41	28	283	145	153	219	43.25	-6
Pu2-23	6951	76	86	30	7083	227	-57	284	164	-5	164	-18	596	85	28	41	241	87	241	90	49.42	16.36
Ra-0	6958	107	104	39	5819	253	-12	265	164	44	182	32	688	85	38	27	221	121	216	128	46	3.3

Rak-2	8365	85	91	31	7127	240	-49	289	174	5	174	-9	607	83	30	37	235	96	235	98	49	16
Rou-0	7320	108	86	38	5102	233	8	225	78	71	173	43	671	71	43	14	201	143	153	177	49.44	1.098
Sap-0	8378	75	91	32	7002	229	-55	284	164	-4	164	-16	670	89	35	34	253	116	253	119	49.49	14.24
Se-0	6961	151	120	37	6838	342	19	323	104	244	244	70	498	68	5	48	183	33	33	163	38.33	-3.53
Sg-1	7344	92	83	30	6722	237	-32	269	177	17	177	4	1004	127	54	30	367	169	367	180	47.67	9.5
Sha	6962	157	132	35	8389	360	-12	372	107	250	264	46	451	97	0	81	231	2	5	169	38.35	68.48
Si-0	7337	86	76	31	5980	217	-21	238	147	45	162	9	828	81	54	12	226	176	226	210	50.87	8.023
Sorbo	6963	157	132	35	8389	360	-12	372	107	250	264	46	451	97	0	81	231	2	5	169	38.35	68.48
Sp-0	7343	91	82	30	6877	238	-32	270	178	42	178	1	570	68	35	21	186	111	186	127	52.53	13.18
Sq-1	6966	98	79	34	5234	225	-3	228	40	61	166	31	701	71	43	14	207	150	160	182	51.41	-0.64
St-0	8387	72	63	23	7114	220	-44	264	157	12	168	-14	495	59	24	28	168	79	155	109	59	18
Tamm-2	6968	51	72	23	7905	214	-89	303	143	-15	156	-46	609	73	29	31	209	94	189	124	60	23.5
Tamm-27	6969	51	72	23	7905	214	-89	303	143	-15	156	-46	609	73	29	31	209	94	189	124	60	23.5
Tottarp-2	6243	73	60	25	6182	198	-33	231	147	18	154	-2	672	73	38	20	205	120	193	161	55.95	13.85
Ts-1	6970	161	71	32	5212	277	56	221	172	208	229	96	644	106	23	36	231	110	142	141	41.72	2.931
Ts-5	6971	161	71	32	5212	277	56	221	172	208	229	96	644	106	23	36	231	110	142	141	41.72	2.931
Tscha-1	7372	80	94	33	6544	224	-55	279	161	6	161	-8	1066	132	57	27	370	181	370	195	47.07	9.904
Tu-0	8395	125	91	30	7250	285	-16	301	163	30	216	30	813	100	38	27	274	132	203	132	45	7.5
Ty-0	7351	89	64	35	4369	186	4	182	44	111	147	35	1778	213	88	29	604	281	338	544	56.43	-5.23
Uk-1	7378	105	85	32	6433	251	-10	261	187	22	187	22	806	103	46	26	273	150	273	150	48.03	7.767
UII2-3	6973	76	61	26	6234	204	-30	234	152	22	159	1	640	71	36	21	198	113	185	151	56.06	13.97
Uod-1	6975	83	100	33	7178	244	-55	299	174	1	174	-11	875	118	46	34	331	155	331	160	48.3	14.45
Uod-7	6976	83	100	33	7178	244	-55	299	174	1	174	-11	875	118	46	34	331	155	331	160	48.3	14.45
Utrecht	7382	93	75	34	5317	213	-5	218	66	49	160	26	804	79	47	16	232	157	217	195	52.09	5.115
Wa-1	7394	79	83	27	7876	239	-60	299	178	-16	178	-24	490	70	22	39	192	68	192	76	52.3	21
Wei-0	6979	82	76	30	6186	219	-31	250	160	13	160	2	1172	145	71	27	414	221	414	224	47.25	8.26
Wil-2	7413	64	81	26	8313	224	-87	311	167	-37	167	-45	656	81	33	26	224	112	224	126	54.68	25.32
Ws-0	6980	67	87	25	9081	242	-100	342	179	-44	179	-53	624	87	30	34	241	99	241	111	52.3	30
Wt-5	6982	86	79	32	5967	217	-23	240	162	43	162	10	744	79	47	16	230	151	230	172	52.3	9.3

Zdr-1	6984	73	86	30	6974	222	-59	281	159	-7	159	-20	623	87	30	40	249	93	249	97	49.39	16.25
Zü-1	7418	93	78	30	6383	234	-23	257	173	22	173	10	1087	132	65	26	381	201	381	205	47.37	8.55

Supplemental Table 8. List of primers used in this thesis.

Cloning with GreenGate method

proBSK3pENTR_F	CACCAAACAAACTCTGATGATCAAATCAA
proBSK3pENTR_R	CTAAATAAAACCACGCTCCAAAA
proBSK3_BsaMut_F	GAACGAGTCCACTTGCTTTAACAGG
proBSK3_BsaMut_R	GCAAGTGGACTCGTTCATAGAAC
ggproBSK3_F	AACAGGTCTCAACCTAAACAAACTCTGATGATCAAATCAA
ggproBSK3_R	AACAGGTCTCATGTTCTAAATAAAACCACGCTCCAAAA
ggCvi_BSK3cds(P)_F	AACAGGTCTCAGGCTATGGGAGGTCAATGCTCTA
ggCvi_BSK3cds(P)_R	AACAGGTCTCACTGACTTCACTCGGGGAACTCCAT
ggCol0_BSK3cds(L)_F	AACAGGTCTCAGGCTATGGGAGGTCAATGCTCTA
ggCol0_BSK3cds(L)_R	AACAGGTCTCACTGACTTCACTCGGGGAACTCCAT
ggYUC8pro_F	AACAGGTCTCAACCTATCCTCTATAATATTTTCTCT
ggYUC8pro_R	AACAGGTCTCATGTTAAGTATTGAAAGTAAGAGAATTTGAA
ggYUC8cds_F	AACAGGTCTCAGGCTATGGAGAATATGTTTCGTTTGATG
ggCol-0YUC8cds_R	AACAGGTCTCACTGAGAAGTGTGAGAGATACACCTTCG
ggCoYUC8cds_R	AACAGGTCTCACTGAGAAGTGTGAGAGATACATCTTCG

For qRT-PCR analyses

UBQ10-qPCR-F	CTTCGTCAAGACTTTGACCG
UBQ10-qPCR-R	CTTCTTAAGCATAACAGAGACGAG
ACTIN2-qPCR-F	GACCAGCTCTTCCATCGAGAA
ACTIN2-qPCR-R	CAAACGAGGGCTGGAACAAG
BSK3-qPCR-F	TCGAAAGCTTCTGGGTTTACGA
BSK3-qPCR-R	AACTCAGGCTAGAGCATTGACC
ASKØ-qPCR-F	GCAGTAGACCTCGTCTCAAGACTC

ASK0-qPCR-R	GGGTGTGCACAAGCTTCCAATG
BAK1-qPCR-F	TGTCCTGACGCTACAAGTTCTGG
BAK1-qPCR-R	ACAGGAATATCTCCGGTGAGAGG
BRI1-qPCR-F	GTAAACGGCCAACGGATTCACC
BRI1-qPCR-R	TTGCGTGCTGTTTCACCCATCC
YUC3-qPCR-F	ATCAACCCTAAGTTCAACGAGACA
YUC3-qPCR-R	CGGCACAACCTTTCTCAGCG
YUC5-qPCR-F	TCGTCCCGGAATTAACGGTTCT
YUC5-qPCR-R	CCGATTTCCCTTTCCACGCGTTT
YUC7-F-qPCR-F	AGTTTGGTCCGGGAAAGGTC
YUC7-qPCR-R	GGTGAATCCCACCGCATACA
YUC8-qPCR-F	TGTATGCGGTTGGGTTTACGAGGA
YUC8-qPCR-R	CCTTGAGCGTTTCGTGGGTTGTTT
YUC9-qPCR-F	CAAGGAGTCCCATTCGTTGTGGT
YUC9-qPCR-R	TCGAACCGGTTTGCGTATGACTCA
CPD-qPCR-F	TTACCGCAAAGCCATCCAAG
CPD-qPCR-R	TCCATCATCCGCCGCAAG
DWF4-qPCR-F	CATTGCTCTCGCTATCTTCTTC
DWF4-qPCR-R	GACTCTCCTAGTTCCTTCTGG
DWF1-qPCR-F	CACTCAAGGTGAAGCTATCAGG
DWF1-qPCR-R	TAGGACACAGCCAGGTGCGTAG
BR6OX2-qPCR-F	AGCTTGTTGTGGGAAGTCTATCGG
BR6OX2-qPCR-R	CGATGTTGTTTCTTGCTTGGACTC

For genotyping T-DNA lines

LBb1.3	ATTTTGCCGATTTTCGGAAC
GABI-LB	CCATTTGGACGTGAATGTAGACAC
SAIL-LB1	GCCTTTTCAGAAATGGATAAATAGCCTTGCTTCC
SAIL_1286_E04 -LP	GACCCTAAGACTCGATACCCG
SAIL_1286_E04 -RP	AAACTGACATTGCGGATGAAG

SALK_077059-LP	ATCCAATTCAACAACCAGTGG
SALK_077059-RP	CGTAGGTCCATGGATGAGTTG
yuc3-LP	AAAAACAAAGAAAAATCCCCC
yuc3-RP	TTTTTGGGAAATCAACGTTTG
yuc5-LP	CCAAATATTTGGGCCTTTGAG
yuc5-RP	CACAATGCTAATGCATCCATG
yuc7-LP	GAGCTGCTCGGTTATTGTGAG
yuc7-RP	TGGAGTGGGCTTATCTCTTTG
yuc8-1-LP	ATTCTGCATTTGGTTCCACAC
yuc8-1-RP	GACTCACTCTTCGACACGGTC
yuc8-2-LP	ATTCTGCATTTGGTTCCACAC
yuc8-2-RP	GACTCACTCTTCGACACGGTC
BSK3-RT-F	CGGGATCCGTATGGGAGGTCAATGCTCTAG
BSK3-RT-R	ACGCGTCTGACTTACTTCACTCGGGGAAGTC

For genotyping of *yucQ*

CSHL_GT6160-LP/yuc5	CGGACTCTAATCAAAGTCCC
CSHL_GT6160-RP/yuc5	GGAGATTTCAAAGTAGATTTG
Ds3_1	ACCCGACCGGATCGTATCGGT
SAIL_762_D07-LP/yuc9	GCTCGGTAAGCAAAACAAAAGT
SAIL_762_D07-RP/yuc9	GAAGGAAATGCCCAATGAGAC
SAIL-LB1	GCCTTTTCAGAAATGGATAAATAGCCTTGCTTCC
yuc3-LP	AAAAACAAAGAAAAATCCCCC
yuc3-RP	TTTTTGGGAAATCAACGTTTG
yuc8-2-LP	ATTCTGCATTTGGTTCCACAC
yuc8-2-RP	GACTCACTCTTCGACACGGTC
yuc7-LP	GAGCTGCTCGGTTATTGTGAG
yuc7-RP	TGGAGTGGGCTTATCTCTTTG

8 Acknowledgements

Foremost, I would like to express my deepest gratefulness to Prof. Dr. Nicolaus von Wirén for accepting me as a PhD candidate in his group, for constructive advises and careful supervision on my thesis; also for providing me a pleasant and active environment that is full of opportunities, challenges and great freedom to develop as a researcher. Thank you very much, Nico.

Then, I would like to acknowledge China Scholarship Council (CSC), the Federal Ministry of Education and Research (BMBF, Germany) and the IPK Gatersleben for the financial support that enables me to study abroad and complete my dissertation.

Many thanks go to Dr. Ricardo F. H. Giehl. I could not be more grateful to his careful guidance and helpful support during my experiments and writing. I thank him for always being ready for scientific discussions, stimulating ideas as well as constructive advices; also for being a good example showing me how to enjoy science and life. I definitely learnt a lot from him allowing me to benefit a lot for my own life.

Also I greatly appreciate Dr. Ying Liu for his scientific and personal support throughout my PhD period, which allowed me to proceed with my scientific project and successfully complete my PhD dissertation.

For sharing research materials, I would like to greatly thank Prof. Dr. Zhaojun Ding (Shandong University, China) for providing seeds of *yucQ* mutant and reporter lines; Prof. Dr. Stephan Pollman (Centro de Biotecnología y Genómica de Plantas, UPM-INIA, Spain) for *YUC8pro::GUS* line; Prof. Dr. Chunhua Choe (Seoul National University, South Korea) for *DWF4pro::GUS* and *bri1-5* lines; Prof. Dr. Guido Sessa (Tel-Aviv University, Israel) for *bsk* multiple knockouts; Prof. Dr. Abdelali Hannoufa (Agriculture and Agri-Food Canada, Canada) for *DIM1pro::GUS* and RNAi lines; Prof. Dr. Thomas Altmann (IPK, Gatersleben) and Dr. Rhonda Meyer (IPK, Gatersleben) for seeds of Arabidopsis ecotypes and SNP array data; Prof. Dr. Cyril Zipfel (The Sainsbury Laboratory, Norwich, UK) for *bak1-4* mutant and reporters; Prof. Dr. Carsten Müssig (MPI für Molekulare Pflanzenphysiologie, Germany) for *ccb1* mutant; Prof. Dr. Grégory Vert (Université Paris-Saclay, France) for *bri1* mutant and reporters.

I specially thank Dr. Thorsten Schnurbusch, Dr. Ahmad M. Alqudah, Dr. Celestine Wabila for their helpful advice and Dr. Christian Klukas, and Jean-Michel Pape for image analysis on barley project. Also I would like to give my special thanks to Dr. Kerstin Neumann and Dr. Guozheng Liu for assistance and helpful discussions with regard to statistics. Thanks to Dr. Martin Mascher for bioinformatics analysis and Dr. Ben Gruber, Dr. Benjamin Kilian, Prof. Dr. Andreas Graner for their constructive advices and correction of our manuscript. Also thanks to Prof. Dr. Jochen Balbach (Martin-Luther-Universität Halle-Wittenberg, Germany) for protein structure modeling.

Regarding technical assistance, I would like to thank Andrea Knospe, Lisa Unrath, Elis Fraust, Susanne Reiner, Baris Boylu, Cornelia Fessel and Dr. Zhaojun Liu for their excellent technical assistance in the barley root phenotyping project. Special thanks are given to Jacqueline Fuge and Heike Nierig for assistance in plasmid construction and sequencing. Thanks to Dr. Twan Rutten and

Dr. Michael Melzer for training and assistance in microscopy. Special thanks to Annett Bieber for plant transformation and taking care of the plants when I was absent. I greatly appreciate the assistance by Barbara Kettig, Dr. Kai Eggert (deceased), Susanne Reiner and Dr. Yudelsy Antonia Tandron Moya for analytical measurements with IR-MS and ICP-OES/MS.

Many thanks to all the group members of the Molecular Plant Nutrition (MPE) group and the Metalloid Transport (MT) group for active discussions and inspiring ideas in the lab meetings. Also thanks are given to all other department members for constructive criticism and questions in the progress reports.

I am very grateful for the support I received from the gardener team led by Mr. Enk Geyer, especially for taking care of my plants.

Thanks to all IPK administrative staff, in particular to Dr. Britt Leps, for their efforts to make my daily life convenient in Gatersleben.

Many thanks to all my native and abroad friends, in particular to Fang Liu, Dr. Zhaojun Liu, Guojing Jiang, Dr. Yongyu Huang, Dandan Wu, Daiyan Li, Dr. Rongfan Wang, Dr. Jiawen Wu, Dr. Ying Liu, Yingjun Sheng, Cevza Esin Tunc, Bijal Thakkar. Thank you all very much for bringing me happiness and I will cherish forever the happy time we have together.

Last but not least, I would like to express my deep and sincere gratitude to my parents for their endless support and also for the great freedom that allows me to pursue the way I want.

9 Curriculum Vitae

Name: Zhongtao Jia

Gender: Male

Date of birth: 03. 21.1990

Place of birth: Xinyang City, Henan province, China

Address: Leibniz-Institute of Plant Genetics and Crop Plant Research (IPK), Department of Physiology and Cell Biology. Correnstraße 3, 06466 Gatersleben, Germany

E-mail: zhongtao@ipk-gatersleben.de, jjzhongtao1990@163.com

Education

➤ 12/2014-present **Ph.D** in Biology, enrolled at Martin Luther University, Halle, Germany, and the thesis was prepared at the Leibniz-institute of Plant Genetics and Crop Plant Research (IPK), Gatersleben.

Supervisor: Prof. Dr. Nicolaus von Wirén, Molecular Plant Nutrition group.

Dissertation title: "Exploiting natural variation to uncover genes modulating root foraging responses to low nitrogen in Arabidopsis thaliana".

➤ 09/2012-07/2014 **M.Sc** in Plant Nutrition, College of Resources and Environmental Sciences, China Agriculture University (CAU), Beijing, China

Supervisor: Prof. Dr. Fusuo Zhang, Prof. Dr. Lixing Yuan and Prof. Dr. Guohua Mi

Dissertation title: "Molecular mechanisms underlying the regulation of MADS-box transcription factor ANR1 involved in Arabidopsis lateral root development".

➤ 9/2008-6/2012 **B.Sc.** in Agricultural Resources and Environmental Science, College of Resources and Environmental Sciences, Henan Agriculture University, Zheng Zhou, China

Conferences and Scientific training

Conferences-oral presentations:

Zhongtao Jia. Genetic variation in barley grain mineral concentrations. Plant Science Student Conference, Halle, Germany, 2017.

Zhongtao Jia. Natural variation of root morphological responses to nitrogen nutritional status in *Arabidopsis thaliana*. Plant Stress Forum in IPSR, Okayama University, Japan, 2017.

Zhongtao Jia. BSK3-dependent brassinosteroid signaling tunes natural variation of root foraging responses to low nitrogen in *Arabidopsis thaliana*. Plant Science Student Conference, Gatersleben, Germany, 2018.

Conferences-poster presentations:

Zhongtao Jia, Ying Liu, Benjamin D. Gruber, Kerstin Neumann, Nicolaus von Wirén. Genome-wide association study of barley root architectural traits. 1st General COST FA1306 Meeting, Gatersleben, Germany, 2015.

Zhongtao Jia, Ying Liu, Benjamin D. Gruber, Kerstin Neumann, Nicolaus von Wirén. Genome-wide association study of barley root architectural traits. Plant Science Student Conference, Halle, Germany, 2015.

Zhongtao Jia, Ricardo F.H. Giehl, Nicolaus von Wirén. Natural Variation of Root System Architectural Traits in Dependence of the Nitrogen Nutritional Status in *Arabidopsis thaliana*. Plant Science Student Conference, Gatersleben, Germany, 2016.

Zhongtao Jia, Ricardo F.H. Giehl, Nicolaus von Wirén. Natural Variation of Root System Architectural Traits in Dependence of the Nitrogen Nutritional Status in *Arabidopsis thaliana*. Nitrogen 2016. Montpellier, France, 2016.

Zhongtao Jia, Ricardo F.H. Giehl, Nicolaus von Wirén. Natural Variation of Root System Architectural Traits in Dependence of the Nitrogen Nutritional Status in *Arabidopsis thaliana*. Natural variation in plants. Cambridge, UK, 2016.

Practical scientific training:

Histological and ultrastructural analysis of plant tissue using Light, Scanning and Transmission Electron Microscopy. IPK Gatersleben (04.13.2015-04.17.2015).

Barlomics-summer school. IPK Gatersleben (09.14.2015-09.17.2015).

Influence of nutrients on phytohormonal and architectural changes during adventitious root formation. IPK Gatersleben (11.23.2016-11.25.2016).

Selection in plant breeding. IPK Gatersleben (03.12.2018-03.16.2018).

Publications:

Zhongtao Jia, Ying Liu, Benjamin D Gruber, Kerstin Neumann, Benjamin Kilian, Andreas Graner, Nicolaus von Wirén. Genetic dissection of root system architectural traits in spring barley. *Frontiers in Plant Science*. doi.org/10.3389/fpls.2019.00400

Zhongtao Jia, Ricardo F.H. Giehl, Rhonda C. Meyer, Thomas Altmann, Nicolaus von Wirén. Natural variation of BSK3 tunes brassinosteroid signaling to regulate root foraging responses to low nitrogen. *Nature Communications* (Accepted).

Zhongtao Jia, Ricardo F.H. Giehl, Nicolaus von Wirén. Allelic variation of YUC8 modulates the lateral root foraging response to low nitrogen (*in preparation*).

Jia Zhongtao, Wang Wenliang, Tang Jianhua, Liu Fang, Liu Hongen, Liu Shiliang, Han Yanlai, Zheng Jun. Effect of animal manure organic fertilizer and nitrogen combined application on maize soil physical & chemical properties. *In Chinese*. *Environmental Science & Technology*, 2015, 38 (6P): 34-39.

10 Eidesstattliche Erklärung/Declaration under Oath

Ich erkläre an Eides statt, dass ich die Arbeit selbstständig und ohne fremde Hilfe verfasst, keine anderen als die von mir angegebenen Quellen und Hilfsmittel benutzt und die den benutzten Werken wörtlich oder inhaltlich entnommenen Stellen als solche kenntlich gemacht habe.

I declare under penalty of perjury that this thesis is my own work entirely and has been written without any help from other people. I used only the sources mentioned and included all the citations correctly both in word or content.

Datum / Date

*Unterschrift des Antragstellers /
Signature of the applicant*

11 Erklärung über bestehende Vorstrafen und anhängige Ermittlungsverfahren/Declaration concerning Criminal Record and Pending Investigations

Hiermit erkläre ich, dass ich weder vorbestraft bin noch dass gegen mich Ermittlungsverfahren anhängig sind. / I hereby declare that I have no criminal record and that no preliminary investigations are pending against me.

Datum / Date

*Unterschrift des Antragstellers /
Signature of the applicant*